A FUNDAMENTAL STUDY OF THE EFFECTS OF APPLIED ELECTRIC FIELDS ON GAS-SOLID (DIELECTRIC) ADSORPTION

By

Arun V. Someshwar

A DISSERTATION

Submitted to
Michigan State University
in partial fulfillment of the requirements
for the degree of

DOCTOR OF PHILOSOPHY

Department of Chemical Engineering

1982

ABSTRACT

A FUNDAMENTAL STUDY OF THE EFFECTS OF APPLIED ELECTRIC FIELDS ON GAS-SOLID (DIELECTRIC) ADSORPTION

By

Arun V. Someshwar

The effects of applied uniform and non-uniform electric fields on the adsorption characteristics of vapors in porous adsorbents are investigated. The theoretical foundations to describe the thermodynamics of polarized layers and the irreversible thermodynamic formulations for surface and volume flow in porous media are laid out. A theoretical 'Single-Pore' model describing the adsorption kinetics in cylindrical, open pore adsorbent systems like silica gel, in the presence of applied electrostatic fields, is postulated. Given the pore and adsorbate characteristics, along with the diffusion coefficient and adsorption kinetics in the absence of the applied fields, this model predicts satisfactorily the observed enhancements in adsorption rates in the presence of the external fields.

Various experiments conducted with porous adsorbents with only a few layers of adsorbate in the sample have confirmed the inability of applied electric fields to influence either gas-phase diffusion rates or surface diffusion rates. Experiments conducted with porous silica gel, wherein significant multilayer adsorption is known to have occurred,

showed significant adsorption rate enhancements, both due to the polarized adsorbate and the presence of alkali ions on the adsorbent surface.

Further experiments conducted with the silica gel-water vapor system have shown that (a) the extent of adsorption rate enhancement is not dependent on the magnitude of the macroscopic field gradient in the sample, and that (b) desorption kinetics from capillary porous media are essentially unaffected in electrostatic fields. The observation made in the literature that applied electric fields do not affect the adsorption behavior for non-polar adsorbates is confirmed by experiments with C_2Cl_4-silica gel.

The phenomenon of relaxing, internal electric fields in moist capillary porous systems is proposed and the procedure to estimate the magnitudes of the resulting internal field gradients is delineated.

Preliminary experiments conducted with the fly ash-water vapor system have shown that the adsorption kinetics are essentially unaffected by applied electric fields in a humid environment ($p/p_s \simeq 1$). However, the adsorption equilibria are significantly affected in an unsaturated environment ($p/p_s \simeq 2/3$) and electrodynamic (with ionic current flow) fields.

To my Mother

-and-

To my Father
who had to bear so much

ACKNOWLEDGEMENTS

The author would like to express his sincere appreciation to Dr. Bruce W. Wilkinson for providing encouragement and support through every single phase of this work. His concern for this student will be long remembered.

The author would also like to thank Drs. Carl Cooper, Charles Petty and MacKenzie Davis for their useful comments and criticisms. Special gratitude is offered to Dr. Carl Cooper for providing this author with various opportunities during the early stages of graduate work.

The excellent workmanship provided by the staff of the Engineering Workshop in fabricating the research equipment is much appreciated.

The author gratefully acknowledges the financial support obtained from the National Science Foundation (CPE-8111276) and the Michigan State University Division of Engineering Research.

The patience and perseverance of Karen Goodman in typing this thesis is gratefully acknowledged.

TABLE OF CONTENTS

Chapter

Chapter

LIST OF TABLES

LIST OF FIGURES

NOTATION

a	Radius of interparticle contact circle.
a_m	Area occupied by single adsorbed molecule.
A	Specific surface area of adsorbent.
c	B.E.T. parameter defined by Eq. (3.5).
c_i	Polarizabilities defined by Eq. (4.11).
C_i	Concentration of i^{th} species.
d	Diameter.
d_i	Interelectrode distance in Figure 4.1.
D	Diffusion coefficient.
e_v	Internal energy density.
$\underset{\rightarrow}{e}_z$	Unit vector in z direction.
E	Magnitude of electric field.
$\underset{\rightarrow}{E}$	Electric field vector.
f_v	Free energy density.
$\underset{\rightarrow}{f}$	Force acting on molecule defined by Eqs. (1.1) and (1.2).
F	Free energy.
$\underset{\rightarrow}{F}$	Pondermotive force defined in Section 2.1(a).
g	Correlation factor.
$\bar{g}$	Gibbs function.
$\underset{\rightarrow}{i}$	Current density.
J	Mass flux of diffusing species.
k	Boltzmann's constant.

K	Constant used in Eq. (3.15a).
$\mathcal{L}(x)$	Langevin function of x.
L	length of pore in adsorbent.
$\bar{L}_m$	Mean-free path on the surface of adsorbent.
m	Mass of adsorbate in system.
M	Molecular weight.
N_{av}	Avogadro's number.
N_m	Number of molecules per monolayer.
N_γ	Mass fraction of species γ.
p	Pressure.
p_s	Vapor pressure at saturation.
P_K	Specific polarization of a substance defined by Eq. (4.14).
$\vec{P}$	Polarization defined by Eq. (2.0).
q	Heat flux defined in Section 2.1(b).
q_s	Charge on particle at saturation defined by Eq. (4.5).
Q	Heat of adsorption.
$\vec{Q}$	Heat flow vector defined in Section 2.1(b).
r	Radial distance.
r_m	Mean pore radius.
R	Universal gas constant.
R_m	Mean radius of curvature defined in Section 3.1(a).
R_o	Radius.
s_v	Entropy density.
S	Entropy.
t	Time.
t_c	Thickness of bound adsorbate.
T	Temperature.

$U_p(z)$ Gas-solid perturbation potential.

$\bar{u}$ Mean velocity of gas molecules.

U Internal Energy.

$\vec{U}$ Velocity due to external force defined by Eq. (1.3).

v Average drift velocity of diffusing species.

v_s Specific volume of surface adsorbed molecules.

V Applied voltage.

V_m Internal pore volume.

W Adsorbate content of specimen

y_m Mass adsorbed in monolayer.

$\bar{z}$ Average charge per unit mass of body.

Greek Letters

β Ratio defined as r/a.

γ Surface tension.

σ Thickness of surface layer for surface diffusion.

δ_i Volume fraction of i^{th} phase in adsorbent.

ε Dielectric constant.

ε_o Permittivity of vacuum or free space.

η Viscosity.

θ Polar angle.

$\underline{\lambda}$ Mean-free path.

λ Phenomenological coefficient in Eq. (3.13).

μ Magnitude of dipole moment.

μ_i Chemical potential of i^{th} species.

$\vec{\mu}$ Dipole moment vector.

ρ Mass density.

τ	Average residence time of adsorbed molecule.
τ'	Lingering time defined by Eq. (3.12).
τ_o	Time of oscillation defined by Eq. (3.8).
τ_o'	Like τ_o in Eq. (3.12).
ϕ	Relative vapor pressure.
Φ	Scalar potential.
χ	Electric susceptibility.
$\vec{\omega}$	Barycentric velocity.
Ω	Gibbs field potential in Section 3.1(a).

INTRODUCTION

I.1 Motivation for this Research

In the technology of Electrostatic Precipitation, the phenomenon of 'back corona' or 'sparkover,' arising principally due to high ash or dust electrical resistivities, and the attendant problems with collection efficiencies is very well documented [W2]. High ash resistivities owing primarily to the burning of low sulphur coal can lead to severe collection problems. For over a decade it has been known that the ash surface resistivity is sensitive to not only the chemical composition of the coal burned, but also to the composition of the flue-gas [W1,B1]. The enhancement of water vapor concentrations in the gas, as well as the addition of small quantities of 'conditioning' agents such as sulphur-trioxide and some sodium compounds [W2] (which, in turn, bind the water more strongly on the particle surface), have been known to significantly lower ash resistivity.

In their investigations of the sorption phenomena of water vapor on fly ash, Ditl and Coughlin [D1,D2] have ascribed the significant lowering of ash resistivity (for adsorbed amounts less than even a monolayer) to 'capillary condensation' in the ring-like inter-particle crevices. However, the problem of justifying the use of the 'Kelvin' equation to account for the incipience of condensation in pore radii less than a few molecular diameters remains unresolved. In all the analysis carried out thus far to explain the sorption phenomena in the conditioning process, the fact that the bed of fly ash is subjected to high

external electric fields and the charged nature of the particulates prior to precipitation is neglected. Extremely high and non-uniform electric fields are known to exist in the vicinity of the contact spots between particulates in a bed subjected to an external electric field [M1].

Polar gases, and especially liquid-like adsorbates that are highly polarizable, experience additional thermodynamic forces in the presence of non-uniform electric and magnetic fields [D3]. The occurrence of alkali ions in fly ash [W2,B1,B2] and their role in the sorption phenomena have been subjects of much recent study. However, the effects of the strong electric fields involved have so far escaped notice. With these specific goals in mind, the present research efforts are aimed at initiating an understanding of the fundamental concepts that underlie the effects of applied electric fields on the thermodynamics and kinetics of gas-solid adsorption. Both theoretical and experimental investigations are attempted. An understanding of these 'electrical effects' could, of course, be utilized in all such processes where adsorption of gases or vapors takes place on electrically charged particles or particles subject to strong electric fields.

I.2 Research Objective and Outline

In this work the class of adsorbents used to study the electrical effects of gas-solid adsorption will be restricted to porous dielectrics. Conductors and semi-conductors will be excluded. The implications derived from porous dielectrics may, however, be extended to solid dielectrics. In the course of the experimental investigations, it was found that the electric field-induced effects in the sorption phenomena became significant only when multi-layer adsorption and/or capillary

condensation were known to take place. Monolayer adsorbed vapor was unaffected by ordinary laboratory fields ($\underset{\rightarrow}{E} < 1 \times 10^4$ V/cm). Accordingly, the chief emphasis of this research work will be on studying the field-induced phenomena brought into play when significant amounts of polarizable adsorbates are adsorbed.

This study consists essentially of three parts. The first consists of laying out the theoretical foundations of adsorption in porous media and the related thermodynamic field-induced phenomena. Detailed analysis of how to estimate internal, local electric fields in an adsorbent-adsorbate system and the corresponding 'ponderomotive' forces is given. In the second section the various experimental investigations are outlined, and the conclusions derived from each are recorded. Finally, the knowledge gained from the theoretical and experimental work already cited is applied to the problem of fly ash resistivity and conditioning in modern Electrostatic Precipitators. Appropriate recommendations for continued work with fly ash and other adsorbents (especially in the presence of alkali ions) are made.

CHAPTER I

SURVEY OF EXISTING LITERATURE

A polarizable molecule of 'effective' dipole moment $\underset{\rightarrow}{\mu}$ will experience a force when placed in a non-uniform electric field given by [H2]

$$\underset{\rightarrow}{f}^{p} = \underset{\rightarrow}{\mu} \cdot \nabla \underset{\rightarrow}{E} \tag{1.1}$$

where

$\underset{\rightarrow}{f}^{p}$ = force per molecule

$\nabla \underset{\rightarrow}{E}$ = gradient of electric field

This force will act in the direction of the maximum field intensity gradient. Besides the force on a polarizable molecule, a charged body (charged with either ions or electronic charges) will also experience a force given by

$$\underset{\rightarrow}{f}^{c} = \rho \bar{z} \underset{\rightarrow}{E} \tag{1.2}$$

where

$\underset{\rightarrow}{f}^{c}$ = force per unit volume of body

$\bar{z}$ = charge per unit mass of body

ρ = density of body

Several researchers have attempted to study the consequences of these two forces in solid-gas, solid-liquid, liquid-liquid and liquid-gas systems. In this chapter a detailed review of the effects of

external electric fields on the characteristics of gas-solid adsorption is made. Among solids only dielectrics are chosen, though the gaseous adsorption in metals and semi-conductors in the presence of an external field is also briefly touched upon. In the final section some instances where the external fields have been used to study liquid-liquid, liquid-gas systems are cited.

1.1 Field-Induced Effects in Solid-Gas Adsorption

For some inexplicable reason, almost all of the research concerning the adsorption of gases and vapors on disperse dielectric solids in the presence of electric fields seems to have been carried out in the Soviet Union.† Panchenko et al. [P1 to P3, P5 to P11] have conducted experiments to study the adsorption of moisture on various kinds of silica gel, potato starch, cellulose-acetate and some natural polymers in the presence of both sub-discharge and corona electric fields.

In references [P3,P5,P6] the authors have studied the water vapor adsorption characteristics in two kinds of silica gel, KSM-5 (mean pore radius = 12 A^{o}) and KSK-2 (mean pore radius = 59 A^{o}) in the presence of electric (both d.c. and a.c. ≃ 50 Hz) and magnetic fields. Figure 1.1 shows the effect of cylindrical, non-uniform electric fields on the rate of water vapor adsorption in KSK-2 silica gel [P3].

The same authors studied the sorption kinetics of water-vapor in silica gel in the presence of uniform constant and uniform alternating (50 Hz) electric fields (with field strengths up to about 2 KV/cm) and

---

†Much of the literature (none of which was felt to have any direct significance in this work, judging from the short paragraphs in Chemical Abstracts) is in Russian and is unavailable in the MSU libraries.

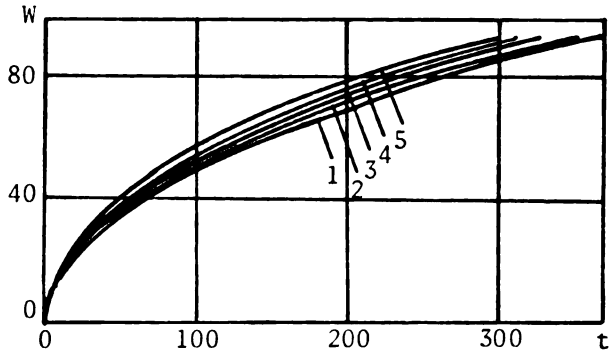

Figure 1.1. Curves of moisture content W(%) in grade KSK-2 silica gel, as a function of time t (mins.): 1) without an electrical field; 2) U = 700 V; 3) U = 800 V; 4) U = 900 V; 5) U = 1,000 V. Relative pressure of water vapor $\phi_s \simeq 1$, T = 293° K.

failed to see any enhancement in the adsorption kinetics [P3]. Also, measurements made in non-uniform electric fields for the adsorption of carbon tetrachloride (dipole moment = 0, dielectric constant ≃ 2) in KSK-2 silica gel yielded no discernible effects. The low frequency (50 Hz) alternating fields were identical in their effects to the constant d.c. fields of similar intensities [P3], probably implying that the frequencies were yet too low to affect the adsorption. In non-uniform electric fields the authors also observed that the time required for attaining a given moisture content decreased linearly with increasing voltage on the electrodes [P6]. The presence of magnetic or electric fields had no influence on the maximum hygroscopic moisture content of the samples and did not change the shape of the adsorption or the desorption branches of the isotherm [P6]. In [P5] the authors studied the temperature effect on the sorption kinetics of water-vapor in silica gel. They observed that an increase in the temperature from 293° K to 323° K weakens the field-induced phenomena.

The preceding authors also studied the effects of applied, non-uniform electric fields on the sorption kinetics of water-vapor in ion-saturated (K^+, Ca^{++}) silica gel KSM-5 (mean pore radius = 12 A^o) [P1]. The ions, especially bivalent Ca^{++}, are assumed to provide additional sorption centers to enhance the adsorption. Further, the mobility of the hydrated ions is presumed to be significantly enhanced in the presence of applied non-uniform fields, thereby influencing the adsorption kinetics. Figures 1.2 and 1.3 describe the equilibrium and kinetic characteristics of water-vapor sorption in ion-saturated silica gel KSM-5, respectively. As these figures clearly indicate, the applied non-uniform fields are seen to enhance both the maximum amount adsorbed, as well as the rate of adsorption in ion-saturated porous silica gel.

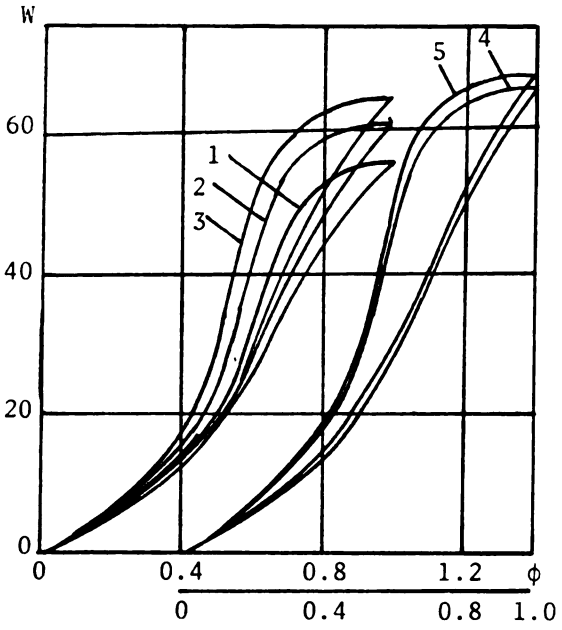

Figure 1.2. Sorption isotherms for plain and ion-saturated specimens of grade KSM-5 silica gel without a field: 1) plain KSM-5, 2) with K^+, 3) with Ca^{2+}; in an electric field: 4) with K^+, 5) with Ca^{2+}.

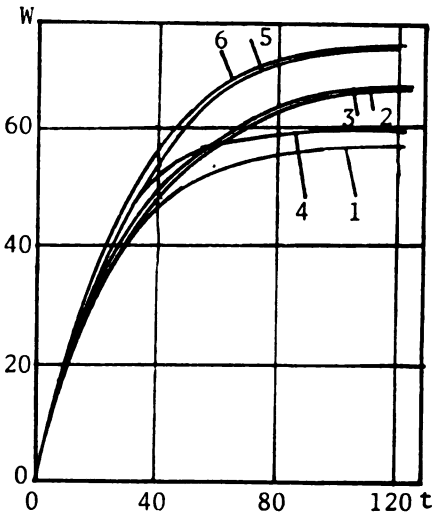

Figure 1.3. Sorption kinetics. Moisture content W(%) vs. time t (min.), T = 303° K without a field: 1) plain KSM-5, 2) with K^+, 3) with Ca^{2+}; in an electric field: 4) plain KSM-5, 5) with K^+, 6) with Ca^{2+}.

In [P10] the authors have investigated the effects of field intensity and homogeneity on the kinetics and statics of water-vapor adsorption by silica gel KSM-5, sulfite cellulose and potato starch. The 'sub-discharge' electric fields had no effect on the maximum adsorption capacity of KSM-5. However, the capacity of cellulose and starch was reduced strongly. They concluded that the sub-discharge electric field shrinks the total pore volume by shifting the pore distribution to smaller radii. The adsorption kinetics were affected to different extents for the different adsorbents.

In [M5] Mosievich has studied the effects of applied electric fields on the internal mass transfer during sorption of moisture by natural polymers. Non-uniform fields increased the rate of adsorption, while uniform fields of the same intensity had no effect on the rate. An increase in temperature weakened these effects.

In [P11] the authors have researched the possibility of using a corona discharge to provide the electric field and the energy supply in the drying of a model capillary-porous body (KSM-5 silica gel). Significant enhancement is observed in the kinetic curves of drying, with the total duration of the process reduced by almost three fold in comparison with convective drying. An attempt is made to establish the physical mechanism underlying this phenomenon in [P12] (to be described soon).

Panchenko et al. [P2] have postulated a mechanism to help explain the field-induced effects on the internal mass transfer in porous bodies. They maintain that since a polar molecule of dipole moment $\vec{\mu}$ will experience a force $\vec{f}$ in a non-uniform electric field (given by equation 1.1), this molecule will acquire a velocity component in the direction of increasing values of $\nabla\vec{E}$ given by

$$\underset{\rightarrow}{U} = D\underset{\rightarrow}{f}/kT \tag{1.3}$$

where

D = vapor diffusion coefficient

k = Boltzmann's constant

T = temperature

To the normally existing diffusive flux, J_v, is then added a convective flux, $J_e = \underset{\rightarrow}{U}C$, and the total flux, J, becomes

$$J = J_v + J_e = -D\frac{dC}{dx}\left[1 + \frac{(\underset{\rightarrow}{\mu}\cdot\underset{\rightarrow}{\nabla E})C}{kT(-dC/dx)}\right] \tag{1.4}$$

In the same work they have conducted experiments to yield the adsorption isotherms (Figure 1.4) and the adsorption kinetics (Figures 1.5, 1.6) for water-vapor adsorption in silica gel KSS-4 (mean pore radius = 22 A^o). Field gradients of up to $\underset{\rightarrow}{\nabla E} = 8{\cdot}5\times10^4$ V/cm^2 were used. As before, the adsorption isotherms were unaffected, while the kinetics were affected noticeably. They ascribe to the former result the fact that applied external fields are much less than the internal fields acting in the adsorbate-adsorbent system and governing the molecular bond energy. The latter result is attributed primarily to a mechanism explained by equation (1.4) and also, possibly, to field effects on the surface transfer of adsorbed material.

In [P9] the authors have reported an increasing amount of water adsorbed with increasing field gradients in the case of hydration of beads of a styrene-divinyl benzene (8%) copolymer modified by SO_3H groups in the Na^+, Cu^{2+} or Ca^{2+} form and at 298^o K. In [P8] the intensification of the drying process in bleached sulfite cellulose and starch, saturated

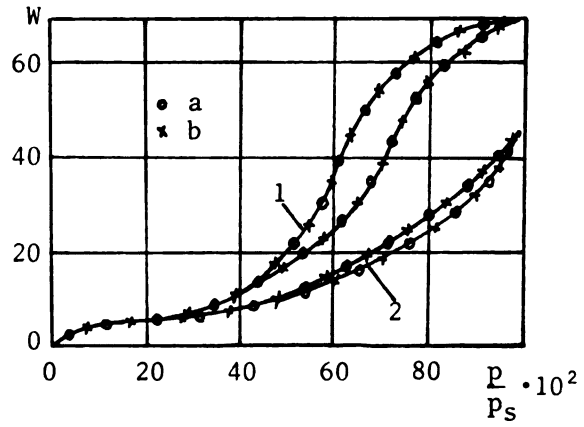

Figure 1.4. Adsorption-desorption isotherms of water vapor in KSS-4 silica gel at various temperatures: 1) 293° K, 2) 308° K; a) without a field, b) in an inhomogeneous electric field ($\nabla \vec{E}$ = 8•5x10^8 V/m^2).

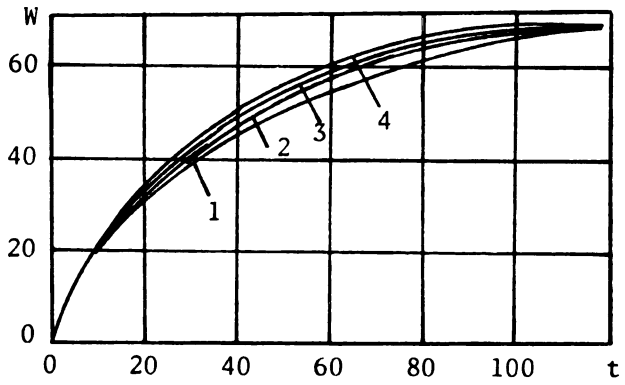

Figure 1.5. Percentage adsorption W vs. time t (min.) for KSS-4 silica gel at T = 293° K. 1) Without a field; inhomogeneous electric fields: 2) $\nabla \vec{E}$ = .76x10^8 V/m^2, 3) 2.03x10^8, 4) 8.5x10^8 V/m^2.

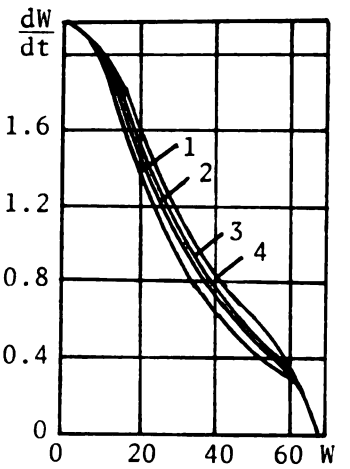

Figure 1.6. Adsorption rate dW/dt (%/min.) of water vapor by KSS-4 silica gel vs. moisture content W(%). 1) Without a field; in an inhomogenous electric field: 2) $\nabla E = .76 \times 10^8$ V/m^2, 3) 2.03×10^8, 4) 8.5×10^8 V/m^2.

with EtOH and water (at 333^{o} K), was studied in the presence of a non-uniform field. The fields did not increase the material temperature nor cause any decomposition.

In an attempt to define the physical mechanisms involved in the intensification of drying of moist capillary porous systems in corona discharges, the authors in [P12] have studied the effects of these discharge fields on the evaporation of water and aqueous KCl solution from quartz capillaries 2-30 μm in radius. Fields of the order of 2.7×10^4 V/cm and gradients of 9.9×10^4 V/cm^2 were created by a needle-plane electrode system. Appreciable increases in the rates of evaporation were observed, especially when the surrounding relative vapor pressures (p/p_s) approached 1. The various factors that were cited as possible reasons for the observed enhancement are: (1) additional electroconvective flow J_e (given by equation 1.4); (2) reduction in vapor pressure above the capillary mouth (where the corona needle is located), due to either a

screening of the capillary in the corona discharge zone by excess space charge of high density [K3], or by sorption of vapor molecules on nuclei (ions) produced in the corona discharge [P12]; (3) liberation of Lentz-Joulean heat in the discharge gap (small). Further experiments to determine the relative extents of mechanisms (1) and (2) revealed the dominance of (2) over (1).

Besides the group of Panchenko et al., another Russian group, that of Kuliev et al. [K4,K5,R2], have studied gas-solid adsorption in the presence of electric fields. In [K4] the authors have investigated the adsorption of p- and o-xylene and of H_2O in silica gel KCM (at 350^{o} K) in an external electric field. They concluded that with increasing field potential, the adsorption on KCM increased with increasing adsorbate-molecular polarity and that on SKT was unaffected by the field. The silica gel KCM had apparently some concentration of foreign ions. In [K5] the same authors conduct adsorption studies with mixtures (1:1) of octane-octene, and p-xylene-o-xylene, on silica gel in the presence of a corona discharge field. The separation coefficient (relative concentrations of adsorbate) was found to be two to three times higher in the presence of the field than without it. Rasulov et al. [R2] studied the surface properties of adsorbents to elucidate the mechanism of processes which take place on solid surfaces in applied electric fields. The electrical conductivity of silica gel NS-62 and zeolite NaA was determined during H_2O-vapor adsorption. The adsorption on NS-62 was observed to increase significantly in the field.

Other than the work detailed above, no relevant information seems to be available relating the effects of external fields on the physical adsorption of gases on disperse, dielectric media. Considerable work,

however, has been carried out to study the effects of applied fields in the chemisorption of mostly non-polar gases on metallic and semiconducting surfaces. The externally applied field is known to enhance or suppress (depending on the polarity) the movement of electrons to the surface and thus affect the electron transfer mechanism in chemisorption bond formation [S3]. Bennett [B7] has formulated a theoretical model with a quantum-mechanical approach to determine strong electric-field induced changes in the binding energy, equilibrium position and vibrational frequency of the adsorbate in chemisorption at a metal-vacuum interface. Lincoln and Olinger [L1] observed an increase in the adsorption rate and quantity of C_2H_4 on a porous nickel catalyst, but saw no change in the case of H_2. Hoenig and Lane [H3] concluded that the adsorption of O_2 on ZnO (known to take place by an electron transfer mechanism) could be suitably altered by imposing an appropriate electric field. The adsorption of O_2 on W [D6], ZnO [D7], Ge [R3], of CO_2 on ZnO [D7] and of Cs, Na, Li on W [T1] in an applied d.c. field were all seen to be significantly affected.

1.2 Field-Induced Effects in Other Systems

In the areas of liquid-liquid and liquid-gas systems, considerable work has been done to study the effects of either applied electric fields or charged liquid droplets. Sawistowski and Banczyk [S4,B8] obtained a more than tenfold increase of the mass transfer coefficient for two-component systems during horizontal laminar flow of the phases and an electric field intensity of about 1KV/cm. They also observed the formation of additional turbulence near the interface, probably caused by electrodynamic forces acting on the liquid [R4]. Agaev and Abdullaev [A1] and Kowalski and Ziolkowski [K6] have independently utilized

electric fields in extraction columns with much success. Besides increased turbulence resulting from the application of non-uniform electric fields in association with inhomogeneous dielectric media [T2,G2,S5,K8], the occurrence of an increased velocity and reduced interfacial tension of charged drops of the dispersed phase in relation to the continuous phase is exploited in various liquid-gas, liquid-liquid systems [B9,K7,H4]. Further mention of the various interesting phenomena arising from electric fields applied to these systems is outside of the scope of this work.

CHAPTER II

THERMODYNAMICS OF CHARGED AND POLARIZED LAYERS

In a system containing polarizable constituents and unequally distributed charges, classical thermodynamics are of dubious value. Prigogine [P13] was the first to derive a formulation of the thermodynamics of charged and polarized systems. He has shown that an elegant combination of the thermodynamics of irreversible processes and of the Maxwell-Lorentz electromagnetic theory, along with a local rather than global character, yields information about thermodynamic functions and equilibrium conditions of charged and polarized matter under more general conditions than comprise the use of classical thermodynamics alone. Using the contributions of Prigogine, Mazur and Defay [P14,M6,D8], Sanfeld [S6] has prepared an excellent monograph which makes a general survey of the thermodynamics of matter in a field.

In this chapter some of the fundamental concepts developed by the above authors are presented. The significance of these concepts on the various aspects of this work is mentioned whenever applicable. Starting with the Kelvin concept of the 'ponderomotive' force, the laws of conservation of momentum and energy in charged and polarized systems are formulated. Next, the Gibbs-Duhem type of equation for these systems is derived. In Section 2.2 the effects of applied fields on various thermodynamic quantities in systems where the permittivity depends on the macroscopic field are investigated, both theoretically and with appropriate numerical examples. In Section 2.3 the very interesting concepts

of 'pressure' in a dielectric and the ponderomotive force, according to the Kelvin and the Helmholtz approaches are presented. Also, the advantages of the Kelvin method over that of the Helmholtz method are noted. In the final section the distribution of matter in charged and polarized systems is discussed for various specific instances.

2.1 Local Balance Thermodynamics in Electrochemical Systems

The phenomena due to electromagnetic forces are, in general, non-conservative. The basic conservation laws of momentum and energy are therefore reformulated to account for the presence of the electromagnetic fields. For the sake of convenience, the assumption that no magnetic fields are applied will be made here.

The electric polarization $\underset{\rightarrow}{P}$ is defined as

$$\underset{\rightarrow}{P} = \varepsilon_o(\varepsilon - 1)\underset{\rightarrow}{E} = \chi\underset{\rightarrow}{E} \tag{2.0}$$

where

$\underset{\rightarrow}{E}$ = macroscopic electric field strength (V/cm)

ε = dielectric constant (dimensionless)

ε_o = permittivity of free space ($= 8{\cdot}854\text{x}10^{-12}\ \frac{N}{V^2}$)

χ = electric susceptibility = $\varepsilon_o(\varepsilon - 1)$

$\underset{\rightarrow}{P}$ = polarization per unit volume

$\underset{\rightarrow}{E}$ = -grad Φ

Φ = scalar potential

2.1(a) Ponderomotive Force

For a non-viscous fluid in the absence of gravity, the force acting upon each isotropic volume element δV is

$$(\underset{\rightarrow}{F} - \text{grad } p)\delta V$$

where

$\underset{\rightarrow}{F}$ = electromagnetic force or ponderomotive force

In general,

$$\underset{\rightarrow}{F} = \underset{\rightarrow}{F}^{L} + \underset{\rightarrow}{F}^{p}$$

where

$$\underset{\rightarrow}{F}^{L} = \sum_{\gamma}(\rho_{\gamma}\bar{z}_{\gamma})\underset{\rightarrow}{E} = \rho\bar{z}\underset{\rightarrow}{E} = \text{force on a volume element having a realized charge } \bar{z}\rho\delta V$$

and

$\underset{\rightarrow}{F}^{p}$ = force on polarized volume element with electric moment $\underset{\rightarrow}{P}\delta V$

If one follows Kelvin, one may define

$$\underset{\rightarrow}{F}^{p} = \underset{\rightarrow}{F}^{k} = \underset{\rightarrow}{P}\cdot\text{Grad } \underset{\rightarrow}{E}$$

2.1(b) Conservation of Momentum and Energy

The dynamical equation for continuous media, viz.,

$$\rho\frac{d\underset{\rightarrow}{\omega}}{dt} = \underset{\rightarrow}{F} - \text{grad } p$$

(where $\underset{\rightarrow}{\omega}$ = barycentric velocity of the system, at a point) now becomes

$$\rho\frac{d\underset{\rightarrow}{\omega}}{dt} = \rho\bar{z}\underset{\rightarrow}{E} + \underset{\rightarrow}{P}\cdot\text{Grad } \underset{\rightarrow}{E} - \text{grad } p \qquad (2.1)$$

Equation (2.1), when combined with the equation of continuity, viz.,

$$\frac{\partial\rho}{\partial t} = -\text{div } \rho\underset{\rightarrow}{\omega}$$

and after some vector manipulations [S6, p. 20], yields the following macroscopic kinetic energy balance:

$$\frac{\partial}{\partial t}\left(\frac{1}{2}\rho\underset{\rightarrow}{\omega}^2 + \frac{\varepsilon_o}{2}\underset{\rightarrow}{E}^2\right) = -\mathrm{div}\left[\left(\frac{1}{2}\rho\underset{\rightarrow}{\omega}^2\right)\underset{\rightarrow}{\omega} - \left(\underset{\rightarrow}{P}\cdot\underset{\rightarrow}{E}\right)\underset{\rightarrow}{\omega}\right] - \rho\underset{\rightarrow}{E}\cdot\frac{d\overline{\underset{\rightarrow}{P}}}{dt} - \underset{\rightarrow}{E}\cdot\underset{\rightarrow}{i} - \underset{\rightarrow}{\omega}\cdot\mathrm{grad}\ p \tag{2.2}$$

where $\overline{X} = \frac{X}{\rho}$ (X is any arbitrary function) and the current density $\underset{\rightarrow}{i} = \sum_\gamma \overline{z}_\gamma \rho_\gamma (\omega_\gamma - \omega)$ arises from the diffusion of charged components.

The energy term $\left(\frac{1}{2}\rho\underset{\rightarrow}{\omega}^2 + \frac{\varepsilon_o}{2}\underset{\rightarrow}{E}^2\right)$ in equation (2.2) is not conservative due to the source term

$$-\rho\underset{\rightarrow}{E}\cdot\frac{d\overline{\underset{\rightarrow}{P}}}{dt} - \underset{\rightarrow}{E}\cdot\underset{\rightarrow}{i} - \underset{\rightarrow}{\omega}\cdot\mathrm{grad}\ p$$

To get the conservation of energy balance equation, the internal energy balance is to be added to the kinetic energy balance equation (2.2). To make the total energy conservative, the internal energy density e_v is defined in such a way that, in addition to the usual convective flow $e_v\underset{\rightarrow}{\omega}$, the flow $p\underset{\rightarrow}{\omega}$ related to mechanical work, and the flow $\underset{\rightarrow}{Q}$ related to pure heat flow, the above source term is added to get

$$\frac{\partial e_v}{\partial t} = -\mathrm{div}\left(e_v\underset{\rightarrow}{\omega} + \underset{\rightarrow}{Q} + p\underset{\rightarrow}{\omega}\right) + \rho\underset{\rightarrow}{E}\cdot\frac{d\overline{\underset{\rightarrow}{P}}}{dt} + \underset{\rightarrow}{E}\cdot\underset{\rightarrow}{i} + \underset{\rightarrow}{\omega}\cdot\mathrm{grad}\ p \tag{2.3}$$

Adding (2.2) and (2.3) and using the relations

$$\rho\frac{d\overline{e}}{dt} = \frac{\partial e_v}{\partial t} + \mathrm{div}\left(\underset{\rightarrow}{\omega}e_v\right)$$

and

$$\rho\frac{dq}{dt} = -\mathrm{div}\ \underset{\rightarrow}{Q} \quad ; \quad \overline{v} = \frac{1}{\rho}$$

one gets the local formula for the first law of thermodynamics for charged and polarized systems, viz.,

$$\frac{d\bar{e}}{dt} = \frac{dq}{dt} - p\frac{d\bar{v}}{dt} + \underset{\rightarrow}{E}\cdot\frac{d\bar{\underset{\rightarrow}{P}}}{dt} + \frac{\underset{\rightarrow}{E}\cdot\underset{\rightarrow}{i}}{\rho} \tag{2.4}$$

2.1(c) The Gibbs-Duhem Equation for Polarized Systems

By assuming the polarization to be in statistical equilibrium with the field (i.e., $\underset{\rightarrow}{i} = 0$) and by considering a one-component fluid without viscosity, the following relations can be obtained:

$$\frac{d\bar{s}}{dt} = \frac{1}{T}\frac{dq}{dt}$$

and since $\underset{\rightarrow}{i} = 0$

$$\frac{df_v}{dt} = -s_v\frac{dT}{dt} + \underset{\rightarrow}{E}\cdot\frac{d\underset{\rightarrow}{P}}{dt} + (\bar{f} - \underset{\rightarrow}{E}\cdot\bar{\underset{\rightarrow}{P}} + p\bar{v})\frac{d\rho}{dt} \tag{2.5}$$

where the free energy density f_v is defined by

$$f_v = e_v - Ts_v$$

Since f_v must be a state function of the volume element, one can write

$$f_v = f_v(T, \underset{\rightarrow}{P}, \rho)$$

with

$$\left(\frac{\partial f_v}{\partial T}\right)_{\underset{\rightarrow}{P},\rho} = -s_v \quad (a) \qquad \left(\frac{\partial f_v}{\partial \underset{\rightarrow}{P}}\right)_{T,\rho} = \underset{\rightarrow}{E} \quad (b)$$

$$\left(\frac{\partial f_v}{\partial \rho}\right)_{T,\underset{\rightarrow}{P}} = \bar{f} - \underset{\rightarrow}{E}\cdot\bar{\underset{\rightarrow}{P}} + p\bar{v} \quad (c) \tag{2.6}$$

Prigogine, Mazur and Defay [P14, §10] have argued that equations (2.6) are valid even when irreversible processes occur, such as heat conduction or viscous dissipation. But polarization here is always considered to be a reversible phenomenon. The entropy production by orientation of dipoles has been treated elsewhere [P15,P16,D3].

For a system of several components, one may rewrite (2.6) as

$$f_V = f_V(T, \underset{\rightarrow}{P}, \rho_1, \ldots \rho_c) \quad (a)$$

$$\left(\frac{\partial f_V}{\partial T}\right)_{\underset{\rightarrow}{P},\rho_1,\ldots\rho_c} = -s_V \quad (b) \qquad \left(\frac{\partial f_V}{\partial \underset{\rightarrow}{P}}\right)_{T,\rho_1,\ldots\rho_c} = \underset{\rightarrow}{E} \quad (c) \tag{2.7}$$

Prigogine et al. then define the mass chemical potential as follows:

$$\left(\frac{\partial f_V}{\partial \rho_\gamma}\right)_{T,\underset{\rightarrow}{P},(\rho)} = \bar{\mu}_\gamma \tag{2.8}$$

From (2.7) and (2.8) and using

$$\frac{d\rho_\gamma}{dt} = N_\gamma \frac{d\rho}{dt} \qquad (N_\gamma = \text{mass fraction})$$

one gets

$$\frac{df_V}{dt} = -s_V \frac{dT}{dt} + \underset{\rightarrow}{E} \cdot \frac{d\underset{\rightarrow}{P}}{dt} = \left(\sum_\gamma N_\gamma \bar{\mu}_\gamma\right)\frac{d\rho}{dt} \tag{2.9}$$

Comparing (2.9) with (2.5), one obtains

$$\sum_\gamma N_\gamma \bar{\mu}_\gamma = \bar{f} + p\bar{v} - \underset{\rightarrow}{E} \cdot \underset{\rightarrow}{\bar{P}} \tag{2.10}$$

which is equivalent to the classical Gibbs function $\bar{g} = \bar{f} + p\bar{v}$ for non-polarized systems.

From equations (2.7) and (2.8), a virtual variation of $T, P, \rho_1 \ldots \rho_C$ leads to

$$\delta f_v = -s_v dT + \underset{\rightarrow}{E} \cdot \delta \underset{\rightarrow}{P} + \sum_\gamma \bar{\mu}_\gamma \delta \rho_\gamma$$

which, when combined with the differentiated form of (2.10) yields the Gibbs-Duhem equation for polarized systems:

$$\delta p - s_v \delta T - \underset{\rightarrow}{P} \cdot \delta \underset{\rightarrow}{E} - \sum_\gamma \rho_\gamma \delta \bar{\mu}_\gamma = 0 \qquad (2.11)$$

In terms of gradients and at constant T, this may be rewritten as

$$\text{grad } p - \underset{\rightarrow}{P} \cdot \text{grad } \underset{\rightarrow}{E} - \sum_\gamma \rho_\gamma \text{ grad } \bar{\mu}_\gamma = 0 \qquad (2.12)$$

Equation (2.12) is the fundamental relation describing the transport fluxes, both due to a pressure gradient and due to the gradient in the electric field. From an irreversible thermodynamical point of view, the mass fluxes in a system are proportional to the gradient of the chemical potentials. The relationship between the gradient in the chemical potential and the other driving forces in the system, given by equation (2.12), will form the starting point of all theoretical analysis used to describe the electric field-induced adsorption kinetic effects in this work.

2.2 Thermodynamic Relations for Systems in which the Dielectric Constant Depends on the Macroscopic Field

In Section 2.1 the electric polarization $\underset{\rightarrow}{P}$ was defined as

$$\underset{\rightarrow}{P} = \varepsilon_o(\varepsilon - 1)\underset{\rightarrow}{E}$$

The dielectric constant ε is a function of $\underset{\rightarrow}{E}$, the electric field. At low fields $\underset{\rightarrow}{P}$ may be assumed to vary linearly with $\underset{\rightarrow}{E}$ (i.e., ε =

constant). However, at even moderate fields, ε of a polar liquid becomes an explicit function of $\underset{\rightarrow}{E}$, decreasing as $\underset{\rightarrow}{E}$ increases.

In general,

$$\varepsilon = \varepsilon(T, C_1, \ldots C_c, E)$$

2.2(a) Free Chemical Energy Density

Equation (2.7c) may be written as

$$\underset{\rightarrow}{E} = \left(\frac{\partial f_v}{\partial \underset{\rightarrow}{P}}\right)_{T, C_1, \ldots C_c}$$

where $C_\gamma = \rho_\gamma / M$ is the molar concentration of species γ

which, when integrated at $T, C_1, \ldots C_c$ constant, yields

$$f_v(T, \underset{\rightarrow}{P}, C_1, \ldots C_c) = f_{vo}(T, \underset{\rightarrow}{P} = 0, C_1, \ldots C_c) + \int_{0,C}^{\underset{\rightarrow}{P}} \underset{\rightarrow}{E} \cdot d\underset{\rightarrow}{P} \qquad (2.13)$$

On further expansion, one gets

$$f_v = f_{vo} + \frac{\underset{\rightarrow}{E} \cdot \underset{\rightarrow}{P}}{2} + \frac{\varepsilon_o}{2} \int_{0,C}^{E^2} \frac{\underset{\rightarrow}{E}}{2} \left(\frac{\partial \varepsilon}{\partial E}\right)_{T,C} d\underset{\rightarrow}{E}^2 \qquad (2.14)$$

The last term corresponds to the contribution to f_v, due to the variation of ε with $\underset{\rightarrow}{E}$.

2.2(b) Entropy Density s_v

Differentiation of (2.13) with respect to T, using (2.7b) gives:

$$s_v = s_{vo} - \left(\frac{\partial}{\partial T} \int_{0,C}^{\underset{\rightarrow}{P}} \underset{\rightarrow}{E} \cdot d\underset{\rightarrow}{P}\right)$$

which may be further expanded to give

$$s_v = s_{vo} + \frac{\varepsilon_o}{2} \int_{0,C}^{E^2} \left(\frac{\partial \varepsilon}{\partial T}\right)_{\underset{\rightarrow}{E},C} d\underset{\rightarrow}{E}^2 \qquad (2.15a)$$

or

$$s_v = s_{vo} + \frac{\epsilon_o}{2} \vec{E}^2 \left(\frac{\partial \epsilon}{\partial T}\right)_{\vec{E},C} - \frac{\epsilon_o}{2} \int_{O,C}^{\vec{E}^2} \frac{E}{2} \left(\frac{\partial}{\partial E}\left(\frac{\partial \epsilon}{\partial T}\right)_{\vec{E},C}\right)_{T,C} d\vec{E}^2 \qquad (2.15b)$$

Once again, the last term in (2.15b) corresponds to the contribution to s_v from the variation of $(\partial\epsilon/\partial T)$ with respect to $\vec{E}$.

2.2(c) Internal Energy Density e_v

From (2.14) and (2.15b) since $f_v = e_v - Ts_v$

$$e_v = e_{vo} + \frac{\vec{E}\cdot\vec{P}}{2} + \frac{T\epsilon_o}{2} \vec{E}^2 \left(\frac{\partial \epsilon}{\partial T}\right)_{\vec{E},C} + \frac{\epsilon_o}{2} \int_{O,C}^{\vec{E}^2} \frac{E}{2} \left(\left(\frac{\partial \epsilon}{\partial E}\right)_{T,C} - T\left(\frac{\partial^2 \epsilon}{\partial E \partial T}\right)_C \right) d\vec{E}^2 \qquad (2.16)$$

2.2(d) Chemical Potential μ_γ

From the definition $\mu_\gamma = \left(\frac{\partial f_v}{\partial C_\gamma}\right)_{T,\vec{P},(C)}$ and equation (2.13), one gets

$$\mu_\gamma(T,\vec{E},C_1,\ldots C_c) = \mu_{\gamma o}(T,O,C_1,\ldots C_c) - \frac{\epsilon_o}{2} \int_{O,C}^{\vec{E}^2} \left(\frac{\partial \epsilon}{\partial C_\gamma}\right)_{T,(C),\vec{E}} d\vec{E}^2 \qquad (2.17a)$$

which may be rewritten as

$$\mu_\gamma = \mu_{\gamma o} - \frac{\epsilon_o}{2} \vec{E}^2 \left(\frac{\partial \epsilon}{\partial C_\gamma}\right)_{T,\vec{E},(C)} + \frac{\epsilon_o}{2} \int_{O,C}^{\vec{E}^2} \frac{E}{2} \left(\frac{\partial^2 \epsilon}{\partial E \partial C_\gamma}\right)_T d\vec{E}^2 \qquad (2.17b)$$

2.2(e) Numerical Estimates

In this section, some estimates are made of the deviations in entropy, free energy and internal energy densities for pure water at 25^o C, due to a local electric field $\vec{E}$. The effect of the electric field ϵ, $(\partial\epsilon/\partial T)$ and its resulting influence on the above thermodynamic quantities are also noted.

For a pure polar substance, Mandel [M7, eqn. (111.3)] has proposed the expression

$$\varepsilon = \frac{\rho N_{av}}{\varepsilon_o M \vec{E}} \mu_d \mathcal{L}\left(\frac{3g\mu_d \vec{E}}{2kT}\right)$$

where

M = molecular weight

N_{av} = Avogadro's number

μ_d = dipole moment in the bulk of the liquid

g = correlation factor ($\simeq$ 2.55 for H_2O at 25° C)

$\mathcal{L}$ = Langevin function ($\mathcal{L}(x)$ = Cot hx - 1/x)

Using this model for the dielectric constant, the following tables for pure water at 25° C can be prepared.

Table 2.1. Influence of Field on the Theoretical Values of $\left(\frac{\partial \varepsilon}{\partial T}\right)_{\rho, \vec{E}}$ and $\frac{\varepsilon_o}{2}\int_0^{\vec{E}^2}\left(\frac{\partial \varepsilon}{\partial T}\right)_{T, \vec{E}} d\vec{E}^2$; from [S6, p. 45]

$\vec{E}$ (V/cm)	$\left(\frac{\partial \varepsilon}{\partial T}\right)_{\rho, \vec{E}}$ (per °K)	$\frac{\varepsilon_o}{2}\int_0^{\vec{E}^2}\left(\frac{\partial \varepsilon}{\partial T}\right)_{\rho, \vec{E}} d\vec{E}^2 \left(\frac{\text{ergs}}{\text{cm}^3\ ^\circ\text{K}}\right)$
1.2×10^5	-0.18	
1.8×10^6	-0.16	
3.0×10^6	-0.10	-14.5×10^6
4.5×10^6	-0.057	-25.0×10^6
6.0×10^6	-0.034	-30.6×10^6
9.9×10^6	-0.014	-42.7×10^6

Table 2.1 clearly shows how the dependence of ε on T drops gradually as the field intensity increases. This is in keeping with the physical

observation that the orientation of the dipoles increases with field intensity whilst disorder increases with temperature (i.e., the disordering effect of temperature is partially corrected for by the field).

Table 2.2. Influence of Field on Entropy Density (T = 25° C)

Case I: $\varepsilon = \varepsilon(T,C,E)$ Case II: $\varepsilon = \varepsilon(T,C,E = 0)$

$\vec{E}$ (V/cm)	Case	$\left(\frac{\partial \varepsilon}{\partial T}\right)_{\rho,\vec{E}}$ (per °K)	$s_v - s_{vo}$ $\frac{erg}{cm^3\ ^oK}$	$\frac{s_v - s_{vo}}{s_{vo}} \times 100$
3×10^6	I	-0.1	-0.58×10^6	-1.48%
	II	-0.25	-1.00×10^6	-2.57%
6×10^6	I	-0.034	-1.22×10^6	-3.12%
	II	-0.25	-4.00×10^6	-10.26%
9.9×10^6	I	-0.014	-1.70×10^6	-4.36%
	II	-0.25	-10.9×10^6	-27.9 %

Table 2.2 demonstrates how the action of the field is to reduce the deviation between s_v and s_{vo} (i.e., $|s_v - s_{vo}|$ is greater for Case II than Case I). For water, $s_{vo} \simeq 3.9 \times 10^7$ erg/cm^3 °K [cf., P17, p. 102].

Table 2.3. Influence of Field on Free Energy Density and Internal Energy Density (T = 25° C); from [S6, pp. 46, 48]

$\vec{E}$ (V/cm)	Case	$f_v - f_{vo}$ $\frac{erg}{cm^3}$	$e_v - e_{vo}$ $\frac{erg}{cm^3}$
3×10^6	I	2.07×10^8	$.35 \times 10^8$
	II	3.09×10^8	$.13 \times 10^8$
6×10^6	I	4.26×10^8	$.63 \times 10^8$
	II	12.34×10^8	$.48 \times 10^8$

Once again, the effect of the field on ε is such as to reduce the difference $(f_v - f_{vo})$; e.g., a reduction in $(f_v - f_{vo})$ of almost 49%

for $\underset{\rightarrow}{E} = 3 \times 10^6$ V/cm. However, as seen from Table 2.3, this saturation effect resulting from the external field increases the chemical internal energy deviation $e_v - e_{vo}$,

It may be noted at this point that fields encountered in the vicinity of ions and other highly charged colloidal particles may be of the order of 10^6 to 10^7 V/cm. However, ordinary applied fields used in the laboratory and in the practice of Electrostatic Precipitation, even when non-uniform, are typically of the order of 10^4 V/cm. Thus, the effect of such fields on the magnitudes of the various thermodynamic quantities is rather negligible.

2.3 Pressure and the Ponderomotive Force

The concepts outlined in the previous pages wherein, starting from a definition of the ponderomotive forces, one can derive thermodynamical quantities such as free energy, entropy, etc., are due to Kelvin. The Helmholtz method, on the other hand, consists in calculating first the free energy due to the field, and afterwards, the work and the ponderomotive forces (indirectly) in the case of a reversible transformation. Nevertheless, the results derived from both methods are in perfect agreement. In the Helmholtz method the pressure in the dielectric (in a field) p is the same as p_o, the pressure with no field. The ponderomotive force $\underset{\rightarrow}{F}$ is given by

$$\underset{\rightarrow}{F}^H = \frac{1}{2} \underset{\rightarrow}{E}^2 \text{ grad } \chi - \frac{1}{2} \text{ grad } \underset{\rightarrow}{E}^2 \rho \left(\frac{\partial \chi}{\partial \rho}\right)_T \tag{2.18}$$

In the Kelvin method $\underset{\rightarrow}{F}$ is defined as

$$\underset{\rightarrow}{F}^K = \underset{\rightarrow}{P} \cdot \text{Grad } \underset{\rightarrow}{E} \tag{2.19}$$

and the pressure p is given in terms of the Helmholtz pressure p_o by the relation [S6]

$$p = p_o - \frac{\varepsilon_o}{2} \underset{\rightarrow}{E}^2 - \frac{\varepsilon_o}{2} \int_{0,C}^{\underset{\rightarrow}{E}^2} \left[\sum_\gamma \rho_\gamma \left(\frac{\partial \varepsilon}{\partial \rho_\gamma} \right)_{T, \underset{\rightarrow}{E}, C} - \varepsilon \right] d\underset{\rightarrow}{E}^2 \qquad (2.20)$$

For weak fields ($\underset{\rightarrow}{E} \leq 3 \times 10^4$ V/cm)ε is almost independent of $\underset{\rightarrow}{E}$, and for a single component system (2.20) reduces to

$$p = p_o + \frac{\underset{\rightarrow}{P} \cdot \underset{\rightarrow}{E}}{2} - \frac{\rho \underset{\rightarrow}{E}^2}{2} \left(\frac{\partial \chi}{\partial \rho} \right)_T \qquad (2.21)$$

Thus, the definitions of pressure and the ponderomotive force in an electric field are quite arbitrary, as long as the 'sum of the mechanical actions exerted on the dielectric is invariant.'[†] Nevertheless, the Kelvin method based on the hypothesis of forces is found to be more convenient for at least two reasons:

First, it leads to a uniform chemical potential for dielectrics in mechanical equilibrium and at uniform temperature; i.e., it can be easily seen from equation (2.12) that the mechanical equilibrium condition

$$\bar{v} \text{ grad } p - \text{Grad } (\underset{\rightarrow}{E} \cdot \underset{\rightarrow}{\bar{P}}) = 0$$

also implies the chemical equilibrium constraint

$$(\text{grad } \bar{\mu})_T = 0$$

Secondly, the Kelvin method can be easily extended to irreversible processes, whereas the Helmholtz method can only be applied to reversible transformations. DeGroot and Mazur [D3, p. 395] give an example of the physical meaning of p (Kelvin) by considering the equilibrium conditions

---

[†]In other words, $\underset{\rightarrow}{F}$ - grad (p) should be the same [S6, p. 56].

between two isotropic systems with different susceptibilities, thereby suggesting that the Kelvin pressure even has physical significance.

The pressure p_o in the absence of an electromagnetic field arises as a consequence of the kinetic energy and the short-range interactions between the constituent particles of the medium. If an electromagnetic field is applied, additional interactions of electromagnetic origin arise. These result in long-range forces (ponderomotive forces) and modify short-range interactions, and thus, the pressure [S6].

2.3(a) Numerical Example for the Kelvin Pressure

For pure water at $T = 25^{o}$ C, using Kirkwood's [K9] model for a pure polar liquid and equation (2.20), Sanfeld [S6, p. 60] has estimated for the pressure deviation

$$p_o - p \simeq 1.4 \text{ atm at } \underset{\rightarrow}{E} = 1.2 \times 10^{6} \text{ V/cm}$$

Once again, for the weaker fields around $\underset{\rightarrow}{E} = 1 \times 10^{4}$ V/cm, one gets a rather small deviation

$$p_o - p \simeq 1.07 \times 10^{-4} \text{ atm}$$

Note that in either case the effect of the electric field is such as to reduce the pressure.

2.4 Distribution of Matter in the Interfacial Layers of Continuous Systems at Uniform Temperature

In this final section, appropriate equations to estimate (a) the hydrostatic pressure difference between two points of the system, (b) the concentration profile of components in a gaseous mixture, (c) the 'polarization' and 'volume' effect in liquids, and (d) the discontinuity of pressure in a surface layer perpendicular to the applied field, are

presented.

2.4(a) Kelvin Pressure Distribution: Mechanical Equilibrium

From (2.1) and the relation $\text{div}(\varepsilon \vec{E}) = \frac{1}{\varepsilon_0} \bar{z}\rho$, one gets for the distribution of the Kelvin pressure

$$\text{grad } p = \varepsilon_0 \vec{E}\ \text{div}(\varepsilon \vec{E}) + \frac{\varepsilon_0}{2}(\varepsilon - 1)\ \text{grad}\ \vec{E}^2 \qquad (2.22)$$

Thus, a knowledge of the geometry of the charged and/or polarized surface, the $\vec{E}$ field profile and the dependence of the dielectric constant ε on $\vec{E}$, can enable one to estimate the 'pressure profile' in the vicinity of such surfaces. As $\varepsilon \simeq 1$ for most gases and vapors and > 1 for liquids, in the absence of real charges ($\bar{z} = 0$) only the profile in the latter will generally be other than flat (for fields $\vec{E} \geq 1 \times 10^5$ V/cm). In Chapter 7 use shall be made of equation (2.22) in estimating the pressure (and, therefore, the concentration) profile in the vicinity of the interparticle contacts in a bed of fly ash.

2.4(b) Equilibrium Distribution of Components in a Gaseous Mixture

For a gaseous mixture of two components 1 and 2 at constant temperature, the condition of thermodynamic equilibrium in a charged and polarized layer, viz.,

$$\bar{\mu}_1 = \bar{\mu}_1' \quad \text{and} \quad \bar{\mu}_2 = \bar{\mu}_2'$$

[where the prime designates the bulk of the medium ($\vec{E} = 0$, $p = p' = p_0$) and μ_γ is the electrochemical potential] leads to the equation [S16, p. 76]

$$\frac{f_{10}N_1}{f_{20}N_2} = \frac{f_{10}'N_1'}{f_{20}'N_2'} \exp\left[\frac{\varepsilon_o}{2RT}\int_{O,C}^{E^2}\left\{\left(\frac{\partial\varepsilon}{\partial C_1}\right)_{C_2} - \left(\frac{\partial\varepsilon}{\partial C_2}\right)_{C_1}\right\}dE^2\right] \qquad (2.23)$$

where

$f_{\gamma o}$ = local activity coefficient of component γ at $\underset{\rightarrow}{E} = 0$

N_γ = local mole fraction of γ

If $f_{20} = f_{20}'$ and $f_{10} = f_{10}'$ and if component 1 is more polarizable than component 2, i.e.

$$\left(\frac{\partial\varepsilon}{\partial C_1}\right) > \left(\frac{\partial\varepsilon}{\partial C_2}\right) ,$$

the integral in (2.23) becomes positive and consequently, for large values of $\partial\varepsilon/\partial C_\gamma$ and $\underset{\rightarrow}{E}$, molecules of 1 will fill the charged layer to an appreciable extent.

2.4(c) Polarization and Volume Effects in Liquids

Sanfeld [S6, p. 80] has derived an expression for the distribution of two uncharged constituents 1 and 2 in the diffuse layer created by ions in a solution. As in the above case, if $f_{10} = f_{10}'$ and $f_{20} = f_{20}'$, he has shown that

$$\frac{C_1}{C_2} = \exp\left[\frac{\varepsilon_o \underset{\rightarrow}{E}^2}{2RT}\left\{2\varepsilon(v_{20}^{**} - v_{10}^{**}) + \frac{\partial\varepsilon}{\partial C_1} - \frac{\partial\varepsilon}{\partial C_2}\right\}\right] \qquad (2.24)$$

where $v_{\gamma o}^{**}$ = standard molar specific volume extrapolated to zero pressure at temperature T in dilute solution.

For 1 being more polarizable than 2, i.e.

$$\frac{\partial\varepsilon}{\partial C_1} > \frac{\partial\varepsilon}{\partial C_2} ,$$

the polarization effect, as was seen in 2.4(b), is such as to increase 1 in the diffuse layer. However, the volume effect $(v_{20}^{**} - v_{10}^{**})$ is able to either increase or counteract the polarization effect. Large components, as can be easily seen from equation (2.24), will tend to avoid the layer. For a mixture of methanol and acetone in electrolytic dilute aqueous solution, methanol concentrates in the layer and the volume effect is even greater than the polarization effect. On the other hand, for a mixture of methanol and urea, the polarization term is greater than the volume term and urea tends to concentrate in the diffuse double layer [S6, p. 81].

2.4(d) Discontinuity of Pressure Across a Plane Interface Perpendicular to the Field

The pressure difference across a surface of discontinuity between two fluids 1 and 2 is given by [S6, p. 181]

$$p_2 - p_1 = \varepsilon_o(\varepsilon_2 \underset{\rightarrow}{E}_2^2 - \varepsilon_1 \underset{\rightarrow}{E}_1^2) - \frac{\varepsilon_o}{2}(\underset{\rightarrow}{E}_2^2 - \underset{\rightarrow}{E}_1^2) \qquad (2.25)$$

where ε_1, ε_2, $\underset{\rightarrow}{E}_1$, $\underset{\rightarrow}{E}_2$ are the dielectric constants and the fields perpendicular to the interface in fluids 1 and 2.

If 1 is water and 2 is air, then since $\varepsilon_1 \underset{\rightarrow}{E}_1 = \varepsilon_2 \underset{\rightarrow}{E}_2$ and $\underset{\rightarrow}{E}_2 > \underset{\rightarrow}{E}_1$, it can be seen from equation (2.25) that $p_2 > p_1$, or the pressure immediately above the water is less than that in the air. The field thus acts as a dryer, reducing the vapor pressure immediately above the water surface. It is this effect that the authors in [P12] allude to when describing the increased evaporation rate of water from a quartz capillary in the presence of a needle corona discharge.

CHAPTER III

GAS-SOLID ADSORPTION IN POROUS MEDIA

The adsorption of gases and vapors on solids is indeed a very vast topic. In this study only solid dielectrics (or insulators) will be considered. The electrical field-induced effects in the adsorption of gases on conductors (W, Cu, etc.) and semi-conductors (ZnO, etc.) are primarily due to the electronic nature of the gas-solid interactions, and these will not be considered here. The subject of gas-solid adsorption with the solid being a dielectric, is in itself quite diverse. However, as various experiments have clearly demonstrated in this work, the formation of a monolayer in gas-solid adsorption is generally unaffected by imposed electric fields of magnitudes less than about 10 KV/cm. This may be due to the fact that the ordinary forces of diffusion operative in the formation of a monolayer are too high when compared with the additional field-induced thermodynamic forces. Multilayer adsorption and/or capillary condensation appears to be a prerequisite before appreciable effects of applied electric fields can be noticed. Of course, for situations in which either extremely high fields exist at the solid-gas interface or when the adsorption forces are relatively weak, the influence of applied electric fields on the extent and rate of monolayer formation cannot be ruled out.

In this study fields of magnitudes generally found in the ESP are applied, fields whose upper limit is fixed by the occurrence of such

phenomena as dielectric breakdown, back-corona, etc. Porous dielectric media constitute a large percentage of solid dielectrics that one encounters in the practical world. The adsorption in porous media, especially at high relative partial pressures, leads to multilayer formation and/or capillary condensation. Fly ash, powdered alumina, porous glass, silica gel, beds of dusts from various cleaning operations, etc., may be classified as porous media. In this study, though experiments have been conducted on various porous, disperse, and dielectric media, the primary emphasis will be on capillary porous silica gel. The reason for this is threefold: (a) the internal structure of silica gel is pretty well understood; (b) the adsorptive forces are strong enough to lead to multilayer adsorption and capillary condensation; and, finally, (c) dielectric studies, as also studies reporting the influence of electric field effects on water-vapor adsorption in silica gel at a relative saturation of $\simeq 1$, have been reported in the literature [P1,P2,P3,K1,M2]. This last factor makes it convenient to refute and justify preconceived ideas and conclusions already arrived at by some authors, and also to propose concepts which are compatible with all available literature.

To understand the nature of the field-induced effects on the thermodynamics and the kinetics of gas adsorption in porous media, one needs to fully comprehend these phenomena in the absence of the external fields. In Section 3.1 the thermodynamics of adsorption in porous media is briefly investigated, with particular reference to silica gel. In Section 3.2 the concepts of surface and volume flow in porous media are defined and, once again, the particular reference to silica gel is made. In the final section the irreversible thermodynamic formulation for mass transfer in porous media developed in Section 3.2 is extended to systems

polarized under the influence of external electric fields.

3.1 Thermodynamics of Adsorption in Porous Solids

The Brunauer-Emmett-Teller (B.E.T.) [B3] theory is generally accepted as providing an accurate description of that part of the adsorption isotherm represented by two or three layers of adsorbate. Surface area calculations based on the B.E.T. monolayer capacity for relative pressures less than about .35 are even today considered to be the most accurate estimates available [S1]. However, for thick films, the B.E.T. theory becomes increasingly inaccurate. The primary reason for this failure is attributed to the assumption that gas-solid interaction energies for molecules beyond the monolayer are zero [S1]. By considering an external potential field to account for the solid-gas interactions, the Frenkel-Halsey-Hill (F.H.H.) theory appears to describe the problem of very thick films most successfully. The adsorption on very finely divided or porous solids, however, cannot be adequately described by either of these theories. The behavior of adsorbates in porous systems is dominated by effects resulting from the curvature of the solid surfaces and of the adsorbed fluid, especially as saturation is reached.

Of the five classes of adsorption isotherms in the B.E.T. classification, the adsorption on porous systems most often falls under the category of class IV.[†] Figure 3.1 shows a typical type IV adsorption isotherm.

[†]More specifically, type IV isotherms are encountered in solids whose pores have diameters in the range of tens to hundreds of angstrom units [G1, p. 123].

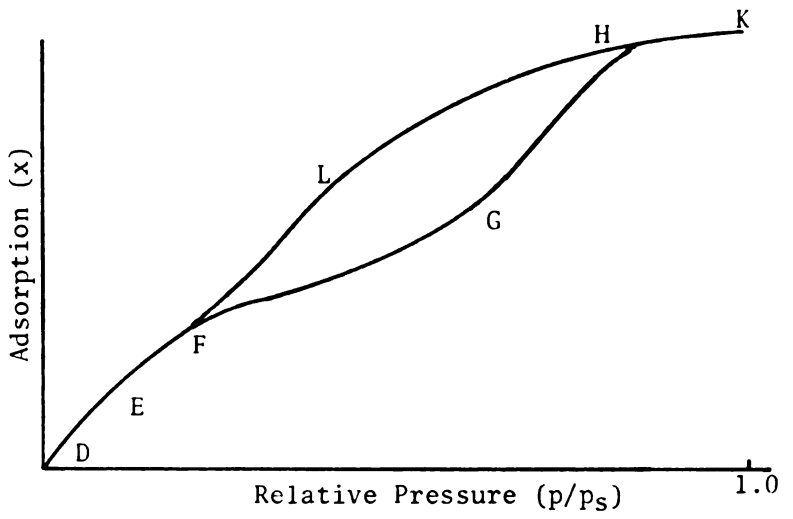

Figure 3.1. A type IV isotherm.

Along low pressure branch DEF, monolayer adsorption is assumed to take place. Opinions differ as to the exact course of events along branch FGH. The most widely accepted view is that a multilayer is gradually built up and that more or less normal liquid-vapor menisci are formed [G1]. At H the pores are filled with a liquid-like adsorbate, and the flat branch HK refers to the negligible adsorption in the outside of the grains. During the desorption process the menisci persist, becoming concave towards the vapor, and the desorption branch HLF is traversed. Evaporation occurs at lower partial pressures and adsorption hysterisis is observed.

Most researchers agree that the desorption branch, especially for high partial pressures, is most adequately described by the Kelvin equation †

---

†A more rigorous relation would have an additional potential energy term $U_p(z)$ in the right-hand side to account for the external field created by the solid surface [S1].

$$RT \ln (p^o/p) = \frac{2\gamma v^{\ell}}{R_m} \cos\theta \qquad (3.1)$$

where

p = adsorption pressure

γ = surface tension of liquid-like adsorbate

v^{ℓ} = specific volume of adsorbate

θ = liquid-solid contact angle

R_m = mean radius of curvature

p_s = saturation vapor pressure

This equation is obtained by the combination of the well-known Laplace equation

$$p^v - p^{\ell} = \gamma\left(\frac{1}{R_1} + \frac{1}{R_2}\right)\cos\theta \qquad (3.2)$$

(where p^v and p^{ℓ} are the pressures in the vapor and liquid across a curved surface of tension with curvatures R_1 and R_2, $2/R_m = 1/R_1 + 1/R_2$, γ is the surface tension) with the thermodynamic relation

$$\delta\mu^v = RT \log \frac{p^v}{p^o} = \delta\mu^{\ell} = v^{\ell}(p^{\ell} - p^v) \qquad (3.3)$$

The Kelvin mechanism implies extremely large negative adsorbate pressures. For example, $\gamma \simeq 72$ dynes/cm for water at $T = 298^o$ K, and for a cylindrical pore of mean radius of curvature $R_m \simeq 30$ A^o and $\cos\theta = 1$, equation (3.2) gives for the pressure in the liquid about $p^{\ell} \simeq -474$ atm. Along increasing pressure paths, nearly all adsorbents show considerable expansion [F1, p. 55]. This implies negative adsorbent and positive adsorbate pressures, and thus, very little of the Kelvin mechanism would seem to be applicable along the path of

adsorption. Rather than large, negative pressures as required by the Kelvin mechanism, Flood [F1, p. 47] has offered the following explanation to justify the hypothesis that the adsorbate layer farthest from the pore walls does, indeed, experience pressures similar to that in the gas phase (along the adsorption path only).

The Gibbs field potential of any thin layer of liquid-like adsorbate can be considered to be the sum of the potentials $\Omega_{sa} + \Omega_{aa}$, the former arising from interactions with the solid surface, the latter from field forces of neighboring adsorbate layers. In the middle of the layer Ω_{aa} would approach zero, whereas in the liquid-like layer most remote from the solid a positive Ω_{aa} should result, just as the last dense layer of the bulk liquid-vapor interface. As saturation is approached along reasonably reversible increasing pressure paths, the net Gibbs potential $\Omega_{aa} + \Omega_{sa}$ of the layer most remote from the solid should approach zero. Consequently, the pressure of this region should be about the same as the saturation pressure. The pressure in this layer will thus be much less than the pressure of the underlying layers, and this layer cannot be considered a surface of tension at all.

Other authors [C1,S1] have attempted to treat the adsorption in cylindrical pores as capillary condensation, but with the meniscus being cylindrical in shape rather than spherical (see Figure 3.2). They arrive at a Kelvin-type relation for the gas pressure p_{ad}, beyond which the pore will fill spontaneously

$$RT \ln (p_{ad}/p_s) = \frac{-\gamma v^{\ell}}{(R_o - t_c)} \tag{3.4}$$

Here t_c = thickness of adsorbate at which the change in $U_p(t)$ (the gas-solid perturbation energy) with t becomes smaller than $\gamma v^{\ell}/(R_o - t_c)^2$;

i.e., beyond t_c adsorption leads to a decrease in chemical potential and, therefore, becomes spontaneous [S1]. This sort of adsorption mechanism, nevertheless, requires extremely high, negative adsorbate pressures, due to the formation of curved surfaces of tension. To form isothermally a number of menisci having relatively high surface tensions and having a large total surface area, considerable pv work must be done on the system to cause condensation and to form the large excess Helmholtz potential of these surfaces of tension [F1, p. 56].

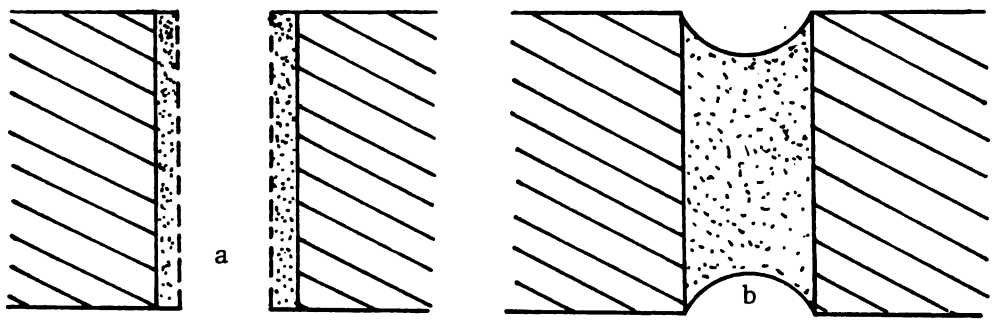

Figure 3.2. a) Cylindrical meniscus; b) hemispherical meniscus.

From the above discussion it would seem that adsorption along increasing pressure paths is essentially a multilayer adsorption phenomenon with normal adsorbate-gas interfaces (rather than curved surfaces of tension). The pressure in the adsorbate is positive, being extremely large in regions close to the solid surface where the gas-solid perturbation energy ($U_p(z)$) is significant, and decreasing rapidly with distance z from the pore wall ($U_p(z) \propto z^{-2.6}$) [S1]. During desorption, the Kelvin-type mechanism holds quite well with the liquid-gas interface for a cylindrical pore being hemispherical rather than cylindrical (see Figure 3.2).

3.1(a) Estimation of Surface Area for Porous Solids

The two-parameter B.E.T. equation goes as follows:

$$\frac{x}{y(1-x)} = \frac{1}{y_m(1-x)} + \frac{(c-1)x}{y_m c} \tag{3.5}$$

where

$x = p/p^o$

y = gms adsorbed/gm of adsorbent

y_m = gms adsorbed in monolayer/gm of adsorbent

c = parameter dependent on the free energy of transfer of the vapor from the liquid state to the surface of adsorbent [B4]

The application of the B.E.T. two-parameter equation to regions of the adsorption isotherm (y vs. x) with $x \leq 0.35$ to determine the monolayer-adsorbed capacity (and hence the surface area) has been known to be extremely satisfactory even in the case of porous solids.

To get the surface area A, one writes

$$A = N_m a_m \tag{3.6}$$

where

N_m = number of molecules in the monolayer (obtained from y_m)

and

a_m = area per molecule in a dense packed layer

As mentioned earlier, the chief disperse, dielectric specimen chosen for this study is silica gel. In particular, Silica Gel No. S-2509, 70-230 mesh, mean pore radius $\simeq$ 30 A^o, made by SIGMA Chemical Company

will be used.

Figure 3.3 represents the adsorption isotherm obtained for the sample in this work, with water as the adsorbate and at 25° C. Note that the applied fields have no discernible effects on the shape of the isotherm.† In Figure 3.4 the B.E.T. plot of x/y(1-x) vs. x is shown, and from the slope and intercept one obtains

$$c = 9.781$$

$$\underline{y_m = 6.491} \text{ gms adsorbed in monolayer/100 gms adsorbent}$$

From reference [D4] (for $r_{mean} \simeq 30$ A°),

$$a_m = 21 \times 10^{-20} \frac{m^2}{\text{molecule}}$$

Hence, from equation (3.6) we get

$$A = .0649 \frac{\text{gms}}{\text{gm adsorbent}} \times \frac{1 \text{ gmole } H_2O}{18 \text{ gm}} \times 6.023 \times 10^{23} \frac{\text{molecules}}{\text{gmole}} \times 21 \times 10^{-20} \frac{m^2}{\text{molecule}}$$

or

$$\underline{A = 456.1} \ m^2/\text{gm silica gel}$$

Also, since the pores in silica gel are known to be the pin-hole or cylindrical type [K1], one can equate the mean pore radius r_m to A by the relation

$$r_m = \frac{2V_m}{A}$$

---

†This confirms the results obtained by Panchenko et al. [P2], represented in Figure 1.4.

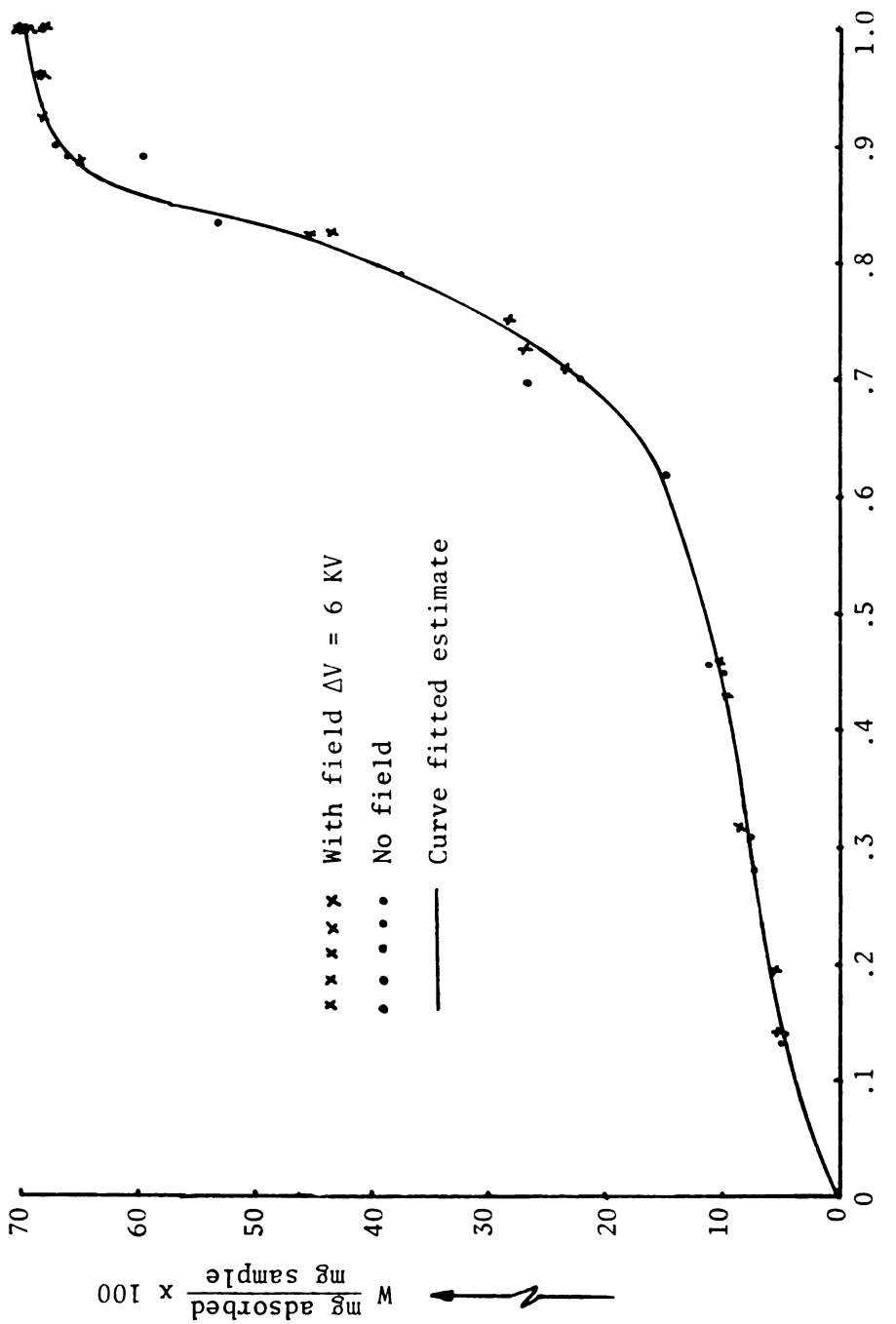

Figure 3.3. Adsorption isotherm for Silica Gel S-2509; amount adsorbed (W) vs. relative pressure (p/p_S); T = 25° C.

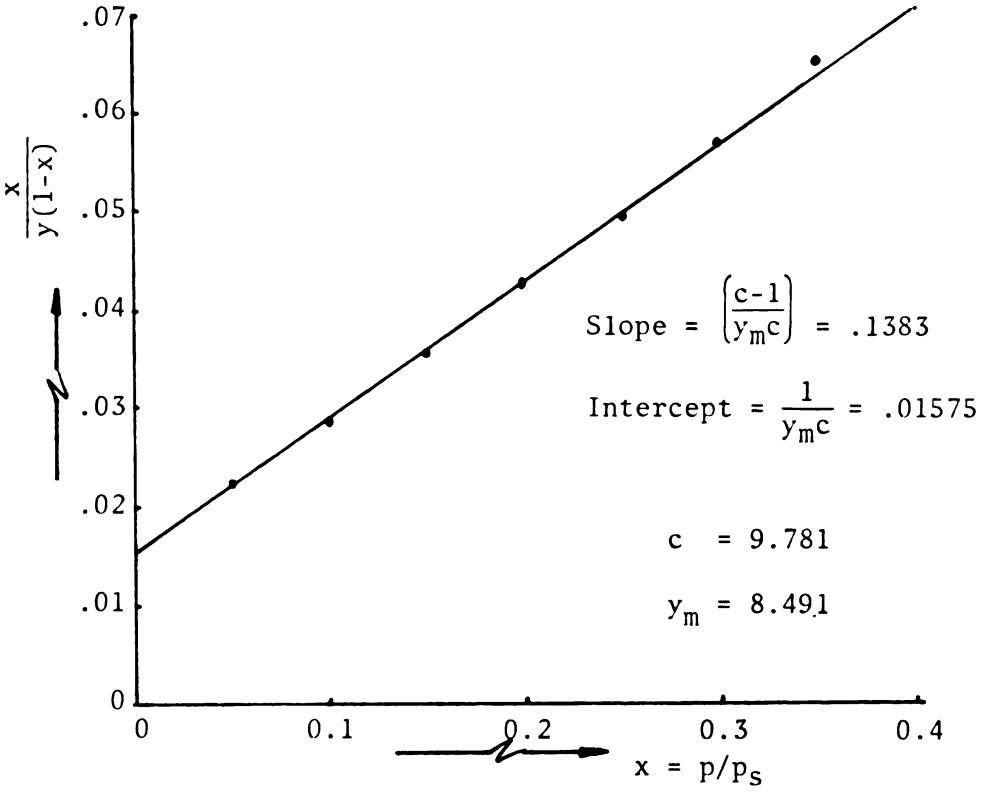

Figure 3.4. B.E.T. plot x/y(1-x) vs. x for Silica Gel S-2509.

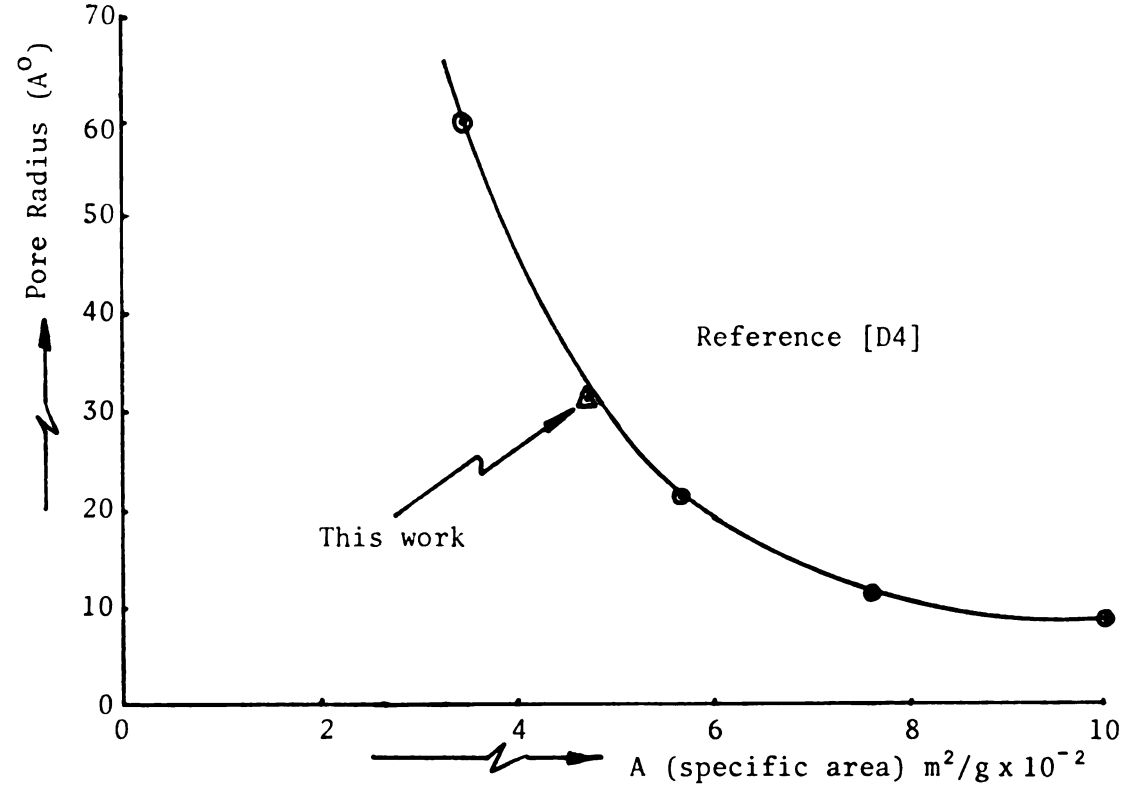

Figure 3.5. Comparison of A with available literature.

where

V_m = internal pore volume of gel

From the experiments conducted in this work for S-2509 gel,

$V_m \simeq \frac{.70 \text{ cc}}{\text{gm adsorbent}}$ (using $\rho_{H_2O} \simeq 1 \frac{\text{gm}}{\text{cc}}$), and hence $\underline{r_m \simeq 30.7 \text{ A}^o}$.

Dushenko et al. [D4] have conducted a careful investigation of the interaction of moisture with four different silica gels (with varying mean pore diameters). Figure 3.5 is a plot of B.E.T. surface area vs. mean pore diameter for the four gels. Note that the area and mean pore radius obtained from this work fits quite well with their work.

The pore size distribution of capillary porous materials can be obtained fairly easily by the application of the Kelvin equation to the desorption branches of the isotherms. With silica gels the distributions are generally quite narrow, indicating that pores with diameters equal to the mean pore diameter are of the dominant variety.

3.1(b) Estimation of 'Bound' Water and 'Capillary-Condensed' Water in Silica Gel

Both dielectric studies [K1] and calorimetric studies [P4] have demonstrated that water adsorbed on the surface of silica gel exists in three distinct states. The first is the monolayer-adsorbed water; the second is the 'bound' or 'adsorbed' water (which, in a sense, has greater degree of freedom of rotation, yet is bound or influenced by the solid surface forces); and finally, the capillary-condensed water which has most of the essential qualities of free, bulk water. Panchenko et al. [P4] have conducted calorimetric experiments to determine the bound energy $T\Delta S$ of the adsorption bond given by

$$T\Delta S = \Delta U - \Delta F$$

where

T = temperature

ΔS = entropy of the bond between moisture and specimen

ΔU = internal energy of the bond between moisture and specimen determined as the difference between the specific heat of isothermal evaporation of moisture and that of free water at the same temperature

ΔF = free energy of the bond determined from the desorption branches of the isotherms for various temperatures and moisture content levels

Figure 3.6 illustrates the variation of the ratio TΔS/ΔU as a function of the moisture content for four different silica gels [D4].

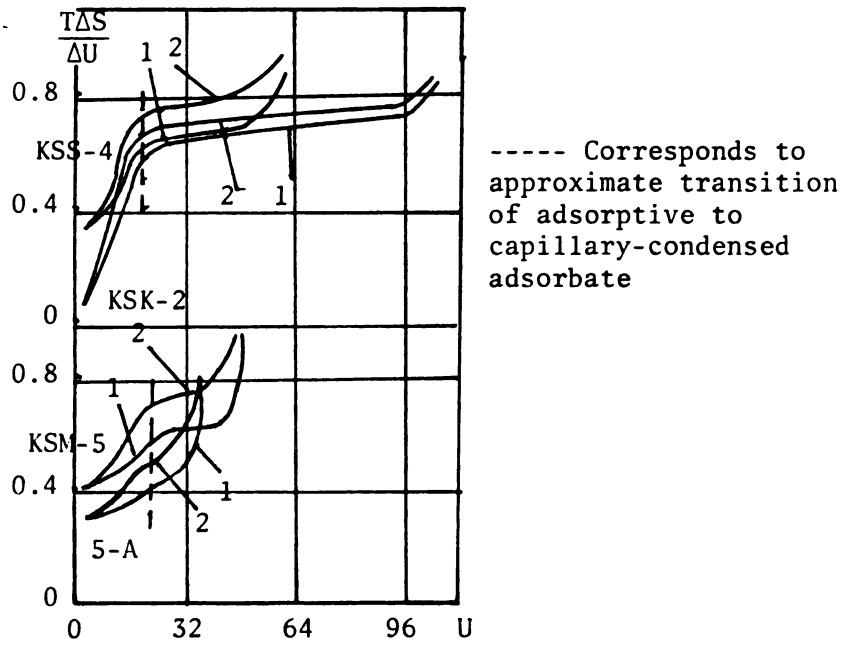

Figure 3.6. Ratio of bound energy to internal energy differentials (TΔS/ΔU) of a moisture bond as a function of the moisture content in four silica gels: 1) 293° K, 2) 308° K.

Figure 3.6 shows very clearly the transition of one form of moisture bond to another; i.e., the energy fraction differential $T\Delta S/\Delta U$ is very sensitive to the change of forces (adsorptive into capillary) which retain moisture in a colloidal dispersion. Dielectric studies of water-vapor adsorption on silica gel have also confirmed this observation [K1]. Figure 3.7(a) gives a plot of the bound water vs. mean pore radius for the four silica gels investigated in [D4,P4]. Using $r_m = 30.7\ A^o$ for the silica gel sample S-2509 used here, one gets

bound water $\simeq$ 13.9 gms/100 gms adsorbent

Hence, water adsorbed beyond the monolayer is $\simeq$ (13.9 - 6.49) = 7.41 gms/100 gms adsorbent, or approximately a second layer. The fact that adsorbed water only extends to about two layers of adsorbate confirms the hypothesis that surface forces extend only to the first few layers adsorbed. Figure 3.7(b) gives the variation of monolayer-adsorbed water (gms/gm adsorbent) with the average pore radius in the four silica gels [D4]. Estimates obtained for Silica Gel S-2509 fit reasonably well with the curve obtained.

The object of estimating the monolayer adsorbed water, the bound water and the remaining capillary-condensed water (70 - 13.9 $\simeq$ 56.1 gms/gm adsorbent) will become clear when these transitions are used to estimate the polarizabilities of the various 'water qualities' in Chapter 4.

3.2 Surface and Volume Flow in Porous Media

The basic mechanisms for gas flow in capillaries include molecular streaming (Knudsen flow), streamline or viscous flow (Poiseuille flow), turbulent flow, and orifice flow. The last two, namely, turbulent flow (high velocities) and orifice flow (smooth, short capillaries), are

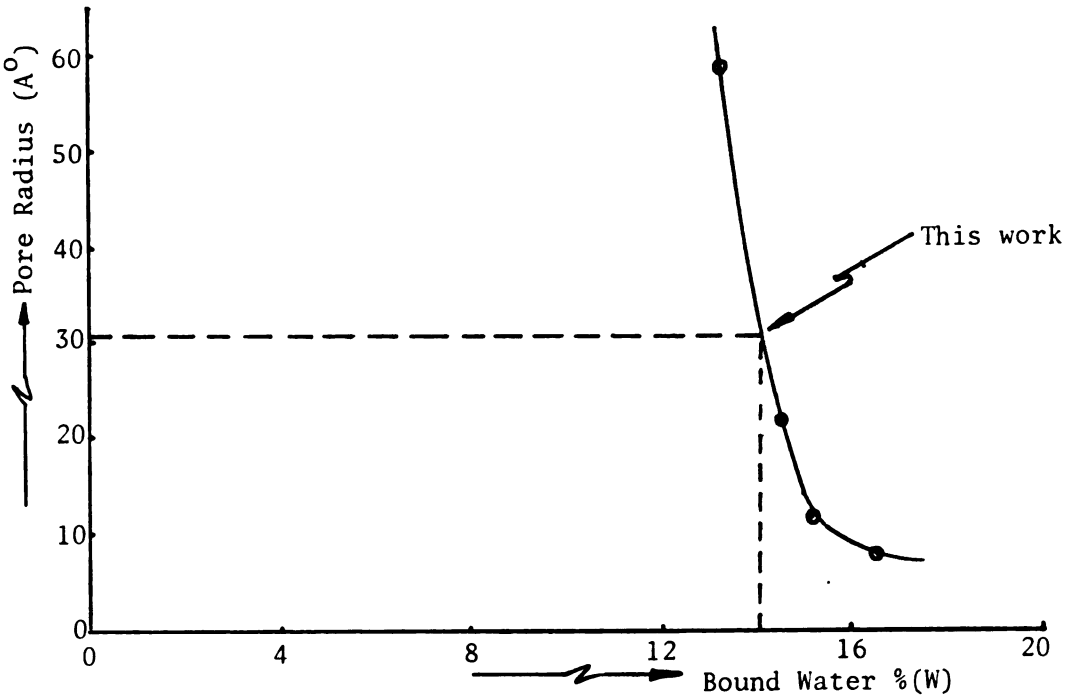

Figure 3.7(a). Bound water vs. mean pore diameter [D4].

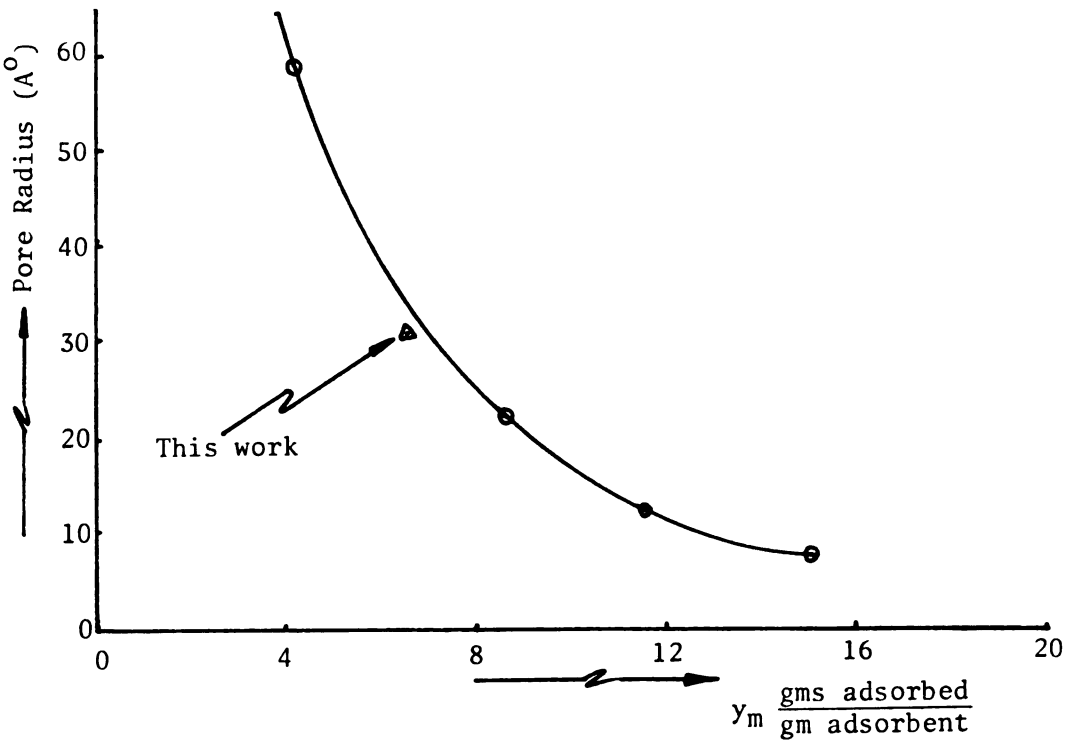

Figure 3.7(b). Monolayer amount adsorbed vs. mean pore diameter [D4].

relatively unimportant in porous media.

Molecular streaming represents a limiting situation in which the mean-free path $\underline{\lambda}$ of the flowing molecules is much greater than either the diameter or the length of the capillary [B5]. The mean-free path of gaseous molecules at 1 atm and room temperature lies between 500 A^{o} and 1000 A^{o}. Thus, in capillary tubes narrower than 500 A^{o}, Knudsen diffusion is expected to be predominant. If the average time that molecules colliding with the wall spend at the wall, τ, were taken to be zero, then the diffusion coefficient D is given by [D5]

$$D = \frac{d\bar{u}}{3} \tag{3.7}$$

where

d = diameter of capillary

$\bar{u}$ = mean velocity of gas molecule = $\left(\frac{8RT}{\pi M}\right)^{1/2}$

M = molecular weight

τ is generally of the form [D5, p. 30]

$$\tau = \tau_o \exp(Q/RT) \tag{3.8}$$

where

τ_o = time of oscillation of the molecules in the adsorbed state (10^{-12} to 10^{-14} secs)

Q = heat of adsorption

The adsorption time τ is usually very significant and the diffusion coefficient is much reduced according to the relation [D5]

$$D = \frac{2d^2\bar{u}}{6(d+\bar{u}\tau)} \tag{3.9}$$

During the time τ, if surface migration is possible, then the diffusion coefficient is enhanced. Two main mechanisms for surface diffusion have been postulated. Clausing [C2] considered a two-dimensional diffusion caused by surface migration. In his model the diffusion coefficient is given by

$$D = \frac{2d^2\bar{u} + 3\tau\bar{L}_m(\bar{u})^2}{6(d+\bar{u}\tau)} \tag{3.10}$$

where $\bar{L}_m$ is the mean-free path on the surface.

If the molecules of the two-dimensional gas behave as 'hopping' molecules, the diffusion coefficient is given by [D5]

$$D = \frac{2d^2\bar{u} + 3\tau a^2\bar{u}/2\tau'}{6(d+\bar{u}\tau)} \tag{3.11}$$

where a is the hopping distance ($\simeq 3\times10^{-8}$ cm) and τ' is the lingering time given by [D5, p. 96]

$$\tau' = \tau_o' \exp(\Delta Q_a/RT) \tag{3.12}$$

with τ_o' being similar to τ_o described above ($\simeq 10^{-13}$ secs), and ΔQ_a being the energy of activation for hopping (some fraction of heat of adsorption).

In this work the hopping mechanism shall be adopted as indicative of the surface diffusion of water-vapor molecules in capillary porous silica gel.†

---

†When the gas flow is by Knudsen diffusion, the 'random' or the 'mechanistic' hopping model has been most widely used [G3,H5,P18,S7,W3,T3] to describe the surface flow mechanism.

$$J_z = Cv = -C\lambda \frac{d\mu}{dz} \tag{3.13}$$

where C is the concentration of the diffusing species.

For a model capillary, an open, cylindrical one is considered in Figure 3.8, shown below.

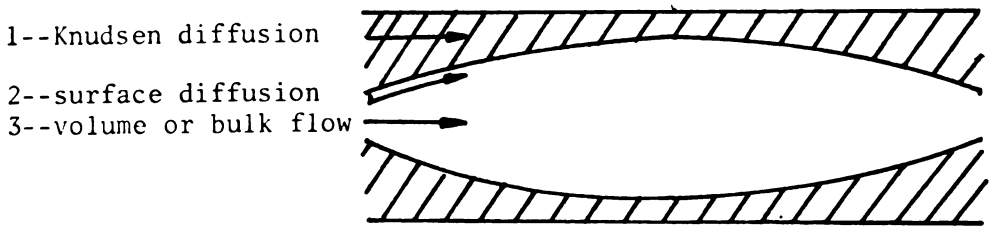

Figure 3.8. Model capillary.

Transport in such a capillary can occur in the following ways [B5,D5]: 1) Knudsen diffusion brought about by molecules banging against the capillary walls, then bouncing back, and so on; 2) Knudsen diffusion with simultaneous surface diffusion (by, say, the hopping mechanism) during the time intervals τ in which the diffusing molecules are temporarily adsorbed; and finally, 3) simultaneous bulk volume flow due to pressure gradients in the adsorbed layers.

For gaseous diffusion at constant T (no external fields)

$$d\mu = vdp$$

As already pointed out in Section (3.1) surface diffusion totally dominates the gas phase diffusion phenomena. Hence,

$$d\mu_s \simeq v_s dp_s$$

where v_s = specific volume of surface adsorbed molecules, and dp_s = pressure differential along surface for 'hopping' molecules. From (3.13), then,

For water-vapor adsorption

$$Q \simeq 10 \text{ Kcal/gmole}, \quad \Delta Q_a \simeq 2.0 \text{ Kcal/gmole (estimate)}$$

and from equations (3.08) and (3.12)

$$\tau \simeq 2\text{x}10^{-6} \text{ secs}; \quad \tau' \simeq 2.9\text{x}10^{-12} \text{ secs}$$

for

$$\bar{u} \simeq 5.87\text{x}10^{4} \text{ cm/sec}$$

For a capillary with diameter $d \simeq 60\text{x}10^{-8}$ cm, one can see from estimating the magnitudes of the first and second terms in equation (3.11) that the surface diffusion contribution to D far exceeds the Knudsenian diffusion term. Thus, surface diffusion by either the hopping mechanism, or any other mechanism, usually fully accounts for the diffusion coefficient in capillaries when adsorption in the pore is significant.

3.2(a) Theoretical Formulation for Surface and Volume Flow

The penetration of molecules into micro-capillaries may be treated as a diffusion problem. The irreversible thermodynamic formulation to describe the transport process is as follows.

For a single substance diffusing in an immobile medium, if the force acting per molecule is proportional to the chemical potential gradient $-\frac{d\mu}{dz}$, the average drift velocity of the molecule is

$$v = -\lambda \frac{d\mu}{dz}$$

where λ is the phenomenological coefficient. Then the total flux in the z direction is given by

$$J_{sz} = -C\lambda v_s \frac{dp_s}{dz} \tag{3.14}$$

At this point, one needs to take a closer look at two things: first, what is the pressure gradient that the surface-hopping molecules experience?, and second, what is the concentration of these hopping molecules?

The pressure in the adsorbed layers, over and above that due to ordinary intermolecular attractions, arises from the gas-solid perturbation energy $U_p(\underset{\rightarrow}{r})$ [S1]. As mentioned earlier, this energy may be neglected beyond the first few adsorbed layers. The pressures in the first and second layer are, however, extremely large. From the discussion in Section 3.1(a), it seems reasonable to assume that beyond the 'bound' layers the pressure exerted on the hopping molecules in the layer farthest from the solid surface is about the same as the gas-phase pressure, and the pressure gradient for the surface-diffusing molecules is the same as it would be in the gaseous phase. Thus,

$$dp_s \simeq dp_g \simeq \frac{RT}{M} dC_g \quad \text{for} \quad C_s > C_{sb}$$

where

C_g = concentration of diffusing species in gas phase

C_{sb} = concentration of adsorbate 'bound' to surface.

The concentration of the hopping molecules may be taken as being proportional to the gas-phase concentration C_g. This is true as the number of molecules hitting any surface is proportional to the partial pressure of that species in the gas phase [D5] and is much larger than the rate at which the molecules are adsorbed.

Thus,

$$C \simeq KC_g \qquad (K = \text{constant})$$

and from (3.14) we then have

$$J_{sz} \simeq -K\lambda C_g v_s \frac{RT}{M} \frac{dC_g}{dz} \tag{3.15a}$$

$$= -D_s \frac{dC_g}{dz} \tag{3.15b}$$

where the surface diffusion coefficient D_s is defined as

$$D_s = K\lambda v_s \frac{RT}{M} C_g = K' C_g \tag{3.16}$$

Equation (3.15b) suggests that the diffusion of molecules along the surface of adsorbate in capillaries may be given by a Fickian model, with the diffusion coefficient dependent on the gas-phase concentration.

For bulk volume flow in adsorbed layers, the most general form of Darcy's equation for a homogeneous fluid may be written [B5]

$$J_c = \frac{K_1 \rho}{\eta} \frac{d\mu_c}{dz} \tag{3.17}$$

where

$$d\mu_c = v_c dp_c \quad ,$$

with

v_c = specific volume of adsorbate

dp_c = average pressure differential in adsorbed layer

K_1 = coefficient (empirical)

ρ = density of fluid

η = viscosity of fluid

Thus,

$$J_c = \frac{-K_1 \rho}{\eta} v_c \frac{dp_c}{dz} \tag{3.18}$$

The average pressure gradient in the adsorbed layers is very large. However, most of the large pressures are very close to the solid surface with the layers farthest from the surface experiencing a pressure similar to that in the bulk fluid at the given temperature [F1]. In attempting to fit the theoretical concepts with the data obtained from the experiments with silica gel (in Chapter VI), the contribution to the overall mass transfer in fine pores from bulk volume flow was found to be very small. This may be attributed to the more ordered structure of the adsorbed species [K1], as also due to strong solid-adsorbate interactions in the silica gel-H_2O system. Of course, as saturation is reached and the cross-sectional area for gaseous diffusion gets to be exceedingly small, bulk volume flow achieves increasing importance in the mass transfer phenomena.

3.3 Irreversible Thermodynamic Formulation Extended to Porous Media in External Electric Fields

The Gibbs-Duhem equation for polarized systems has been derived in Section 2.1(c):

$$\text{grad } p - \underset{\rightarrow}{P} \cdot \text{grad } \underset{\rightarrow}{E} - \sum_\gamma \rho_\gamma \text{ grad } \bar{\mu}_\gamma = 0 \tag{2.12}$$

For a single-component system one may write the 'z' component of equation (2.12) as

$$\frac{d\bar{\mu}}{dz} = \frac{vdp}{dz} - \underset{\rightarrow}{\bar{P}} \cdot \frac{d\underset{\rightarrow}{E}}{dz}$$

where

$$\overrightarrow{\overline{P}} = P\vec{v}$$

Applying equation (3.13) for the mass flux, one gets

$$J_z^e = -\lambda C\left(v\frac{dp}{dz} - \overrightarrow{\overline{P}}\cdot\frac{d\vec{E}}{dz}\right) \tag{3.19}$$

For surface diffusion in a cylindrical pore

$$J_{zs}^e = -K\lambda C_g v_s \frac{RT}{M}\left(\frac{dC_g}{dz} - \frac{M}{RT}\vec{P}\cdot\frac{d\vec{E}}{dz}\right) \tag{3.20}$$

and from (3.16) and (2.0)

$$J_z = -D_s\left(\frac{dC_g}{dz} - \frac{M}{RT}\varepsilon_o\frac{(\varepsilon_s-1)}{2}\frac{dE^2}{dz}\right) \tag{3.21}$$

In equation (3.21) a few of the terms need further elucidation. ε_s is the dielectric strength of the surface adsorbed molecules. $\vec{E}$ represents the field that the hopping molecules see during their motion. As the hopping molecules are neither in the bulk adsorbate phase or fully in the gas phase, the exact magnitude of $\vec{E}$ is difficult to estimate. In this work $\vec{E}$ is assumed to be the field estimated (in Chapter IV) in the gas phase $\vec{E}_g$. The term p in (3.19) stands for the Kelvin pressure. However, as pointed out in Chapter II, for fields $\vec{E} \leq 1\text{x}10^4$ V/cm (rough estimate for values of $\vec{E}_g$ in the silica gel bed from Chapter IV) the pressure remains fairly unaffected and the ideal gas relation $p_g = C_g\frac{RT}{M}$ holds.

Similarly, for the bulk volume flow in a pore

$$J_z = \frac{-K_1\rho}{\eta}\left(v_c \frac{dp_c}{dz} - \overline{P}\cdot\frac{d\vec{E}}{dz}\right)$$
$$= \frac{-K_1}{\eta}\left(\frac{dp_c}{dz} - P\cdot\frac{d\vec{E}}{dz}\right) \qquad (3.22)$$

In (3.22) the electric field $\underset{\rightarrow}{E} = \underset{\rightarrow}{E}_c$, or the field in the adsorbed phase. Also, dp_c = pressure differential in the adsorbate. As $\underset{\rightarrow}{E}_c < \underset{\rightarrow}{E}_g$[†] and $dp_c > dp_g$, one can easily see that the $\underset{\rightarrow}{E}$ field-induced effects will be much larger in the case of surface diffusion than for volume flow. Further clarification of this and other field related observations made up to this point will be dealt with in Chapter V.

The various physical characteristics of silica gel necessary to evaluate the theoretical model presented in Chapter VI have been estimated in this chapter. The fundamental relationships for the mass fluxes, with and without the applied electric fields, have been derived for capillary porous adsorbents. Once the various internal and external electric fields have been estimated in the next chapter, all necessary information for solving the mathematical model proposed in Chapter VI becomes available.

[†]The field in a dielectric in contact with air or vacuum is always lesser in intensity than the field in the latter.

CHAPTER IV

ESTIMATION OF ELECTRIC FIELDS IN DIELECTRIC MEDIA

The Kelvin Ponderomotive Force was defined in Chapter II as

$$\underset{\rightarrow}{F}^{K} = \underset{\rightarrow}{P} \cdot \nabla \underset{\rightarrow}{E} \tag{2.19}$$

where $\underset{\rightarrow}{P} = \varepsilon_o(\varepsilon-1)\underset{\rightarrow}{E}$ is the polarization of the medium and $\nabla \underset{\rightarrow}{E}$ is the gradient of the electric field (a tensor).

It seems imperative, then, that in the absence of any real charges or ions in the system a non-uniform field distribution (at least locally) needs to exist in order for the above force to be effective. Non-uniform fields are created by various configurations, both of the electrodes and the adsorbent system under investigation. In this chapter the various electric field distributions encountered for the several electrode and adsorbent sample geometries are briefly described. Comparisons are made of the relative magnitudes of the ponderomotive forces in each case. Detailed derivations are worked out in Appendix A. In Section 4.2 a popular method for estimating the dielectric properties of crystalline powders and the electric fields in the various phases of an adsorbent-adsorbate system is outlined. In Section 4.3 the phenomenon of relaxation fields, as encountered in moist capillary porous silica gel, is postulated by this author. Numerical estimates for the 'internal' field distribution are also given.

4.1 The Electrostatic Field in Dielectric Media

Six major field configurations are described in this section. The first four refer to experiments conducted in this work, and the last two have direct bearing on the fly ash situation in ESPs.

4.1(a) Bed of Particles in Uniform External Field

Figure 4.1 describes a bed of homogeneous (or near homogeneous), disperse dielectric placed in a uniform, external electric field.

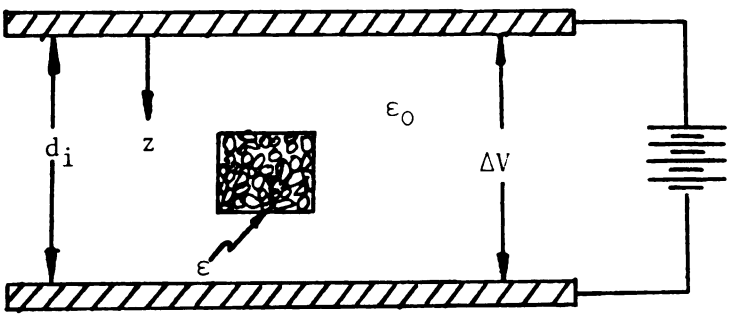

Figure 4.1. Bed of particles in uniform field.

If the particles are fairly small and the bed has fairly uniform dielectric properties (even during adsorption), the field in the bed is uniform and is given by

$$\underset{\rightarrow}{E}_{bed} = \frac{\Delta V}{\varepsilon d_i} \underset{\rightarrow}{e}_z \tag{4.1}$$

ε = dielectric constant of the bed

ΔV = voltage applied between parallel plate electrodes

d_i = inter-electrode distance

$\underset{\rightarrow}{e}_z$ = unit vector in z direction

For typical values used in this work of ΔV = 10 KV, d $\simeq$ 2.5 inches and $\varepsilon \simeq 2$ (dry silica gel)

If

dielect

multila

dependi

in the

parts o

uniform.

used as

field co

4.1(b)
External

Sphe

ween a p

the spher

The

surface)

which redu

$$\underset{\rightarrow}{E} \simeq .79(KV/cm)$$

If only monolayer adsorption is known to take place, then the dielectric properties in the bed will change very little. If, however, multilayer adsorption and/or condensation is known to occur, then, depending on the adsorbate characteristics and the diffusion resistances in the bed, the adsorbate concentrations can differ widely in various parts of the bed and concurrently, the internal field can become non-uniform. In this work crushed alumina, silica gel and fly ash were used as adsorbents and water-vapor as adsorbate for this particular field configuration with ΔV = 10 KV and $d_i \simeq 2.5$ inches.

4.1(b) Spherical Beads in Uniform External Field

Spherical, catalyst-grade, porous alumina particles are placed between a parallel plate capacitor. The field in the immediate vicinity of the spherical particle is non-uniform (see Figure 4.2 below).

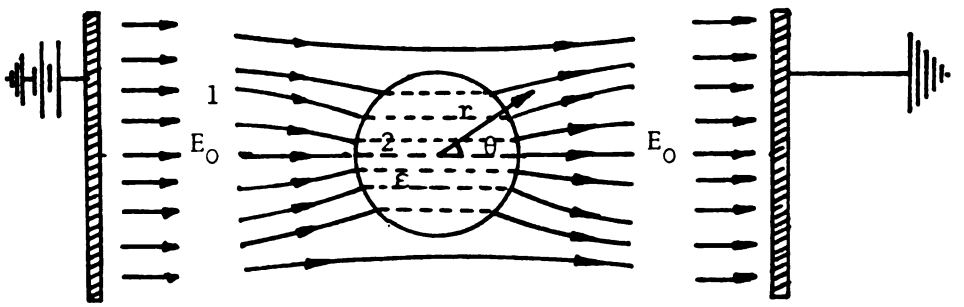

Figure 4.2. Dielectric sphere in uniform field.

The Kelvin force on a dipole molecule of moment $\underset{\rightarrow}{\mu}$ (at the particle surface) is given by (see Appendix A.1)

$$f_{r=R} = (\underset{\rightarrow}{\mu}_{eff} \cdot \nabla E)\Big|_{r=R}$$

which reduces to

$$f_R = \frac{-3(\varepsilon-1)}{RkT} \times \frac{(E_o\mu)^2}{(\varepsilon+2)^2} \times (2\varepsilon\text{Cos}^2\theta - \text{Sin}^2\theta) \qquad (4.2)$$

where

E_o = applied field

θ = polar angle

ε = dielectric constant of particle

μ_{eff} = effective dipole moment = $\frac{\mu^2 \vec{E}}{3kT}$

For $\varepsilon \simeq 5$, $E_o \simeq$ (10 KV/2.5"), $\mu \simeq 6.18\text{x}10^{-28}$ Ccm, $T = 298^o$ K, $k = 1.38\text{x}10^{-23}$ CV/^{o}K

$$f_R \simeq -3.8\text{x}10^{-28}\text{x } f(\theta,\varepsilon) \qquad \text{(Newtons)}$$

where $f(\theta,\varepsilon) = 2\varepsilon\text{Cos}^2\theta - \text{Sin}^2\theta$.

For $\varepsilon = 5$, $f(\theta,\varepsilon)$ is given below:

θ (deg.)	0	30	60	90	120	150	180
$f(\theta,\varepsilon)$	10.0	7.25	1.75	-1.0	1.75	7.25	10.0

The average gradient of the field squared[†] is given by

$$(\nabla E^2)_{\substack{avg \\ at\ r=R}} \simeq \frac{f_R^{avg}}{\mu^2/6kT} \simeq 9.37\text{x}10^7 (V^2/cm^3)$$

Also, $\underset{\rightarrow}{E}_2 = \underset{\rightarrow}{E}_o \times \frac{3}{(\varepsilon+2)}$

The internal field $\underset{\rightarrow}{E}_2$ is uniform and ceases to be so only when significant adsorption can take place in the particle and the adsorbate

---

[†]In all comparisons of electric fields the gradient of the field squared, ∇E^2, is taken, as the ponderomotive force is given by $\underset{\rightarrow}{F} = \varepsilon_o(\varepsilon-1)\nabla E^2/2$.

concentration decreases significantly as the center of the sphere is reached. For porous alumina particles with fine pores, the field in the particle may be expected to be uniform.

4.1(c) Annular Sample Configuration in Cylindrical Field

An annular pan (made of metallic screen material) containing the disperse, dielectric specimen was placed concentric with a cylindrical wire-cylinder electrode system (see Figure 4.3 below).

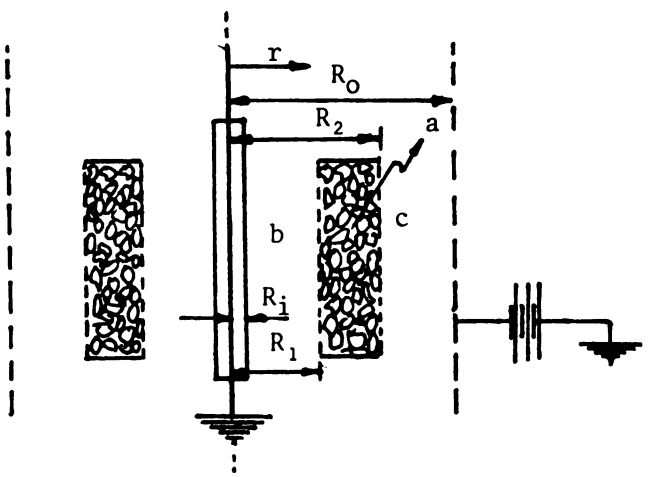

Figure 4.3. Annular sample pan in cylindrical field.

The electrical field distribution has radial symmetry and the gradient of the field squared in the adsorbent phase 'a' for this geometry is given by (see Appendix A.2)

$$\nabla E^2 = \frac{dE^2}{dr} = -\frac{(V_2-V_1)^2}{(\ln R_2/R_1)^2} \times \frac{2}{r^3} \qquad (4.3)$$

where

$$V_1 = \ln(R_1/R_i)^{\varepsilon_a \Delta V} / \ln\left\{\left(\frac{R_2}{R_1}\right)^{\varepsilon_o} \left(\frac{R_1}{R_i}\frac{R_o}{R_2}\right)^{\varepsilon_a}\right\}$$

$$V_2 = \ln\{(R_1/R_i)^{\Delta V} (R_2/R_o)^{V_1}\} / \ln \frac{R_1}{R_i}$$

ΔV = voltage applied across electrodes

ε_a = dielectric constant of adsorbent

ε_o = dielectric constant of air (or vacuum) $\simeq 1$

R_i, R_1, R_2, and R_o are described in Figure 4.3

For $\Delta V = 6000$ V, $\varepsilon_a \simeq 3$, $R_i = .0794$ cm, $R_1 = .3$ cm, $R_2 = .75$ cm and $R_o = 1.25$ cm

$$\nabla E^2 = (-932.23)^2 \times \frac{-2}{r^3} (V^2/cm^3)$$

and

$$\nabla E^2_{avg} \simeq -1.471 \times 10^7 (V^2/cm^3)$$

The field here is non-uniform and depends on the radius r. However, as can be seen from the expression for ∇E^2, most of the non-uniformity is around the central electrode, and therefore, does not involve the cylindrical annular sample holder.

4.1(d) Cylindrical Bed of Dielectric Specimen Coaxial with Cylindrical Electrode Geometry

The sample pan containing the adsorbate is cylindrical in shape, with a fine wire running through its axis and base. The wire serves as the ground electrode and a surrounding cylindrical screen serves as the H.V. electrode (see Figure 4.4).

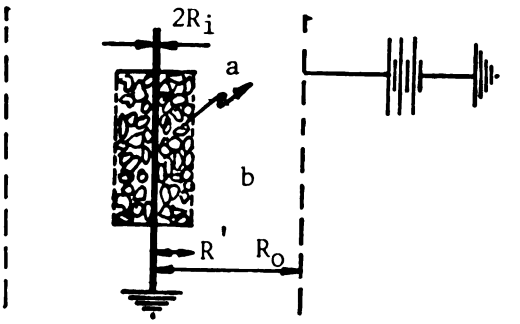

Figure 4.4. Cylindrical sample bed coaxial with cylindrical field.

Once again, the field is radial in nature with the gradient of the field squared, given by (see Appendix A.3)

$$\nabla E_r^2 = \frac{dE_r^2}{dr} = -\frac{(\Delta V)^2}{(\ln R'/R_i + \varepsilon_a \ln R_o/R')^2}\,\frac{2}{r^3} \tag{4.4}$$

For ΔV = 6000 V, R_i = .0089 cm, R' = .16 cm, R_o = 1.25 cm, $\varepsilon_a \simeq 1.50$ (for dry silica gel)

$$\nabla E^2 \simeq -2.02\text{x}10^6/r^3 (V^2/cm^3)$$

and

$$\nabla E^2_{avg} \simeq -1.68\text{x}10^{10} (V^2/cm^3)$$

The average gradient of the field squared in this geometry is seen to be about three orders of magnitude greater than in the annular geometry of Figure 4.3. The central electrode is a fine wire, thus accounting for high fields and field gradients in its immediate vicinity. The average field strength in this geometry for the above parameters and a dry bed is about

$$\underset{\rightarrow}{E}_{r,avg} \simeq 11.89\ (KV/cm)$$

Of course, as adsorption proceeds, the fields (especially in the case of porous silica gel) get exceedingly complex, varying all along

a single internal pore. A method to estimate the internal pore fields during adsorption is proposed in Sections 4.2 and 4.3.

4.1(e) Charged Spherical Particles in Uniform Field

Fly ash particulates encountered in an ESP are charged to saturation by a stream of ions. The field around a fully-charged particle is shown in the figure below.

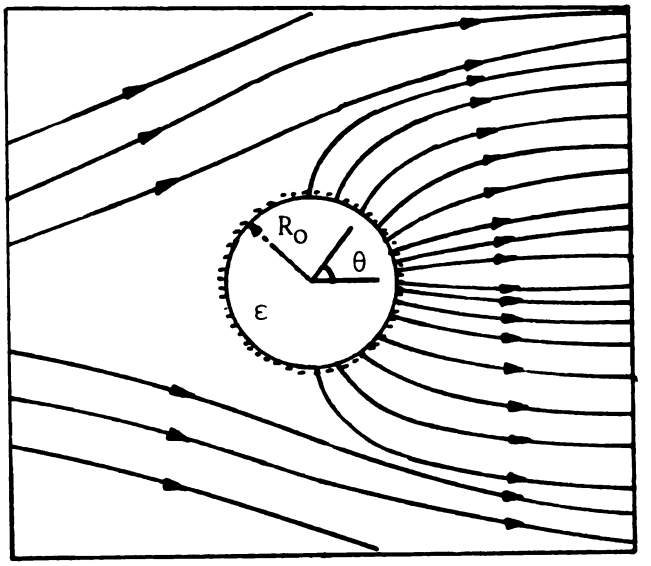

Figure 4.5. Charged particle in uniform external field.

The field on the particle surface for $\pi/2 \leq \theta \leq \pi$ is zero (due to opposing effects of the surface charge and the applied field), while the field on the surface for $0 \leq \theta < \pi/2$ is given by [R1, p. 199]

$$E = E_o \cos\theta \left(2\left(\frac{\varepsilon-1}{\varepsilon+2}\right)\frac{R_o^3}{r^3} + 1 \right) + \frac{q_s}{4\pi\varepsilon_o r^2} \qquad (4.5)$$

where

q_s = maximum free charge on particle = $12(\varepsilon/\varepsilon+2)\pi\varepsilon_o R_o^2 E_o$

ε = dielectric constant of particle

R_o = particle radius

E_o = charging field

For $R_o \simeq 20\times10^{-6}$ m, $E_o = 3\times10^3$ V/cm, $\varepsilon \simeq 4$ (typical values for fly ash particulates in ESPs)

$$E\Big|_{r=R_o}^{avg} \simeq 9.82\times10^3 (V/cm)$$

and

$$\frac{dE_r^2}{dr}\Big|_{r=R_o}^{avg} \simeq 1.79\times10^{11} (V^2/cm^3)$$

Thus, though the field at the particle surface is not very significant, the gradient of the field squared is quite steep. A surface adsorbed dipole molecule (dipole moment μ_s) on this charged particle will experience an additional binding force $\underset{\rightarrow}{f} = \underset{\rightarrow}{\mu_s} \cdot d\underset{\rightarrow}{E}/dr$ due to the field gradient.

4.1(f) Bed of Spherical Particulates Subject to Uniform External Field

A bed of fly ash particulates may be assumed to consist of spherical particles neatly arranged in a cubic array. If such a bed is subject to a uniform external electric field, the typical interparticle contact (shown below) will experience very high non-uniform fields in its immediate vicinity [M2,S2].

The electric field along the plane of contact (in direction r) is estimated to be [S2]

$$E_1 \simeq 2\,\frac{V}{a}\,\frac{R_o}{a}\,\frac{1}{(\beta^2-1)} \quad ; \quad (\beta \geq 1.0) \qquad (4.7)$$

where

V = voltage drop per contact

a = radius of contact circle

R_o = radius of particle

β = r/a (dimensionless distance, $\beta \geq 1$)

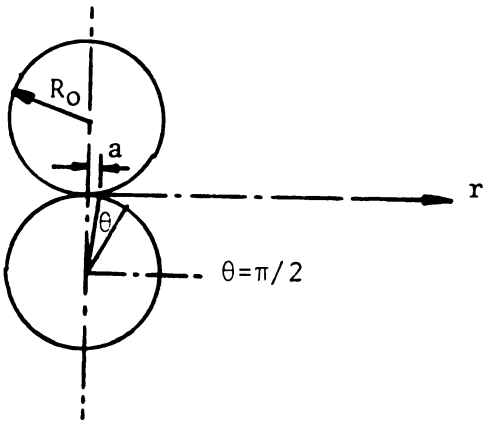

Figure 4.6. Interparticle contact characteristics.

Using typical values encountered in an ESP $R_o/a = 100$, V = 12.5 volts/contact, $a = .10 \times 10^{-6}$ m, one obtains the following field distribution

$\beta \rightarrow$	2	5	10	20	50	100	
E_r	8.3×10^7	1.0×10^7	2.5×10^6	6.3×10^5	1×10^5	2.5×10^4	(V/cm)
$\frac{dE_r^2}{dr}$	1.85×10^{21}	9.04×10^{18}	2.58×10^{17}	7.87×10^{15}	8.0×10^{13}	2.5×10^{12}	(V^2/cm^3)

A field intensity of 5×10^5 V/cm is of the order of the breakdown strength of air, and consequently, field intensities > 5×10^5 V/cm (for $\beta \leq 22$) imply a 'gap charge emission' phenomena. This breakdown is responsible for the non-linear current-voltage characteristics observed with a bed of fly ash [M2].

The field intensity $\vec{E}_s(\theta)$ along the particle surface has also been

estima

where

U

the fo

4.6).

$$\frac{\xi}{(}$$

$$\frac{E_S(}{\rightarrow}$$

$$\frac{1}{R_o}\frac{\partial}{}$$

In

solid p

to esti

all mac

assumpt

as deve

most ea

Bo

17]:

1)

in any

scopic

estimated as [S2]

$$\vec{E}_s(\theta) = \vec{E}_a/(-(\ln \frac{a}{2R_o})\sin^2\theta) \qquad (4.8)$$

where

$\vec{E}_a$ = layer average field = $\Delta V/h$

ΔV = voltage drop across an ash layer of thickness h

Using typical values ΔV = 2 KV, h = .32 cm, R_o/a = 100, one gets the following field variations along the particle surface (see Figure 4.6).

θ (deg.)	1	5	10	40	90	
$\vec{E}_s(\theta)$	3.8×10^{6}	1.5×10^{5}	3.9×10^{4}	2.9×10^{3}	1.2×10^{3}	(V/cm)
$\frac{1}{R_o}\frac{\partial E_s^2(\theta)}{\partial\theta}$	3.44×10^{18}	1.1×10^{15}	3.47×10^{13}	3.89×10^{10}	0.0	(V^2/cm^3)

4.2 Dielectric Properties of Crystalline Powders

In an adsorbate-adsorbent system, there exists three phases: the solid phase, the adsorbate phase and the gaseous phase. The procedure to estimate the dielectric properties of the three phases and the overall macroscopic dielectric constant for the powder involves certain assumptions. The method of Bottcher [B6] (in particular, its extension as developed by McIntosh and his associates [M2,M4]) is considered to be most easily adapted to heterogeneous adsorptive systems.

Bottcher's method is based on the following assumptions [M3, p. 12-17]:

1) The average internal field in the heterogeneous dielectric, and in any phase thereof, is given by the factor $(\varepsilon+2)/3$ times the macroscopic field. ε is the appropriate dielectric constant.

2)

vidual i

3)

by addi

4)

polariz

interna

5)

usual fo

field, w

dielectr

6)

adsorbat

Fro

retical

where th

gaseous

c_i

2) The average internal field is given by the addition of the individual internal fields on a volume-fraction basis.

3) The overall polarization of the composite system is also given by adding the individual polarizations on a volume-fraction basis.

4) The polarization of each phase is related to its volume average polarizability by the relation $P_i = c_i E_i$, where E_i is the average internal field of the i^{th} phase.

5) The macroscopic field in voids or interstices is given by the usual formula for spherical voids, $E_3 = 3\varepsilon/(2\varepsilon+\varepsilon_3)$ times the applied field, where ε refers to the composite dielectric constant and ε_3 to the dielectric constant of the interstices.

6) The average field within the solid phase does not alter with adsorbate concentration in the composite system.

From the above assumptions, all of which are based on some theoretical basis, the following equations are obtained:

$$E\frac{(\varepsilon+2)}{3} = E_1'\delta_1 + E_2'\delta_2 + E_3'\delta_3 \tag{4.9}$$

$$E\frac{(\varepsilon-1)}{4\pi} = c_1\delta_1 E_1' + c_2\delta_2 E_2' + c_3\delta_3 E_3' \tag{4.10}$$

where the subscripts 1, 2, and 3 refer to the solid, adsorbate, and gaseous matter, respectively.

δ_i = volume fraction of i^{th} phase

E_i' = average internal field in phase i given by

$E_i' = (\frac{\varepsilon_i+2}{3})E_i$ (E_i = macroscopic field in phase i)

c_i, the average polarizability in the i^{th} phase, is given by

$$c_i = \frac{3(\varepsilon_i - 1)}{4\pi(\varepsilon_i + 2)} \tag{4.11}$$

From equation (4.10) one has for the initial condition ($\delta_2 = 0$ or no adsorbate)

$$\delta_1 E_1 = (\varepsilon^o - 1)E/4\pi c_1 \tag{4.12}$$

since $\delta_2 = 0$ and $c_3 \simeq 0$ (polarizability of gas phase $\simeq 0$).

ε^o = dielectric constant of composite material when $\delta_2 = 0$

Thus, from assumption (6), when the applied field is $\underset{\rightarrow}{E}$, the field in the solid phase is always given by (4.12), irrespective of whether $\delta_2 = 0$ or not. In cases where $\underset{\rightarrow}{E}$ itself is decreasing with adsorption, an additional assumption that equation (4.12) still holds is made here.

From (4.9) and (4.10) and with the help of (4.12), one arrives at the relation

$$\frac{(\varepsilon+2)}{3} - \frac{3\varepsilon\delta_3}{(2\varepsilon+1)} = \frac{(\varepsilon^o-1)}{4\pi c_1} + \frac{(\varepsilon-\varepsilon^o)}{4\pi c_2} \tag{4.13}$$

where ε_3 has been taken to be $\simeq 1$ (gas phase).

Thus, a knowledge of the variation of the composite dielectric constant ε as a function of the amount adsorbed, and of ε_1, the solid dielectric constant, yields ε_2, the average dielectric constant of the adsorbate phase. Conversely, if the permittivity of the adsorbed phase is known, an approximate estimate of the overall dielectric constant may be obtained.

Once the dielectric constants are obtained, the evaluation of the average fields in the various phases can be easily carried out from equations (4.9), (4.10) and (4.12). If the adsorbed phase is a multi-layer, very often distinct phases in the adsorbed phase are known to

exist (see Section 4.3). In such a case, equations (4.9) and (4.10) may be reapplied to the adsorbed phase to yield the electric fields in the respective adsorbed intra-phases.†

The electric fields in equations (4.9) and (4.10) are, in general, not uniform. For example, if one wishes to estimate the dielectric properties of a powder subjected to a cylindrical external field, the overall macroscopic field becomes radial in nature (as seen in Section 4.1(c)). The local fields depend on both the overall field and the local environment. In the next section an approximate methodology for estimating the local and global electric fields as a function of applied voltage, adsorption amount and powder characteristics is proposed.

4.3 Relaxation Fields: Estimation of Electric Fields in Moist, Capillary Porous Silica Gel

Due to the cylindrical shapes of pores in silica gel, and the rather long, narrow pore structures, the adsorption of water vapor in silica gel may be represented by diffusion-controlled mass transfer phenomena in open, cylindrical pores (see Figure 4.7 below):

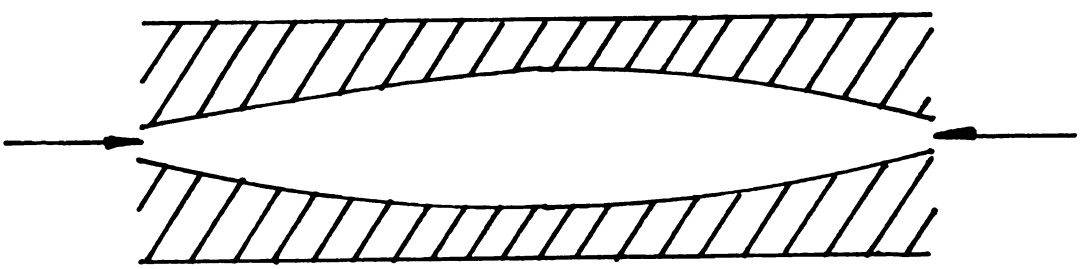

Figure 4.7. Single cylindrical open pore with adsorbate.

---

†Calculations show that this procedure yields almost the same values for the average field as when equations (4.9) and (4.10) were not reapplied.

As

tend to

center.

monolay

and vap

vary al

be smal

at the

up with

gradien

ously w

so to s

seen th

though

are, ne

existin

4.3(a)
Adsorbe

Th

the ear

amyl al

tion of

with am

this wo

As adsorption is taking place, the regions close to the pore mouths tend to have a greater concentration of adsorbate than those deep in the center. Owing to the different dielectric constants associated with monolayer adsorbate, bound layer adsorbate, condensed layer adsorbate and vapor phase adsorbate (to be seen shortly), the local fields will vary all along the pore. In general, the fields at the pore mouths will be smaller (due to higher average dielectric constants) than the fields at the middle of the pore. Consequently, a local field gradient is set up with the gradient pointing towards the center of the pore. This field gradient, and the corresponding ponderomotive force, will vary continuously with the adsorption process. Thus, the fields in the pore will, so to say, relax with the progress of adsorption. In this work, it is seen that the internal field gradients produced by such relaxation, though depending on the magnitude of the overall external applied field are, nevertheless, much larger than the macroscopic field gradients existing in the bulk adsorbent sample.

4.3(a) Dielectric Constant of Adsorbed Water in Silica Gel

The dielectric behavior of porous adsorbents has been studied since the early 1940s. Higuti [H1] examined the behavior of n-propyl and iso-amyl alcohols adsorbed in titanium oxide gel. In Figure 4.8 the variation of the capacitance (or dielectric constant) of the porous sample, with amount adsorbed, is shown. Three linear regions were reported in this work.

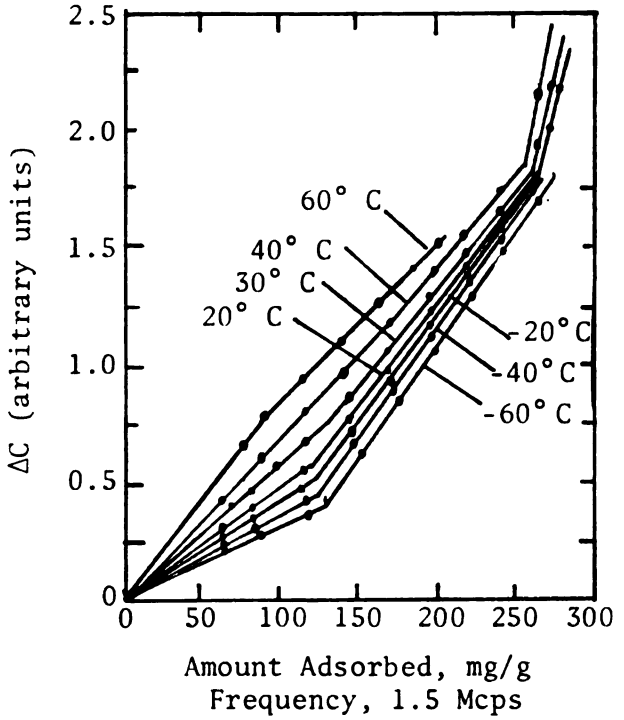

Figure 4.8. n-propyl alcohol-titania gel system.

Kurosaki [K1] investigated the silica gel-water system. He also reported three linear regions for the variation of sample dielectric constant with amount adsorbed (see Figure 4.9). The discontinuity in the slope from the first to the second region is considered by most to be proof that the monolayer has been completed [M3, p. 67]. The third linear region is not observed with most adsorbates. With water vapor adsorbed on silica gel, Kurosaki has given as a possible explanation the existence of very strongly developed hydrogen bonds in the adsorbate for this third linear region. All researchers agree that the plots are linear. This experimental result shows that the dielectric property of an amount of adsorbate added is independent of the amount already present [M3, p. 67], which then implies that the adsorbate in the two or three regions described above have more or less uniform dielectric constants (at least within a linear region).

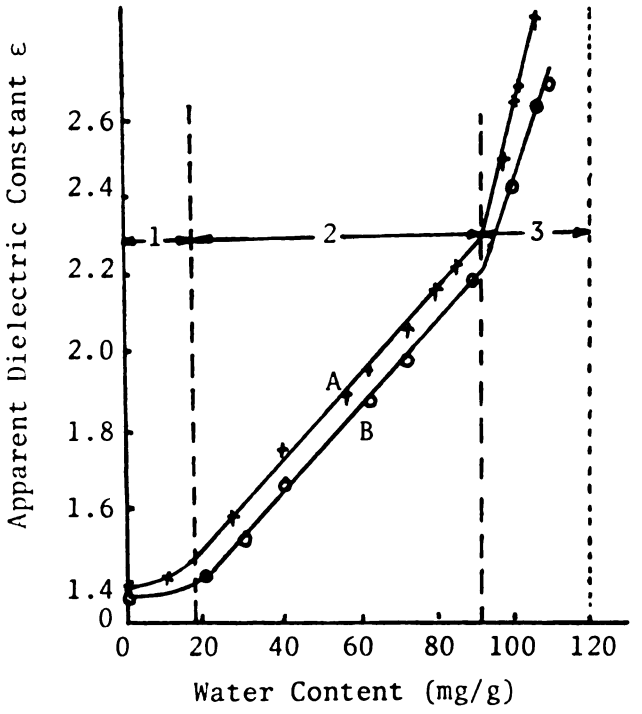

Figure 4.9. Relations between dielectric constants and sorbed amount of water (25° C): A. 500 kc; B. 1,000 kc.

The Onsager-Kirkwood formula [K2] yields the following relationship between the specific polarization of a substance P_k and its dielectric constant ε

$$P_k = \frac{(\varepsilon-1)(2\varepsilon+1)}{9\varepsilon\rho} \tag{4.14}$$

ρ = density of substance

When water is adsorbed on to, say, silica gel, the differential specific polarization of water can be shown [K1] to be

$$\overline{P}_w = \frac{\partial P_k}{\partial W} = \frac{(2\varepsilon^2+1)(\partial\varepsilon/\partial W)}{9\varepsilon^2\rho} \tag{4.15}$$

where

δW = small amount of water added to the composite dielectric

ε = dielectric constant of composite dielectric

ρ = density of moist composite dielectric

$\overline{P}_w$ = differential specific polarization of adsorbed water

Using the experimental results obtained in the silica gel-H_2O vapor system Kurosaki has obtained for the three regions described above

	Region 1	Region 2	Region 3
$\overline{P}_w$	$\simeq 1$	8-11	$\simeq 23$

If one uses the Onsager-Kirkwood formula for the adsorbate only (an assumption), one then obtains a rough estimate for the adsorbate dielectric constants ε_s

	Region 1	Region 2	Region 3
ε_s	$\simeq 1.05$	$\simeq 43.26$	$\simeq 104$

The dielectric constant of pure liquid water at 25^{o} C is $\simeq 80$, and of pure ice $\simeq 100$. Thus, region 3 corresponds to an 'ice-like structure' arising from tightly bonded 'clusters' of water molecules [K1]. Similar ice-like structures have been observed with water-vapor adsorbed on α - Fe_2O_3 [Z1]. In this work the transition from region 2 to 3 will be taken to imply that adsorptive forces (bound layer) have been converted to bulk liquid intermolecular forces (condensed layer). This fits very well the numerical estimates of Kurosaki's work and the estimates of bound water in Figure 3.7(a). Zettlemoyer [Z1,Z2] has suggested a doubly hydrogen bonded monolayer, singly bonded second layer and ordered 'ice-like' multilayer for water adsorbed on oxide surfaces, which is consistent with the analysis presented here.

4.3(b) Strategy for Internal Field Calculations

Detailed numerical calculations are described in Appendix B. The procedure outlined below (estimating local fields) is divided into two parts.

Part I

To Obtain Overall Dielectric Constant and Electric Field

1) Knowing W (gms adsorbed/gm adsorbent), the assumption that the water is adsorbed uniformly in the whole silica gel bed is made. Next, the average dielectric constant of adsorbate (volume average of the three layers) is estimated, and using equation (4.13), the average dielectric constant of each spherical silica gel particle, $\varepsilon = \varepsilon_p$, is obtained.

2) The whole bed is treated as composed of silica particles of dielectric constant ε_p interspersed with air (see Figure 4.10).

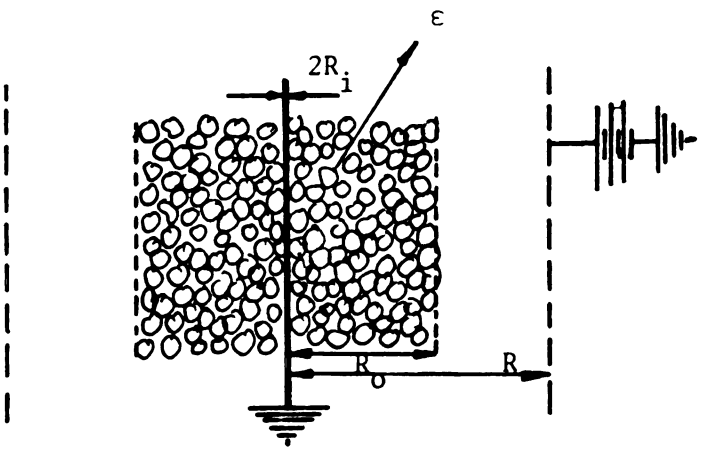

Figure 4.10. Spherical, porous dielectric particles in air; subjected to electric field.

Using equation (4.13) with $4\pi c_1 = 3(\varepsilon_p-1)/(\varepsilon_p+2)$ and $4\pi c_2 = 0$ (only two phases here), one gets ε, the overall dielectric constant of

the bed as a function of W.

3) The overall electric field for the field geometry shown in Figure 4.10 is obtained from equation (4.4) as

$$E_r = \frac{\Delta V}{(\ln R_o/R_i + \varepsilon \ln R/R_o)} \times \frac{1}{r} \tag{4.4}$$

Part II

To Obtain Local Dielectric Constant and Local Field

4) The average macroscopic field in a particle, E_p, is obtained from applying equations (4.9) and (4.10).

5) As the adsorbate concentration is, in reality, non-uniform all along the particle (decreasing as the center of the particle is approached), the local field will be different from the average particle field. The field inside a spherical particle subjected to an external field $\underset{\rightarrow}{E}$ is given by (see Section 4.2)

$$\underset{\rightarrow}{E}_p = \left(\frac{3}{\varepsilon_p + 2}\right)\underset{\rightarrow}{E} \tag{4.16}$$

The assumption is made here that the local field $\underset{\rightarrow}{E}_{pi}$ is related to the average field $\underset{\rightarrow}{E}_p$ in the particle by the relation

$$\underset{\rightarrow}{E}_{pi}(\varepsilon_{pi}+2) = \underset{\rightarrow}{E}_p(\varepsilon_p+2) \tag{4.17}$$

based on the above observation (equation 4.16).

6) Using Bottcher's method (equation 4.13) for a small local segment, one can estimate ε_{pi}, the local particle dielectric constant (knowing the local adsorbate concentration C_i). Next, using $\underset{\rightarrow}{E}_p$ from (4) and ε_p from (1) along with equation (4.17), the local average particle

field $\underset{\rightarrow}{E}_{pi}$ is obtained.

7) Finally, by applying (4.9) and (4.10) to the small local section of adsorbent, $\underset{\rightarrow}{E}_{2i}$ and $\underset{\rightarrow}{E}_{3i}$, the local average fields in the adsorbate and the gas phase, respectively, are estimated.

The following tables give some numerical estimates of the local and global fields calculated.

Table 4.1. Estimates of Overall Dielectric Constants and Macroscopic Electric Fields as a Function of W for Silica Gel S-2509 and Water Vapor System

$W \frac{gm}{gm\ ads}$	ε_2^{avg}	ε_p	ε	$\vec{E}r$ (V)	$\vec{E}_p r$ (V)
.10	15.88	3.53	2.08	837.2	678.7
.20	48.09	9.63	4.18	522.6	364.2
.30	66.73	19.94	7.39	331.71	211.9
.40	76.04	31.85	10.98	237.3	145.3
.50	81.65	44.12	14.63	182.0	108.9
.60	85.36	47.12	18.48	146.8	86.5
.70	88.03	70.11	22.30	123.1	71.8

W = gms adsorbed/gm adsorbent dry

ε_2^{avg} = average dielectric constant of adsorbed phase

ε = average overall dielectric constant of bed

$\underset{\rightarrow}{E}$ = average overall electric field = $\frac{B}{r}$ ($B = f(\varepsilon)$)

r = radial position in bed

$\underset{\rightarrow}{E}_p$ = average electric field in silica gel particle

Table 4.1 illustrates how the overall dielectric constant of the bed rises with W, and correspondingly, how the field in the bed

decreases. The variation of ε with W is approximately linear (within the respective adsorbate regions), which confirms the experimental observations made earlier.

For a given W, Table 4.2 gives the adsorbate concentration profile in a typical pore (obtained from computer calculations in Chapter VI) and the corresponding ε_{pi} (local dielectric constant), $\underset{\rightarrow}{E}_{pi}$ (local average field), $\underset{\rightarrow}{E}_{2i}$ (field in adsorbate) and $\underset{\rightarrow}{E}_{3i}$ (field in vapor space in pore).

Table 4.2. Estimates of ε_{pi}, E_{pi}, E_{2i}, E_{3i} for W = .3085 $\frac{\text{gm adsorbed}}{\text{gm adsorbent}}$, $\varepsilon_p^{avg} = 20.95$, $(E_p r)^{avg} = 206.2$ V (from Table 4.1)

$\zeta \rightarrow$	0	.24	.25	.26	.49	.50	.51
C_i	.9888	.3556	.3497	.3441	.2744	.2741	.274
ε_{pi}	69.22	14.42	13.98	13.57	9.12	8.91	8.91
$(E_{pi}r)$	66.45	284.73	296.1	303.9	425.6	433.8	433.8
$(E_{2i}r)$	85.02	263.8	281.7	292.4	396.5	392.8	392.8
$(E_{3i}r)$	99.7	412.8	428.8	439.65	563.9	557.9	557.9

$\zeta = \frac{z}{L}$, z = distance in pore, L = length of pore, C_i = dimensionless adsorbate concentration.

Thus, when the amount of adsorbate in the silica gel bed is about 30.85 gm/100 gm dry adsorbent, a typical pore will have the adsorbate phase and the gas phase field increasing towards the center of the pore ($\zeta \simeq .50$). All the fields up to now have been obtained as a product of $\underset{\rightarrow}{E}$ and r, the latter being the radial position in the bed of particles. To obtain an average estimate of the field distribution, r is taken to

correspond to the radial position of the average field squared $\langle E^2 \rangle$. This is due to the ponderomotive force being defined as

$$\underset{\rightarrow}{F} = \underset{\rightarrow}{P} \cdot \nabla \underset{\rightarrow}{E_i} = \frac{1}{2} \varepsilon_o (\varepsilon_s - 1) \nabla |E_i|^2$$

and the observation that by 'gradient of the field squared' (∇E_i^2) is meant the gradient in the internal pore fields. The latter depend on the magnitudes of the overall field squared (E^2) and not on the gradient of the overall field squared (∇E^2).

4.3(c) Comparison of Internal Field Gradients and External Field Gradients

For a cylindrical bed of silica gel subject to a cylindrical electrical field as in Figure (4.10), the gradient of the overall $(\text{field})^2$ is given by differentiating equation (4.4)

$$\frac{dE_r^2}{dr} = \frac{(\Delta V)^2}{(\ln R_o/R_i + \varepsilon \ln R/R_o)^2} \times \frac{2}{r^3} \qquad (4.18)$$

For R_o = .16 cm, R_i = .0089 cm, R = 1.25 cm, ΔV = 6000 V, ε = 7.70 and W = .3085, the average component of the ponderomotive force ($F = \varepsilon_o \frac{(\varepsilon - 1)}{2} \frac{dE^2}{dr}$) is given by

$$\left\langle \frac{dE^2}{dr} \right\rangle = \frac{6000^2}{(\ln(.16/.0089) + 7.7 \times \ln(1.25/.16))^2} \times \frac{4}{(.16^2 - .0089^2)} \left(\frac{1}{.0089} - \frac{1}{.16} \right)$$

or

$$\left\langle \frac{dE^2}{dr} \right\rangle \Bigg|_{\text{overall}} = 1.71 \times 10^9 \, (V^2/cm^3)$$

For the internal field gradients, for example, at ζ = 0.25 (L = .01693 cm) from Table 4.2 (for same R_o, R_i, R, ΔV, ε and W as above)

$$\frac{dE_{2i}^2}{dr} = \frac{\left\{\left(\frac{292.4}{.0667}\right)^2 - \left(\frac{263.8}{.0667}\right)^2\right\}}{.02x.01693} = \underline{1.06x10^{10}(V^2/cm^3)}$$

and

$$\frac{dE_{3i}^2}{dr} = \frac{\left\{\left(\frac{439.65}{.0667}\right)^2 - \left(\frac{412.8}{.0667}\right)^2\right\}}{.02x.01693} = \underline{1.519x10^{10}(V^2/cm^3)}$$

where $r_{avg} \simeq .0667$ cm is substituted for the radial position of the average field squared $\langle E^2 \rangle$ (see Appendix B.2).

Thus, it can be seen that the internal field gradients set up by the relaxing fields are much larger (one order of magnitude, in this case) than the overall external field gradients. In essence, then, it would seem that the field-induced effects should be observed in moist silica gel, even with uniform externally-applied electric fields of magnitudes comparable with those calculated for non-uniform fields. More on this in Chapter V, Section 5.6(b).

CHAPTER V

EXPERIMENTAL VERIFICATION OF FIELD-INDUCED MASS TRANSFER EFFECTS

In this chapter the various experiments conducted in the M.S.U. laboratory to study the effects of both uniform and non-uniform, externally-applied electric fields are presented. In Section 5.1 a brief outline of the rationale that determined the sequence of experiments conducted is given. In Section 5.2 the apparatus used in these experiments, the schematic diagram and a step-by-step procedure for conducting the experiments are illustrated. Section 5.3 deals with the application of uniform electric fields to various adsorbents and adsorbent geometries. In Section 5.4 the effects of non-uniform applied fields to several adsorbents are described in the context of water-vapor adsorption. Both 5.3 and 5.4 deal with a maximum of two to three layers of adsorbed gas. Section 5.5 involves multilayer adsorption and/or capillary condensation in porous silica gel in the presence of non-uniform, cylindrical fields. Section 5.6 covers various interesting sub-topics such as the adsorption of non-polar adsorbates, the field-induced effects on the desorption process in silica gel, the relative significance of internal and external field gradients, etc. Finally, in Section 5.7, preliminary experiments conducted with silica gels treated with concentrated HCl, and also impregnated with traces of K^+ ions, are presented.

5.1 Rationale Behind the Order of Experiments

At the outset of the experimental investigations, available literature [P2] seemed to suggest that the kinetics of gas(polar)-solid adsorption was enhanced or depressed due to an additional electro-convective vapor-phase flux, defined in equation (1.4) as

$$\underset{\rightarrow}{J}_e = \frac{D}{kT}(\underset{\rightarrow}{\mu}\cdot\nabla\underset{\rightarrow}{E})\,C \qquad (1.4)$$

where $\underset{\rightarrow}{\mu}$ is the molecular dipole moment and a vector.

For a gas not subjected to any external field, its effective dipole moment (even when the gas is polar, like water-vapor) is zero. When a fairly strong field is applied, however, the polar molecules assume an effective dipole moment in the direction of the field which for most laboratory fields encountered ($E \leq 1\text{x}10^6$ V/cm) is given by [R5, p. 108]

$$\underset{\rightarrow}{\mu}_{eff} = \frac{\mu^2 \underset{\rightarrow}{E}}{3kT} \qquad (5.1)$$

The magnitude of $\underset{\rightarrow}{\mu}_{eff}$ for E of, say, $1\text{x}10^4$ (V/cm), is about four orders of magnitude smaller than μ itself, and numerical estimates of the electro-convective flux using $\underset{\rightarrow}{\mu}_{eff}$ yield negligible increases over the ordinary concentration gradient-driven diffusive fluxes, i.e.

$$\frac{D}{kT}(\underset{\rightarrow}{\mu}_{eff}\cdot\nabla E)\,C \,/\, D\,\frac{\partial C}{\partial x} \;<<\; 1$$

Consequently, if the electro-convective flux of equation (1.4) above were indeed the correct mechanism for increased mass transfer rates, then the value of $\underset{\rightarrow}{\mu}$ in this equation should be other than that of $\underset{\rightarrow}{\mu}_{eff}$. Equation (5.1) is arrived at by assuming a Boltzmann distribution for the potential energy of permanent gas dipoles and estimating the average

value of the effective dipole moment (component in field direction) [R5, p. 107]. If, however, the time scale over which the force acting upon a dipole gas molecule is much smaller than the time scale over which an equilibrium Boltzmann distribution is applicable, then the instantaneous force on a dipole is much larger (as, then, $\mu_{eff} = \mu$) though the direction of the force is absolutely random. This could conceivably lead to an increase in 'local turbulence,' and therefore an increase in the mass transfer rates. With these rather 'undeveloped' ideas in mind, the adsorption of water-vapor in individual, spherical, catalyst-grade alundum (Al_2O_3) particles in uniform external fields were initiated. Also, the adsorption of H_2O-vapor in the same field in a bed of silica gel particles was studied to observe, if possible, any increases of mass transfer rates due to the presumed 'electro-turbulence' phenomenon. At this point all the experiments were conducted at a relative water-vapor pressure $p/p_s \simeq 2/3$ (at which pressure no condensation is expected) and $T = 37^{o}$ C. More experiments were undertaken with uniform fields applied across beds of alundum particles and crushed alumina. No significant effects were observed with the applied uniform fields under the above conditions. The kinetics of adsorption was next studied in cylindrical annular sample pans containing, mainly, crushed alumina particles (non-spherical). Cylindrical fields across a wire cylinder geometry were applied. The reasoning behind using an annular pan went as follows: the gradient of the electric field in a wire-cylinder geometry always points towards the central wire (see Figure 4.3 for geometry details). If the electro-convective flux given by equation (1.4) is indeed the correct transport mechanism, then, blocking the inner face of the annular pan (see Figures 4.3 and 5.2(c)) would simulate a closed pore

adsorbent sample. Thus, according to reference [P2], this should lead to an acceleration of adsorption kinetics and an exponential equilibrium concentration distribution limited only by the Kelvin concentration for condensation. On the other hand, blocking the outer face of the pan should lead to a deceleration of the adsorption kinetics, due to the ponderomotive forces acting towards the mouth of the closed pore system (i.e., away from the sample). With both faces unblocked, only adsorption kinetics should be affected and not the equilibria.

In spite of the cylindrical fields imposed on the sample in annular pans, no appreciable changes in the adsorption kinetics or equilibria were observed, and it was concluded that somehow much higher fields and field gradients were essential before any effects could be expected. To this end, cylindrical sample pans with a fine metallic filament running through their axis of symmetry were constructed. The fine wire was grounded when the pan was positioned directly over the grounded electrode. A cylindrical screen formed the High-Voltage electrode (see Figure 4.4). In this way, very high fields and field gradients existing in the immediate vicinity of the filament electrode were utilized. Crushed alumina, porous glass, $CaCO_3$ powder, alundum beads individually strung on the central filament, zeolite catalyst beads and 'drying grade' silica gel were used as adsorbents and water-vapor as adsorbate (with relative vapor pressures varying from 0.5 to 1) in this electrode-sample configuration. The extent of adsorption was as yet at most two or three layers. In spite of fairly high fields and field gradients employed, no discernible effects could be detected in either the rate of adsorption or the maximum hygroscopic moisture content in the various porous adsorbents, except drying grade silica gel. In the latter, small

increases in the rates of adsorption were observed, especially as the relative vapor pressure was increased towards $p/p_s \simeq 1$. In order to conduct more careful investigations into the observed enhancements of adsorption rates in drying grade silica gel, highly porous samples of Silica Gel S-2509 and S-4133 (from SIGMA Chemical Company) were procured. Significant capillary condensation was observed in S-2509, owing to the large pore diameters. At this point, it was realized that multilayer adsorption and/or condensation was essential to notice appreciable electric field-induced effects. Various related experiments were then carried out with Silica Gel S-2509 as adsorbent, and water-vapor (μ = 1.85 debye) as adsorbate. Besides the field configurations mentioned above, a point-plane field was also briefly tested in the adsorption of water-vapor in crushed alumina particles. Finally, preliminary experiments were conducted with silica gel, first treated with HCl to remove any foreign ions in the gel, and next, treated with a saturated KCl solution to introduce some K^+ ions.

5.2 Experimental Apparatus and Procedure

The gravimetric method was adopted to study the gaseous adsorption of water-vapor in the various disperse, dielectric adsorbents.[†] A CAHN Gram Electrobalance (see Appendix D) was modified to perform remote weighing. Figure 5.1 is a schematic diagram illustrating the experimental

---

[†]An indirect volumetric technique would probably have been better suited to conduct these experiments, especially in the light of the various problems associated with weighing a sample when the latter is subject to an electric field. However, the Gram Electrobalance was the only measuring equipment available at the outset.

set-up.

A rectangular plexi-glass box served as the adsorption chamber. The chamber was immersed in a constant temperature water bath. The electrode geometry and sample pan configurations used in this work are described in Figure 5.1 and also in Figures 5.2(a), (b) and (c). The sample was suspended from the central hook of the electrobalance during weighing. The balance was located directly above the chamber and outside the water bath. A 'Spellman' high voltage D.C. supply was used to provide the required voltage across the electrodes. A 'Simpson' ultra-high sensitivity multimeter was used to measure the leakage current through the electrodes. Dry nitrogen brought up to the bath temperature by heating coils was passed through two separate lines. The N_2 passing through one remained dry as it entered the adsorption chamber, while the N_2 passing through the other picked up moisture (became saturated with it) as it bubbled through pure distilled water contained in bubbling bottles. The relative flow rates could be adjusted to control the humidity of the entering N_2 stream.

Using the gravimetric method to measure the progress of adsorption in the presence of strong electric fields can cause innumerable 'background' problems. The pan material, the string from which the pan is hung, the distance of pan from the electrodes, the pan geometries and charging characteristics, etc., all have to be taken into account for a 'background-free' reproducible reading. 'Strip Teeze' teflon tape (dielectric constant low) was found to be best suited to serve as the string on which the adsorbent sample was suspended. For the uniform field electrode geometry polystyrene foam (dielectric constant $\simeq$ 1) was found to serve best as the sample pan without distorting the field

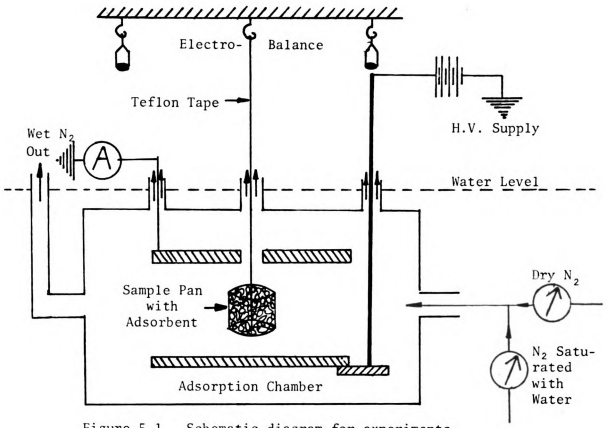

Figure 5.1. Schematic diagram for experiments.

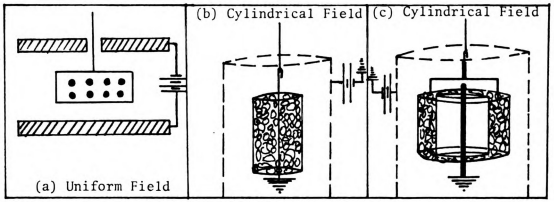

Figure 5.2. Sample pan configurations (other than that in Fig. 5.1)

characteristics. In the case of the cylindrical fields, metallic screen material formed concentric constant voltage surfaces, thus leaving the cylindrical applied fields unaffected.

5.2(a) Step-By-Step Procedure for Conducting Experiments

The procedure followed in conducting all the experiments consisted of essentially two parts:

Part I

Preparation for Start of Experiment

a) The water bath was filled with water until the entire adsorption chamber was submerged. The temperature control knob was set at the required bath temperature (either 25^{o} C or 37^{o} C in this work).

b) The power to the microbalance was switched on and so was the current for the two N_2 heaters.

c) If the adsorbent was to be desorbed by passing dry N_2 at the adsorption temperature (as for all cases except silica gel in this work), then dry N_2 was passed into the adsorption chamber with the adsorbent in the sample pan. If silica gel was the adsorbent, the dry, water-free silica gel was removed from the oven (at $\simeq 110^{o}$ C) and placed inside a dessicator at room temperature for about one-half hour prior to the start of an experiment. In this case, the N_2 fed to the chamber (without the adsorbent but with the sample pan, etc.) was moist and of the same humidity as that required for the experiment.

d) The microbalance was zeroed and calibrated and the adsorbent sample (or the sample pan only) allowed to come to temperature and concentration equilibrium with the N_2 environment ($\simeq$ 1 hour).

e) The weight of the dry adsorbent sample (or the wet sample pan)

was recorded as the initial reading.

Part II

During the Experiments

f) For the case with the dry adsorbent sample at time t = 0, the moist N_2 was started through the bubblers and the required voltage applied across the electrodes. For the case of silica gel, the adsorbent sample pan was removed from the chamber and the dry, room temperature adsorbent immediately filled into the narrow, cylindrical sample pan. The pan was then lowered back into the wet adsorption chamber and the time recorded as t = 0. In both the cases, the field was applied only after the sample pan was unhooked from the balance and placed firmly in the required configuration. In the cylindrical field case, proper care was taken to ensure that the sample pan was concentric with the wire cylinder electrode geometry and that, in the case of the filament electrode, the latter was in good contact with the grounded terminal.

g) For silica gel the reading on the balance was recorded after one minute, the pan unhooked and placed in the chamber securely, and then the H.V. started.

h) After four minutes, the voltage was turned off (for ≃ 1 minute) and the reading at t = 5 minutes was recorded. From this reading and the readings at t = 1 minute and t = 0 minutes, the weight of the dry silica gel sample was estimated (see Appendix C.20).

i) At successive intervals of time (e.g., at t = 15, 30, 45, . . . minutes) the voltage was turned off for one minute and the adsorbent weight recorded. The time for which the adsorbent sample was not subjected to the field in this weighing procedure ranged from about 4 to 8% of the total time. This on-off procedure was essential to ensure that

the weighings were not affected by the imposed fields.

j) All experiments were repeated for the blank data, i.e., the data without any adsorbent in the sample pan. The actual amount adsorbed was then obtained by subtracting the blank readings for both the 'no-field' and 'with-field' case.†

k) The zero was periodically checked for error. Calibration error was usually found to be negligible when a 'stabilized line source' was used to power the balance.

5.3 Adsorption in Uniform, Applied Electric Fields

In the following experiments a uniform field was created between two parallel plates two and one-half inches apart, and across which a 10 KV voltage drop was maintained (see Figures 5.1 and 5.2a).

5.3(a) Spherical, Porous, Alundum Beads in Uniform Field

Spherical beads of catalyst-grade porous alumina of about .25 to .30 cm. diameter were stuck on a rectangular strip of polystyrene foam and suspended from the balance as shown in Figure 5.2(a). The temperature of the bath was maintained at $T = 37^{o}$ C and the relative humidity of the moist N_2 was about 67%. Only monolayer adsorption is expected in the fine pores of this catalyst at $p/p_s \simeq .67$. The nature of the fields and field-induced forces in this geometry was discussed briefly in Section 4.1(b). The average of the field gradient squared†† existing at the spherical particle surface has been shown in Appendix A.1 to be

---

†In some cases the pan experienced a push from the surroundings during weighing, possibly due to residual charges left by the field.

††$\vec{F} = \varepsilon_o(\varepsilon-1)\nabla E^2/2$ and hence, the comparison of ∇E^2.

about $\nabla E^2_{avg} \simeq 1.11 \times 10^7$ (V^2/cm^3) and the average field at the surface $\underset{\rightarrow}{E}_{avg} \simeq 2.19$ (KV/cm). The internal field is uniform and of smaller magnitude than the external applied field.

Figure 5.3 is a plot of the experimental data obtained. Within experimental error, no change is observed either in the adsorption kinetics or the maximum amount adsorbed. As discussed in Chapter IV, Section 4.3(a), molecules adsorbed in the monolayer have very low dielectric constants (or low polarizabilities) and, consequently, the effect of field-induced forces on surface diffusion in the monolayer is negligible. This and the added factor of relatively low fields and field gradients could account for the lack of any observed effects in these experiments.

5.3(b) Bed of Silica Gel in Uniform, Applied Field

Drying grade silica gel (6-16 mesh, 'Baker Analyzed' Reagent) was crushed and placed in a cylindrical polystyrene foam pan of length = 0.5 cm and diameter = 1.2 cm (see Figure 5.1). The gel was placed overnight in an oven at 115° C and degassed under vacuum for ≃ 2 hours just before being introduced into the adsorption chamber. Dry N_2 was passed through the chamber for ≃ 1 hour, or until the sample could be assumed to have come to equilibrium with the bath temperature (= 37° C). At the start of experiments, the N_2 flow rates were adjusted to give $p/p_s \simeq 2/3$ and a voltage drop of $\Delta V = 10$ KV was applied across the electrodes. Results of water-vapor adsorption in drying grade silica gel at 37° C, $p/p_s \simeq 2/3$ and $\Delta V = 10$ KV are shown in Figure 5.4. On the y axis is plotted the ratio of the weight of water-vapor adsorbed to the dry sample weight, W, and on the x axis is time, t. As shown in Section 4.1(a), the average field in the sample is about $\underset{\rightarrow}{E} \simeq .79$ V/cm (when sample is

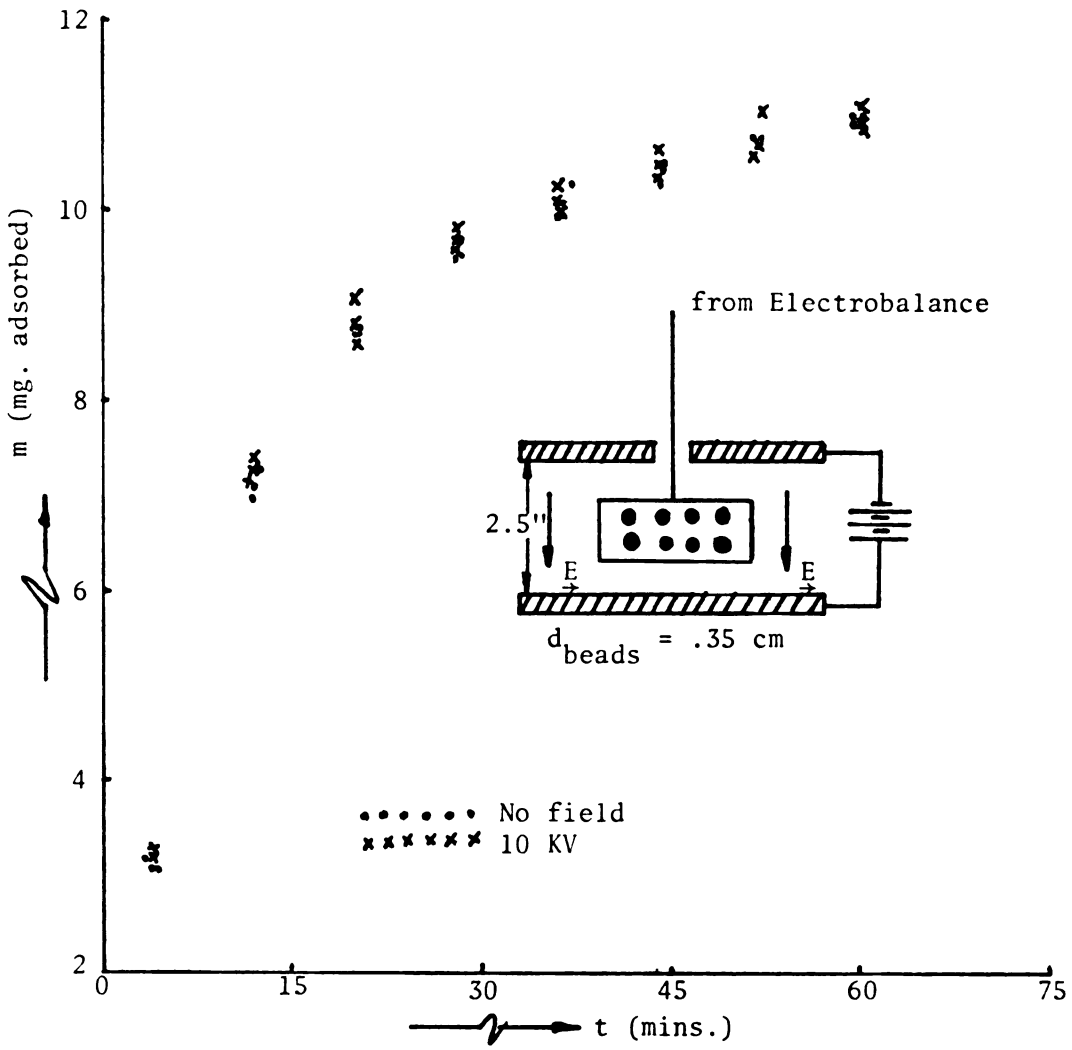

Figure 5.3. Spherical porous alumina beads in uniform electric field--adsorption of water vapor, T = 37° C, p/p_s = 2/3, ΔV = 10 KV.

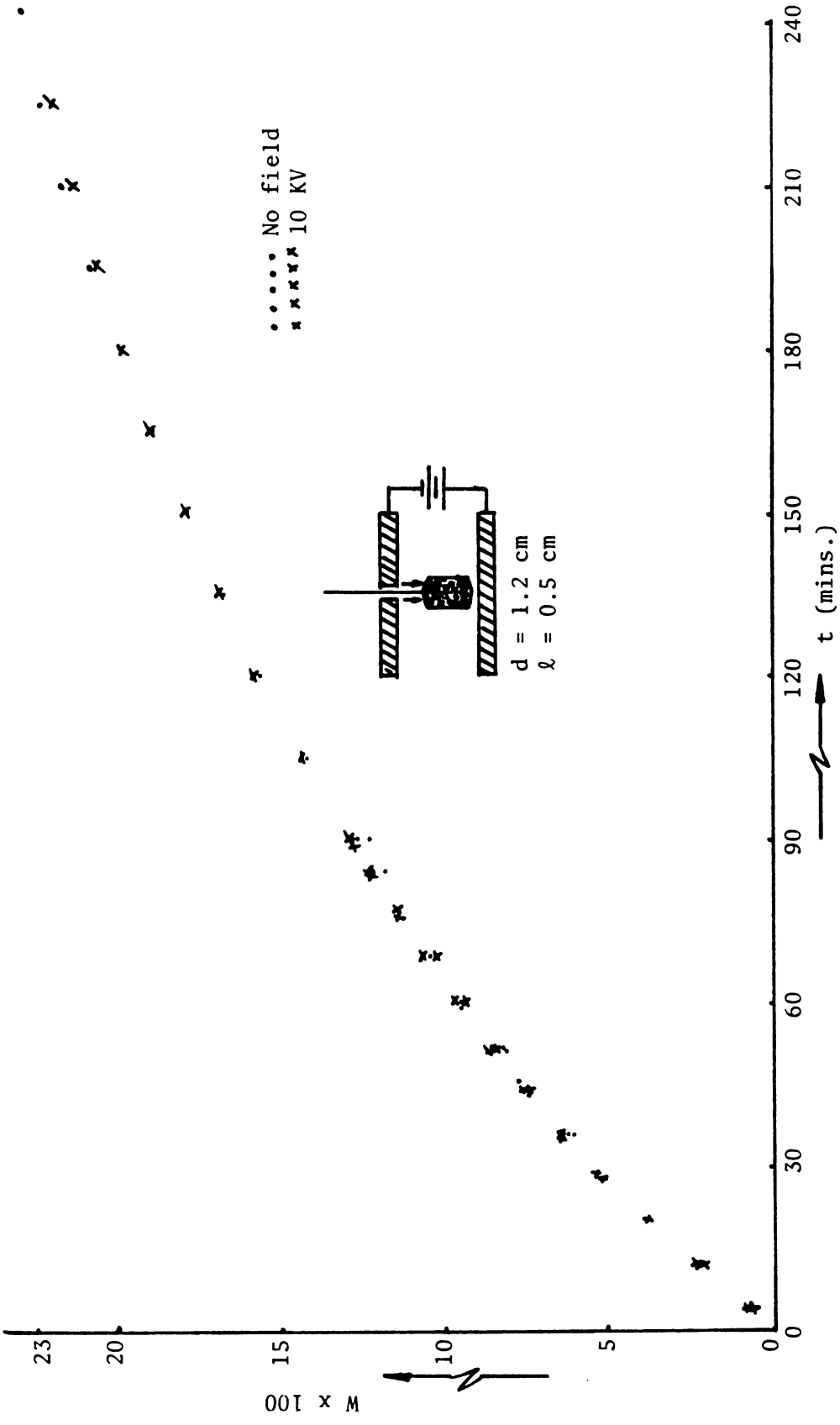

Figure 5.4. Water vapor adsorption in drying grade silica gel in uniform, applied field; T = 37° C, p/p_s = 2/3, ΔV = 10 KV.

dry). Once again, within experimental error, no discernible effects are observed due to the imposed uniform field. However, it is not essential to conclude from this that uniform applied fields have no effect on the adsorption kinetics, as has been suggested by some authors [P3,P5,P6]. Rather, as discussed later in Section 5.6(b), the magnitudes of the applied fields (and therefore the applied voltage drops) have to be much larger in order to expect any field-induced effects. In comparison, the average field magnitudes for non-uniform applied fields are much larger for similar applied voltage drops, ΔV. Also, from a knowledge of the maximum adsorption capacity of this silica gel and comparisons with other silica gels mentioned in Chapter III, it may be concluded that only three or four layers of adsorbate are formed. Surface diffusion, which predominates in such fine pored solids, may thus be expected to be influenced very little.

5.3(c) Bed of Spherical, Alundum Beads in Uniform Field

The interparticle contact points between spherical particles experience extremely high, non-uniform electric fields [M1]. To investigate the effects of such fields on the adsorption characteristics, spherical catalyst Al_2O_3 particles used in Section 5.3(a) were piled one upon the other to form a bed of spheres. This bed was subjected to a uniform field of $\Delta V \simeq 10$ KV and the environment was maintained at $p/p_s \simeq 2/3$, $T = 37^{o}$ C. The experiments were conducted just as in 5.3(a). Figure 5.5 shows the adsorption kinetics for this system with and without the field. The results imply that the above mentioned non-uniform fields are obviously too 'local' to affect appreciably the adsorption in the internal pores of alundum catalyst beads.

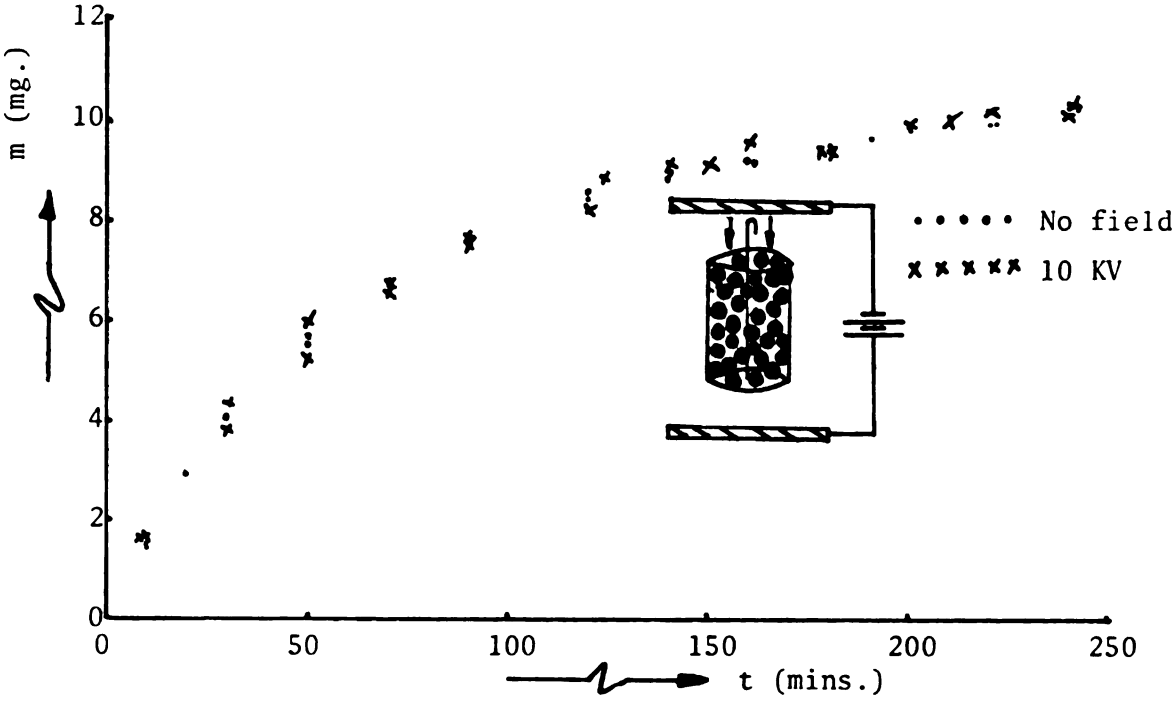

Figure 5.5. Water vapor adsorption on alundum beads in uniform electric field, ΔV = 10 KV, T = 37° C, $p/p_s \simeq 2/3$.

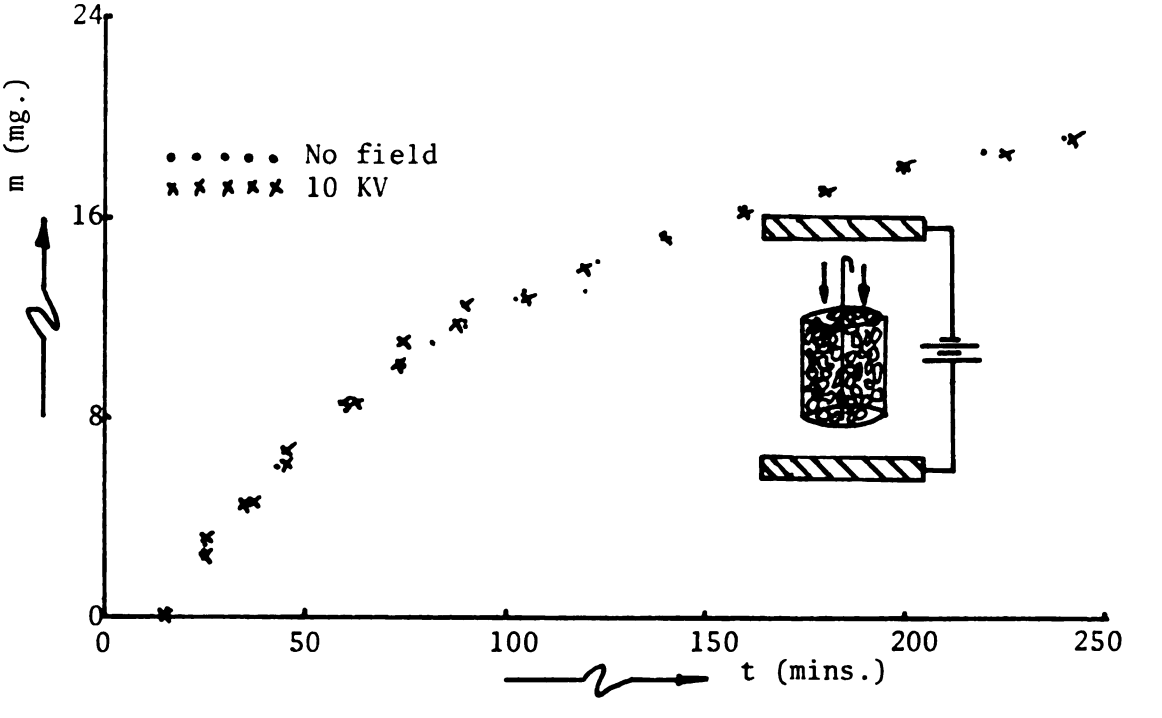

Figure 5.6. Water vapor adsorption on crushed Al_2O_3 in uniform electric field, ΔV = 10 KV, T = 37° C, $p/p_s \simeq 2/3$.

5.3(d) Bed of Crushed Alumina Beads in Uniform Electric Field

In Figure 5.6 is represented the experimental data for water vapor adsorption in crushed Al_2O_3 particles in the presence of a uniform external field of $\Delta V \simeq 10$ KV, $T = 37^{o}$ C, $p/p_s \simeq 2/3$. Once again, no appreciable effects are observed.

5.4 Adsorption in Cylindrical, Non-Uniform Electric Fields

In the following experiments a cylindrical field was created between a thin rod (or filament) and a cylindrical screen. Two sample pan geometries were utilized. In the first, an annular pan (see Figure 5.2(c) and also Figure 4.3) made of metal screen was filled with the adsorbent, and the central electrode was a thin metal rod of radius = 1/32 inch. In the second, a cylindrical metal (screen) or polystyrene foam pan with a fine filament (r = .0089 cm) passing through the axis of the pan and serving as the grounded electrode (see Figures 5.2(b) and 4.4) was filled with the adsorbent. In both cases the High-Voltage electrode was a cylindrical, metal screen of diameter = 2.5 cm.

5.4(a) Crushed Alumina in Annular Pan and Cylindrical Field

The adsorption of water-vapor in crushed alumina in the presence of a cylindrical field ($\Delta V \simeq 5.5$ to 6 KV across electrodes) was studied in four different configurations. In Figure 5.7(a) the only face of the annular pan open to adsorption was the top face. In 5.7(b) the inner cylindrical face was open with the other faces being blocked. In Figure 5.7(c) only the outer cylindrical face was open to adsorption. Finally, in Figure 5.7(d) both the cylindrical faces were open with the top and bottom faces closed off. In all four cases field calculations in Appendix

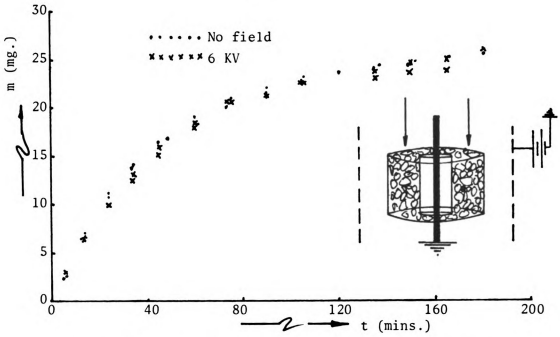

Figure 5.7(a). Water vapor adsorption in crushed alumina.

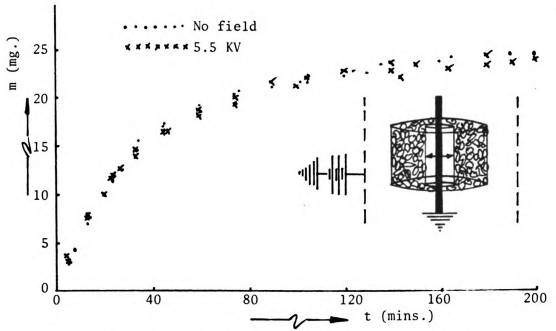

Figure 5.7(b). Water vapor adsorption in crushed alumina.

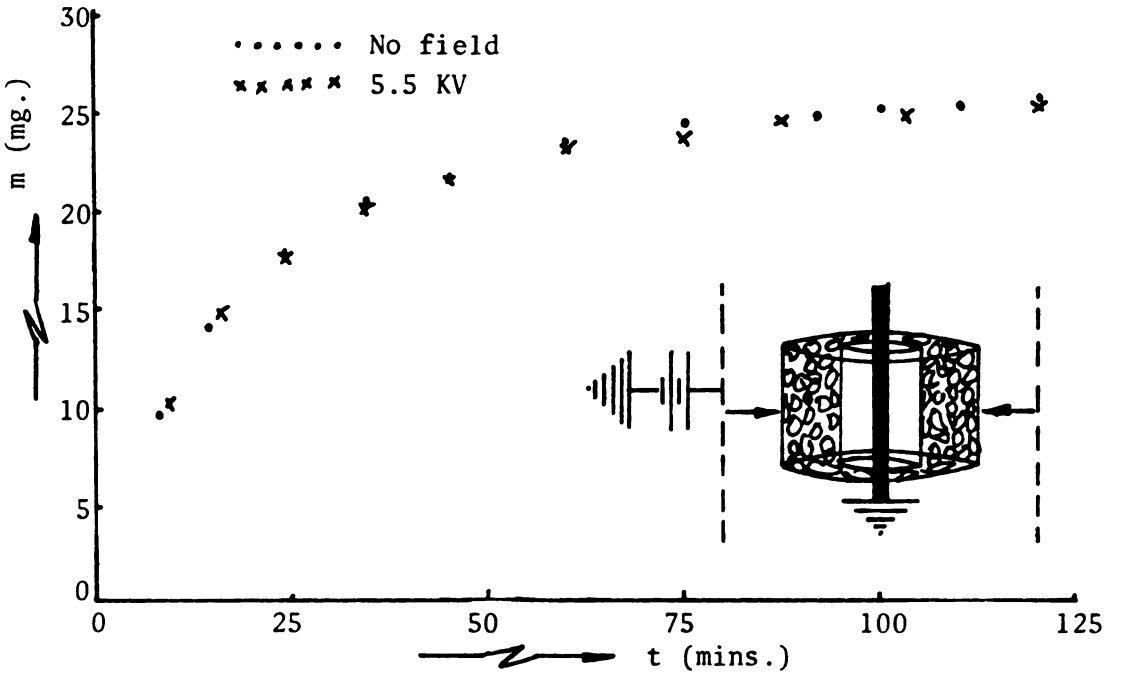

Figure 5.7(c). Water vapor adsorption in crushed alumina.

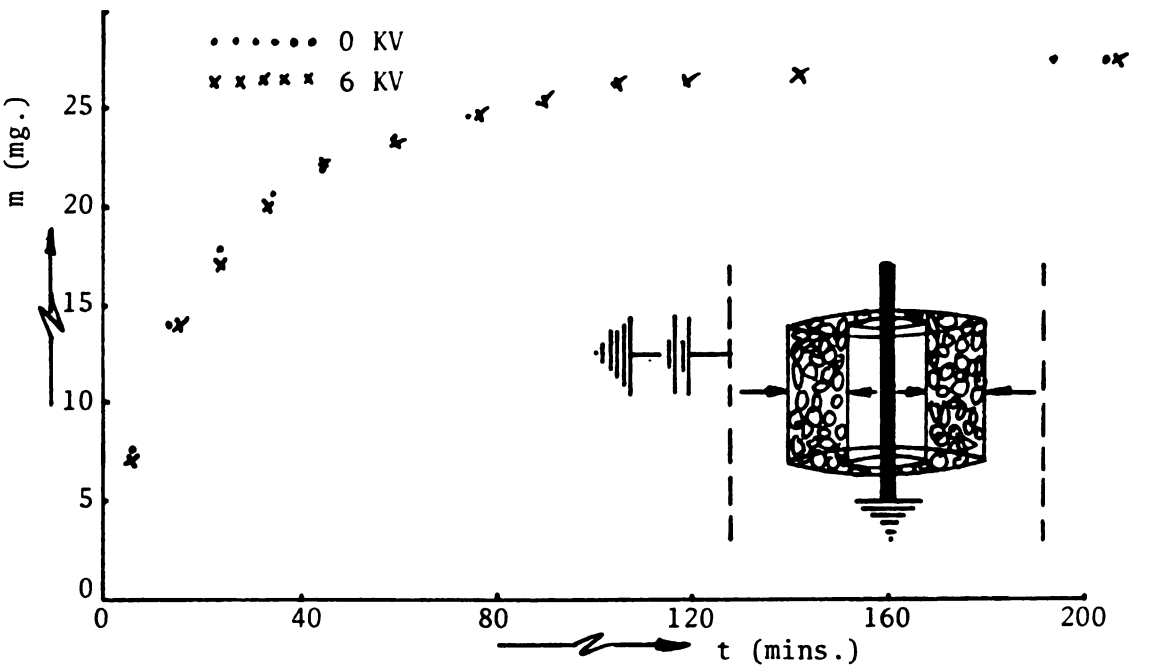

Figure 5.7(d). Water vapor adsorption in crushed alumina.

A give estimates of $\nabla E^2_{avg} = 1.97 \times 10^7$ (V^2/cm^3) and $\underset{\rightarrow}{E}_{avg} \simeq 1.78$ KV/cm. At the time these experiments were undertaken, one was still looking for the electro-convective vapor-phase flux of equation (1.4) (described earlier in this chapter). The exact significance of the dipole moment and the Boltzmann equilibrium distribution was still not very clear. If instead of μ_{eff} ($= \mu^2 E/3kT$) one used μ for the magnitude of $\underset{\rightarrow}{\mu}$ in equation (1.4) with the resulting direction of the force being random, one would then expect some sort of a local turbulence phenomenon. It was to observe this phenomenon, if possible, that the experiment in Figure 5.7(a) was conducted. From the results in that figure, it appears as though the Boltzmann equilibrium distribution is valid and the electro-turbulence phenomenon is, therefore, non-existent.† In Figures 5.7(b), (c) and (d) the objective was to simulate a closed-pore model, as mentioned earlier. Once again, it is obvious from the results obtained that the fields to which the adsorbents are subjected are too weak to have any effect on the gaseous diffusion of water vapor. In the following experiments available field strengths are further increased and so is the surrounding vapor pressure.

5.4(b) Crushed Alumina, $CaCO_3$ Powder, Porous Glass and Zeolite Beads in Strong Cylindrical Fields

Figures 5.8, 5.9 and 5.10 represent the adsorption kinetics of water vapor in crushed, porous Al_2O_3 particles, $CaCO_3$ powder and porous

---

†Rough calculations made later for the comparison of time scales over which collisions occur with those over which the electrical forces act, indicated that the former were much smaller than the latter, thus justifying the use of the Boltzmann equilibrium distribution.

glass, respectively, in the presence of a non-uniform cylindrical field. The sample pan-electrode geometry is described in Figure 5.2(b). Field calculations give (for a dry sample bed) $\nabla E^2_{avg} \simeq 3.46 \times 10^8$ (V^2/cm^3) and $\underset{\rightarrow}{E}_{avg} \simeq 1.74$ KV/cm. In these experiments $p/p_s \simeq 2/3$ and $T = 37^o$ C. Within experimental accuracy no appreciable effects are observed due to the imposed electric fields. Field gradients are as yet quite low and the amount adsorbed at $p/p_s \simeq 2/3$ is limited to the first few bound layers. Figure 5.11 shows the kinetics for water-vapor adsorption in zeolite, catalyst beads (Linde Type 3A, 1/16" pellets) at $p/p_s \simeq 1/2$ and $T = 37^o$ C. Fields estimated in this case were about $\nabla E^2_{avg} \simeq 10.2 \times 10^8$ (V^2/cm^3) and $\underset{\rightarrow}{E}_{avg} \simeq 2.98$ KV/cm. Once again, insufficient adsorption at $p/p_s \simeq 1/2$ may be cited as the major cause of insignificant field-induced effects.

5.4(c) Alundum Catalyst Beads Strung on Filament Electrode

Three cylindrical porous alundum catalyst beads were strung on the central ground electrode filament used in the previous experiments. A voltage drop of $\Delta V = 4$ KV was applied with $p/p_s \simeq 1/2$ and $T = 37^o$ C. In this configuration the average fields experienced by the beads (estimated in Appendix A.3) are $\nabla E^2_{avg} \simeq 1.90 \times 10^9$ (V^2/cm^3), $\underset{\rightarrow}{E}_{avg} \simeq 4$ KV/cm. Figure 5.12 depicts the amount adsorbed m (in mg.) vs. time t (in mins.) for this system. Again, the applied fields (higher than before) have no discernible effect on the monolayer formation rate.

5.4(d) Water Vapor Adsorption in 'Drying Grade' Silica Gel

The adsorption rate of water vapor in silica gel has been known to be enhanced in the presence of strong, non-uniform electric fields [P1, P2,P3,P5]. Having observed no discernible effects with unsaturated N_2

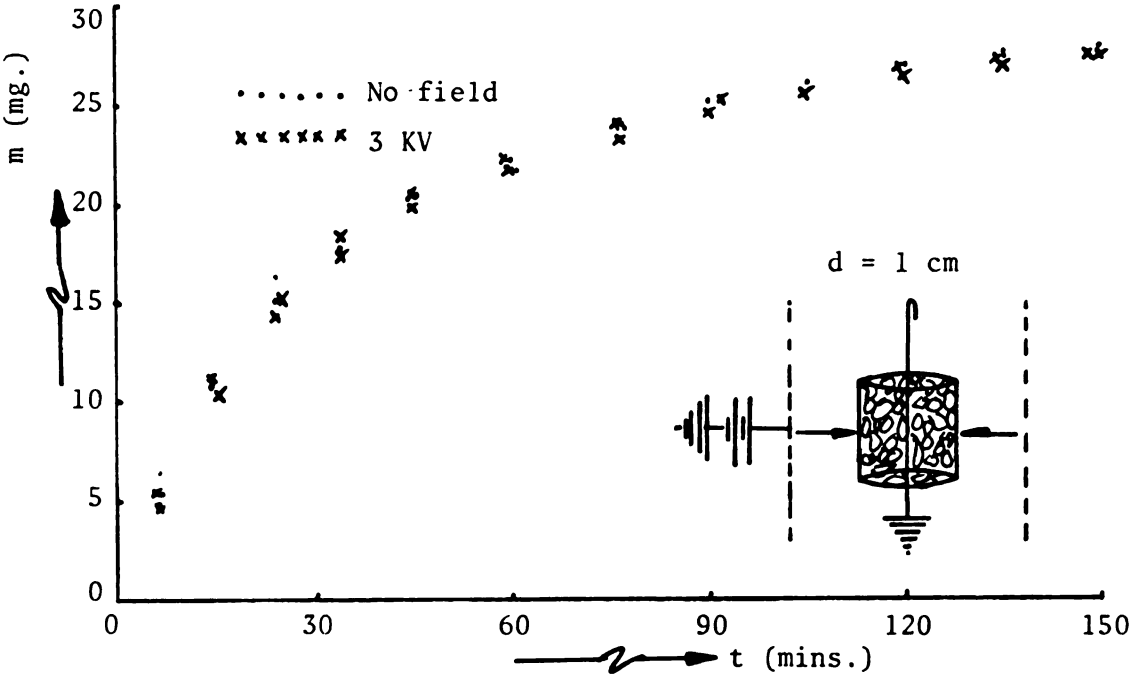

Figure 5.8. Water vapor adsorption on crushed Al_2O_3 in cylindrical field, $p/p_s \simeq 2/3$, T = 37° C.

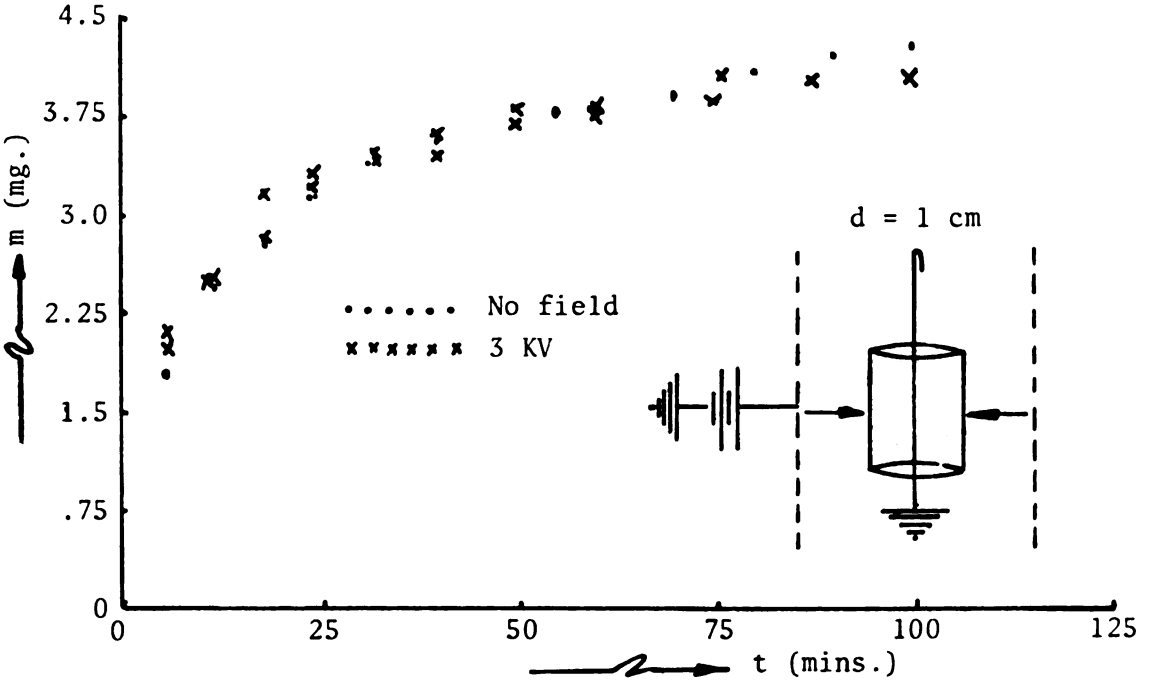

Figure 5.9. Water vapor adsorption on $CaCO_3$ powder in cylindrical field, $p/p_s = 2/3$, T = 37° C.

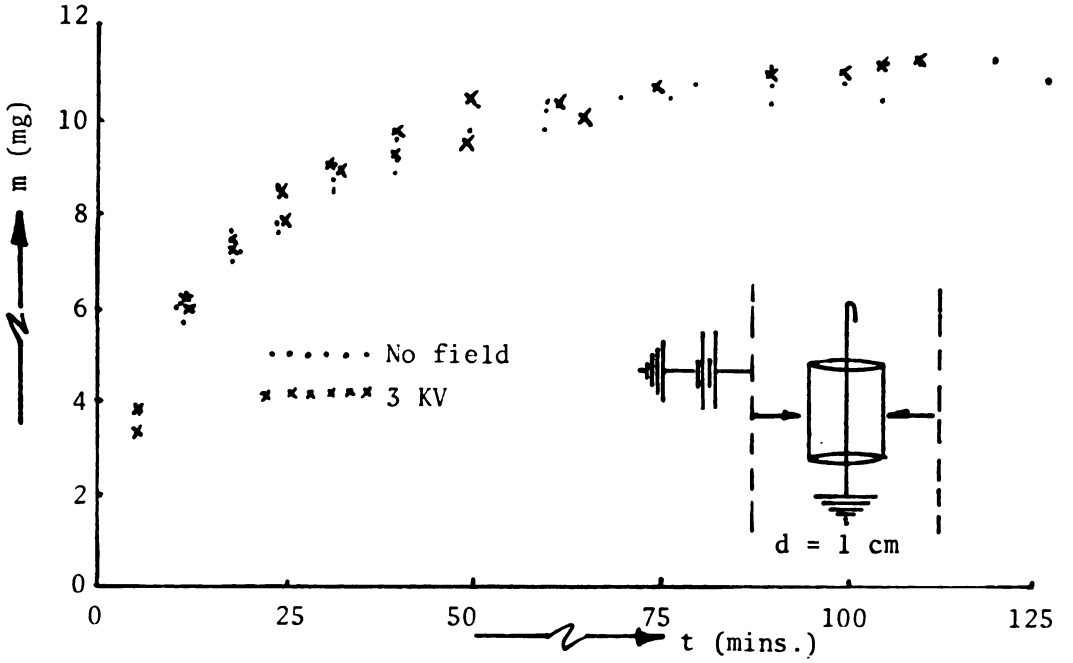

Figure 5.10. Water vapor adsorption on porous glass in cylindrical field, $p/p_s \simeq 2/3$, $T = 37^{o}$ C.

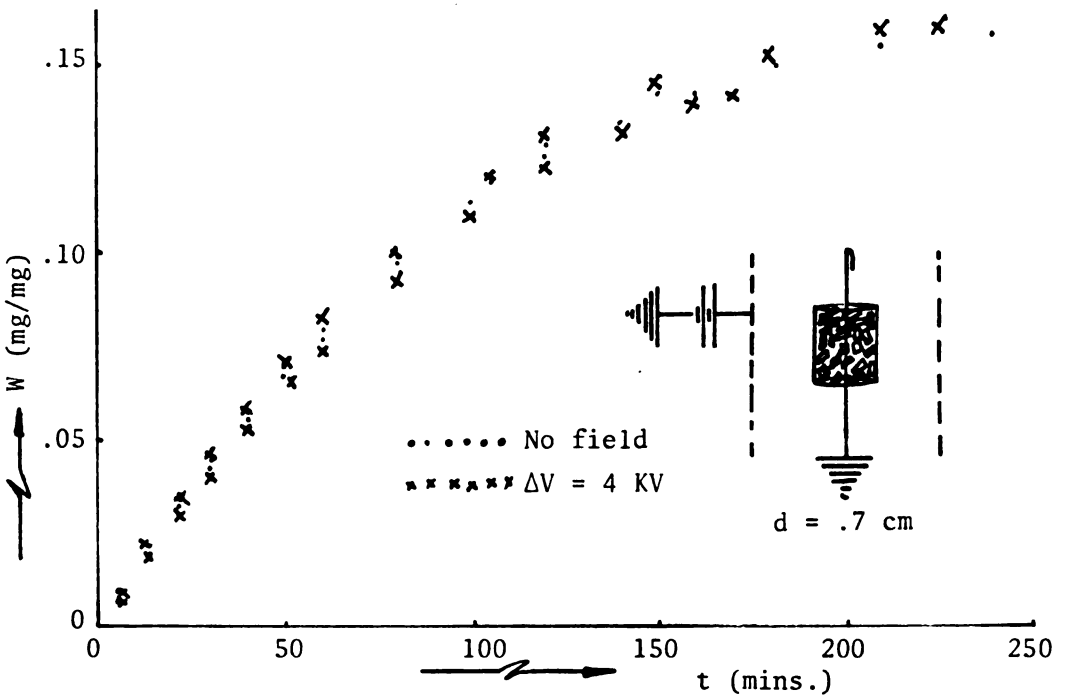

Figure 5.11. Water vapor adsorption in zeolite catalyst beads, $p/p_s \simeq .5$, $\Delta V = 4$ KV, $T = 37^{o}$ C, in cylindrical field.

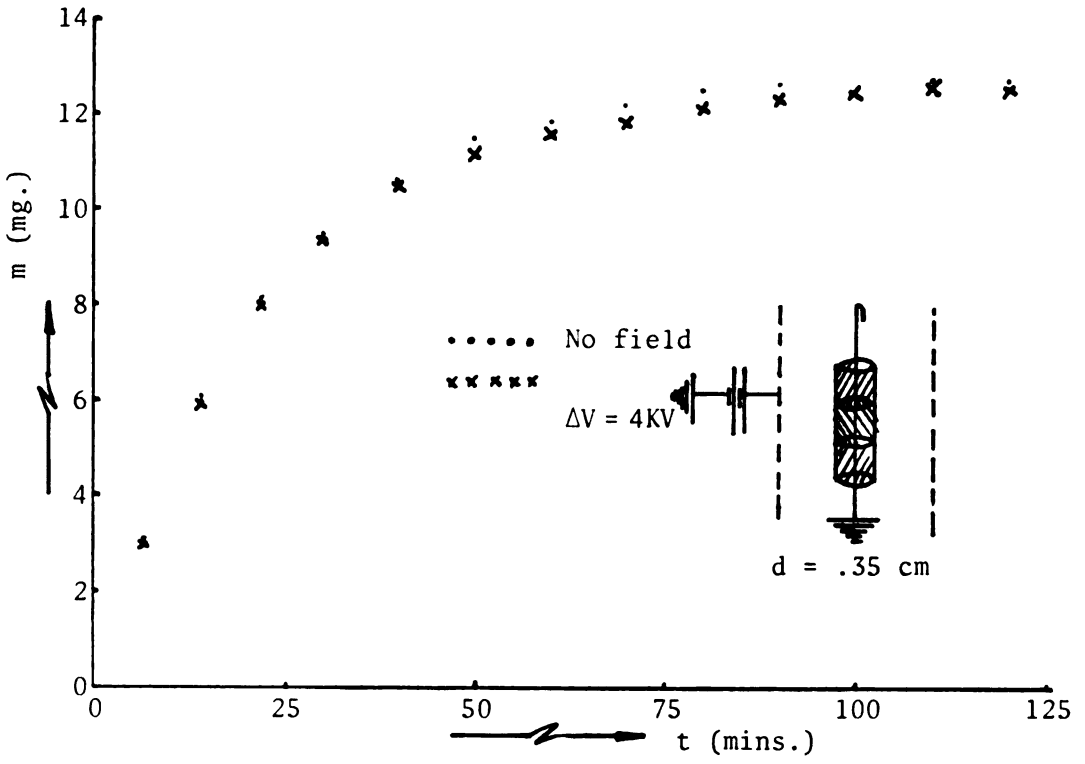

Figure 5.12. Alundum beads strung on ground filament, $p/p_s \simeq 0.5$, $T = 37^{o}$ C, V = 4 KV.

environments and fields of the order of $E_{\rightarrow avg} < 4$ KV/cm and $\nabla E^2_{avg} < 1.9 \times 10^9$ (V^2/cm^3), the relative humidity p/p_s was raised to $\simeq 1$ and available field strengths were slightly increased in order to duplicate the Russian experiments. The bath temperature was lowered to 25^{o} C, so as to avoid condensation in the tubes exposed to the surrounding laboratory temperatures. Figures 5.13(a) and (b) represent the adsorption kinetics in 'drying grade' (D.G.) silica gel with $p/p_s \simeq 1$, $T = 25^{o}$ C. In Figure 5.13(a) the pan diameter d = .7 cm and the field strengths are estimated to be $\nabla E^2_{avg} \simeq 3.91 \times 10^9$ (V^2/cm^3) and $E_{\rightarrow avg} = 5.82$ KV/cm (when $\Delta V = 6.5$ KV). Applied fields of $\Delta V = 4$ KV show no effect in the rate data. When the voltage drop is raised to 6.5 KV some enhancement is observed. In Figure 5.13(b) a narrower pan of diameter .35 cm is used and the available field strengths are consequently higher; ∇E^2_{avg}

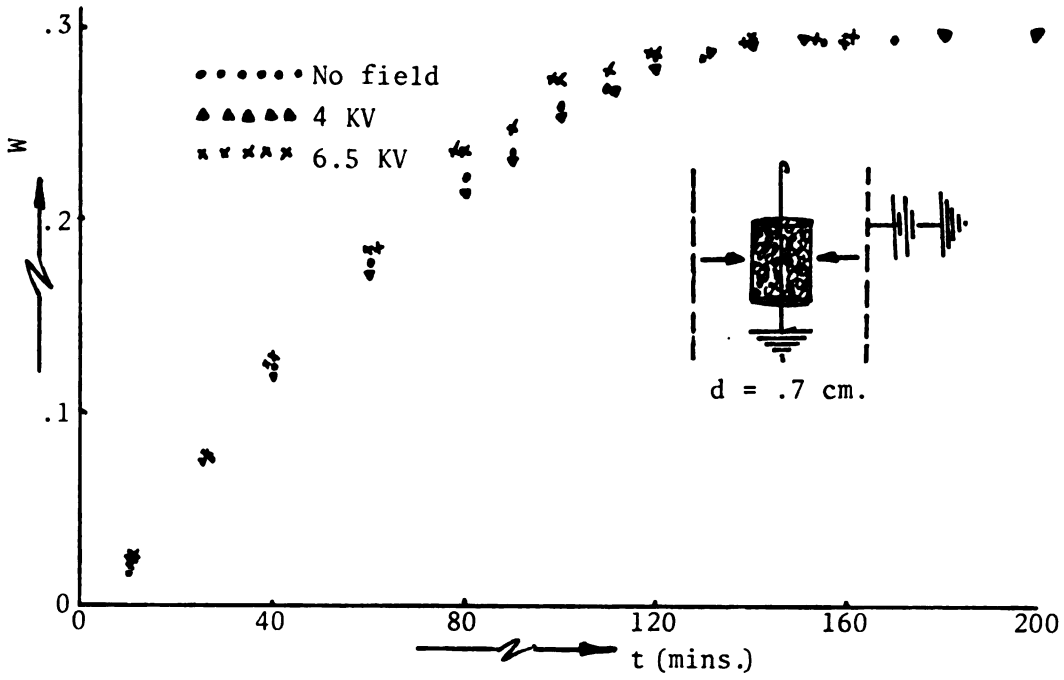

Figure 5.13(a). H_2O - silica gel (D.G.), $p/p_s \simeq 1$, $T = 25^{\circ}$ C, $\Delta V = 4$, 6.5 KV.

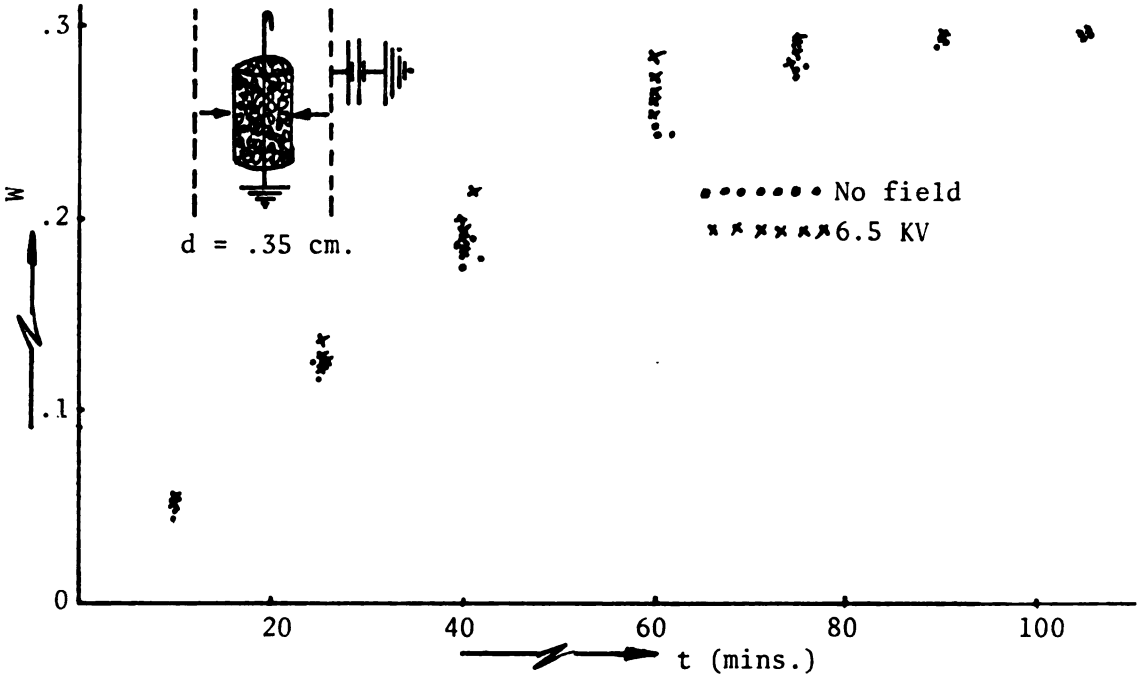

Figure 5.13(b). H_2O - silica gel (D.G.), $p/p_s \simeq 1$, $T = 25^{\circ}$ C, $\Delta V = 6.5$ KV

$= 1.24 \times 10^{10}$ (V^2/cm^3) and $E_{\rightarrow avg}$ = 10.23 KV/cm. Significant enhancement in the rate of adsorption is observed in this case. However, owing to the non-uniformity of the crushing process (to facilitate packing the gel into the narrow pan) and the resultant differences in the available surface areas and pore volumes for adsorption (each sample used only once), much scatter is observed in the data. To rectify this, uniform-sized, fine, chromatographic silica gels were procured and used in the following experiments.

For the sample electrode configurations in Figure 5.13(a) and (b), experiments were also conducted in such a way as to take only one reading after a sufficient length of time, both with and without an electric field applied. The object here was to verify whether the off-on procedure for the applied field was resulting in depolarization of the polarized adsorbate, and thus preventing any significant field-induced effects from occurring. The results in Appendix C.11 suggest that this was not the case. In view of the relaxation time for polarization for water being of the order of 10^{-11} secs., polarization is essentially instantaneous in the adsorbate and the above result is to be expected.

5.4(e) Water Vapor Adsorption in S-4133 (25 A° dia.) Silica Gel

Adsorption of water vapor was studied in uniform sized (70-140μ) chromatographic silica gel with approximate mean pore diameter of 25 A° (made by SIGMA). The cylindrical screen pan dimensions were d = .35 cm., ℓ = 2.5 cm. For applied voltages of ΔV = 6 KV, fields estimated in Appendix A.3 for this geometry give $\nabla E^2_{avg} \simeq 1.43 \times 10^{10}$ (V^2/cm^3) and $E_{\rightarrow avg} \simeq 11.01$ KV/cm. Figure 5.14 represents the adsorption kinetics for this system. The enhancement in the rate of adsorption is clearly

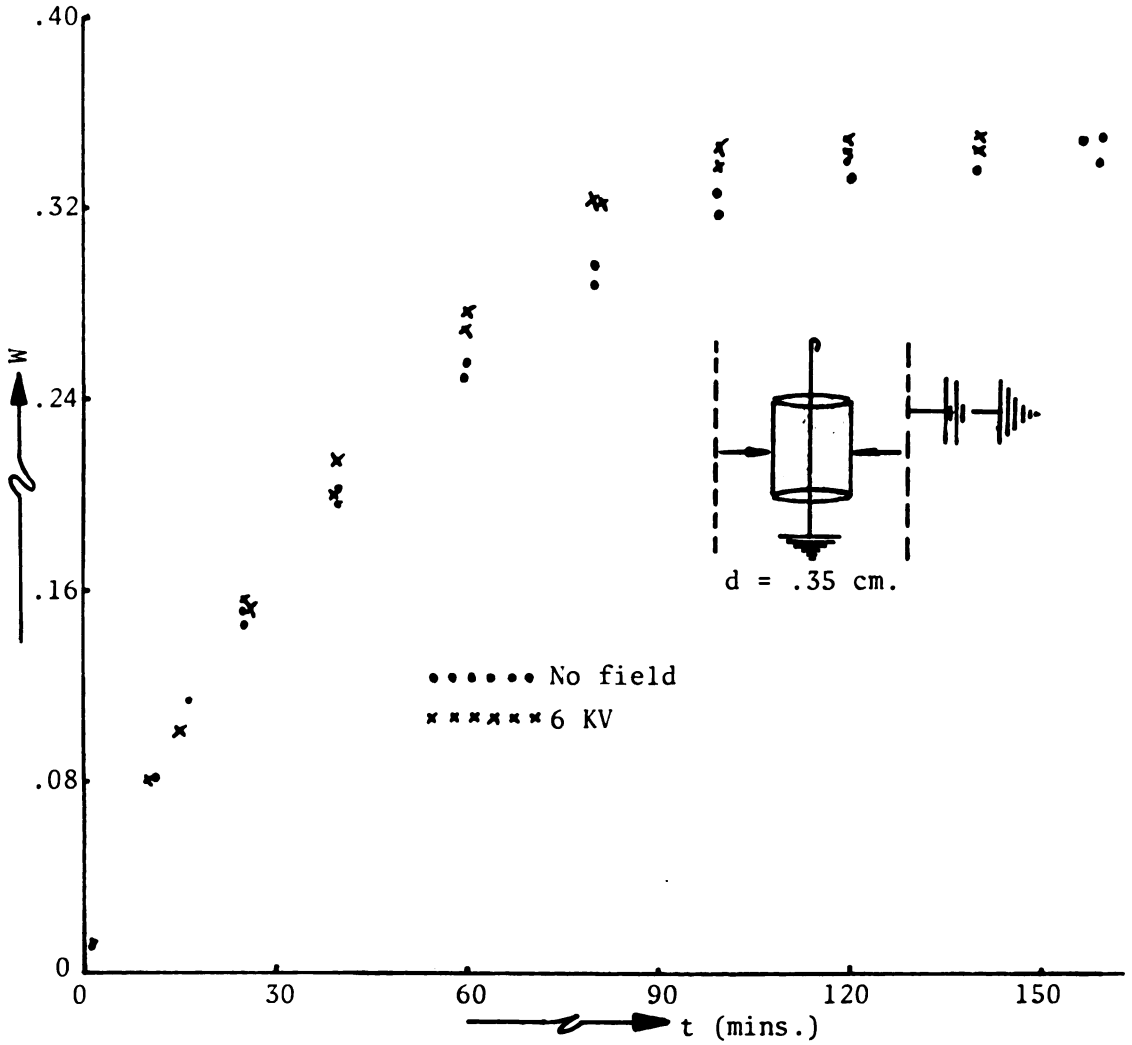

Figure 5.14. Adsorption of water vapor in Silica Gel S-4133 (25 A^{o} M.P.D.), ΔV = 6 KV, T = 25^{o} C, $p/p_s \simeq 1$.

indicated by the data obtained. A maximum amount of about 35% by weight of dry sample is adsorbed. For a mean pore diameter of about 25 A^o, the monolayer amount adsorbed corresponds to about 11.5% of dry sample weight (see Figure 3.7b). Thus, only three to four layers of adsorbate may be expected in this sample.

5.4(f) Monolayer Adsorption in S-2509 (60 A^o dia.) Silica Gel

Chromatographic grade Silica Gel S-2509 (63-200μ) with mean pore diameter around 60 A^o was placed in a highly unsaturated ($p/p_s \simeq 1/3$) humid environment at 25° C. In Section 5.5 the maximum water capacity of this gel is seen to be around 70% by weight of dry gel and the monolayer capacity around 6.5%. In Figure 5.15 the adsorption kinetics show a maximum of around 8% by weight, which corresponds to a little over a monolayer. Fields of the same magnitude as in the previous section yield no discernible effects in monolayer adsorption kinetics. More on this in Chapter VIII.

5.4(g) Water Vapor Adsorption in Porous Alundum Catalyst Beads Strung on Ground Filament Electrode at $p/p_s \simeq 1$ and T = 25° C

The experiment described in Section 5.4(c) is repeated here, but for a saturated, moist N_2 environment ($p/p_s \simeq 1$) and T = 25° C. The beads of diameter ≃ .35 cm are subjected to even higher fields of ΔV = 6 KV, $\nabla E^2_{avg} \simeq 4.28 \times 10^9$ (V^2/cm^3), $E_{\rightarrow avg} \simeq 6.02$ KV/cm. The results of the adsorption kinetics are shown in Figure 5.16. The fact that even such high fields and moist surroundings fail to produce any discernible effects in the rates indicate mainly that the field effects on the first few bound layers of adsorbate are negligible for the given field


W
mg. adsorbed (%)

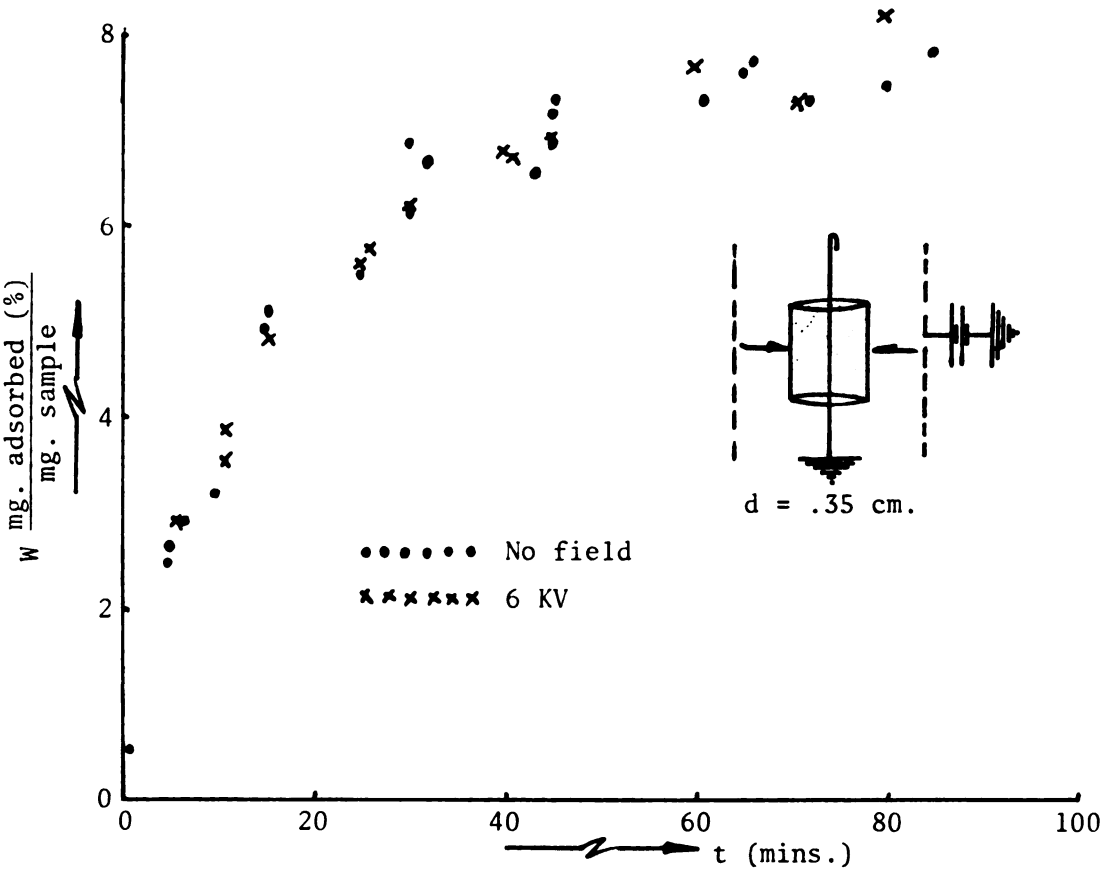

Figure 5.15. Monolayer adsorption in porous silica gel (S-2509)-H_2O vapor adsorbate - ΔV = 6 KV, $p/p_s \simeq 1/3$, T = 25° C.

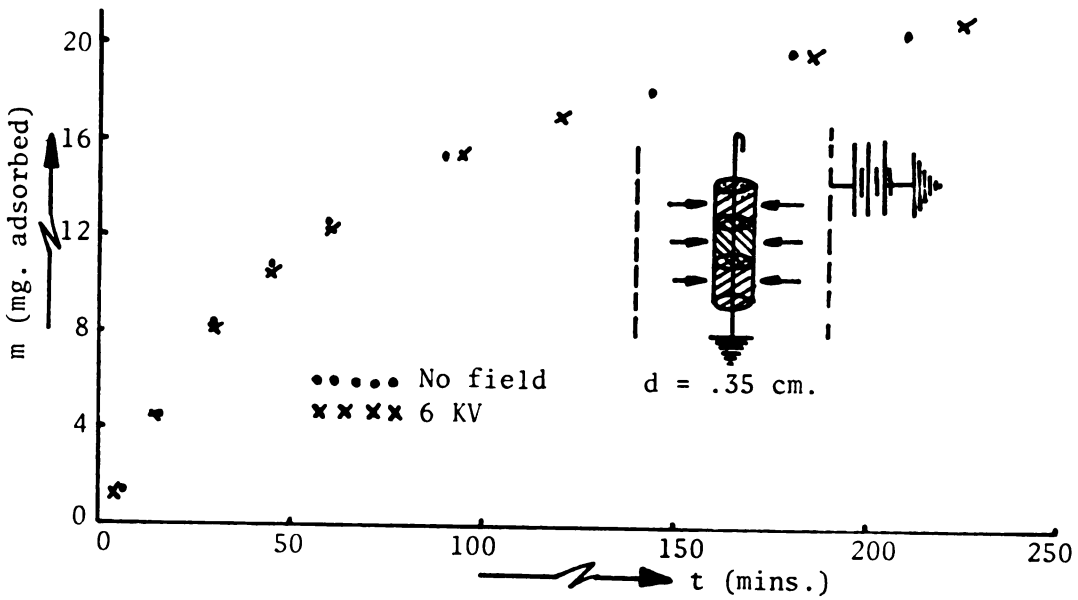

Figure 5.16. Alundum beads strung on ground filament, $p/p_s \simeq 1.0$, $T = 25^o$ C, $\Delta V = 6$ KV.

strengths. The pores in the catalyst beads are extremely fine, leading to only a few layers of adsorbate at saturation.

5.4(h) Water Vapor Adsorption in Crushed Alundum in the Presence of a Corona Field

The lower plate of the parallel plate capacitor described in Figures 5.1 and 5.2(a) was removed and a needle electrode inserted in the center, as shown in Figure 5.17. In this point-plane electrode configuration was placed a shallow polystyrene foam pan filled with crushed alundum. The pan was suspended just above the needle tip. The results of water-vapor adsorption at $T = 37^o$ C, $p/p_s \simeq 2/3$, with and without the external field are represented in Figure 5.17. A slight dielectrophoretic push on the pan due to the field was observed during the experiments. The push varied linearly with the amount of adsorbate in the system. The data in Figure 5.17 are plotted after accounting for this push. There seems to be a definite, though small, increase in the rate, as well as

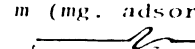
m (mg. adsorbed)

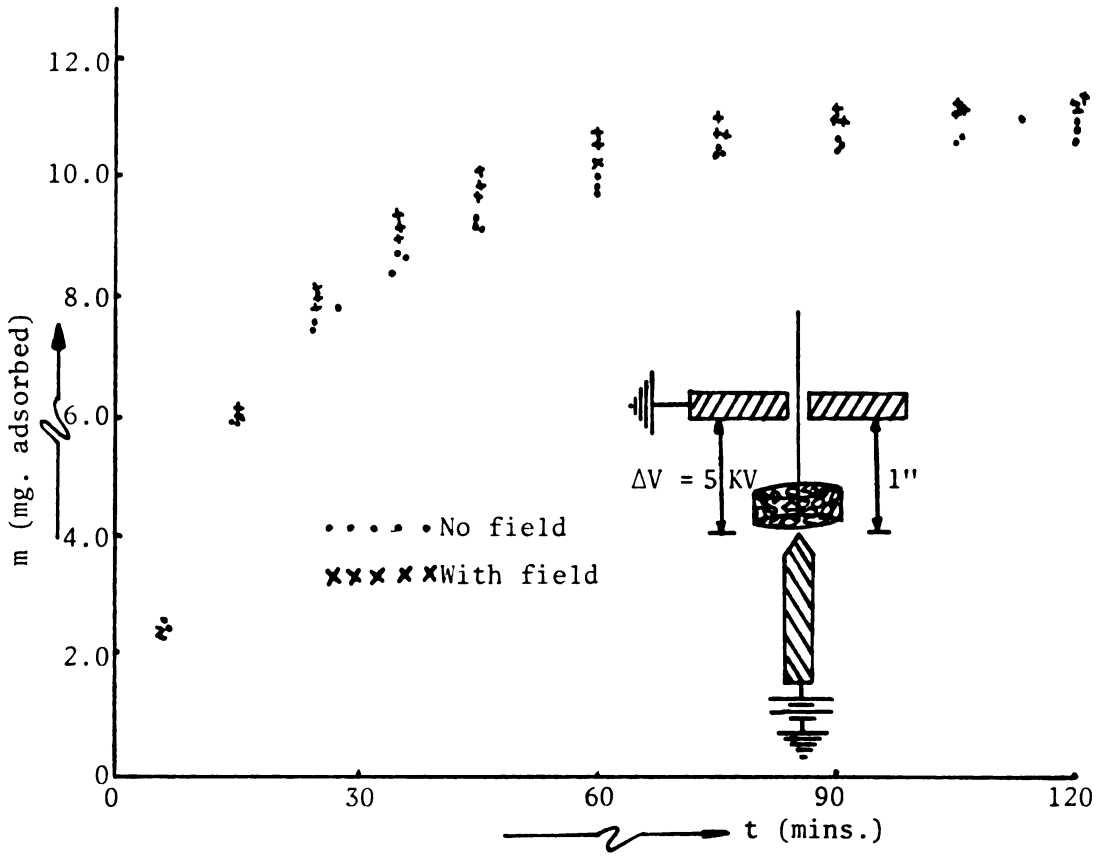

Figure 5.17. Water vapor adsorption in point-plane geometrical field--crushed alundum adsorbent.

extent of adsorption in this system. The voltage drop across the point and plane was ΔV = 5 KV and the point-plane gap was about 1 inch. Further, careful experiments have to be conducted to verify the claim made in the literature [P11,P12,K5] that corona discharge fields affect adsorption-desorption kinetics appreciably.

5.5 Multilayer Adsorption in Cylindrical Electric Fields

Figure 5.18 represents the adsorption kinetics of water vapor adsorbed in Silica Gel S-2509 (M.P.D. $\simeq$ 60 A^{o}) already used in 5.4(f), however at conditions of $p/p_s \simeq 1$. The large pore diameters of this gel allow for multilayer adsorption and/or condensation. Monolayer adsorbed water accounts for about 6.49% by weight of dry sample (see Section 3.1a). Bound layer adsorbate accounts for $\simeq$ 13.9% by weight (Section 3.1b). The mean pore radius for this gel is calculated in Section 3.1(a) to be $\simeq$ 30.7 A^{o}. Beyond 13.9% by weight adsorbate, the remaining 56.1% by weight corresponds to free, multilayer adsorbed water. Figure 5.18 indicates a significant enhancement in the adsorption kinetics of this sample, reducing the time required for saturation ($W_s \simeq$ 70% by weight) by almost 20%. Fields existing in the dry bed are estimated to be about $\nabla E^2_{avg} \simeq 1.68 \times 10^{10}$ (V^2/cm^3), $E_{\rightarrow avg} \simeq$ 11.89 KV/cm. In Figure 3.3 the adsorption isotherm for this silica gel was plotted, both with and without the applied non-uniform field. As observed in [P2], the isotherm is unaffected by the field indicating that the adsorptive forces are much stronger than the ponderomotive forces. In Chapter VI a theoretical model is proposed for the multilayer adsorption of a vapor in a single, open, cylindrical capillary pore with and without applied electric fields, and the results obtained therein are used to predict the adsorption

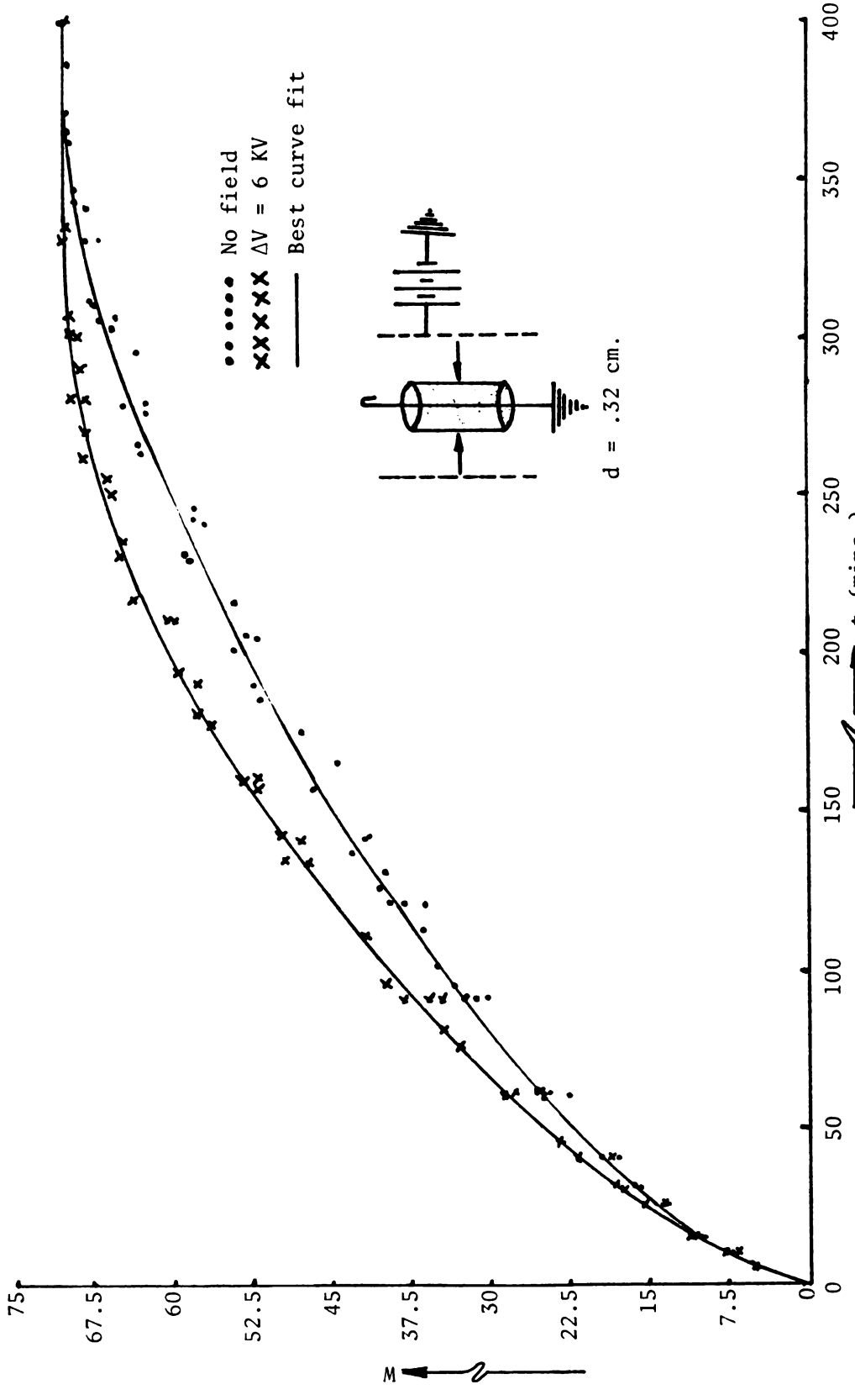

Figure 5.18. Multilayer adsorption in capillary porous Silica Gel S-2509 (M.P.D. = 60 A^{o}), $p/p_s \simeq 1$, $T = 25^{o}$ C, $\Delta V = 6$ KV, in cylindrical electrical field.

kinetics in the silica gel-water vapor system.

5.6 Further Experiments with Silica Gel S-2509 (60 A° dia.)

In this section, various experiments aimed at verifying proposed notions of the field-induced forces and also experiments to further probe the exact nature of the field and its effects on both adsorption and desorption phenomena are discussed.

5.6(a) Non-Polar Adsorbate (C_2Cl_4) and Silica Gel

Ethylene tetrachloride (dipole moment = 0, dielectric constant ≃ 2) was chosen as an excellent representative of the non-polar adsorbate group. C_2Cl_4 was adsorbed in Silica Gel S-2509 at T = 25° C.† Figure 5.19 represents the adsorption kinetics for this system. As seen in this figure, the kinetics are essentially unchanged, although the maximum amount adsorbed (≃ 106% by weight of dry sample) corresponds to capillary condensed liquid. The adsorption time is much smaller (≃ 60 mins.) than for water vapor (≃ 5 hrs.) in the same adsorbent, owing to the higher molecular weight and greater saturation partial pressure of C_2Cl_4 at 25° C. Working with CCl_4 (same dielectric properties as C_2Cl_4), the adsorption time was found to be even smaller (≃ 30 mins.), owing to the still higher partial pressures at T = 25° C; and thus the experiments were, as such, found to be inconclusive, owing to the scarcity of experimental points obtainable. In references [P2,P3,P6] CCl_4 was used to

---

†Tetrachloroethylene is toxic in nature, and therefore the entire experiment was conducted under a hood with the air suction being turned on at all times except when readings were being taken (to avoid external effects on weighing).

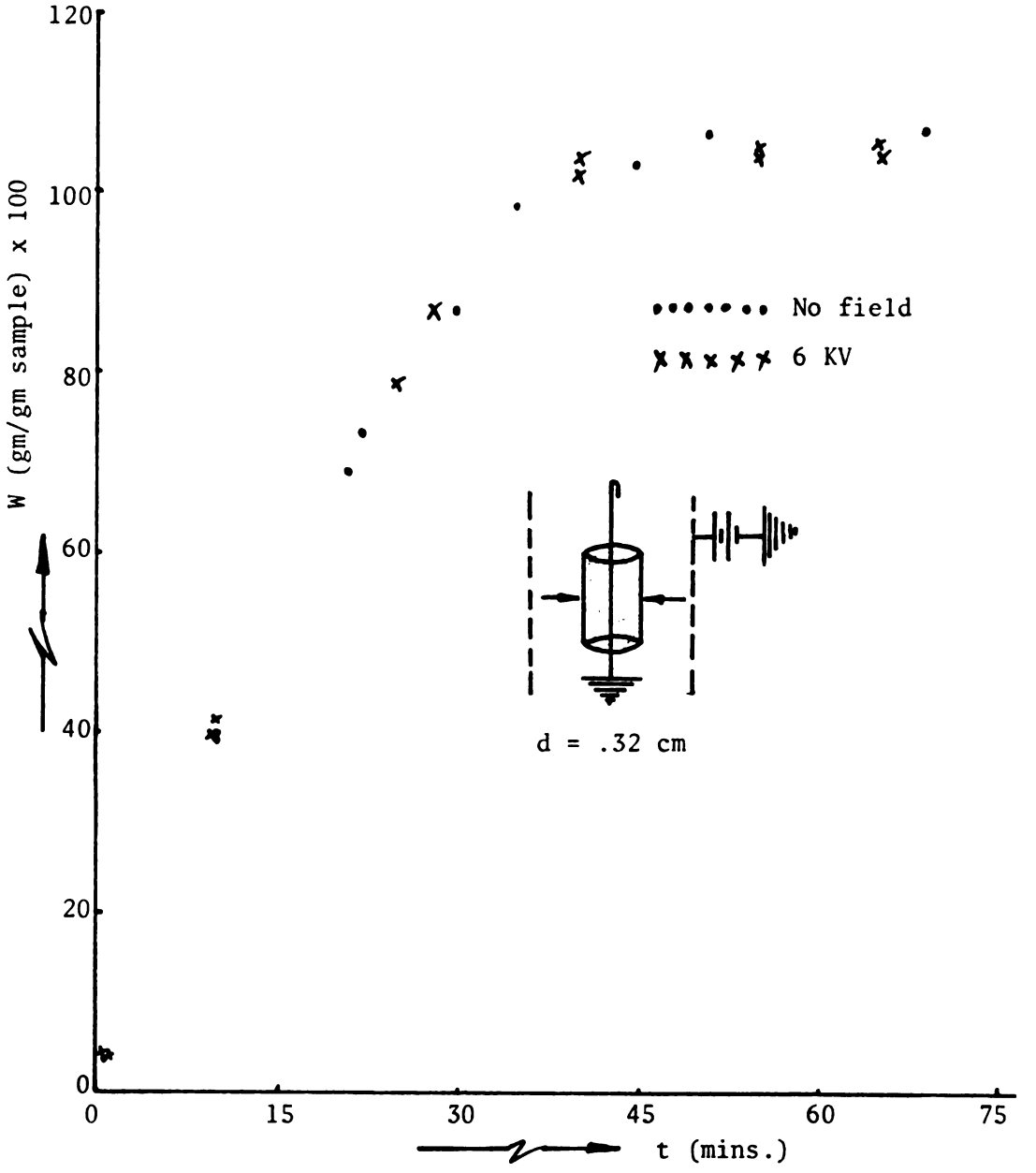

Figure 5.19. Adsorption of non-polar adsorbate C_2Cl_4 on Silica Gel S-2509, p/p_s = 1, T = 25° C, ΔV = 6 KV.

demonstrate the inability of applied fields to affect the adsorption kinetics of non-polar adsorbates. In the light of the above-mentioned observation, this seems hardly justifiable.

5.6(b) Effect of Decreasing the Gradient of External Field Squared, $\langle \nabla E^2 \rangle$, but Maintaining the Average Field Strength Squared, $\langle E^2 \rangle$

In the course of carrying out the calculations for the external field gradients (in the silica gel sample) as a function of adsorbate concentration, it was observed that the magnitudes of the macroscopic gradient of the externally applied field squared (∇E^2) were not sufficient to account for the observed enhancement in the adsorption kinetics. Further analysis showed that the internal field gradients in the fine micro-pores (resulting from fields relaxing as adsorption in the pores proceeds towards saturation) were much higher than the above-mentioned external, overall field gradients (shown in Section 4.3c). To verify the validity of this calculation, an adsorption pan was constructed as before, but instead of a fine filament ($r \simeq .0089$ cm), a thick metallic wire ($r \simeq .0348$ cm) formed the grounded, central electrode. In this fashion by increasing the applied voltage somewhat (see Appendix A.4), the average of the field squared was maintained essentially the same but the average gradient of the field squared was reduced by almost one-third the value estimated for the original pan geometry. The experimental results for the adsorption kinetics are represented in Figure 5.20. The rate of adsorption in the presence of the field changes very little due to the reduction of the overall average $\langle \nabla E^2 \rangle$. For similar average $\langle E^2 \rangle$s in the two cases compared, the adsorption kinetics are essentially similar. This seems to justify the assumption that in estimating the

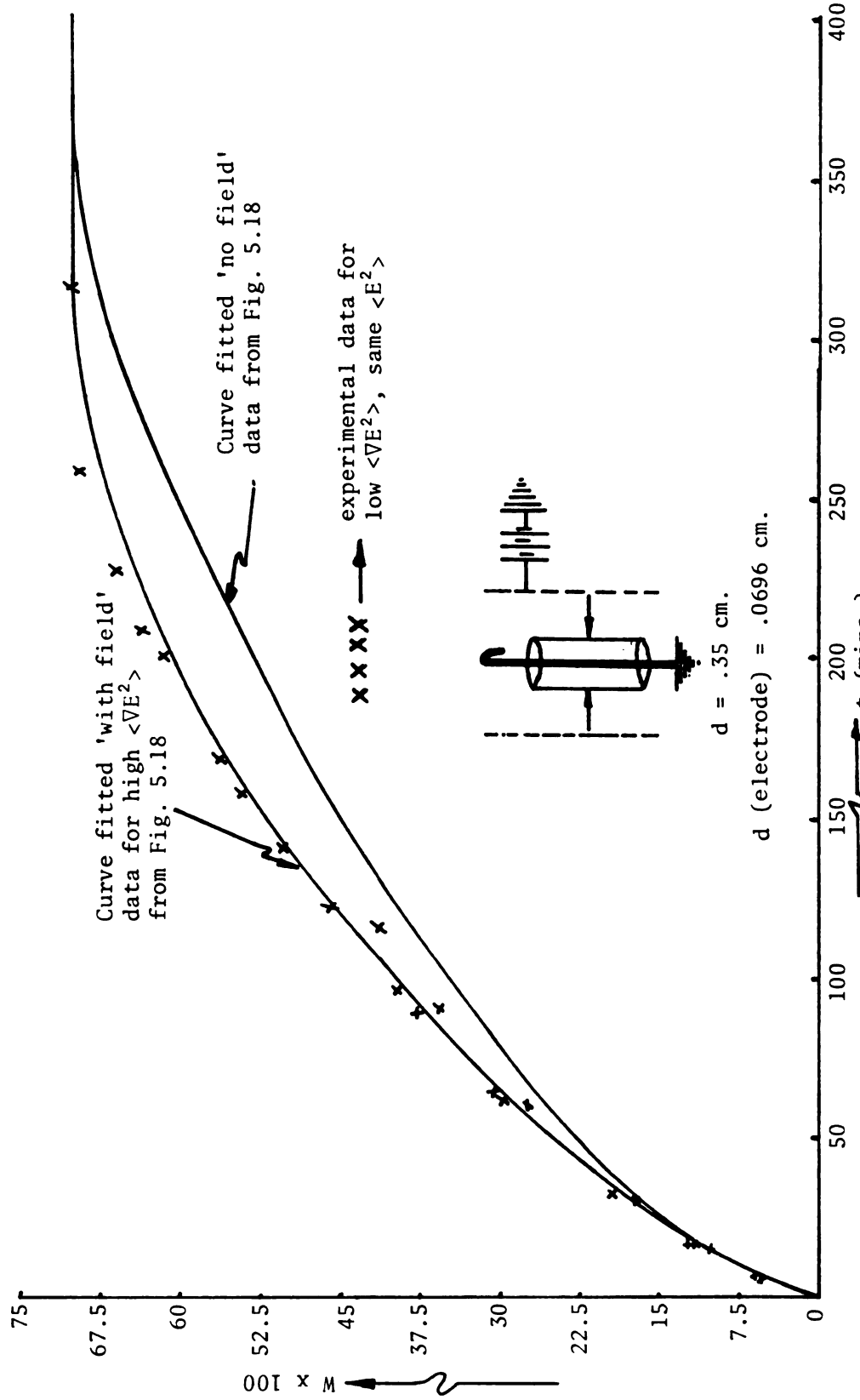

Figure 5.20. Adsorption of water vapor on Silica Gel S-2509 in the same average $\langle E^2 \rangle$ but smaller average $\langle \nabla E^2 \rangle$.

ponderomotive forces which cause the enhancement in the mass transfer rates, the internal relaxation fields in the fine pores ought to be considered rather than any overall, macroscopic, applied fields. To carry the conclusions even further, this result seems to imply that it is not really essential that the applied fields be non-uniform for the field-induced effects to be observed. Indeed, the average $\langle E^2 \rangle$s in non-uniform field configurations is quite high compared to the average $\langle E^2 \rangle$s obtainable by applying uniform external fields. For example, in Figures 5.18 and 5.20 the average $\langle E^2 \rangle$ for the dry silica gel bed is estimated to be about 2.24×10^8 (V^2/cm^2). If a uniform field between two parallel plates were to produce the same average $\langle E^2 \rangle$, then one would require an average field strength $\langle E \rangle$ of 14.97 KV/cm or a voltage drop of ΔV = 58.1 KV needs to be applied across an inch of interelectrode space (from equation 4.1, with $\varepsilon \simeq 1.53$). Thus, it may well be the extremely high voltages that must be applied across electrodes in a uniform field geometry that preclude the possibility of observing any field-produced phenomenon, rather than the experimental constraint of an externally applied uniform field.

5.6(c) Desorption Experiments: Water Vapor-Silica Gel

As explained in Section 3.1(a), the desorption process from narrow cylindrical pores filled with capillary-condensed liquid is supposed to take place by a very different mechanism than in the case of adsorption. The liquid meniscus contracts and becomes concave towards the vapor. It is hemispherical in shape with the radius of curvature given by $(R_o - t_c)$, where R_o is the capillary radius and t_c is the thickness of the adsorbed film (see Figure 5.21). The pressures at the gas-liquid interface

(given by the Kelvin equation for curved surfaces of tension, equation 3.2) are extremely high, and ordinary applied electric fields may not be expected to alter them significantly. Also, the desorption mechanism is best visualized as brought about by vapor molecules diffusing to the mouth of the pore along the adsorbed mono- or di-layer film on the pore walls (see Figure 5.21). The pressure gradient driving force for this kind of surface diffusion is due to much higher surface pressures than in the case of multilayer adsorption. The magnitudes of theoretically derived electric field-induced diffusion fluxes do not compare favorably with the ordinary surface fluxes just described. Figure 5.22 represents the kinetics of desorption of water vapor in Silica Gel S-2509 (M.P.D. = 60 A^{o}). The experiments were conducted both with and without an applied, cylindrical electric field (ΔV = 6.6 KV). Within experimental error, no appreciable changes in the desorption kinetics were noted. Of course, the literature abounds with results of enhanced evaporation rates from capillary porous bodies in the presence of corona discharge fields [P11,P12,K5]. The enhancement in the fine-pored bodies (diameters 20-60 A^{o}) has to be ascribed to the presence of ionic charges and the resultant reduction in the vapor pressure above the capillary mouths [P12] and not to any field-induced phenomenon.

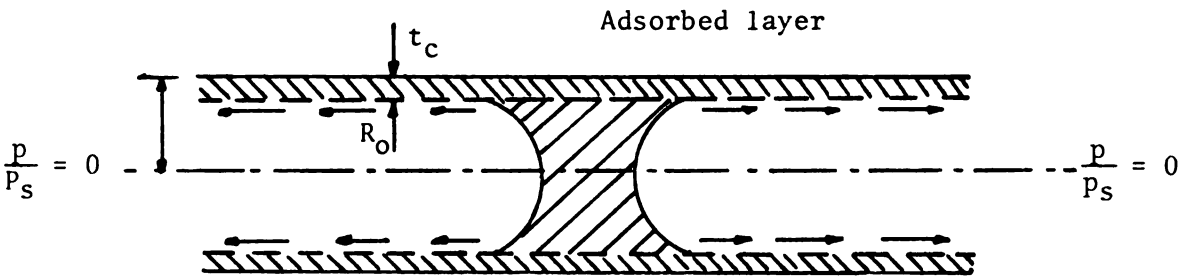

Figure 5.21. Desorption from a cylindrical pore.

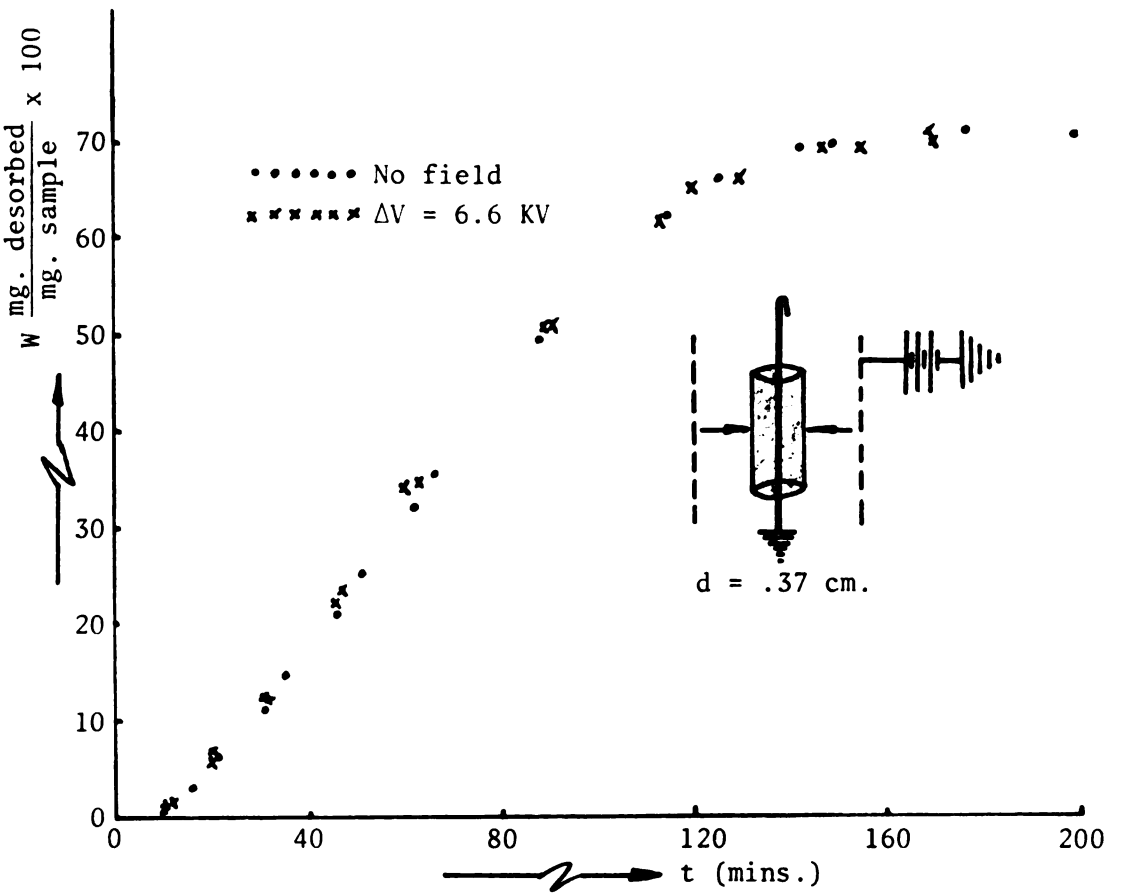

Figure 5.22. Desorption kinetics, water vapor - Silica Gel S-2509, $p/p_s \simeq 0$, T = 25° C, $\Delta V \simeq 6.6$ KV.

5.7 Preliminary Experiments with Treated Silica Gel S-2509

In this final section, the industrial Silica Gel S-2509 was subjected to chemical treatment with the intention of obtaining some preliminary information on the role of alkali ions in the adsorption process. Industrial specimens of silica gel always contain various ionic impurities [A2]. The Silica Gel S-2509 was found to contain significant amounts of sodium.† The gel was placed in concentrated hydrochloric acid overnight to remove any foreign ions [D4] and then washed thoroughly with deionized water. The sample treated in this way (Sample I) had significantly lesser amounts of sodium and essentially no chlorine. The deionized silica gel was next placed in a saturated KCl solution for about 24 hours. The KCl-treated sample was then thoroughly washed with deionized water. The resulting chlorine-free sample contained small amounts of K^+ ions (Sample II).

In Figure 5.23 are shown the adsorption kinetics of water vapor in silica gel samples I and II, with and without an imposed, cylindrical electric field. As can be seen from the results, the two samples, I and II, behave rather identically. This might indicate that the potassium concentrations are much too small to show any specific differences. The 'no field' adsorption data are somewhat higher than that for the 'untreated' Silica Gel S-2509 used until now. The 'with field' data are, however, not correspondingly higher than that for the 'untreated' sample. Two reasons may be offered at this point to help explain this decrease

---

†The relative concentrations of Na, K, Cl and other elements in the silica gel samples were estimated by the "Neutron Activation Analysis' technique in the M.S.U. nuclear laboratory.

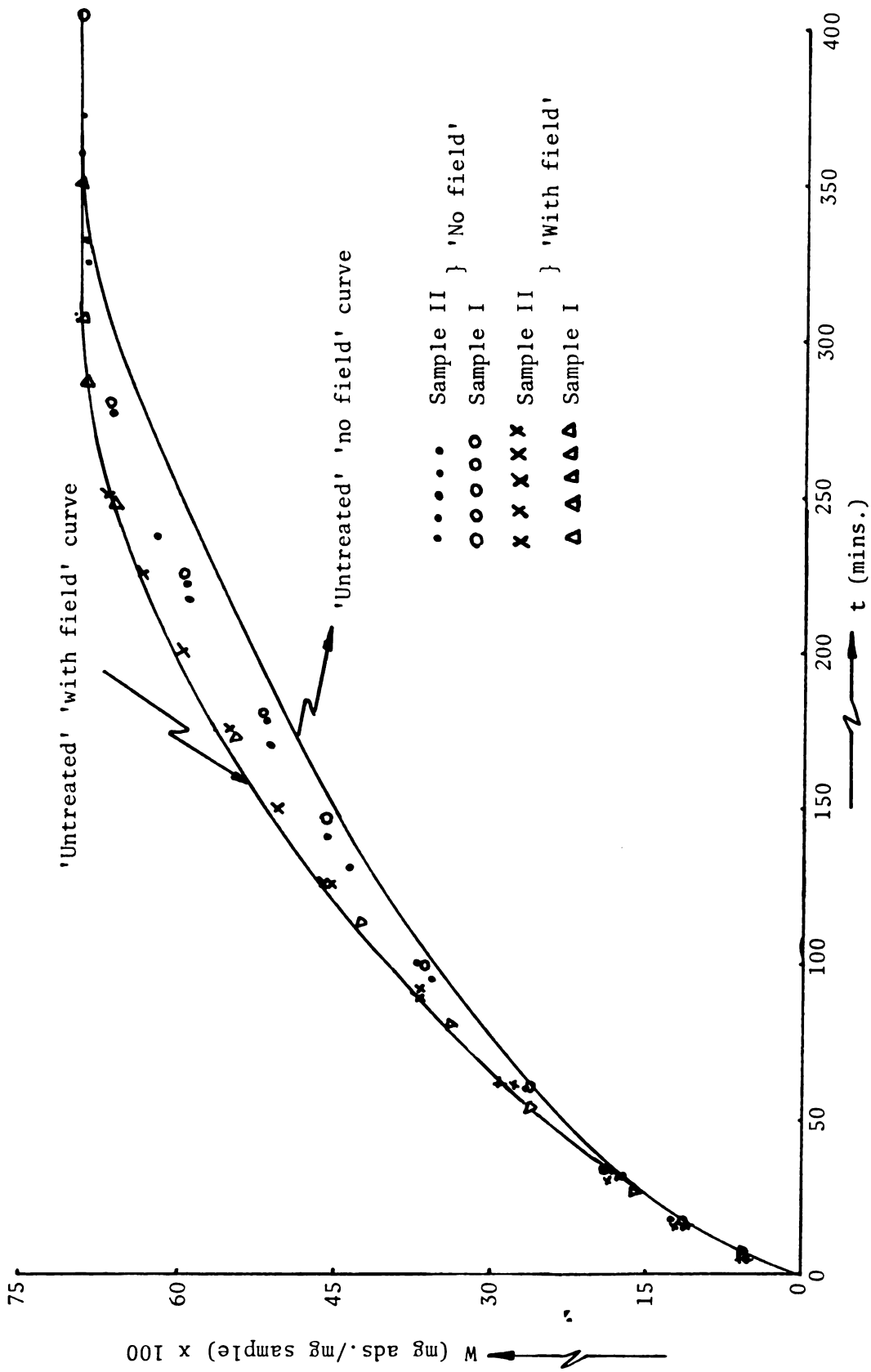

Figure 5.23. Water vapor adsorption in silica gel treated with HCl and KCl solutions at T = 25° C, $p/p_s \simeq 1$, $\Delta V = 6$ KV.

of 'field-induced' adsorption rate due to the chemical treatment: (1) the Na^+ ions which were originally in the sample also played a role in the 'enhancement' of field-induced adsorption kinetics;† (2) the removal of significant quantities of sodium from the gel matrix could have altered the gel surface characteristics considerably, thereby also affecting the polarizabilities of the adsorbed water and the resultant field forces.

One is tempted to choose the first explanation over the second one. However, the removal of Na^+ ions from the sample should have decreased the activity of the gel by providing fewer sorption centers at the inner surface of micropores in the gel [P1]. Instead, the activity is actually slightly increased. Whatever the actual explanation, it seems clear that the enhancement of adsorption kinetics in the untreated silica gel sample is at least partially due to reasons other than the impact of ponderomotive forces on the adsorbed water. The authors in [P1] have observed definite improvements in the adsorption kinetics due to the introduction of significant amounts of Ca^{2+} and K^+ ions. More work needs to be done to estimate the exact role of the alkali ions in the field-induced adsorption phenomena.

---

†As mentioned earlier, the field-induced adsorption kinetics in the system Silica Gel S-2509-water vapor is predicted in a theoretical 'single-pore' model described in Chapter VI. Since only the effects on polarized adsorbate is considered in this model (the role of surface alkali ions, Na^+ in this case, is excluded), the HCl treated silica gel 'no-field' kinetics of Figure 5.23 are used to predict the 'with field' adsorption rate curve.

CHAPTER VI

MATHEMATICAL MODELING: MASS TRANSPORT IN A SINGLE, OPEN CAPILLARY PORE IN THE PRESENCE OF AN ELECTRIC FIELD

In this chapter the mathematical mass transport model for water vapor diffusion and adsorption in an open, cylindrical pore is presented. Boundary and initial conditions similar to those existing in the silica gel bed used in the experiments are imposed. The mass balance equation is solved numerically on the computer, using the implicit finite difference scheme. Solutions for the concentration profiles in the pore are obtained for both the 'with field' and 'without field' cases. Finally, the relative adsorption rates obtained in the 'single pore' model are applied to the actual experimental 'no field' data in order to predict the 'with field' adsorption kinetics. The predicted and experimentally obtained adsorption rate curves are then compared.

6.1 The Mathematical Problem

Figure 6.1 depicts a single, cylindrical, open pore of radius R_o and length L. Diffusion of water vapor into this pore can be brought about by primarily two mechanisms (see discussion in Chapter III, Section 3.2a): first, by a combination of Knudsen and surface diffusion in the vapor phase, and second (simultaneously), by a bulk adsorbate volume flow.

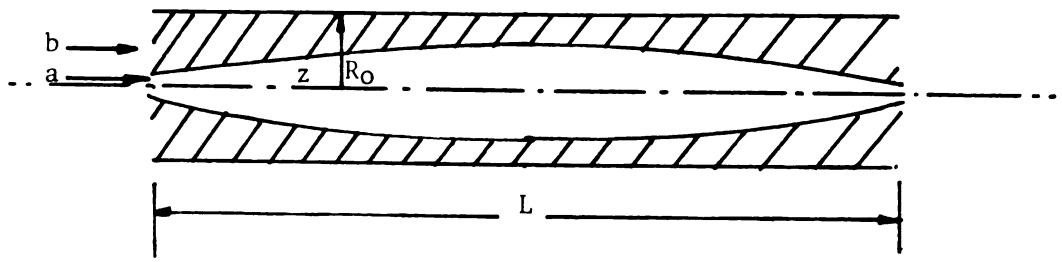

Figure 6.1. Single, cylindrical, open pore: (a) Knudsen and surface diffusion; (b) bulk adsorbate volume flow.

As briefly discussed in Chapter III, the bulk adsorbate volume flow is generally expected to be small, owing to the strong adsorbate-adsorbent interactions. For gaseous diffusion with surrounding relative pressure $p/p_s \simeq 1/3$, bulk volume flow in silica gel is non-existent, as only a monolayer is known to form. Estimates for the diffusion coefficient for monolayer formation rate are obtained by fitting the mathematical model (to be described) to the experimental data. Correcting this coefficient for the concentration dependence, as given by equation (3.16), and using the corrected estimate for the coefficient in the mathematical model when the surrounding $p/p_s \simeq 1$, gives a fairly good fit for the experimental data. This seems to suggest that surface diffusion is the predominant mode of transport in the fine-pored capillaries. Gaseous Knudsen diffusion combined with surface diffusion of adsorbed molecules during the residence time of adsorption will be considered here to represent fully the mechanisms of mass transport. Further, in equation (3.10) it was seen that the contribution to the overall diffusion coefficient from the surface diffusion mechanism far exceeds that due to Knudsenian diffusion. Equation (3.21), then, represents the mass flux into this cylindrical pore in the presence of an electric field

$$J_z = -D_s\left(\frac{dC_g}{dz} - \frac{M}{RT}\,\frac{\epsilon_o(\epsilon_s-1)}{2}\,\frac{d\vec{E}^2}{dz}\right) \tag{3.21}$$

where the surface diffusion coefficient D_s is defined in equation (3.16) as

$$D_s = K\lambda v_s \frac{RT}{M} C_g = K' C_g \tag{3.16}$$

Equation 3.21 may be rewritten as

$$J_z = -D_s\left[1 - \frac{M\epsilon_o(\epsilon_s-1)}{RT \times 2 \times (dC_g/dz)} \times \frac{d\vec{E}^2}{dz}\right] \times \frac{dC_g}{dz} \tag{6.1}$$

$$= -D_s^e \frac{dC_g}{dz}$$

where

$$D_s^e = D_s\left[1 - \frac{M\epsilon_o(\epsilon_s-1)}{RT \times 2 \times (dC_g/dz)} \times \frac{d\vec{E}^2}{dz}\right] \tag{6.2}$$

is the enhanced diffusion coefficient in the presence of the electric field (note that in the pore the gradient of the field squared and dC_g/dz are always opposite in sign, thus always enhancing D_s).

Writing a mass balance for the water vapor adsorption in this single, cylindrical pore is made exceedingly complex due to two main reasons:

1) The cross-sectional area through which diffusion takes place varies all along the pore, as the adsorbate concentration profile is dependent on the gas-phase concentration profile in the pore.

2) The electric field is a function of the adsorbed amount which, in turn, is a function of C_g (thus introducing a second source of

non-linearity).

In Figure 6.2 is shown an elemental volume in the pore. The mass balance over such a volume is given as

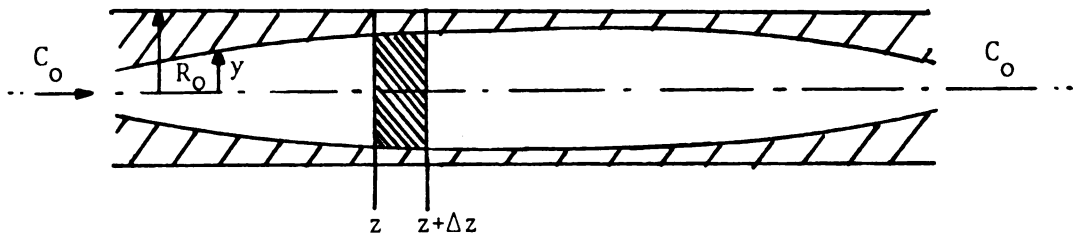

Figure 6.2. Elemental mass balance.

$$J_z A\big|_z - J_z A\big|_{z+\Delta z} = \frac{\partial C_g}{\partial t} \Delta V_g + \frac{\partial C_s}{\partial t} \times 2\pi R_o \Delta z \qquad (6.3)$$

where $A\big|_z$ is the area of cross section for diffusion. For surface diffusion $A\big|_z$ is given by

$$A\big|_z \simeq 2\pi\sigma y\big|_z$$

where σ is the thickness of the surface layer through which the surface diffusion occurs (assumed to be a constant).

R_o = radius of empty pore

$(R_o - y)$ = thickness of adsorbed layer, y is defined in Figure 6.2

C_g = gas phase concentration (g/cm^3)

C_s = adsorbate surface concentration (g/cm^2)

$\Delta V_g = (\pi y^2\big|_z + \pi y^2\big|_{z+\Delta z}) \frac{\Delta z}{2}$ = volume of gas in element

In general, when adsorption is present

$$\frac{\partial C_s}{\partial t} \times 2\pi R_o \Delta z >> \frac{\partial C_g}{\partial t} \Delta V_g$$

and one may neglect the latter term. From equations (6.1) and (6.2) the mass flux may be written as

$$J_z = -D_s \frac{\partial C_g}{\partial z}$$

or

$$J_z' = -D_s^e \frac{\partial C_g}{\partial z}$$

where the prime refers to the presence of an electric field. Therefore, from equation (6.3)

$$-D_s \frac{\partial C_g}{\partial z} \times 2\pi y\sigma\Big|_z + D_s \frac{\partial C_g}{\partial z} \times 2\pi y\sigma\Big|_{z+\Delta z} = \frac{\partial C_s}{\partial t} \times 2\pi R_o \Delta z$$

Dividing by Δz and taking the limit as $\Delta z \to 0$, one gets

$$\frac{\partial}{\partial z}\left(D_s \frac{\partial C_g}{\partial z} y\sigma\right) = R_o \frac{\partial C_s}{\partial t} \tag{6.4}$$

or

$$\frac{\partial}{\partial z}\left(D_s^e \frac{\partial C_g}{\partial z} y\sigma\right) = R_o \frac{\partial C_s}{\partial t} \tag{6.5}$$

Inserting the expression for D_s^e given by equation (6.2) and the relation $D_s = K'C_g$ from equation (3.16) into equation (6.5), one obtains

$$\frac{\partial}{\partial z}\left[K'C_g\left(\frac{\partial C_g}{\partial z} - \frac{M\varepsilon_o}{2RT} \times (\varepsilon_s - 1) \frac{dE^2}{dz}\right) y\sigma\right] = R_o \frac{\partial C_s}{\partial t} \tag{6.6}$$

At this point, the often used assumption that the adsorbate phase and the gas phase are at all times in dynamic equilibrium is invoked; i.e., $C_s = f(C_g)$, where the relationship between C_s and C_g is obtained from the adsorption isotherm. Once again, since C_s is not a linear

function of C_g (see Figure 3.3), the adsorption isotherm is broken into several regions, each of which may be approximated as a linear variation of C_s with C_g. Thus, one may write

$$C_s = k_1 C_g + k_2$$

where k_1 and k_2 are constants varying with each region of C_g chosen.

Inserting the above expression for C_s and carrying out the required differentiations in equation (6.6), one obtains

$$(C_g y)\frac{\partial^2 C_g}{\partial z^2} + \frac{\partial (C_g y)}{\partial z}\frac{\partial C_g}{\partial z}$$

$$-\frac{M\varepsilon_o}{2RT}\left[(C_g y)(\varepsilon_s - 1)\frac{d^2 E^2}{dz^2} + (C_g y)\frac{d\varepsilon_s}{dz}\frac{dE^2}{dz} + (\varepsilon_s - 1)\frac{d(C_g y)}{dz}\frac{dE^2}{dz}\right]$$

$$= \frac{R_o}{K'\sigma}\frac{\partial}{\partial t}(k_1 C_g + k_2) \qquad (6.7)$$

The boundary conditions for this problem are

a) Initial condition: $C_g = 0$ at $t = 0$, for all z.

b) Boundary condition: $C_g = C_o$ at $z = 0, L$, for all $t > 0$.

C_o = surrounding vapor concentration

Equation (6.7) is a non-linear, second-order partial differential equation with the non-linearity arising from: (1) The concentration dependence of the diffusion coefficient, $D_s = K'C_g$; (2) The surface concentration (C_s) dependence of the radius of gas-phase cross-section area, y (see Figure 6.2); (3) The dependence of the electric fields on the adsorbate concentration profiles; and finally, (4) The adsorbate concentration dependence of the surface hopping molecules' dielectric constant, ε_s.

To avoid having to solve non-linear PDEs, the following procedure

is adopted in solving equation (6.7) numerically.

A first estimate based on the values available at the beginning of a time interval are used for all the terms arising from the above non-linearities, and the equation to be solved reduces to

$$a_1 \frac{\partial^2 C_g}{\partial z^2} + a_2 \frac{\partial C_g}{\partial z} - a_3 = a_4 \frac{\partial}{\partial t} (k_1 C_g + k_2) \qquad (6.8)$$

where

a_1, a_2, a_3 and a_4 are constants.

Having obtained a first approximation for the concentration profile, the coefficients a_1, a_2 and a_3 are corrected for by using values corresponding to 'average' concentrations over the same time interval. This 'iterative' procedure is repeated three times over each time interval before moving on to the next time interval.

Using dimensionless variables

$$G = C_g/C_o \ , \quad Y = (C_g y)/(C_m R_o) \ , \quad \zeta = z/L$$

one obtains for equation (6.7)

$$Y \frac{\partial^2 G}{\partial \zeta^2} + \frac{\partial G}{\partial \zeta} \frac{\partial Y}{\partial \zeta} = \frac{L^2}{D_\zeta} \frac{\partial}{\partial t} (k_1 G + k_2/C_o) + \frac{M\varepsilon_o}{2RTC_o} \left[Y(\varepsilon_s - 1) \frac{d^2 \vec{E}^2}{d\zeta^2} + Y \frac{d\varepsilon_s}{d\zeta} \frac{d\vec{E}^2}{d\zeta} + (\varepsilon_s - 1) \frac{\partial Y}{\partial \zeta} \frac{d\vec{E}^2}{d\zeta} \right] \qquad (6.9)$$

where

$$D_\zeta = K_1' C_m \sigma \quad \text{(constant)}$$

and

C_m = gas-phase concentration C_g for monolayer coverage

with the boundary conditions

a) $G = 0$ at $t = 0$, for all ζ.

b) $G = 1$ at $\zeta = 0,1$, for all $t > 0$.

6.2 Numerical Solution of the Second Order Partial Differential Equation (6.8)

The Implicit Finite Difference scheme was used to solve equation (6.8) for the concentration profiles. Let $G = G(I,N)$, where the index I refers to position in the pore and N refers to time. Also, let $C = C_s/C_{so}$ be the dimensionless adsorbate concentration ($C = C(I,N)$).

$$Y = Y(I),\ k_1 = k_1(I,N),\ k_2 = k_2(I,N),\ \alpha = L^2/D_\zeta$$

$$\beta = M\varepsilon_o/(2RTC_o)\ ,\quad E = E(I)\ ,\quad \varepsilon_s = \varepsilon_s(I)$$

In the Implicit Finite Difference scheme

$$\frac{\partial^2 G}{\partial \zeta^2} = \frac{G(I+1,N+1) - 2xG(I,N+1) + G(I-1,N+1)}{\Delta Z^2}$$

where ΔZ = step size in ζ ($\simeq .01$ in this work)

$$\frac{\partial G}{\partial \zeta} = \frac{G(I+1,N+1) - G(I-1,N+1)}{2x\Delta Z}$$

$$\frac{\partial Y}{\partial \zeta} = \frac{Y(I+1) - Y(I-1)}{2x\Delta Z}$$

$$\frac{d^2 \vec{E}^2}{d\zeta^2} = \frac{E^2(I+1) - 2 \times E^2(I) + E^2(I-1)}{\Delta Z^2}$$

$$\frac{dE^2}{d\zeta} = \frac{E^2(I+1) - E^2(I-1)}{2 \times \Delta Z}$$

$$\frac{d\varepsilon_s}{d\zeta} = \frac{\varepsilon_s(I+1) - \varepsilon_s(I-1)}{2 \times \Delta Z}$$

$$\frac{\partial}{\partial t}(k_1 G + k_2/C_o) = (k_1(I,N+1)xG(I,N+1) + k_2(I,N+1)/C_o$$

$$-k_1(I,N)xG(I,N) - k_2(I,N)/C_o)/\Delta t$$

where Δt = step size in time t (varies from 2 to 5 to 15 to 20 mins.).

With these notations equation (6.9) may now be written as

$$XA(I) \times G(I-1,N+1) + XB(I) \times G(I,N+1) + XC(I) \times G(I+1,N+1) = XD(I) \qquad (6.10)$$

where

$$\begin{aligned}
XA(I) &= Y(I)/\Delta Z^2 - (Y(I+1)-Y(I-1))/(4x\Delta Z^2) \\
XB(I) &= -2 \times Y(I)/\Delta Z^2 - \alpha \times k_1(I,N+1)/\Delta t \\
XC(I) &= Y(I)/\Delta Z^2 + (Y(I+1)-Y(I-1))/(4 \times \Delta Z^2) \\
XD(I) &= -\alpha \times [k_1(I,N) \times G(I,N) + k_2(I,N)/C_o - k_2(I,N+1)/C_o]/\Delta t \\
&\quad +\beta[Y(I) \times (\varepsilon_s(I)-1) \times (E^2(I+1)-2 \times E^2(I) + E^2(I-1))/\Delta Z^2 \\
&\quad +Y(I) \times (\varepsilon_s(I+1)-\varepsilon_s(I-1)) \times (E^2(I+1)-E^2(I-1))/(4 \times \Delta Z^2) \\
&\quad +(\varepsilon_s(I)-1) \times (Y(I+1)-Y(I-1)) \times (E^2(I+1)-E^2(I-1))/(4 \times \Delta Z^2)]
\end{aligned} \qquad (6.11)$$

The index I runs from 1 to 101 (as $\Delta\zeta = .01$). From the boundary conditions, one obtains

$$\begin{aligned}
XD(2) &= XD'(2) - XA(2) \times 1 \\
XD(100) &= XD'(100) - XC(100) \times 1
\end{aligned}$$

where the prime refers to values obtained from equation (6.10).

Equation (6.9) for I = 1 to 101 comprises a Tri-Diagonal Matrix, which is readily solved by a Gaussian elimination method [C3, p. 441]. The diffusion coefficient D_ζ is obtained from a best fir of experimental data when the experiments are carried out at a relative partial vapor pressure $p/p_s = GO \simeq 0.3$ (Figure 5.15). (Note: the conclusion that D_ζ is a proportional function of the gas phase concentration C_g, arrived at in Chapter III, is used here. Also, for $GO \simeq 0.3$ only monolayer adsorption is observed, and therefore, no bulk volume flow is possible,

indicating that $D_{\zeta o}$ represents fully the mass transport phenomena for the low surrounding concentrations.)

Other constants in equation (6.2) are

$$M = 18 \text{ gms/gmole} \quad , \quad R = 8.30 \times 10^2 \text{ Ncm/gmole } ^{o}K$$

$$T = 298^{o} \text{ K}$$

$$\varepsilon_o = 8.854 \times 10^{-12} \text{ N/V}^2$$

Appendix E lists the computer program used to estimate the concentration profile in the gas phase (G(I,N)) and the adsorbate phase (C(I,N)).

6.3 Results of Numerical Calculations

Numerical values for W (gms adsorbed/gm sample) and the concentration profile in a single, cylindrical pore, as obtained from the computer calculations, are given in Appendix E. Figure 6.3 represents the adsorption kinetics in an idealized bed of silica gel consisting of only cylindrical, open pores of length L = .01693 cm, $R_o = 30.7$ A^{o}, $A = 4.56 \times 10^6$ (cm^2/gm) (values corresponding to Silica Gel S-2509 from Chapter III), and subjected to an average field (corresponding to the radial position of the average field squared $\langle E^2 \rangle$, $r_{avg} \simeq .0667$ cm) of $\langle E \rangle = 11.89$ KV/cm (see Appendix B.2).

In the actual experiments certain non-idealities exist. Among them are: (1) the gas-phase concentration at the mouth of <u>each</u> pore is not $= C_o$ (the surrounding concentration), at time t = 0; (2) A distribution of pore sizes exists resulting in the smaller pores being filled first and the larger pores filled last; (3) The overall dielectric constant is not uniform over the entire bed, especially at small times, owing to the

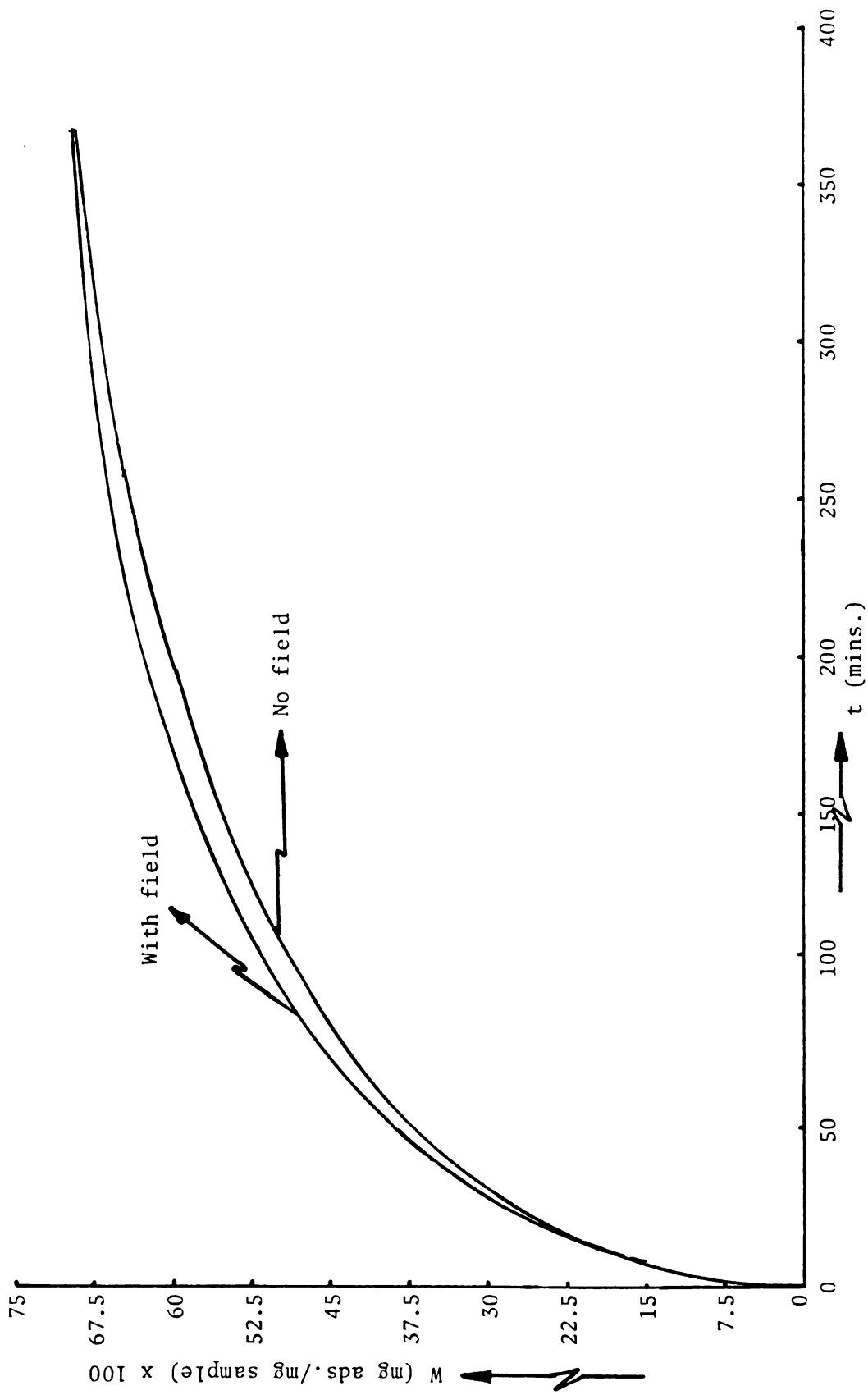

Figure 6.3. Adsorption rate in single-pore model, with and without electric field (theoretical curves).

particles closer to the bed boundaries being exposed to the humid environment earlier than the particles in the center of the bed.

Nevertheless, the single-pore model can give valuable qualitative and quantitative estimates of the effects of the applied fields in the real laboratory situations, once the 'no field' adsorption rate curve is known. For a given W (i.e., for a given amount adsorbed in the single pore), the ratio of the rates of adsorption in the field and no field cases $(dW'/dt)/(dW/dt)$ can be used to predict the rate of adsorption in the actual bed for the same W, given the (dW/dt) for the non-ideal bed.† In this fashion, the adsorption kinetics in a bed of silica gel for a given applied field may be predicted, given the kinetics without the field.

Figure 6.4 gives dW/dt vs. W for both 'with' and 'without' field for the single pore. Table 6.1 lists the ratio $(dW'/dt)/(dW/dt)$ vs. W, obtained from Figure 6.4. Also listed is dW/dt for the actual experiments with Silica Gel S-2509, represented in Figure 5.23.†† Next, the predicted dW'/dt is obtained for the experiments in Figure 5.23 $(dW'/dt = (dW'/dt)/(dW/dt)\big|_{\text{single pore}} \times (dW/dt)_{\text{bed}})$. In Figure 6.5 is plotted dt/dW' for the bed vs. W. The area under the curve gives $t\ (= \int_0^{W'} \frac{dt}{dW'}\, dW')$. Thus, W' is obtained as a function of t. Figure 6.6 shows the experimental and predicted adsorption kinetics for this sample. The electric field-induced surface diffusion enhancement of the polarized

---

†The prime refers to the case with the field applied.

††As mentioned earlier, this theoretical model is applied to the HCl treated Silica Gel S-2509 so as to exclude possible ion-related adsorption rate effects.

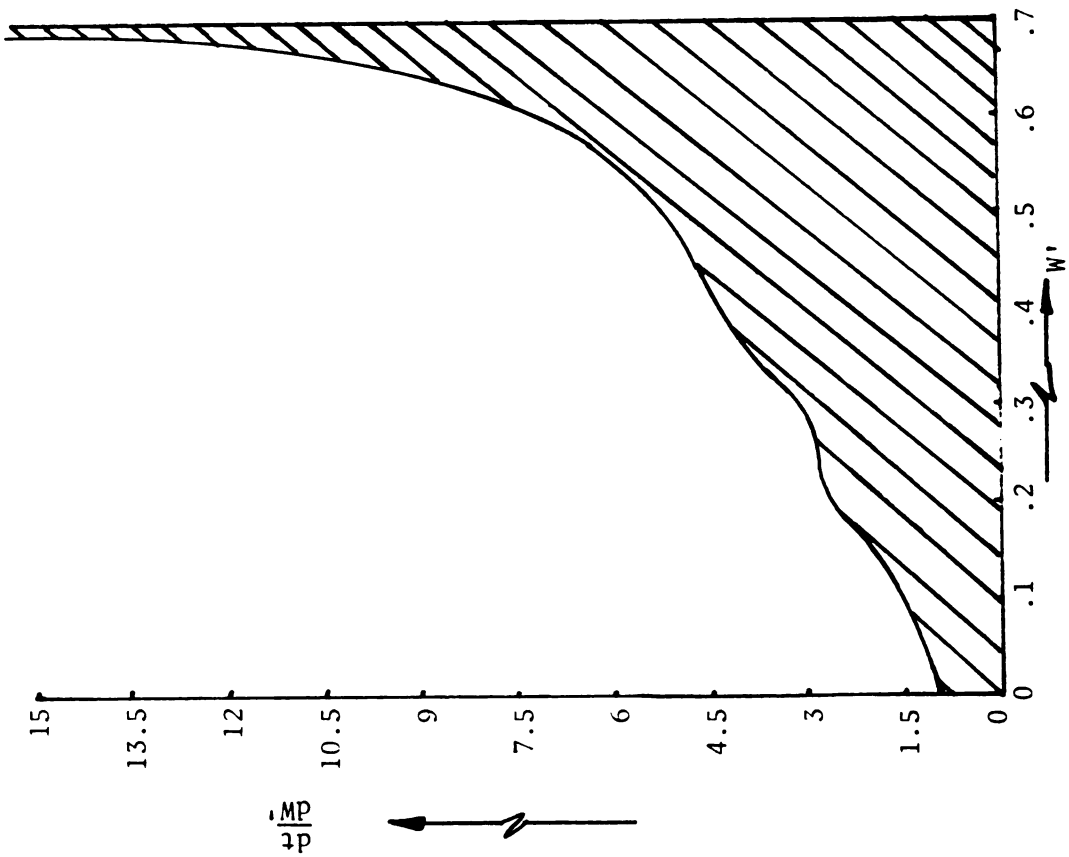

Figure 6.5. Integral curve to yield W' vs. t for Silica Gel S-2509.

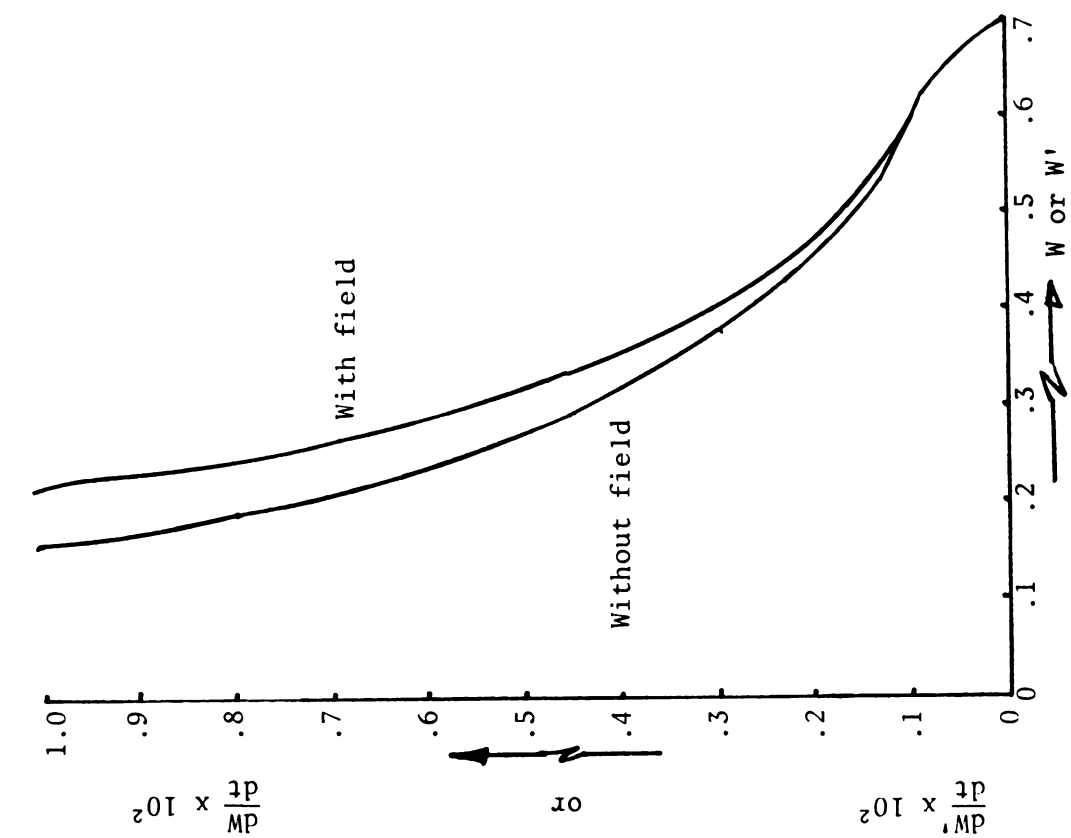

Figure 6.4. Rate of adsorption vs. amount adsorbed for single-pore model.

Table 6.1. Estimation of Adsorption Rate Curve in the Presence of an Electric Field.

W or W'	$\left(\frac{dW'/dt}{dW/dt}\right)$ For Single Pore	$\left(\frac{dW}{dt}\right)$ Experimental for Bed	$\left(\frac{dW'}{dt}\right)$ Estimate for Bed	$\frac{dt}{dW'}$	W'	t (min) for W'
0	1.00	1.0526	1.0526	.950	0	0
10	1.000	.5556	.5556	1.800	5	5.9
15	1.117	.3704	.4137	2.417	10	13.7
20	1.340	.3226	.4323	2.313	20	36.2
25	1.362	.3077	.4191	2.386	30	61.3
30	1.3084	.2500	.3271	3.057	40	99.1
40	1.128	.1980	.2233	4.478	50	146.6
50	1.088	.1869	.1972	5.072	60	205.8
60	1.055	.1316	.1388	7.203	65	250.7
65	1.000	.1077	.1077	9.285	67.5	276.2
67.5	1.00	.0773	.0773	12.93	68.5	288.2
70.0	1.00	.00	0.0	∞		

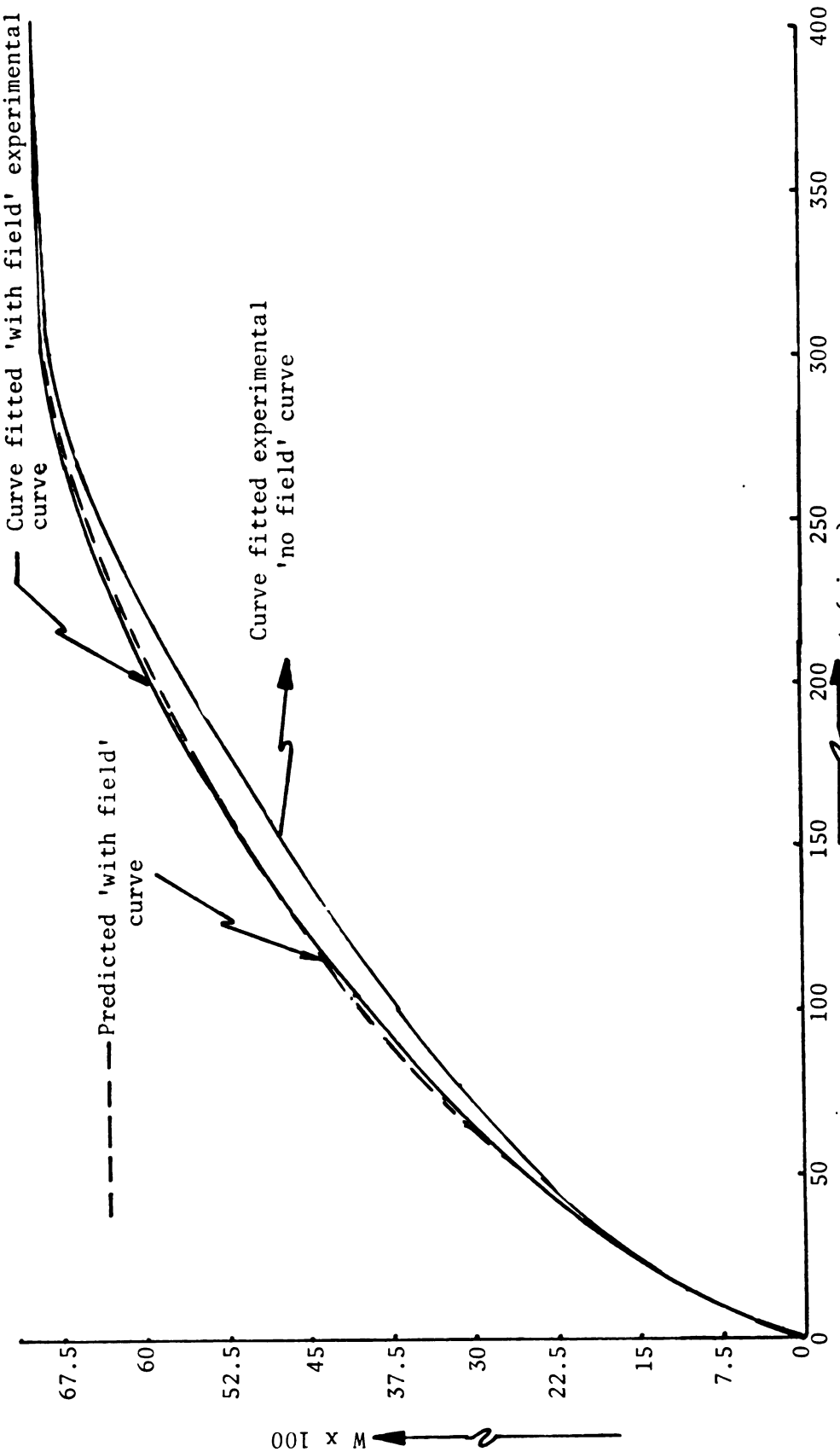

Figure 6.6. Predicted and experimental adsorption rate curves in silica gel-water vapor system at $T = 25^{o}$ C, $\Delta V = 6$ KV, $p/p_s = 1.0$.

adsorbate molecules seems to represent fairly well the observed experimental enhancements in the case of silica gel free of any surface ions. That the field-induced effects in the untreated Silica Gel S-2509 in Figure 5.18 is larger may indicate the additional role played by the ions in the ion-assisted field-induced effects.

CHAPTER VII

FLY ASH RESISTIVITY, CONDITIONING AND THE EFFECTS OF APPLIED ELECTRIC FIELDS

Both from widespread experience and theoretical investigations, the electrical resistivity of fly ash (and other highly resistive dusts) is reckoned to be one of the most common causes of poor precipitator performance [W2]. In an Electrostatic Precipitator (ESP) gas ions are formed in the high field regions near the wires and flow to the grounded plate. The ions attach onto particles in the gas to be cleaned, and the particles, in turn, are precipitated on the grounded collecting plate. However, as the ion densities produced in the corona wire vicinity are much larger than those used in charging the particles [W4], the bulk of the ions have to pass through the particle deposits which form on the ground electrode, thus constituting the D.C. corona current. When the bed of fly ash or dust has a high electrical resistivity, a significant voltage drop develops across the bed causing dielectric breakdown by ionization of the gas within the interstices of the particle layer [D2]. This phenomenon, known as sparking or back corona, can severely limit the effective voltages used in the precipitation process, and consequently bring down the collection efficiencies [W2].

The mode of conduction through a bed of fly ash particles may be either due to volume conduction or surface conduction. The former involves the motion of electrical charges through the interior of the particles and is dependent on the composition and temperature of the

particle. In surface conduction, electrical charges are carried in the surface moisture and chemical films adsorbed on the particles. Below about 300^{o} to 400^{o} F (the temperature at which most ESPs operate), surface conduction becomes the predominant mechanism due to the increased adsorption of moisture and chemical films which occur at these lower temperatures [W2]. In an effort to lower the bed resistivity, various 'conditioning' agents have been introduced into the gas stream, so as to increase either directly or indirectly the amount of moisture adsorbed on the particles. Often, much success has been achieved due to such conditioning. However, all attempts to explain the significant lowering of bed resistivity have thus far omitted the possible effects that high, non-uniform electric fields existing in the bed may have on the adsorption process, and also on the equilibrium distribution of the adsorbate in the bed.

Ditl and Coughlin [D1,D2] have proposed a model composed of neat, spherical fly ash particles stacked on each other, with the interparticle contact resistances accounting for the entire layer resistance (see Figure 7.1). While conducting equilibrium experiments with fly ash as adsorbent and argon and water as adsorbates (at T = 20^{o} C), they observe hysterisis and conclude this to be proof of capillary condensation (see Figure 7.2). By introducing a ring-like liquid condensate at the points of contact between the spherical particles (see Figure 7.3), they then go on to explain how the ash layer resistivity is significantly lowered due to this condensation phenomenon.

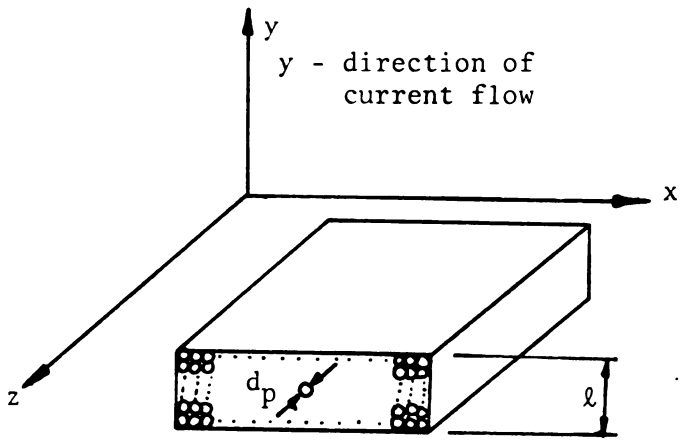

Figure 7.1. Idealized array of uniform, spherical fly ash particles packed in a layer.

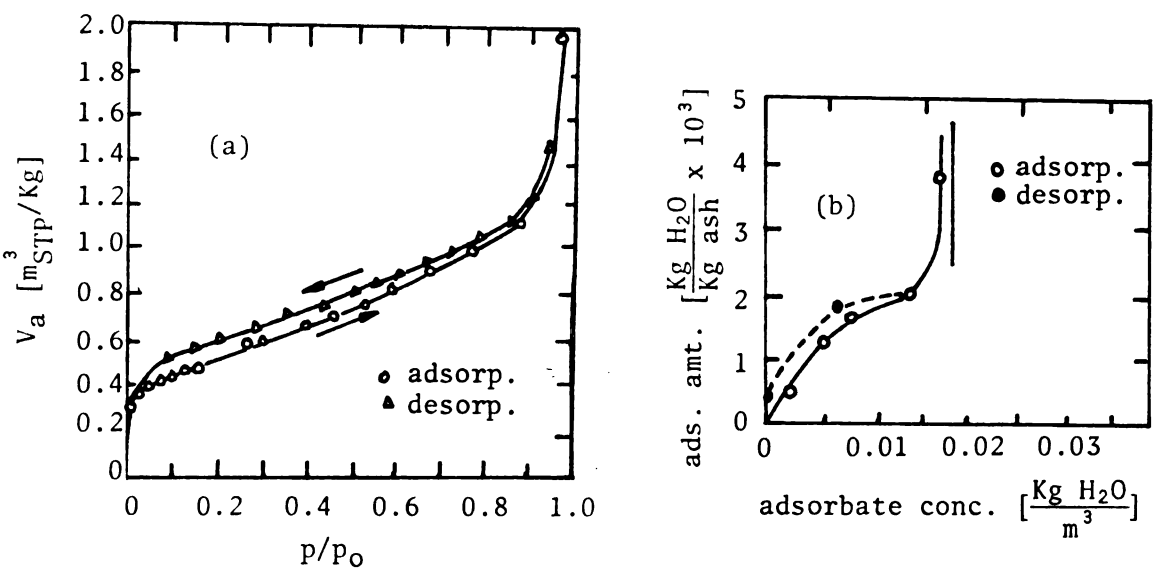

Figures 7.2(a) and (b). Equilibrium curves for fly ash-argon (a); and fly ash-H_2O-air (b) [D1,D2].

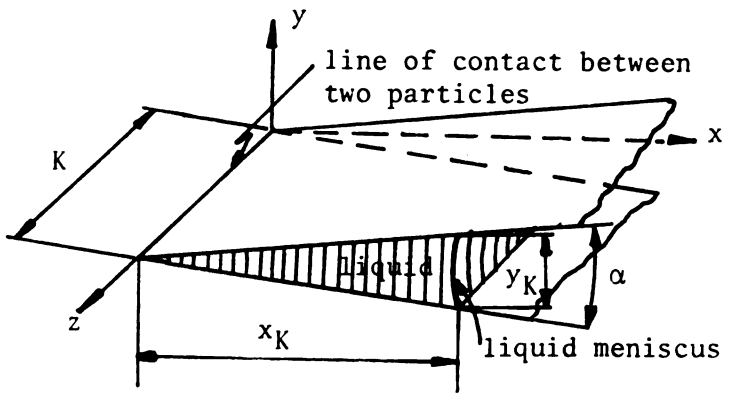

Figure 7.3. Geometrical properties of capillary condensed liquid at a point of contact between spherical particles.

However, certain discrepancies seem to exist in this model. First, in expressing the dimension y_K in Figure 7.3, the authors have taken recourse to the Kelvin equation (with certain simplifying assumptions)

$$y_K = \frac{v^{\ell}\gamma}{\ln(p_s/p_K)RT} \tag{7.1}$$

where

v^{ℓ} = molar volume of condensate

γ = surface tension of condensate

p_s = vapor pressure at saturation of condensate

p_K = partial pressure of vapor in gas phase

T = temperature ^{o}K and R = gas constant

For typical conditions in an ESP with water being the adsorbate,

v^{ℓ}= 18 cc/gmole, γ = 46.73 dynes/cm at T = 430.9^{o} K [S2],

$(p_K/p_s) \simeq .09$, R = 8.3x10 (dyne cm)/(gmole ^{o}K)

and one obtains from equation (7.1)

$y_K = .98\ A^{o}$

Thus, y_K, the radius of curvature of the wedge-shaped interparticle pore, is of submolecular dimensions, and as such, the Kelvin equation is inapplicable.† Also, the argument they put forward to explain the presence of capillary condensate even at low, relative, partial pressures (p/p_s) is quite ambiguous. As the relative pressure p/p_s is increased beyond a reasonably high value (say, $0.6 \simeq 0.7$) capillary condensation may become possible and is indeed observed experimentally by the authors. In the desorption process the liquid-like adsorbate begins to evaporate and as the desorption mechanism is often quite different from the adsorption one, especially when capillary condensation is involved, hysterisis is observed in the isotherms. The fact that hysterisis persists even at low relative pressures is due to the decreasing radii of curvature of the condensed liquid and does not, by itself, prove the possibility of condensation at such low relative pressures.

The moisture contents of conductive fly ash have been reported by White to be typically 0.1 to 0.3% by weight [W4]. The specific surfaces of these ashes were about .5 to 1 m^2/g. For these values an elementary calculation leads to the presence of five to ten molecular layers on the fly ash particles [W4], assuming that all the moisture is present in the adsorbed form. As the adsorptive force fields for water adsorbed on fly ash are known to be rather weak††, this would tend to imply that much of

---

†Actually, the application of the Kelvin equation is strictly impermissible for radii of curvature less than about 10 to 15 A^o [F1].

††It is as a result of this that a 'conditioning' agent is used, so as to bind the water molecules more strongly onto the fly ash surface indirectly [W2].

the adsorbed moisture is in the capillary-condensed liquid state, primarily at the interparticle contacts.

Thus, though it is hard to explain capillary condensation in fly ash based on a Kelvin mechanism, the phenomenon, nevertheless, would seem to occur, especially for conductive fly ash. On the other hand, even when less than a monolayer of water has been adsorbed by a bed of fly ash, Ditl and Coughlin [D2] have reported a significant decrease in the fly ash resistivity.

These observations would lead one to seek an explanation for the presence of capillary condensation in a fly ash bed (that has been exposed to an applied electric field either in the ESP, or in the course of a resistivity experiment when a voltage drop has to be imposed across the ash bed) in the phenomena attendant with the extremely high interparticle contact electric fields that are known to exist. In addition, the charged nature of the ash particulates prior to precipitation may play some role in the equilibrium moisture content of these particles. In the following section, a possible mechanism leading to the enhancement of surface adsorbate concentrations at the interparticle contact regions, due to the field characteristics, is postulated.

7.1 Interparticle Field and Concentration Gradients

Equation (2.22) of Section 2.4(a) gives the Kelvin pressure distribution in the presence of external electric fields and realized charges

$$\text{grad } p = \varepsilon_o \underset{\rightarrow}{E}\ \text{div}(\varepsilon \underset{\rightarrow}{E}) + \frac{\varepsilon_o}{2}(\varepsilon - 1)\ \text{grad}\ \underset{\rightarrow}{E}^2 \qquad (2.22)$$

The first term on the right-hand side is due to an average realized charge $\bar{z}$, and the second is due to the local electric field $\underset{\rightarrow}{E}$.

Neglecting any real charges in the bed, one gets

$$\text{grad } p = \frac{\varepsilon_o}{2} (\varepsilon-1) \text{ grad } \underset{\rightarrow}{E}^2 \tag{7.2}$$

This equation implies that the Kelvin pressure distribution (and, therefore, the concentration distribution) will be such that in regions of high field strengths, higher pressures (or concentrations) will result in the limit of thermodynamic and mechanical equilibrium.

The fields estimated at the interparticle contact briefly mentioned in Section 4.1(f) are reconsidered here.

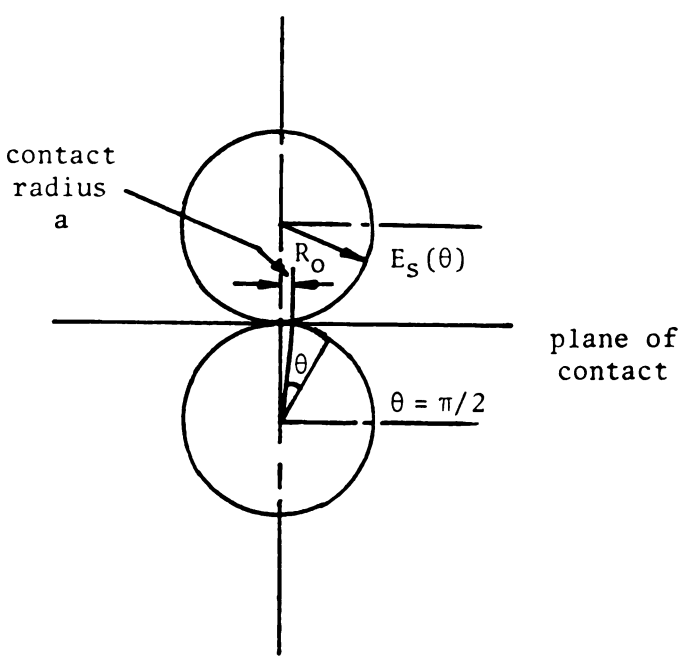

Figure 7.4. Interparticle contact dimensions.

In particular, the equation for the field $\underset{\rightarrow}{E}_s(\theta)$ along the particle surface went as

$$\underset{\rightarrow}{E}_s(\theta) = \underset{\rightarrow}{E}_a/(-(\ln \frac{a}{2R_o})\text{Sin}^2\theta) \tag{4.8}$$

Along the surface

$$\nabla_s E_s^2(\theta) = \frac{d}{d(R_o\theta)}[\underset{\rightarrow}{E}_s^2(\theta)] = \frac{\underset{\rightarrow}{E}_a^2}{R_o} \times \frac{1}{(\ln a/2R_o)^2} \times \frac{-4\mathrm{Cot}\theta}{\mathrm{Sin}^4\theta}$$

For typical ash bed values quoted in Section 4.1(f)

$$\underset{\rightarrow}{E}_a = \frac{2\times10^3\ \mathrm{V}}{.32\ \mathrm{cm}}\ ,\quad R_o = 10\times10^{-6}\ \mathrm{m}\ ,\quad R_o/a \simeq 100$$

one has

$$\begin{aligned}\nabla_s E_s^2(\theta) &= 3.44\times10^{18}\ \mathrm{V^2/cm^3} \quad \text{for } \theta = 1^o\\ &= 1.10\times10^{15}\ \mathrm{V^2/cm^3} \quad \text{for } \theta = 5^o\\ &= 3.47\times10^{13}\ \mathrm{V^2/cm^3} \quad \text{for } \theta = 10^o\end{aligned}$$

The equations for the fields estimated in Section 4.1(f) were for a dry particle-particle contact with the presupposed assumption that the interparticle air gap does not break down electrically. Actual fields should take into account the existence of adsorbate and also some dielectric breakdown in the contact vicinity. These factors would reduce the field magnitudes somewhat, but nevertheless, the above numbers may be used as an upper limit. Using a crude estimate for the dielectric constant of water vapor adsorbed on fly ash (ε) to be about 30, one obtains from equation (7.2)

$$\text{grad } p = 4.36\times10^9\ \mathrm{atm/m} \quad \text{at } \theta = 1^o$$

and

$$\text{grad } p = 1.39\times10^6\ \mathrm{atm/m} \quad \text{at } \theta = 5^o$$

where p is the hydrostatic pressure in the adsorbate. Thus, in the equilibrium limit, extremely high pressure gradients (and, therefore, adsorbate concentration gradients) need to exist at the interparticle contact points, so as to overcome the ponderomotive forces created by

the high fields.

The above analysis may be used to explain why the resistivity of a bed of fly ash is reduced significantly, even for adsorbed amounts of less than a monolayer of water vapor. However, it does not necessarily predict an enhancement in the total amount of adsorbate in the bed, due to the imposed fields, as the redistribution of matter, due to the extremely high and non-uniform interparticle contact fields, is a very 'local' phenomenon affecting a rather small percentage of the available surface area (specifically, at the interparticle contacts).

In Section 4.1(e), the field characteristics around a charged spherical particle were estimated. Estimates for typical charged fly ash particulates yielded very strong field gradients at the particle surface. It is to be remembered that the fly ash particulates prior to being collected on the grounded plate are charged. The adsorption kinetics and equilibria of moisture adsorbed from the surrounding flue gas could well be affected by these charges. From the knowledge gathered thus far, it seems improbable that the rate of gaseous adsorption onto the particles will be affected, as the rate controlling mechanism is gas phase diffusion. However, it is probable that the presence of ionic charges on the particle surfaces could affect the equilibrium amount of water vapor adsorbed, possibly, by altering the adsorbate-adsorbent bond characteristics (for example, by more strongly binding the adsorbate, much like 'conditioning' agents such as NH_3, SO_3, etc.). If this hypothesis were indeed proven to be true, then, as the particles give up their charges on precipitation, this would lead to further redistribution of the adsorbate on the particle surface, due to altered surface properties. In this way, one could visualize a significant amount of interparticle

capillary condensate brought about by a combination of particle charges and local non-uniform fields in the ash layer.

7.2 Preliminary Experiments with Fly Ash

The results of experiments dealing with the adsorption of water vapor on fly ash (conducted in the M.S.U. laboratory) are represented in Figures 7.5 and 7.6. Owing to the limited sensitivity of the electrobalance used, the necessity of keeping the entire sample weight to the minimum possible and the extremely small water vapor adsorption capacity of fly ash (relative to silica gel, porous alumina, etc.), there is understandably some scatter in the data corresponding to $p/p_s \simeq 2/3$ (no condensation). Figure 7.5 represents the adsorption of water vapor on fly ash at a relative saturation of 2/3. In case (2) the cylindrical sample pan was of much smaller diameter than the one used in case (1), and consequently, the sample experienced a higher average field. In both the cases the application of the cylindrical field seems to result in a net reduction in the maximum amount of moisture adsorbed. A small corona current was recorded when the field was on. The current flow reduced significantly when the fly ash particles were removed from the sample pan, indicating that the presence of the fly ash led to interparticle air gap breakdown and the resultant ionic current. On shutting off the voltage, the bed seemed to gradually adsorb more moisture until the water content reached almost the same capacity as with no field on. This phenomenon occurred repeatedly, both at $T = 25^{o}$ C and at $T = 37^{o}$ C. Three possible causes may be given to explain this behavior: (1) As observed by Panchenko et al. [P10], the application of strong electric fields led to a significant reduction in the water vapor adsorption capacity of cellulose and potato starch, possibly due to a rearrangement of

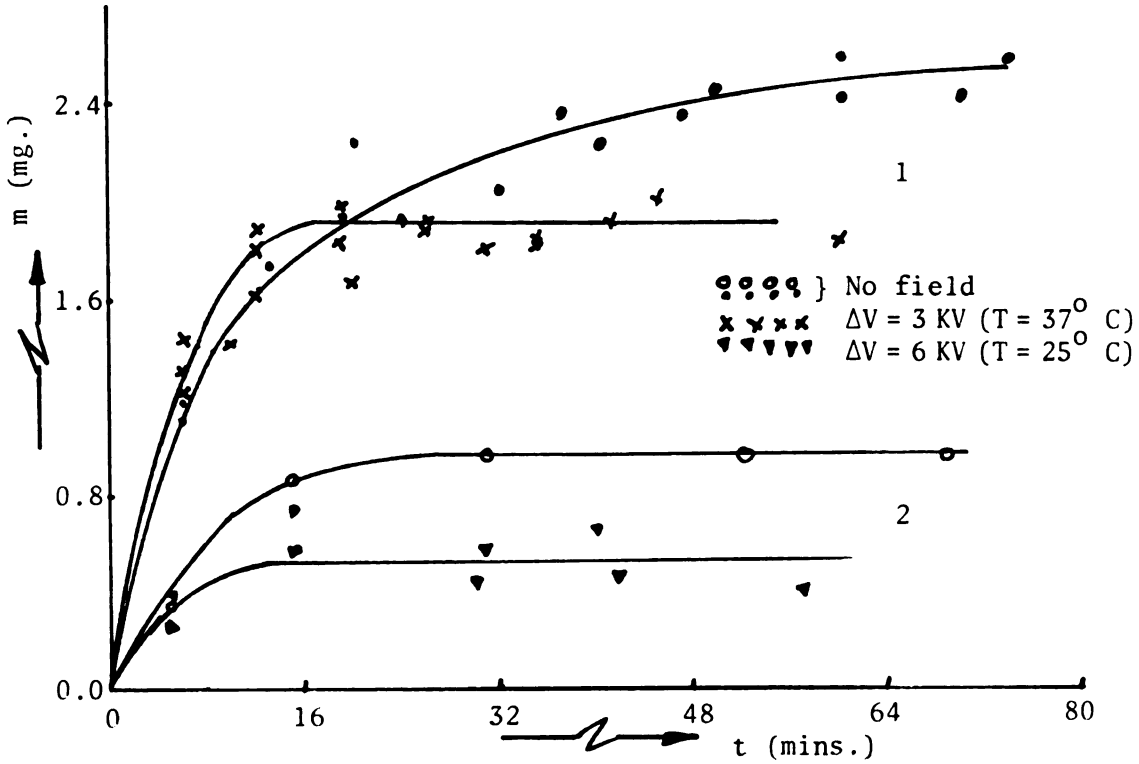

Figure 7.5. Fly ash-H_2O vapor, $p/p_s \simeq 2/3$: (1) 1.6 cm dia. pan; (2) .7 cm dia. pan.

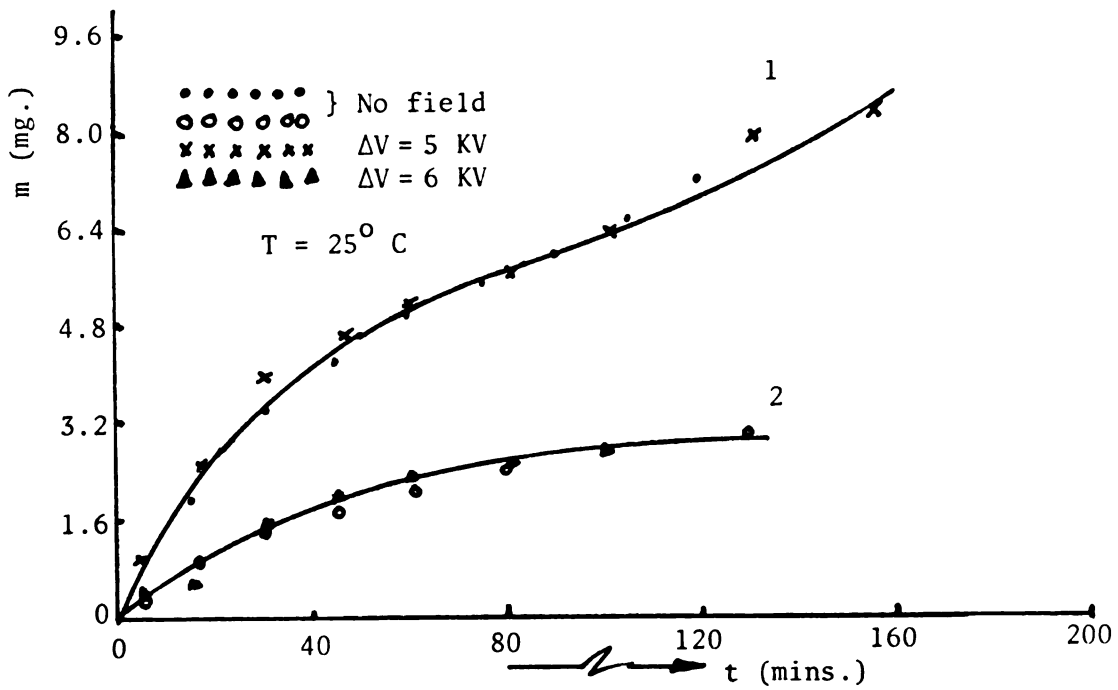

Figure 7.6. Fly ash-water vapor, $p/p_s \simeq 1$.

the particles in the regions of smaller available surface area. The fact that the fly ash bed seems to regain its original capacity fairly soon once the field is turned off, seems, however, to eliminate this hypothesis. (2) The ionic current could be sufficient to heat up the bed, and thereby reduce its adsorption capacity. Rough calculations made in Appendix A.5 offer some credibility to this explanation. (3) The presence of positive ions (negative corona) may itself be responsible for a net reduction of adsorption capacity (how, it is unclear).

Changing the central filament electrode from the negative terminal (negative corona) to the positive terminal (positive corona) essentially eliminates the current flow (at $\Delta V = 3$ KV) and, surprisingly, even the observed reduction in adsorption capacity. In Figure 7.6 is represented the adsorption kinetics of water vapor on fly ash at $p/p_s \simeq 1$ and $T = 25^{o}$ C. Within experimental error, no effects were observed, even with sufficiently high fields and significant adsorption. The adsorption kinetics remained unaffected, even though a corona current (for a negative corona) was still observed. This may be due to the fact that though the corona current was essentially of the same magnitude as in Figure 7.5 (3 to 4 μA), the net voltage drop across the bed is much smaller in this case, owing to significant decrease in resistivity (or increase in dielectric constant) of the bed.

To summarize the experiments conducted with fly ash, one might say: (1) When no ionic current is present, the adsorption kinetics and equilibria of water vapor on fly ash are essentially unaffected by the applied fields for $2/3 \leq p/p_s \leq 1$. (2) The ionic current seems to affect the maximum amount of adsorbate adsorbed when the relative pressure of surrounding vapor is less than 1.

Based on these observations and the conclusions derived from the experiments in Chapter V, appropriate recommendations for future work with fly ash, especially in relation to its resistivity, are made in Chapter VIII.

CHAPTER VIII

CONCLUSIONS AND RECOMMENDATIONS FOR CONTINUED RESEARCH

8.1 Conclusions

The various conclusions arrived at from the theoretical and experimental investigations conducted in this work are listed below:

a) The gas-phase electro-convective flux is negligible. Various experiments described in Chapter V, wherein the gas-phase diffusion fluxes determine the rate of adsorption, have shown that the field-induced enhancements are negligible. Considering that the polarizabilities of even polar gases are extremely small (when compared with adsorbate or liquid-phase polarizabilities), this result is only to be expected. The theoretical analysis conducted in the available literature thus far [P2,P12] has proposed the electro-convective gas-phase flux described by equation (1.4) as the predominant field-induced transport flux. This is certainly not true.

b) Field-induced surface diffusion fluxes are negligible for diffusion over monolayer covered adsorbents. For adsorbents with micropores in which surface diffusion and simultaneous Knudsen diffusion is predominant, the effect of applied fields is minimal when only a few layers of adsorbate are present in the sample. The polarizabilities of molecules adsorbed in the monolayer are comparable to those in the gas phase and, as such, the ponderomotive forces are weak. Interactions with the

adsorbent surface tend to further weaken the field-induced phenomena.

c) Field-induced surface diffusion fluxes are appreciable for diffusion over multilayers of adsorbed vapor. The polarizabilities of multilayer adsorbed vapor are generally large and could even exceed that corresponding to the bulk liquid state. Surface interactions are weaker, and strong internal field gradients could exist in the pores of the adsorbent. Adsorption kinetics in moist capillary porous adsorbents of a polar vapor like H_2O is definitely enhanced by applied electric fields.

d) Internal relaxation field gradients are responsible for the enhanced fluxes and not the nature of the overall, externally applied fields. Theoretical calculations of field gradients in a moist silica gel bed have led to the conclusion that the gradients resulting from local fields in a pore (relaxing with the progress of adsorption) are much larger in magnitude than the gradients existing in the macroscopic adsorbent bed. Experiments conducted in Section 5.6(b) seem to confirm this hypothesis. Uniform externally applied fields of the same average field squared ($\langle E^2 \rangle$) as those existing in a bed subjected to a non-uniform external field should produce similar adsorption rate enhancements. Observations to the contrary have been made in references [P1, P2,P3], but for much lower $\langle E^2 \rangle$s in the uniform field case.

e) Surface ions in adsorbents definitely alter the adsorption kinetics. Silica Gel S-2509 containing significant Na^+ ions showed definite reduction in the field-induced effects when treated with concentrated HCl to remove all surface ions (Figure 5.23). The surface ions play a significant role in the field-induced mass transport phenomena.

f) The 'single-pore' theoretical model represents the field-enhanced

adsorption kinetics in ion-free porous adsorbents with cylindrical pores fairly well. Given the adsorption characteristics (including the surface diffusion coefficient) for diffusion in porous adsorbents like silica gel in the absence of an external field, the field-induced enhancements due to the action of the ponderomotive forces on polarized adsorbate molecules is satisfactorily predicted by the application of this mathematical model. The procedure of translating the enhanced mass flux ratios obtained in the 'single-pore' model to the actual adsorbent-adsorbate system works fairly well, as long as the pore characteristics and the adsorbate characteristics in the pore are known quite adequately.

g) The adsorption kinetics of non-polar adsorbates in porous media is unaffected by applied fields. The observation that non-polar, low dielectric constant vapors do not experience additional field-assisted mass fluxes [P2,P3] is confirmed in this work. C_2Cl_4 was used as adsorbate at $p/p_s \simeq 1$ and $T = 25^{o}$ C.

h) Desorption or evaporation phenomena from moist capillaries in electrostatic fields are essentially unaffected. Enhancements in evaporation rates from fine capillaries observed in [P11,P12] are due primarily to the ionic corona discharge and not the applied fields. Experiments conducted in Section 5.6(c) to observe the field-related effects on the desorption process of water vapor from silica gel yielded no discernible changes when electrostatic fields were used. Theoretical investigations of the desorption phenomena seem to consolidate this observation.

i) Field-induced adsorption phenomena are significantly influenced by a flow of ionic current through the bed. Various experiments conducted when small but steady ionic currents were registered through the

adsorbent sample seemed to affect the adsorption kinetics significantly. In the case of silica gel the kinetics were enhanced. For fly ash the maximum adsorbed vapor was lowered in a partially saturated surrounding. The reasons behind these phenomena arising from electrodynamic effects or possible Lentz-Joulean heat production are, at present, unclear.

j) Adsorption characteristics of water vapor on fly ash are unaffected for a humid environment ($p/p_s \simeq 1$) but noticeably affected for a partially saturated environment ($p/p_s \simeq 2/3$). The flow of ionic current through a bed of fly ash (the current resulting from interparticle air-gap breakdown) seems to affect the adsorption equilibria of water vapor for $p/p_s \simeq 2/3$. In the presence of capillary condensation observed at $p/p_s \simeq 1$ the equilibria seems to be unaffected. The rate of gas-phase diffusion into a bed of fly ash is expected to remain unaffected (from (a) above). However, theoretical calculations for the equilibrium between ponderomotive and mass flux driven forces at the interparticle contact region seem to indicate a possible enhancement of local, adsorbate concentrations.

8.2 Recommendations for Continued Research

The number of experiments that could be conducted to further probe into the effects of applied electric fields and electric discharges on gas-solid adsorption characteristics is endless. A few ideas that strike the author's mind, and that fall along the lines over which this work has developed thus far, are mentioned below. In Section 8.2(a) various experiments that could be conducted on capillary porous dielectrics, in order to further consolidate one's understanding of field-induced

phenomena in these well defined systems, are listed. In Section 8.2(b) experiments that could have a more direct bearing on the consequences of fly ash conditioning in the presence of particle charges, ESP fields and interparticle contact fields are suggested. In all these experiments it is to be noted that the experimenter would do very well to come up with some indirect means of measuring the adsorbed quantities, rather than use the existing direct gravimetric techniques. This would significantly reduce the problems associated with shutting off the field when making measurements, and of having to account for the repulsion-attraction effects due to accidental or unavoidable charging of the adsorption sample and pan. This would also help in constructing a heavier adsorbent pan, sturdier electrode assembly and provide the facility of making current and voltage drop measurements exclusively across the sample.

8.2(a) Further Experiments with Capillary Porous Materials

1) A method to significantly enhance the alkali ion concentrations in silica gel has to be found. Experiments of water vapor adsorption in gel samples with predetermined concentrations of surface ions will yield important information on the relative magnitudes of the ponderomotive forces acting on the polarized adsorbate and on the hydrated ion complexes.

2) Experiments conducted in Section 5.6(b) seemed to suggest that the field-induced adsorption rate phenomena were on account of internal relaxation fields and did not depend (explicitly) on the nature of the applied overall field. To confirm this observation, one needs to create uniform fields (between two parallel plate electrodes) of intensities at least five times larger than those used in this work ($\simeq$ 2 KV/cm). In

such high fields the adsorption behavior of water vapor in porous silica gel at $p/p_s \simeq 1$ should be studied.

3) A.C. fields of low frequencies were found to have no discernible effects on the water vapor adsorption characteristics in silica gel [P3, P5]. A.C. fields of high frequencies (several KHz) should be applied across the adsorbents and the resulting phenomena arising from oscillating ponderomotive forces and decreased dielectric constants ($\varepsilon \propto 1/\text{frequency}$) investigated. The effect of alternating fields on the maximum amount of adsorbed material should be noted, especially for those instances where the adsorbate-adsorbent bond strengths are known to be relatively weak.

4) Just as for Silica Gel S-2509, water vapor adsorption studies should be investigated in the presence of non-uniform fields for other adsorbents like porous glass, zeolite beads, etc., at a relative pressure of $\simeq 1$. The relative magnitudes of the electrical effects on the multilayer adsorbate formation in these adsorbents should provide information on the relative polarizabilities of water vapor adsorbed on these surfaces.

5) Adsorption experiments in point-plane electrode configurations should be further investigated to estimate the role of a discharge of ions in both the kinetics and equilbrium characteristics of gas-solid adsorption. If possible, the adsorbent temperature should be monitored so as to estimate the role played by the production of Lentz-Joulean heat. The adsorbent sample pan should be constructed in such a way that the adsorbent geometry lends itself to easy field analysis around a point electrode.

8.2(b) Experiments with Fly Ash

As mentioned in Chapter VII, a bed of fly ash particulates may be assumed to consist of ideal spheres arranged one on top of another (see Figure 8.1). The diffusion of water vapor into this bed is through the macropores formed in between the particles. Diffusion through the gas phase is expected to be far greater than surface diffusion. As such, the rate of adsorption on the fly ash particles is not expected to be enhanced due to any field-induced effects. However, besides the effects of electric fields on gas-phase diffusion phenomena, two other effects need to be considered. First, What is the role of the ionic current passing through the ash bed in influencing the adsorption characteristics?, and second, What is the influence of the strong, non-uniform interparticle fields on the equilibrium distribution of adsorbate in the interparticle contact region?

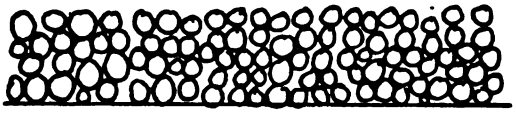

Figure 8.1. Bed of ideal spheres.

The ionic current in a bed of fly ash subjected to an electric field can be due to two sources: 1) breakdown of the gas in the interparticle contact vicinities, resulting from extremely high fields; and 2) a current, due to a corona discharge from a fine wire, point, etc., placed away from the bed, as in Figure 8.2. For the experiments conducted in Chapter VII, it was confirmed that the current registered was due to the first of the two sources mentioned above. At $p/p_s \simeq 0.67$, the adsorption capacity of water vapor on fly ash was found to be reduced when the

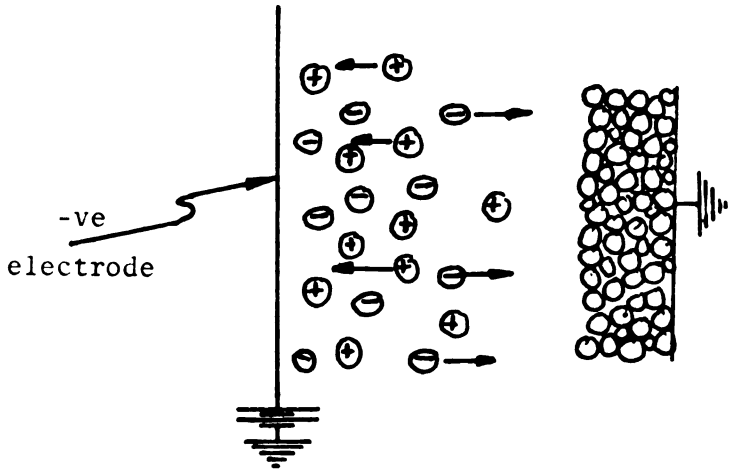

Figure 8.2. Corona discharge through bed (negative corona).

current passed through the bed. It was hypothesized that this could be due to a heating effect, though this hypothesis is open to question. To more nearly simulate the ash bed in a precipitator and to study the effect of an ionic current through the bed, the following experiment is proposed.

Fly ash is packed into an annular sample container and placed concentric with a central high voltage electrode (shown in Figure 8.3 below).

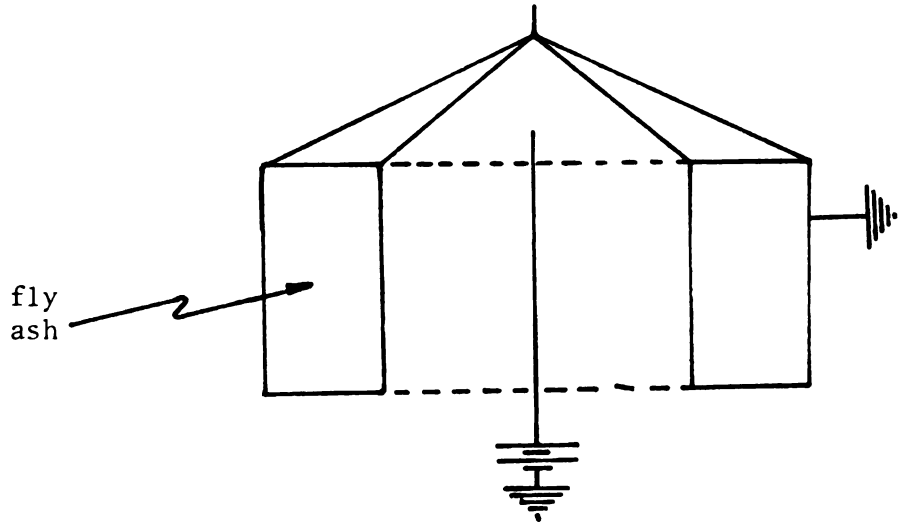

Figure 8.3. Annular pan with fly ash.

If the central electrode is a fine filament, then, by applying a high enough voltage, a corona discharge could be maintained (negative and/or positive). By replacing the central filament with a rod, similar fields could be applied across the ash bed without any current flow. In the case of the experiments in Chapter VII, positive ions passed through the bed to the negative filament electrode. In this experiment both positive ions and electrons (the latter would simulate the ESP) could be made to pass through the bed. It remains to be seen whether the passage of electrons through the bed would have an opposite effect from the one observed in Chapter VII.

As for the influence of strong, non-uniform interparticle contact fields, one needs to conduct the following experiments:

a) Obtain capacitance measurements of fly ash as a function of moisture content in a dielectric cell. From these measurements, as shown in Chapter IV, the adsorbed water vapor dielectric constants may be estimated.

b) Knowing the dielectric constants of water adsorbed on fly ash, one needs to estimate precise field distributions on the particle surface in the contact regions, taking into account the simultaneous effects of adsorbate concentrations on the field strengths themselves.

c) The equilibrium surface adsorbate concentration distribution should then be estimated based on equations referred to in Chapter VII. The results should help verify (theoretically) whether sufficient adsorbate exists in the contact vicinities to justify condensation.

Other experiments on fly ash that would help throw considerable light on the problem of fly ash conditioning include: 1) determining the maximum moisture content of charged versus uncharged particles in a

humid environment, and 2) determining the effects of applied electric fields on the diffusion of water vapor through fly ash impregnated with significant concentrations of alkali ions. The motivation for the former lies in the possible role that surface electronic charges may play in the adsorbate-adsorbent bond formation, and also in the influence that highly non-uniform radial fields may have on the adsorption phenomena. As for the latter, the role of alkali ions in the transport phenomena over fly ash particulates has been investigated [B1,B2], but their role in the rate of adsorption of water vapor in a fly ash bed in the presence of an imposed field (and ionic leakage current) is not well understood. The ion-related surface transfer of water molecules is especially significant when only a monolayer or so of water vapor has been adsorbed.

APPENDICES

APPENDIX A

ESTIMATION OF OVERALL ELECTRIC FIELDS

APPENDIX A

ESTIMATION OF OVERALL ELECTRIC FIELDS

A.1 Dielectric Sphere in a Uniform Electric Field

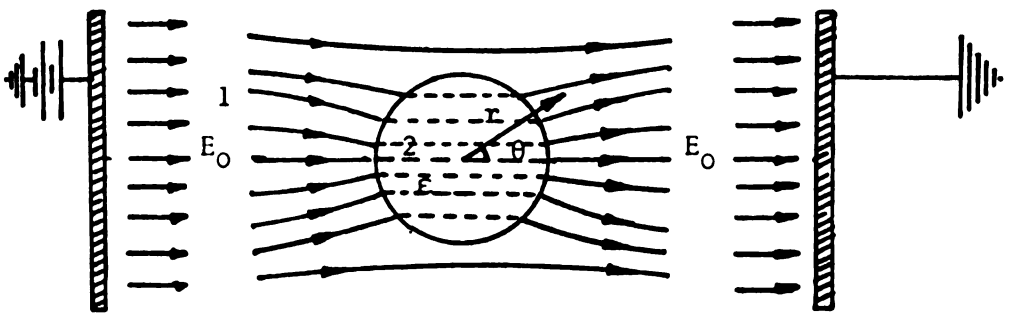

Figure 4.2. Dielectric sphere in uniform field.

The potential distribution around a dielectric sphere subjected to a uniform external field is given by [R5, p. 93]

$$\Phi_1(r,\theta) = -E_o r\cos\theta + \frac{(\varepsilon-1)}{(\varepsilon+2)} \frac{R_o^3}{r^2} E_o \cos\theta \qquad (A.1)$$

where ε is the dielectric constant of the sphere, R_o its radius and E_o the applied external field intensity. The field intensity in medium 1 is given by

$$\begin{aligned} \underset{\rightarrow}{E}_1 &= -\nabla\Phi_1 = -\frac{1}{r}\frac{\partial\Phi_1}{\partial\theta}\underset{\rightarrow}{e}_\theta - \frac{\partial\Phi_1}{\partial r}\underset{\rightarrow}{e}_r \\ &= E_o\left(\frac{(\varepsilon-1)}{(\varepsilon+2)}\frac{R_o^3}{r^3}\sin\theta - \sin\theta\right)\underset{\rightarrow}{e}_\theta \\ &\quad + E_o\left(2\frac{(\varepsilon-1)}{(\varepsilon+2)}\frac{R_o^3}{r^3}\cos\theta + \cos\theta\right)\underset{\rightarrow}{e}_r \end{aligned} \qquad (A.2)$$

The force on a dipole molecule in a non-uniform field is given by

$$\underset{\rightarrow}{f} = \underset{\rightarrow}{\mu}_{eff} \cdot \nabla \underset{\rightarrow}{E} \tag{A.3}$$

where $\mu_{eff} = \frac{\mu^2}{3kT} \underset{\rightarrow}{E}$ is the effective dipole moment.

$$\therefore \quad \underset{\rightarrow}{f} = \frac{\mu^2}{3kT} \underset{\rightarrow}{E} \cdot \nabla \underset{\rightarrow}{E} = \frac{\mu^2}{6kT} \nabla |E^2| \tag{A.4}$$

From (A.2) then,

$$\begin{aligned} |E|^2 = E_o^2 [& \left(\frac{\varepsilon-1}{\varepsilon+2}\right)^2 \frac{R_o^6}{r^6} \sin^2\theta + 4\left(\frac{\varepsilon-1}{\varepsilon+2}\right)^2 \frac{R_o^6}{r^6} \cos^2\theta \\ & + 1 - 2\left(\frac{\varepsilon-1}{\varepsilon+2}\right)\frac{R_o^3}{r^3} \sin^2\theta + 4\left(\frac{\varepsilon-1}{\varepsilon+2}\right)\frac{R_o^3}{r^3} \cos^2\theta] \end{aligned} \tag{A.5}$$

and

$$\nabla |E^2| = \frac{1}{r} \frac{\partial}{\partial \theta} |E^2| \underset{\rightarrow}{e}_\theta + \frac{\partial}{\partial r} |E^2| \underset{\rightarrow}{e}_r \tag{A.6}$$

The radial component of the force $\underset{\rightarrow}{f}_r = f_r \underset{\rightarrow}{e}_r$

$$\therefore \quad f_r = \frac{\mu^2}{6kT} \frac{\partial}{\partial r} |E^2|$$

$$= \frac{\mu^2 E_o^2}{6kT} \left[-6\left(\frac{\varepsilon-1}{\varepsilon+2}\right)^2 \frac{R_o^6}{r^7} \sin^2\theta - 24\left(\frac{\varepsilon-1}{\varepsilon+2}\right)^2 \frac{R_o^6}{r^7} \cos^2\theta \right.$$

$$\left. + 6\left(\frac{\varepsilon-1}{\varepsilon+2}\right) \frac{R_o^3}{r^4} \sin^2\theta - 12\left(\frac{\varepsilon-1}{\varepsilon+2}\right) \frac{R_o^3}{r^4} \cos^2\theta \right]$$

At the particle surface

$$f|_{r=R_o} = \frac{\mu^2 E_o^2}{6kT} \times \frac{1}{R_o} \left\{6\left(\frac{\varepsilon-1}{\varepsilon+2}\right) \times \frac{3\sin^2\theta}{(\varepsilon+2)} - 12\left(\frac{\varepsilon-1}{\varepsilon+2}\right) \times \frac{3\varepsilon}{(\varepsilon+2)} \cos^2\theta\right\}$$

or

$$f_{R_o} = \frac{-3(\varepsilon-1)}{R_o kT} \times \frac{(E_o\mu)^2}{(\varepsilon+2)^2} \times (2\varepsilon\text{Cos}^2\theta - \text{Sin}^2\theta) \qquad (A.7)$$

A.1(a) Average Field Gradient at Particle Surface

Let $f(\theta) = 2\varepsilon\text{Cos}^2\theta - \text{Sin}^2\theta$

then

$$f(\theta)_{avg} = \frac{2}{\pi}\int_o^{\pi/2} (2\varepsilon\text{Cos}^2\theta - \text{Sin}^2\theta)d\theta$$

$$= \varepsilon - 1/2$$

$$\therefore f(\theta)\Big|_{r=R_o}^{avg} = -\frac{3}{R_o}\frac{(\varepsilon-1)}{kT}\left(\frac{\mu E_o}{\varepsilon+2}\right)^2 (\varepsilon-1/2) \qquad (A.8)$$

For H_2O, $\mu = 6.18\text{x}10^{-28}$ C cm and k = Boltzmann's constant = $1.38\text{x}10^{-23}$ CV/^oK, T = 298^o K, ε = 5 and R_o = .175 cm (for alumina beads).

If

$$E_o = \frac{10\text{ KV}}{2.5''} = 1.575\text{ KV/cm},$$

then

$$f\Big|_{r=R_o}^{avg} = -\frac{3}{.175\text{ cm}} \times \frac{(5-1)}{(1.38\text{x}10^{-23}\text{ x }298)\text{CV}}$$

$$\times \left(\frac{6.18\text{x}10^{-28}\text{ C cm x }1.575\text{x}10^{3}\text{ V/cm}}{5+2}\right)^2$$

$$\times (5-1/2) \times 100\ \frac{\text{cm}}{\text{m}} \times 1\ \frac{\text{Nm}}{\text{CV}}$$

$$= -1.451\text{x}10^{-25}\text{ (Newtons)}$$

$$(\nabla E^2)_{\substack{avg \\ at\ r=R}} \simeq \frac{f_R^{avg}}{\mu^2/6kT} \simeq 9.37\text{x}10^7 (V^2/cm^3)$$

A.1(b) Average Field Intensity at Surface

At $r = R_o$, equation (A.5) reduces to

$$|E| = \frac{3E_o}{(\varepsilon+2)} \sqrt{\text{Sin}^2\theta + \varepsilon\text{Cos}^2\theta} = \frac{3E_o}{(\varepsilon+2)} f(\theta)$$

$\theta \rightarrow$	0	30	60	90^o
$f(\theta) \rightarrow$	5	4.359	2.646	1

$\therefore \quad f(\theta)_{avg} \simeq 3.251$

and $|E|_{avg} \simeq \frac{3E_o}{(\varepsilon+2)} \times 3.251 = 2.19$ (KV/cm)

A.2 Annular Bed of Dielectric Particles in Cylindrical Electrical Field

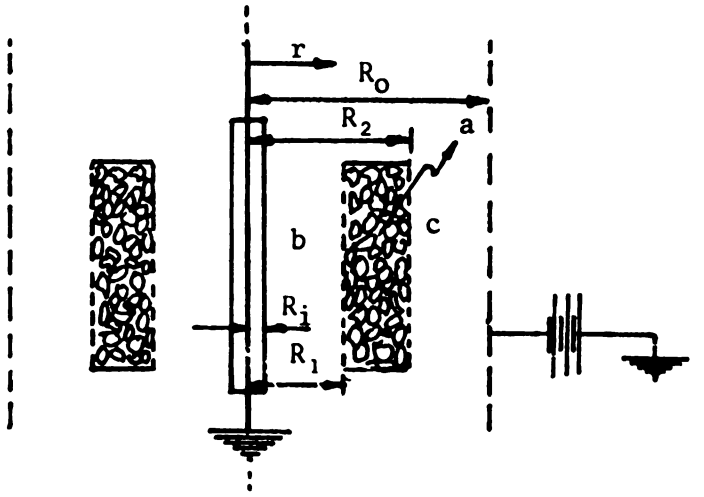

Figure 4.3. Annular sample pan in cylindrical field.

In the absence of any real charges, the Laplace equation for the voltage distribution gives

$$\nabla^2 V = 0$$

or

$$\frac{d^2V}{dr} + \frac{1}{r}\frac{dV}{dr} = 0$$

The two boundary conditions required to solve this differential equation are: (1) the potential is continuous at the boundary, and (2) the normal component of the electric displacement ($\underset{\rightarrow}{D} = \varepsilon \underset{\rightarrow}{E}$) is continuous across an interface. Using these two boundary conditions over regions a, b and c, one obtains for the field in the region of the dielectric 'a'

$$\underset{\rightarrow}{E}_a = \frac{-(V_2 - V_1)}{\ln R_2/R_1} \frac{1}{r} \underset{\rightarrow}{e}_r$$

where

$$V_1 = \ln(R_1/R_i)^{\varepsilon_a \Delta V} / \ln\left\{\left(\frac{R_2}{R_1}\right)^{\varepsilon_o} \left(\frac{R_1}{R_i}\frac{R_o}{R_2}\right)^{\varepsilon_a}\right\}$$

and

$$V_2 = \ln\{(R_1/R_i)^{\Delta V} (R_2/R_o)^{V_1}\} / \ln \frac{R_1}{R_i}$$

For $\varepsilon_a \simeq 3$ (guestimate for bed of Al_2O_3 particles)

$\varepsilon_o = 1$, $\Delta V = 6000$ V, $R_i = .0794$ cm, $R_1 = .3$ cm, $R_2 = .75$ cm and $R_o = 1.25$ cm

one gets

$$V_1 = 3716.7 \text{ (V)} \quad \text{and} \quad V_2 = 4570.9 \text{ (V)}$$

$$E_a = -\frac{932.23}{r} \text{ (V/cm)}$$

$$\langle E_a \rangle_{avg} = \frac{-932.23}{\pi(.75^2 - .30^2)} \int_{.30}^{.75} 2\pi r \frac{1}{r} dr = 1.776 \text{ (KV/cm)}$$

$$\nabla E_a^2 = (-932.23)^2 \times \frac{-2}{r^3} (V^2/cm^3)$$

and

$$\nabla E_{avg}^2 \simeq -1.471 \times 10^7 (V^2/cm^3)$$

A.3 Cylindrical Bed of Dielectric Particles in Cylindrical Electrical Field

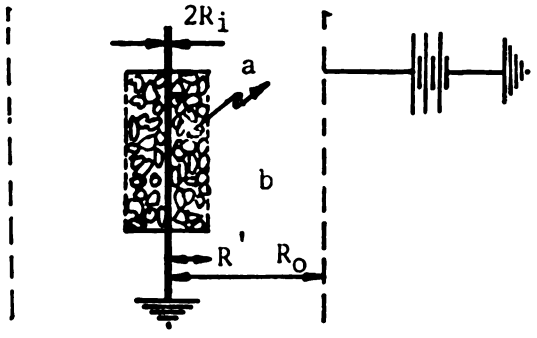

Figure 4.4. Cylindrical sample bed coaxial with cylindrical field.

Once again, the Laplace equation in cylindrical coordinates, combined with the two boundary conditions mentioned in Section A.2, lead to the relations

$$\underset{\rightarrow}{E}_a = \frac{-dV_a}{dr} = \frac{(V_i - V_{R'})}{\ln R'/R_i} \frac{1}{r} \underset{\rightarrow}{e}_r$$

$$V_R = \frac{(\varepsilon_a V_i \ln R_o/R_i + \varepsilon_o V_{R_o} \ln R'/R_i)}{(\varepsilon_o \ln R'/R_i + \varepsilon_a \ln R_o/R')}$$

and therefore,

$$E_a = \frac{(V_i - V_{R_o})}{(\ln R'/R_i + \varepsilon_a \ln R_o/R')} \frac{1}{r} = \frac{B}{r} \quad (B = f(\varepsilon))$$

$$\langle E_a \rangle = \frac{Bx2}{(R'+R_i)} \quad ; \quad \langle \nabla E_a^2 \rangle = \frac{B^2 x -4}{(R'^2 - R_i^2)} \left(\frac{1}{R_i} - \frac{1}{R'} \right)$$

For Figures 5.8, 5.9 and 5.10:

$(V_i - V_{R_o}) = \Delta V = 3000$ V, $R_o = 1.25$ cm, $R' = 0.5$ cm, $R_i = .0089$ cm

and $\varepsilon_a \simeq 3\varepsilon_o$ (approximate value for Al_2O_3 particles, $CaCO_3$ powder and porous glass).

$\langle E_a \rangle = 1.739$ (KV/cm)

$\langle \nabla E_a^2 \rangle = 3.46 \times 10^8$ (V^2/cm^3)

For Figure 5.11:

Same as above, with $\Delta V = 4000$ V, $R' = .35$ cm

$\langle E_a \rangle = 2.975$ (KV/cm)

$\langle \nabla E_a^2 \rangle = 10.2 \times 10^8$ (V^2/cm^3)

For Figure 5.12:

$\Delta V = 4000$ V, $R' = .175$ cm, $\varepsilon_a = 4\varepsilon_o$

$\langle E_a \rangle = 4.01$ (KV/cm)

$\langle \nabla E_a^2 \rangle = 1.90 \times 10^9$ (V^2/cm^3)

For Figure 5.13(a):

$\Delta V = 6500$ V, $R' = .35$ cm, $\varepsilon_a = 2\varepsilon_o$

$\langle E_a \rangle = 5.82$ (KV/cm)

$\langle \nabla E_a^2 \rangle = 3.913 \times 10^9$ (V^2/cm^3)

For Figure 5.13(b):

$\Delta V = 6500$ V, $R' = .175$ cm, $\varepsilon_a = 2\varepsilon_o$

$\langle E_a \rangle = 10.23$ (KV/cm)

$\langle \nabla E_a^2 \rangle = 1.24 \times 10^{10}$ (V^2/cm^3)

For Figure 5.14:

$\Delta V = 4000$ V, $R' = .35$ cm, $\varepsilon_a = 3\varepsilon_o$

$\langle E_a \rangle = 2.975$ (KV/cm)

$\langle \nabla E_a^2 \rangle = 1.02 \times 10^9$ (V^2/cm^3)

For Figure 5.15:

$\Delta V = 6000$ V, $R' = .175$ cm, $\varepsilon_a = 1.5\varepsilon_o$

$$\langle E_a \rangle = 11.01 \text{ (KV/cm)}$$

$$\langle \nabla E_a^2 \rangle = 1.43 \times 10^{10} \text{ (V}^2\text{/cm}^3\text{)}$$

For Figure 5.16:

$\Delta V = 6000$ V, $R' = .175$ cm, $\varepsilon_a \simeq 4\varepsilon_o$

$$\langle E_a \rangle = 6.02 \text{ (KV/cm)}$$

$$\langle \nabla E_a^2 \rangle = 4.28 \times 10^{9} \text{ (V}^2\text{/cm}^3\text{)}$$

For Figure 5.18:

$\Delta V = 6000$ V, $R' = .16$ cm, $\varepsilon_a \simeq 1.5\varepsilon_o$

$$\langle E_a \rangle = 11.893 \text{ (KV/cm)}$$

$$\langle \nabla E_a^2 \rangle = 1.680 \times 10^{10} \text{ (V}^2\text{/cm}^3\text{)}$$

A.4 Calculations for Section 5.6(b); Keeping Average E^2 Constant but Decreasing the Average ∇E^2

For the pan-electrode geometries used in Figures 5.18 and 5.20, the overall electric field is given by (see Section A.3)

$$\underset{\rightarrow}{E} = \frac{(\Delta V)}{\ln R/R_i + \varepsilon \ln R_o/R} \frac{1}{r} \underset{\rightarrow}{e}_r$$

For the grounded filament electrode geometry used in Figure 5.18, $R_i = .00889$ cm, $R' = .16$ cm, $R_o = 1.25$ cm; and for the thick grounded electrode geometry in Figure 5.20, $R_i = .0348$ cm, $R' = .18$ cm and $R_o = 1.25$ cm.

The average field squared is given by

$$\langle E^2 \rangle = \frac{1}{\pi(R'^2 - R_i^2)} \times 2\pi \int_{R_i}^{R'} r(E^2) dr$$

or

$$\langle E^2 \rangle = \frac{\Delta V^2}{(\ln R'/R_i + \varepsilon \ln R_o/R')^2} \times \frac{2}{(R'^2 - R_i^2)} \ln \frac{R'}{R_i} \qquad \text{(A.9)}$$

For Figure 5.18

$$\Delta V = 6000 \text{ V, and } \therefore \langle E^2 \rangle = \frac{6000^2}{(2.89+\varepsilon x 2.056)^2} \times 226.5$$

ε, the dielectric constant of the bed, varies as adsorption proceeds towards saturation. The variation of amount adsorbed, W vs. ε, may be taken from Table 4.1. For Figure 5.20, one has

$$\langle E^2 \rangle = \frac{(\Delta V)^2}{(1.67 + \varepsilon x 1.911)} \times 101.21 \qquad \text{(A.10)}$$

Table A.1 lists W, ε and the ΔV obtained from equation (A.10), so as to keep the $\langle E^2 \rangle$ same as in equation (A.9) (for the same W). Also listed in Table A.1 are the average field gradient squared $\langle \nabla E^2 \rangle$ for the two cases where $\langle \nabla E^2 \rangle$ is given by

$$\langle \nabla E^2 \rangle = \frac{\Delta V^2}{(\ln R'/R_i + \varepsilon \ln R_o/R')^2} \times 4\left\{\frac{1}{R_i} - \frac{1}{R'}\right\}$$

Note that while the average $\langle E^2 \rangle$ are maintained the same, the average $\langle \nabla E^2 \rangle$ in Figure 5.20 is only 38% of the same quantity in Figure 5.18.

A.5 Approximate Calculations for Temperature Rise of Bed Due to Ionic Current

For Silica Gel:

mass of dry sample $\simeq$ 60 mg

$$Q = (1 \times 10^{-6} \text{ A})(1000 \text{ V}) \times 14.33 \frac{\text{cals/min}}{(\text{AV})}$$

$$= \underline{.0143 \text{ cals/min}}$$

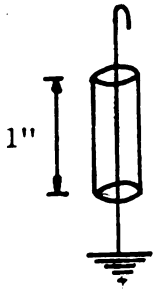

d = .32 cm

At equilibrium

$$Q = hA\Delta T_{eq}$$

Table A.1. Comparison of Fields for Figures 5.18 and 5.20.

W	ε	ΔV (KV)	$\langle \nabla E^2 \rangle'$ for Figure 5.18	$\langle \nabla E^2 \rangle^2$ for Figure 5.20	$\frac{\langle \nabla E^2 \rangle^2}{\langle \nabla E^2 \rangle'}$
0	1.53	6.83	1.646×10^{10}	6.25×10^{9}	0.38
.10	2.08	7.07	1.167×10^{10}	4.44×10^{9}	0.38
.20	4.18	7.55	4.55×10^{9}	1.73×10^{9}	0.38
.30	7.39	7.84	1.83×10^{9}	6.96×10^{8}	0.38
.40	10.98	7.99	9.24×10^{8}	3.51×10^{8}	0.38
.50	14.63	8.07	5.52×10^{8}	2.1×10^{8}	0.38
.60	18.48	8.12	3.59×10^{8}	1.36×10^{8}	0.38
.70	22.30	8.16	2.52×10^{8}	9.59×10^{7}	0.38

where

h = heat transfer coefficient of N_2 - gel interface

A = area of heat transfer

ΔT_{eq} = temperature difference at equilibrium between bed and surroundings for constant Q

For heat transfer by natural convection, h may be obtained from Figure 13.5-I of reference [S8]. For air, Pr $\simeq$ .73, $\rho_{air} \simeq 7.36 \times 10^{-4}$ gm/cc at T = 298^{o} K, $\mu \simeq 1.754 \times 10^{-4}$ g/cm sec, $k_f \simeq 6.27 \times 10^{-5}$ cal/sec cm ^{o}K; and for d = .32 cm

$$Gr = \frac{d^3 \rho^2 g \Delta T}{\mu^2 T_f} \simeq 1.897\ \Delta T$$

For $\Delta T \simeq 0.5^{o}$ K (estimate), Gr $\simeq$ .95; and from Figure 13.5-I of [S8]

$$h \simeq 2.05 \times 10^{-4}\ \text{cal/cm}^2\ \text{sec}\ ^{o}\text{K}$$

$$\therefore\ \Delta T_{eq} \simeq Q/hA \simeq \frac{.0143\ \text{cals/min} \times 1\ \text{min/60 secs}}{2.05 \times 10^{-4}\ \text{cal/cm}^2\ \text{sec}\ ^{o}\text{K} \times \pi \times .32\ \text{cm} \times 2.5\ \text{cm}}$$

$$\simeq \underline{.46^{o}\ \text{C}}$$

For Fly Ash:

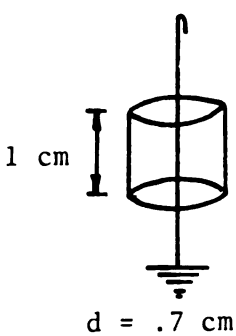

mass of dry sample $\simeq$ 150 mg

$$Q \simeq (3 \times 10^{-6}\ \text{A})(2000\ \text{V}) \times \frac{14.33\ \text{cals/min}}{(AV)}$$

$$\simeq .0858\ \text{cals/min}$$

$$Gr \simeq 19.86\ \Delta T$$

For $\Delta T \simeq 5^{o}$ C (estimate), Gr $\simeq$ 99.3; and from Figure 13.5-I of [S8]

$$h \simeq 1.79 \times 10^{-4} \text{ cal/cm}^2 \text{ sec } {}^{o}\text{K}$$

$$\Delta T_{eq} \simeq Q/hA \simeq \frac{.0858 \text{ cals/min} \times 1 \text{ min/60 secs}}{1.79 \times 10^{-4} \text{ cal/cm}^2 \text{ sec } {}^{o}\text{K} \times \pi \times .7 \text{ cm} \times 1 \text{ cm}}$$

$$\simeq \underline{3.64^{o} \text{ C}}$$

NOTE: The unsteady state temperature rise of protions of the bed away from the heat transfer surface could be higher than the equilibrium temperature rises estimated here.

A.6 Charged Spherical Dielectric Particle in Uniform Electric Field

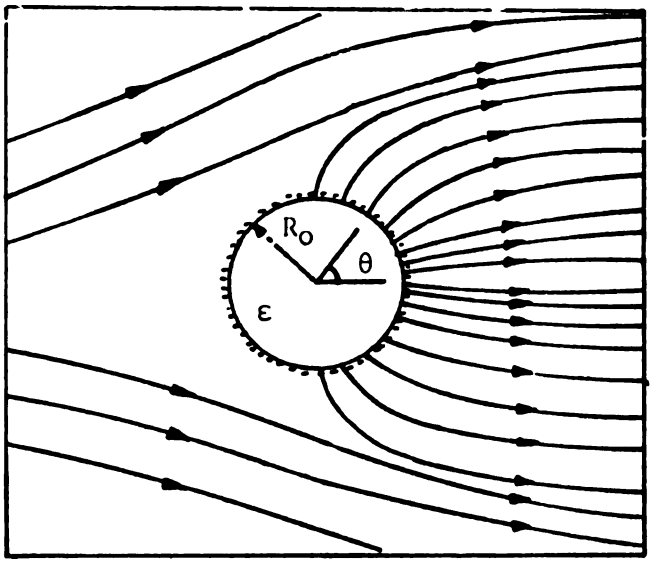

Figure 4.5. Charged particle in uniform external field.

$$E = E_o \text{Cos}\theta \left[2\frac{(\varepsilon-1)}{(\varepsilon+2)} \frac{R_o^3}{r^3} + 1\right] + 3\left(\frac{\varepsilon}{\varepsilon+2}\right) \frac{R_o^2 E_o}{r^2} \qquad \text{(A.11)}$$

The first term is due to the dielectric sphere existing in the external uniform field, while the second term is due to the charges on the sphere. At saturation the force on an approaching ion $\underset{\rightarrow}{F} = q_{ion}E = 0$, i.e., no

more ions are caught (for $\pi/2 < \theta < \pi$). The field for $0 < \theta < \pi/2$ is given by equation (A.11)

The average field is obtained from

$$E_{avg} = \frac{2}{\pi}\int_{o}^{\pi/2} E\Big|_{r=R_o} d\theta$$

$$= E_o \times \frac{\varepsilon}{(\varepsilon+2)} + 3\left(\frac{\varepsilon}{\varepsilon+2}\right)E_o$$

$$\frac{dE^2}{dr}\Big|_{r=R_o}^{avg} = -36\frac{\varepsilon(\varepsilon-1)}{(\varepsilon+2)^2} \times \frac{E_o^2}{R_o} \times \frac{2}{\pi}\int_{o}^{\pi/2} \mathrm{Cos}^2\theta d\theta \; -36\left(\frac{\varepsilon}{\varepsilon+2}\right)^2\frac{E_o^2}{R_o}$$

$$-36\frac{\varepsilon(\varepsilon-1)}{(\varepsilon+2)^2} \times \frac{E_o^2}{R_o} \times \frac{2}{\pi}\int_{o}^{\pi/2} \mathrm{Cos}\theta d\theta \; -36\left(\frac{\varepsilon}{\varepsilon+2}\right)^2\frac{E_o^2}{R_o} \times \frac{2}{\pi}\int_{o}^{\pi/2} \mathrm{Cos}\theta d\theta$$

For $R_o \simeq 20\times10^{-6}$ m, $E_o = 3\times10^3$ V/cm, $\varepsilon \simeq 4$ (typical values for fly ash particulates in ESPs)

$$E\Big|_{r=R_o}^{avg} \simeq 9.82\times10^3 (V/cm)$$

and

$$\frac{dE_r^2}{dr}\Big|_{r=R_o}^{avg} \simeq 1.79\times10^{11} (V^2/cm^3)$$

APPENDIX B

ESTIMATION OF INTERNAL RELAXATION FIELDS

APPENDIX B

ESTIMATION OF INTERNAL RELAXATION FIELDS

B.1 Internal Field Calculations for Silica Gel S-2509

B.1(a) Dielectric Constant of Solid Content in Dry Silica Gel

Density of fused transparent silica ≃ 2.24. From Kurosaki's paper [K1], for a bed of dry silica gel (specific area ≃ 143 m^2/g), apparent density ≃ .37 gm/cc and apparent dielectric constant ≃ 1.4. If

δ_1 = volume fraction of solid adsorbent in bed

δ_2 = volume fraction of voids in bed

and if the bed is dry (no adsorbate), then

$2.24 \times \delta_1 + 0 \times \delta_3 = .37$ (density of void ≃ 0)

$\therefore \delta_1 = .1652$ and

$\delta_3 = 1 - \delta_1 = .8348$ or 83.48% total voids (internal and external) in this silica gel.

For the dry bed, the last term in equation (4.13) drops out, and rearranging the remaining terms, one has

$$4\pi c_1 = (\varepsilon^o - 1)/\left\{\left(\frac{\varepsilon^o + 2}{3}\right) - \left(\frac{3\varepsilon^o \delta_3}{2\varepsilon^o + 1}\right)\right\} \qquad (B.1)$$

From [K1], ε^o (apparent dielectric constant of composite material when no adsorbate is present) ≃ 1.4

$\therefore 4\pi c_1 = 1.8988$

But $\frac{4\pi c_1}{3} = \frac{\varepsilon_1 - 1}{\varepsilon_1 + 2}$ and $\therefore$ $\underline{\varepsilon_1 = 6.173}$, where ε_1 is the dielectric constant of the silica gel solid content.

B.1(b) To Get ε^o for Silica Gel S-2509 Used in this Work

ε_1 is assumed to be the same for both the gels (a good assumption). For Silica Gel S-2509, apparent density of bed = .461 gms/cc

$$\therefore \delta_1 = .461/2.24 \simeq .2058 \quad \text{and}$$

$$\delta_3 \text{ (for a dry bed)} = 1 - \delta_1 = .7942$$

Once again, from equation (4.13) for $\varepsilon = \varepsilon^o$

$$\left(\frac{\varepsilon^o + 2}{3}\right) - \frac{3\varepsilon^o \delta_3}{(2\varepsilon + 1)} = \frac{(\varepsilon^o - 1)}{3(\varepsilon_1 - 1)} \quad (\varepsilon_1 + 2) \qquad \text{(B.2)}$$

Solving for ε^o, one gets

$$\varepsilon^o \simeq 1.529$$ (composite dielectric constant for dry Silica Gel S-2509)

B.1(c) Dielectric Constant of Single, Spherical, Porous Particle

All the adsorption in this silica gel may be safely assumed to take place in the internal micro-pores.

The maximum water vapor amount adsorbed in S-2509 (from experiments) $\simeq$ .70 gm/gm adsorbent. If average density of adsorbate is taken as 1 gm/cc, then internal pore space

$$\simeq .70 \text{ cc/gm adsorbent dry}$$

or

$$.70 \frac{\text{cc}}{\text{gm ad. dry}} \times .461 \frac{\text{gm ad. dry}}{\text{cc ad. dry}} = .3227 \frac{\text{cc}}{\text{cc adsorbent}}$$

From above, one has δ_1 = .2058 cc solid matter/cc adsorbent, $\therefore$ inter-particle void volume (macropore)

$$= 1 - .3227 - .2058 = .4715 \text{ cc/cc total}$$

Now, if one considers a single, spherical, porous particle, the internal pore volume fraction

$$= \frac{.3227}{(.3227+.2058)} \simeq .6105 \frac{\text{cc}}{\text{cc particle}}$$

and δ_1 (solid volume fraction of particle) = 1 - .6105 = .3895. If δ_2 is the volume fraction adsorbate in particle, and δ_3 is the volume fraction free gas space in particle, then

$$\delta_2 + \delta_3 = .6105$$

In order to proceed further, one needs to estimate the dielectric constant of the adsorbate, ε_2.

Let C_i be the dimensionless adsorbate concentration. Since the adsorbate is assumed to have uniform density of 1 gm/cc, then

$$\delta_2 = .6105 \times C_i \quad \text{(volume fraction adsorbate)} \quad \text{and}$$

$$\delta_3 = .6105 - \delta_2$$

For the adsorbate, the average dielectric constant is obtained by an averaging of the monolayer ($\varepsilon \simeq 1.05$, $C_i < .0927$), bound layer ($\varepsilon \simeq 43.26$, $.0927 \leq C_i \leq .1986$) and the capillary condensed layer ($\varepsilon \simeq 104$, $C_i > .1986$). Thus, if $C_i \leq .0927$, then $\varepsilon_2 = 1.05$. If $.0927 < C_i \leq .1986$, then

$$\varepsilon_2 = .0927 \times 1.05 + (C_i - .0927) \times 43.3$$

and if $C_i > .1986$, then

$$\varepsilon_2 = .0927 \times 1.05 + (.1986 - .0927) \times 43.3 + (C_i - .1986) \times 104$$

Rewriting equation (4.13), one has

$$\left(\frac{\varepsilon_p+2}{3}\right) - \frac{3\varepsilon_p\delta_3}{(2\varepsilon_p+1)} + \frac{(3\varepsilon^o-1)}{3(\varepsilon_1-1)}(\varepsilon_1+2) + \frac{(\varepsilon_p-\varepsilon^o)(\varepsilon_2+2)}{3(\varepsilon_2-1)} \qquad (B.3)$$

where

ε_p = dielectric constant of particle

Thus, knowing W (gms adsorbate overall/gm dry adsorbent) and assuming a uniform adsorbate layer (as in 4.3(b), Part I(1)), one can obtain C_i (= W/W_{max}) and then δ_3 and ε_2 as described above. Finally, from the above equation (B.3), the dielectric constant for the particle ε_p may be estimated as

$$\varepsilon_p = \frac{-b - \sqrt{b^2-4ac}}{2a}$$

where

$$b = 5 - 9\delta_3 - \frac{6(\varepsilon^o-1)}{4\pi c_1} + \frac{(6\varepsilon^o-3)}{4\pi c_2}$$

$$a = 2 - \frac{6}{4\pi c_2} \quad \text{and} \quad c = 2 - \frac{3(\varepsilon^o-1)}{4\pi c_1} + \frac{3\varepsilon^o}{4\pi c_2}$$

B.1(d) Overall Bed Dielectric Constant, ε

Treating the bed as spherical solid particles of dielectric constant ε_p interspersed with air, one has

$4\pi c_2 = 0$ (only two phases, particle and air)

$4\pi c_1 = 3\,(\varepsilon_p-1)/(\varepsilon_p+2)$

From (4.9) and (4.10), then,

$$E(\varepsilon+2)/3 = E_p'\delta_1 + \left(\frac{3\varepsilon}{2\varepsilon+1}\right)E\delta_3 \qquad (B.4)$$

and

$$E(\varepsilon-1)/4\pi = 3(\varepsilon_p-1)\delta_1 E_p'/\{4\pi(\varepsilon_p+2)\} \qquad (B.5)$$

which can be solved for ε, knowing

ε_p = particle dielectric constant

δ_3 = volume fraction of macropore (or interparticle) void volume (= .4715) (see B.1(c))

δ_1 = volume fraction of particle space in bed = $(1-\delta_3)$

$$\varepsilon = \frac{-b + \sqrt{b^2-4ac}}{2a}$$

where

$$b = -\left(\frac{\varepsilon_p+2}{\varepsilon_p-1}\right) - 5 + 9\delta_3$$

$$a = 2(\varepsilon_p+2)/(\varepsilon_p-1)-2 \quad \text{and} \quad c = -\left(\frac{\varepsilon_p+2}{\varepsilon_p-1}\right)-2$$

B.1(e) Overall Electric Field Estimate

$$E_r = \frac{\Delta V}{(\ln R'/R_i + \varepsilon \ln R'/R_o)}\,\frac{1}{r} \qquad \text{(see Figure 4.10)}$$

In this work with Silica Gel S-2509, ΔV = 6000 V, R' = .16 cm, R_i = .00889 cm, and R_o = 1.25 cm.

The value of r to be used is that corresponding to the average of the field squared in the bed, and has been estimated in Section B.2 as

$$r_{avg} \simeq .0667 \text{ cm}$$

B.1(f) Obtaining the Local Particle Field

Having obtained the macroscopic overall field E, equation (B.5) may be used to estimate $E_p' = E_p(\varepsilon_p+2)/3$, where E_p is the average particle particle field. However, due to the long, narrow pores in silica gel and the extended diffusion time periods, the adsorbate concentration in the pore will be non-uniform, decreasing as the pore center is reached. Consequently, the local particle dielectric constant ε_{pi} may be very different from the average particle dielectric constant ε_p. In Section 4.3(b), Part II, it was shown that the local particle fields E_{pi} may be obtained from the relation

$$E_{pi} \simeq E_p(\varepsilon_p+2)/(\varepsilon_{pi}+2) \tag{B.6}$$

Knowing the local adsorbate concentration C_i, the analysis undergone in B.1(c) may be reapplied to the small, local segment whose adsorbate concentration is C_i, and thus the local dielectric constant ε_{pi} may be obtained. Knowing ε_{pi}, E_{pi} is easily obtained from equation (B.6). Finally, equations (4.9) and (4.10) may be rewritten as

$$E_{pi}\frac{(\varepsilon_{pi}+2)}{3} = \left(\frac{\varepsilon_1+2}{3}\right)E_1\delta_1 + \left(\frac{\varepsilon_2+2}{3}\right)E_2\delta_2 + \left(\frac{3\varepsilon_{pi}}{2\varepsilon_{pi}+1}\right)E_{pi}\delta_3 \tag{B.7}$$

$$E_{pi}\frac{(\varepsilon_{pi}-1)}{4\pi} = c_1\delta_1\left(\frac{\varepsilon_1+2}{3}\right)E_1 + \left(\frac{\varepsilon_2+2}{3}\right)c_2\delta_2E_2 \tag{B.8}$$

where ε_2 = local adsorbate dielectric constant (obtained from knowing C_i and applying equations as in Section B.1(c))

δ_1 = local gel solid volume fraction

δ_2 = local adsorbate volume fraction

δ_3 = local gas phase volume fraction

From (B.7) and (B.8), the fields E_1 and E_2 can be estimated, and E_3 (gas phase field) is next obtained as $E_3 = 3\varepsilon_{pi}E_{pi}/(2\varepsilon_{pi}+1)$. Thus, E_2 and E_3, the required adsorbate and gas phase average, internal fields respectively, are obtained as functions of the local C_i.

B.2 Estimation of r_{avg}: Radial Position of $\langle E^2 \rangle$ Average

For the internal fields, the gradients of the internal field squared $\nabla E_{2_i}^2$ are dependent on the magnitudes of the overall field squared E^2, and not the overall gradient of the field squared ∇E^2. Hence, one needs to estimate the magnitude of the average field squared $\langle E^2 \rangle$. In Figure 5.18 and the model described in Chapter VI, the bed has dimensions $R_i = .0089$ cm, $R' = .16$ cm, $R_o = 1.25$ cm, and consequently,

$$E^2 = \frac{\Delta V^2}{(\ln R'/R_i + \varepsilon \ln R_o/R')^2} \frac{1}{r^2}$$

$$= \frac{B^2}{r^2} \quad , \quad \text{where } B = f(\varepsilon)$$

The average E^2 is given by

$$\langle E^2 \rangle = B^2 \frac{x2\pi}{\pi(R'^2 - R_i^2)} \int_{R_i}^{R'} r \frac{1}{r^2} dr = \frac{2B^2}{(R'^2 - R_i^2)} \ln\left(\frac{R'}{R_i}\right)$$

or

$$\langle E^2 \rangle = B^2 \times \frac{2 \cdot \ln .16/.0089}{(.16^2 - .0089^2)} = 226.5\ B^2$$

Also, r_{avg} may be defined as

$$\langle E^2 \rangle = \frac{B^2}{r_{avg}^2}$$

which then gives $r_{avg} = .0667$ cm

APPENDIX C

EXPERIMENTAL DATA & DATA ANALYSIS

APPENDIX C

EXPERIMENTAL DATA & DATA ANALYSIS

C.1 Spherical, Porous, Alundum Beads in Uniform Field (for Figure 5.3)

BLANK DATA: (averaged)

(Field data same as No Field data)

t:	0	4	12	20	28	36	44	52	60
mg:	0	.30	.55	.70	.80	.90	.90	.90	.90

DATA FOR ADSORPTION OF WATER VAPOR ON BEADS:

(Corrected for blank readings)

No Field data

t	mg	t	mg	t	mg
4	3.12	0	0	4	3.2
12	7.11	12	7.26	12	6.93
20	8.7	20	8.77	20	8.68
28	9.69	28	9.51	28	9.54
36	10.10	36	9.95	36	10.29
44	10.52	44	10.29	44	10.47
52	10.79	52	10.63	52	10.78
60	11.01	60	10.96	60	11.03

With Field data

t	mg	t	mg	t	mg
4	3.18	4	3.27	4	3.2
12	7.39	12	7.27	12	6.93
20	9.08	20	8.80	20	8.68
28	9.84	28	9.72	28	9.54
36	10.27	36	10.10	37	10.29
44	10.68	44	10.51	44	10.47
52	11.11	52	10.68	52	10.78
60	11.15	60	10.95	60	11.03

C.2 Drying Grade Silica Gel-Water Vapor in Uniform Field

(for Figure 5.4)

(Blank readings negligible)

No Field data

t	W	t	W	t	W	t	W	t	W
4	.0095	4	.0067	4	.0067	4	.0071	105	.1435
20	.0378	12	.0244	20	.0373	20	.0395	135	.1689
36	.0622	28	.0520	36	.0614	36	.0658	165	.1910
52	.0830	44	.0756	52	.0823	52	.0865	195	.2100
68	.1025	60	.0956	68	.1004	68	.1056	225	.2253
84	.1181	76	.1138	84	.1174	84	.1230	250	.2237
90	.1240	90	.1283	90	.1226				

With Field data

t	W	t	W	t	W	t	W	t	W
4	.0066	4	.0068	4	.0064	4	.0070	105	.1443
12	.0255	20	.0393	12	.024	20	.0396	135	.1691
28	.0530	36	.0653	28	.053	36	.0657	165	.1907
44	.0770	52	.0871	44	.0778	52	.0847	195	.2068
60	.0979	68	.1076	60	.097	68	.1039	210	.2147
76	.1157	84	.1241	76	.1152	84	.1238	225	.2212
90	.1296	90	.1304	90	.1293				

C.3 Water Vapor Adsorption on Bed of Alumina Beads in Uniform Field

(for Figure 5.5)

(Blank readings small)

Without Field data

t	mg	t	mg
5	1.45	5	1.45
10	2.88	15	4.01
25	5.74	25	5.67
35	6.76	35	6.78
45	7.63	45	7.57
60	8.43	60	8.49
70	8.89	70	8.93
80	9.28	80	9.25
90	9.53	95	9.71
100	9.78	110	10.00
110	9.95	120	10.17
120	10.12		

With Field data

t	mg	t	mg
5	1.61	5	1.50
15	4.27	15	3.72
25	5.89	25	5.15
35	6.76	35	6.46
45	7.55	45	7.51
62	8.87	60	8.18
70	9.10	75	9.08
80	9.57	90	9.46
90	9.43	105	10.02
100	9.87	120	10.21
110	10.17		
120	10.21		

C.4 Water Vapor Adsorption in Crushed Al_2O_3 Particles in Uniform Field

(for Figure 5.6)

(Trouble during weighing with field on for approximately first 15 mins. Reading at t = 15 mins. taken as start of adsorption.)

Without Field data

t	mg	t	mg	t	mg
15	0	15	0	140	15.46
25	2.54	25	2.78	160	16.47
35	4.47	82	11.01	180	17.35
45	6.21	90	11.89	200	18.09
60	8.39	105	13.08	220	18.82
75	10.16	123	14.38	240	19.30
90	11.64				

With Field data

t	mg	t	mg	t	mg
15	0.00	15	0.00	105	12.86
25	2.46	25	3.30	120	14.00
35	4.62	35	4.66	140	15.31
45	6.18	45	6.71	160	16.36
60	8.63	60	8.62	180	17.09
75	11.18	75	10.17	200	18.11
90	12.59	90	11.68	220	18.72
				240	19.34

C.5 Adsorption of Water Vapor in Crushed Alumina in Cylindrical Field and Annular Screen Sample Container

(for Figures 5.7a, b, c, and d)

BLANK DATA: (averaged)

t	No Field mg	With Field mg	t	No Field mg	With Field mg
6	.80	.80	90	2.37	1.56
14	1.46	1.24	105	2.39	1.58
24	1.78	1.43	120	2.44	1.58
34	1.94	1.50	135	2.47	1.58
45	2.06	1.51	150	2.50	1.58
60	2.18	1.52	165	2.51	1.58
75	2.27	1.54	180	2.52	1.58

(All the following data obtained after subtracting blank.)

For Figure 5.7(a)

Without Field data

t	mg	t	mg	t	mg	t	mg
6	2.61	90	22.33	6	2.53	75	20.53
9	7.13	105	23.23	14	6.74	90	21.85
24	11.13	120	23.86	24	10.96	105	22.72
34	14.21	137	24.50	34	13.96	120	23.32
45	16.70	151	24.93	48	16.93	135	24.19
60	19.19	166	25.28	60	18.64	150	24.63
75	21.13	180	25.86				

With Field data

t	mg	t	mg	t	mg	t	mg
0	0	90	22.33	0	0	75	20.53
6	2.61	105	23.23	6	2.54	90	21.85
19	7.13	120	23.86	14	6.74	105	22.72
24	11.13	137	24.50	24	10.96	120	23.32
34	14.21	151	24.93	34	13.96	135	24.19
45	16.70	166	25.28	48	16.93	150	24.63
60	19.19	180	25.86	60	18.44		
75	21.13						

For Figure 5.7(b)

Without Field data

t	mg	t	mg	t	mg	t	mg
8	4.18	105	21.57	6	3.0	105	22.31
14	7.49	120	22.10	14	8.49	120	23.18
24	11.84	130	22.45	25	13.25	135	23.39
34	14.64	190	24.44	35	15.84	150	23.60
45	16.68	200	24.37	45	18.22	165	24.09
60	18.54	210	24.61	60	20.15	180	24.08
75	19.64	220	24.65	76	20.96	200	24.33
90	21.18			90	21.71		

t	mg	t	mg
6	2.69	92	21.71
14	6.97	105	22.29
24	11.35	124	22.84
34	14.76	140	23.43
45	17.10	160	23.87
60	19.03	306	26.15
75	20.55	317	25.82

With Field data

t	mg	t	mg	t	mg	t	mg
0	0	90	21.48	6	2.98	90	19.90
20	9.98	105	22.29	14	7.60	115	21.68
27	12.47	120	22.61	24	11.84	144	21.96
34	14.74	130	23.19	34	14.29	154	22.28
45	16.52	140	22.79	45	16.26	165	22.93
60	18.67	150	23.49	60	18.02	180	23.18
75	19.89	212	24.02	75	19.19	210	24.26
		220	24.22			220	24.41

t	mg	t	mg
6	3.2	105	21.95
14	7.94	120	22.79
24	10.96	140	23.55
34	13.71	160	23.72
45	16.47	180	24.16
60	18.13	288	24.36
75	19.95	298	24.21
90	21.16		

For Figure 5.7(c)

Without Field data

t	mg	t	mg
8	9.43	91	24.92
14	13.99	100	25.12
24	17.82	110	22.34
34	20.31	120	25.69
45	21.67	242	27.03
60	23.33	250	27.03
75	24.21		

With Field data

t	mg	t	mg
9	9.95	75	23.62
16	14.45	90	24.46
24	17.52	105	24.80
34	19.98	120	25.18
45	21.51	220	26.39
60	22.98	228	26.52

For Figure 5.7(d)

Without Field data

t	mg	t	mg
6	7.5	60	23.63
14	13.84	76	24.61
24	17.86	195	27.62
35	20.59	205	27.62
45	21.92	215	27.62

With Field data

t	mg	t	mg
6	6.91	60	23.24
15	13.87	77	24.57
24	17.05	90	25.27
34	20.01	105	26.36
45	22.17	120	26.36
		143	26.78
		221	27.60

C.6 Water Vapor Adsorption in Crushed Alumina in Cylindrical Field

(for Figure 5.8)

BLANK DATA FOR C.6, C.7, C.8: (averaged)

Without Field data

t	mg	t	mg
0	0	40	1.46
6	.51	50	1.50
12	.87	60	1.54
18	1.11	70	1.55
24	1.27	80	1.55
32	1.39	90	1.55
		100	1.55

With Field data (3KV)

t	mg	t	mg
0	0	40	1.20
6	.42	50	1.26
12	.69	60	1.28
18	.90	75	1.30
24	1.02	90	1.30
32	1.15	100	1.30

(Blank data subtracted)

Without Field data

t	mg	t	mg
6	5.27	77	24.09
14	10.82	90	25.07
24	15.13	105	26.19
34	17.99	120	27.08
46	20.51	135	27.72
60	22.17	150	27.95
		324	30.47

With Field data

t	mg	t	mg	t	mg	t	mg
6	4.91	90	24.51	6	5.34	120	26.81
15	10.62	105	25.64	14	11.18	135	27.23
24	14.64	120	26.48	24	15.18	150	27.47
34	17.63	135	26.88	34	18.36	170	27.82
45	19.96	150	27.49	45	20.33	190	28.44
60	21.76	202	30.4	60	22.21	210	28.90
75	23.19			76	24.08	230	29.03
				92	25.07		

C.7 Water Vapor Adsorption on $CaCO_3$ Powder in Cylindrical Electric Field

(for Figure 5.9)

(Same blank data as in C.6, with blank subtracted)

Without Field data

t	mg	t	mg
6	1.76	55	3.80
12	2.46	70	3.90
18	2.77	80	4.09
24	3.13	90	4.19
32	3.41	100	4.29
40	3.57	110	4.19

With Field data

t	mg	t	mg	t	mg
6	2.09	6	1.97	50	3.98
11	2.49	12	2.50	60	3.78
18	3.15	18	2.78	76	4.05
24	3.29	24	3.21	90	3.99
32	3.44	32	3.44	100	4.05
40	3.42	40	3.62		
50	3.67				
60	3.75				
75	3.85				

C.8 Water Vapor Adsorption in Porous Glass in Cylindrical Electric Field

(for Figure 5.10)

(Same blank data as in C.6, with blank subtracted)

Without Field data

t	mg	t	mg	t	mg
6	3.77	6	3.77	6	3.79
12	6.26	12	5.62	12	5.93
18	7.46	19	7.12	18	6.90
24	8.54	24	7.58	24	7.71
32	9.05	32	8.49	32	8.68
40	9.57	40	8.84	40	9.14
51	10.33	50	9.43	40	9.68
60	10.34	60	9.80	60	10.18
75	10.70	77	10.77	70	10.48
90	11.11	91	10.33	80	10.77
106	11.28	105	10.43	90	10.77
120	11.28	128	10.79	99	10.77

With Field data

t	mg	t	mg	t	mg	t	mg
6	3.86	40	9.68	6	3.29	32	8.94
12	6.22	50	10.41	12	5.99	40	9.19
18	7.41	62	10.33	18	7.22	50	9.38
24	8.46	75	10.67	24	7.83	65	10.04
32	9.02	90	11.01				
		100	11.03				
		110	11.16				

C.9 Water Vapor Adsorption in Linde Zeolite Beads in Cylindrical Electrical Field

(for Figure 5.11)

(Blank data negligible)

Without Field data

t	W	t	W	t	W	t	W
6	.0085	60	.0797	6	.0073	80	.0977
14	.0219	80	.0986	14	.0200	105	.1183
22	.0346	100	.1137	22	.0332	120	.1283
30	.0447	120	.1256	30	.0432	150	.1419
40	.0575	140	.1351	40	.0559	182	.1501
50	.0687	160	.1415	50	.0671	210	.1544
				60	.0784	240	.1577

With Field data

t	W	t	W	t	W	t	W
6	.0072	80	.0923	6	.009	80	.0999
14	.0188	100	.1090	14	.0213	105	.1197
22	.0303	120	.1222	22	.0344	120	.1306
30	.0400	140	.1315	30	.0456	150	.1443
40	.0525	160	.1387	40	.057	180	.1522
52	.0657	170	.1413	50	.070	210	.1585
60	.0736			60	.0813	225	.1594

C.10 Water Vapor Adsorption in Al_2O_3 Beads Strung on Ground Electrode Filament in Cylindrical Field

(for Figure 5.12)

BLANK READINGS: (averaged)

t	No Field mg	With Field mg
6	.01	- .30
14	.03	- .40
22	.07	- .46
30	.07	- .50
40	.07	- .50
50	.07	- .50
60	.07	- .50

Without Field data

(with blank subtracted)

t	mg	t	mg
6	3.06	60	11.81
14	6.08	70	12.17
22	8.11	80	12.51
30	9.47	90	12.65
40	10.60	110	12.75
50	11.51	120	12.68

With Field data

t	mg	t	mg
6	2.96	70	11.86
14	5.94	80	12.11
22	7.98	90	12.30
30	9.36	100	12.41
40	10.50	110	12.55
50	11.17	120	12.55
60	11.63		

C.11 Water Vapor Adsorption in Drying Grade Silica Gel in Cylindrical Non-Uniform Field

(for Figures 5.13a, b)

BLANK DATA:

t:	0	10	25	40	60	80
No field mg:	0	.28	.82	1.02	1.10	1.10
With field mg:	0	.24	.72	.90	.98	1.00

For Figure 5.13(a)

Without Field data

t	W	t	W	t	W
90	.2384	10	.0282	100	.2622
110	.2714	25	.0796	120	.2862
130	.2873	40	.1253	140	.2942
155	.2934	60	.1796	160	.2974
170	.2950	80	.2253		

With Field data (ΔV = 4 KV)

t	W	t	W	t	W
10	.025	120	.2811	90	.2333
25	.0758	140	.2918	111	.2688
40	.120	160	.2960	131	.2893
60	.1719	180	.2986	151	.2962
80	.2156	200	.2995		
100	.2536				

With Field data (ΔV = 6.5 KV)

t	W	t	W	t	W	t	W	t	W
10	.0175	100	.2729	10	.0229	100	.2723	0	0
25	.0746	120	.2885	25	.0750	120	.2886	90	.2486
40	.1296	140	.2935	40	.1257	140	.2923	110	.2780
60	.1850	160	.2961	60	.1844	160	.2936	154	.2912
80	.2380			80	.2371				

For Figure 5.13(b)

Without Field data (All values standardized to $W^{\dagger}_{max}$ = .30)

t	W	t	W	t	W	t	W	t	W
10	.048	10	.0425	10	.0474	10	.9479	10	.0484
25	.1215	25	.1161	25	.1251	25	.1235	25	.1255
42	.1895	40	.1754	40	.1862	40	.1822	40	.187
60	.2463	62	.2445	60	.2499	60	.2449	60	.251
76	.2813	75	.2447	75	.2813	75	.2791	75	.284
90	.2920	90	.2926	90	.2913	90	.2912	90	.295
105	.2972	105	.2980	105	.2952	105	.2958	105	.2994
120	.3000	120	.3000	120	.2980	125	.2994	120	.3000
				135	.3000	135	.3000		

With Field data

t	W	t	W	t	W	t	W
10	.0502	10	.0541	10	.0541	10	.0539
25	.1222	25	.1284	25	.1388	25	.1233
40	.1826	40	.1953	41	.2154	41	.1894
60	.2622	60	.2731	60	.2861	60	.2951
75	.2922	75	.2939	75	.2966	75	.2896
90	.2945	90	.2969	90	.2983	90	.2962
105	.300	105	.2991	105	.300	105	.3000
120	.300	120	.3000	120	.300	120	.3000

---

†Each experiment involves a different geometry and size distribution of silica gel particles. To bring about some uniformity in the comparison, an average maximum value of $W \simeq .30$ is taken for the samples and the corresponding W_{max} are corrected for this maximum.

With Field data (cont'd)

t	W	t	W	t	W	t	W	t	W
10	.0505	10	.0546	10	.0505	10	.0474	10	.0562
25	.1259	25	.1305	25	.1291	25	.1220	25	.1278
40	.1889	40	.1902	40	.1982	40	.1845	40	.1890
60	.2618	60	.2544	60	.2659	60	.2483	61	.2525
75	.2914	75	.2848	75	.2925	75	.2815	75	.2814
90	.2957	90	.2930	90	.2974	90	.2900	90	.2927
105	.2998	105	.2961	105	.2976	105	.2957	105	.2957
120	.3000	120	.2988	120	.3000	120	.3000	120	.3000
		135	.3000						

CHECK FOR POLARIZATION-DEPOLARIZATION EFFECT IN SECTION 5.4(d):

No Field point				With Field point			
t:	150	t:	132	t:	150	t:	132
W:	.2230	W:	.2735	W:	.2220	W:	.2698

C.12 Water Vapor Adsorption in Silica Gel S-4133 (25 A^{o}, M.P.D.) in Cylindrical Field

(for Figure 5.14)

(Blank data negligible)

Without Field data

t	W	t	W	t	W	t	W
1.5	.0112	80	.2874	1	.0071	80	.2956
11	.0818	100	.3171	16	.1136	100	.3274
25	.1446	121	.3319	25	.1516	120	.3418
40	.1956	140	.3359	40	.2023	157	.3493
60	.2478	160	.3384	60	.2558	160	.3496

With Field data

t	W	t	W	t	W	t	W
1.5	.012	60	.2767	1.5	.0100	80	.3210
10	.080	82	.3211	15	.0997	100	.3435
25	.1554	100	.3370	26	.1522	120	.3467
40	.2145	120	.3417	40	.1987	140	.3477
		140	.3429	60	.2678		

C.13 Monolayer Water Vapor Adsorption in Silica Gel S-2509 (60 A°, M.P.D.) in Cylindrical Field

(for Figure 5.15)

(Blank data negligible)

Without Field data

t	W	t	W	t	W	t	W
0	0	0	0	32	.0665	6	.0291
10	.0316	1	.0052	45	.0721	15	.0482
25	.0547	5	.026	66	.0776	30	.0617
43	.0648	15	.0493	85	.0787	45	.069
61	.0733					71	.0729

With Field data

t	W	t	W	t	W
0	0	0	0	0	.0245
11	.0354	1	.0035	15	.0528
25	.0560	11	.0383	30	.0687
40	.0676	26	.0577	45	.0728
60	.0768	41	.0669	65	.0743
80	.0821	109	.0768	80	.0743

C.14 Water Vapor Adsorption on Alundum Beads Strung on Ground Filament Electrode in Cylindrical Field

(for Figure 5.16)

t	mg	t	mg	t	mg	t	mg
0	0	90	15.44	0	0	60	12.30
5.5	1.46	143	18.23	5	1.22	94	15.40
15	4.64	180	19.81	15	4.66	120	17.00
30	8.30	210	20.72	30	8.15	185	19.78
45	10.84			45	10.45	224	21.15
60	12.59						

C.15 Multilayer Water Vapor Adsorption in Silica Gel S-2509 (M.P.D. ≃ 60 A°) in Cylindrical Field

(for Figure 5.18)

(Blank data negligible)

(All values of W corrected for $W_{max} = .70 \frac{\text{gm adsorbed}}{\text{gm adsorbent}}$)

Without Field data

t	W	t	W	t	W	t	W	t	W
15	.1016	10	.0817	10	.0736	10	.0798	5	.0482
25	.1404	25	.1477	25	.1329	31	.1661	15	.1039
40	.1924	40	.1967	40	.1802	60	.2496	31	.1684
60	.2489	60	.2548	60	.2320	141	.4190	60	.2570
90	.3197	90	.3266	90	.3023	204	.5234	93	.3408
112	.3666	120	.3864	120	.3632	240	.5765	124	.4089
130	.4035	175	.4830	165	.4466	278	.6268	137	.4356
205	.5317	215	.5447	294	.6324	306	.6562	201	.5477
240	.5820	242	.5851	330	.6716	421	.7000	263	.6329
275	.6270	275	.6275	363	.7000			310	.6800
302	.6577	364	.7000					343	.6934
332	.6852							362	.6968
370	.700							385	.7000

t	W	t	W	t	W	t	W
5	.0478	183	.5185	5	.0481	157	.4706
16	.1075	230	.5915	15	.1061	188	.5262
30	.1619	278	.6539	30	.1668	228	.5876
61	.2554	312	.6844	61	.2661	265	.6352
101	.3558	346	.6963	90	.3309	304	.6717
139	.4365	366	.7000	121	.3992	341	.6853

With Field data

t	W	t	W	t	W	t	W	t	W
10	.0672	91	.3667	10	.0788	5	.0506	5	.0512
25	.1384	156	.5230	25	.1547	15	.1107	15	.1110
40	.1891	210	.5978	41	.2199	31	.1846	30	.1757
61	.2511	255	.6658	61	.2910	60	.2775	60	.2803
90	.3471	289	.6892	80	.3488	95	.4008	90	.3842
140	.4802	306	.6943	158	.5359	133	.4970	133	.4747
160	.5239	330	.7000	180	.5797	177	.5628	142	.4981
180	.5582			216	.6397	333	.7000	193	.5963
210	.6035			300	.6912			230	.6512
250	.6584			423	.7000			261	.6881
271	.6816							280	.7000
300	.6960								
330	.7000								

With Field data (cont'd)

t:	5	45	75	110	160	190	235	280	300
W:	.0542	.2391	.3305	.4177	.5221	.5751	.6460	.6853	.7000

C.16 Adsorption of Non-Polar C_2Cl_4 in Porous Silica Gel S-2509 in Cylindrical Electric Field

(for Figure 5.19)

(Blank data negligible)

(All values of W corrected for W_{max} = 1.05)

Without Field data

t	W	t	W
1	.0396	1	.0398
10	.3964	10	.3933
21	.6996	22	.7215
30	.8845	35	.9658
45	1.046	51	1.048
60	1.05	69	1.050

With Field data

t	W	t	W
1	.0406	1	.0399
10	.4061	10	.3996
28	.8646	25	.7955
40	1.032	40	1.0304
55	1.05	55	1.05
65	1.05	65	1.05

C.17 Adsorption of Water Vapor on Silica Gel S-2509 in the Same Average $\langle E^2 \rangle$ but Smaller Average $\langle \nabla E^2 \rangle$

(for Figure 5.20)

(No Field data same as in C.15)

(All values of W corrected for W_{max} = .70)

With Field data

t	W	KV	t	W	KV	t	W	KV
5	.0495	6.9	5	.052	7.0	6	.06	6.9
15	.1037	7.2	15	.12	7.2	16	.123	7.2
30	.1705	7.2	31	.179	7.3	32	.195	7.5
61	.2952	7.4	60	.270	7.5	63.5	.304	7.5
95	.3977	7.5	91	.354	7.5	88.5	.377	7.5
121	.4589	7.9	116	.409	7.5	139.5	.506	7.5
157	.5421	7.5	343	.700	7.5	166.5	.563	7.5
208	.6383	7.5				200	.626	7.5
257	.7000	7.5				227	.665	7.5
						316	.700	7.5

C.18 Desorption Kinetics: Water Vapor-Silica Gel S-2509 (M.P.D. = 60 A°)

(for Figure 5.22)

Without Field data

t	W	t	W
16	.0293	10	.0085
31	.1117	21	.0627
46	.2111	35	.147
62	.3221	51	.2528
125	.6617	66	.3551
142	.6922	88	.4945
171	.7062	115	.6230
239	.7109	149	.6979
		177	.7112

With Field data

t	W	t	W
10	.0127	11	.0177
20	.0599	20	.0655
30	.1254	30	.1255
47	.2352	45	.2265
63	.3475	60	.3410
89	.5040	90	.5087
113	.6184	120	.6344
130	.6614	147	.6906
155	.6921	169	.7043
170	.6991		

C.19 Data for Adsorption Isotherm

(for Figure 3.3)

(All data corrected for blank experimental data)

Without Field data

W	p/p_s	W	p/p_s	W	p/p_s	W	p/p_s
.0467	.140	.0447	.1368	.1000	.451	.675	.898
.0711	.280	.0738	.3090	.2214	.701	.689	.960
.1148	.457	.1650	.6170	.5980	.893	.690	1.000
.2681	.697						

W:	.664	W:	.3758	W:	.5369	W:	.697
p/p_s:	.889	p/p_s:	.7922	p/p_s:	.833	p/p_s:	1.0

With Field data

W	p/p_s	W	p/p_s	W	p/p_s	W	p/p_s
.0494	.1413	.0507	.195	.651	.882	.104	.456
.0824	.3187	.0931	.427	.684	.960	.2854	.753
		.2709	.7233	.686	1.000	.709	1.000

W:	.6839	W:	.4561	W:	.2347	.4835	W:	.7024
p/p_s:	.923	p/p_s:	.8235	p/p_s:	.705	.825	p/p_s:	1.0

W:	.701
p/p_s:	1.0

C.20 Procedure for Obtaining Initial Dry Silica Gel Sample Weight

Example

Maximum 'calibrated' weight = 100 mg.

Weight of sample pan (without adsorbent) brought to equilibrium with surrounding moist atmosphere ($p/p_s = 1$) = W_s + 50 mg. (reading = .1293, say); 50 mg. acts as counterweight.

Sample pan removed from chamber, filled with dry R.T. sample and immediately inserted back in chamber (t = 0).

After 1 min. reading taken (50 mg. wt. removed), reading = .1449

After 5 min. reading = .1663

$\therefore$ initial reading = $.1663 - \frac{(.1663 - .1449)}{0.8} = .1396$ (4 min/5 min = 0.8)

$\therefore$ sample weight (when dry) = (.1396 - .1293) x 100 + 50 (counter wt.)

= 51.03 mg. sample

C.21 Fly Ash-Water Vapor Data (for Figures 7.5 & 7.6)

FOR FIGURE 7.5, CURVES 1

(Same blank data as in C.6; corrected for blank data)

Without Field data

t	mg	t	mg	t	mg
6	1.09	6	1.18	6	1.3
13	1.73	12	1.81	12	1.81
19	1.94	20	2.26	19	1.83
24	1.93	37	2.36	26	1.92
32	2.05	47	2.36	35	1.82
40	2.24	60	2.59		
50	2.48	70	2.60		
60	2.42				
70	2.44				

With Field data

t	mg	t	mg
6	1.45	10	1.42
12	1.61	20	1.67
19	1.98	31	1.80
26	1.89	41	1.92
35	1.84		
45	2.02		
60	1.84		

FOR FIGURE 7.5, CURVES 2:

Without Field data

t	mg
0	0
5	.35
15	.86
31	.98
52	.97
69	.97

With Field data

μA	t	mg	t	mg
	5	.26	5	.39
	15	.56	15	.74
3.1	31	.57	30	.43
3.4	42	.47	40	.65
			51	.39

FOR FIGURE 7.6, CURVES 1:

Without Field data

t	mg	t	mg
5	.93	105	6.54
15	1.92	120	7.18
30	3.44	229	9.33
45	4.18	249	9.74
60	4.94	271	10.10
75	5.44		
90	5.93		

With Field data

μA	t	mg	μA	t	mg
.6	5	.96		81	5.66
	17	2.52		102	6.29
2.5	30	3.91		132	7.93
	47	4.61	3.7	157	8.29
3.3	60	5.09		346	10.85

FOR FIGURE 7.6, CURVES 2:

Without Field data

t	mg
5	.32
16	.94
30	1.43
45	1.7
61	2.11
80	2.41
100	2.70
131	3.05

With Field data

μA	t	mg
	5	.37
5.4	15	.54
5.2	30	1.52
	45	1.95
	60	2.3
	81	2.43
	101	2.71

C.22 Water Vapor Adsorption in Crushed Alundum Beads in Point-Plane Electrode System

(for Figure 5.17)

Without Field data

t	mg	t	mg
5	2.29	5	2.45
15	5.88	15	5.88
28	7.62	28	7.88
35	8.74	36	8.66
45	9.41	45	9.11
60	10.12	60	9.89
75	10.54	75	10.40
90	10.72	90	10.47
113	10.96	105	10.61
120	11.03	120	10.65

With Field data

(Push on Pan (final) = 0 mg)

t	mg	t	mg	t	mg
5	2.4	5	2.44	5	2.31
15	6.23	15	6.06	15	5.26
25	7.98	25	8.14	25	7.83
35	8.98	35	9.49	35	9.10
45	9.62	45	10.15	45	9.77
60	10.28	60	10.76	60	10.56
75	10.71	75	11.00	75	10.69
90	11.04	90	11.18	90	11.00
105	11.33	105	11.26	105	11.08
120	11.33	120	11.33	120	11.26
Push on Pan (initial)	= .50 mg		= .76 mg		= .49 mg

C.23 Water Vapor Adsorption in HCl Treated Silica Gel S-2509

(Blank data negligible)

(All values of W corrected for $W_{max} = .70 \frac{\text{gm adsorbed}}{\text{gm adsorbent}}$)

SAMPLE I

Without Field data

t	W
5	.0540
15	.1119
31	.1771
60	.2673
95	.3590
131	.4375
178	.5172
222	.5974
278	.6708
326	.6938
359	.6999
375	.7000

With Field data

t	W
6	.0638
26	.1669
53	.2601
80	.3398
113	.4250
173	.5480
247	.6682
287	.6940
312	.6971
345	.7000

SAMPLE II

Without Field data

t	W	t	W
5	.0526	5	.0533
16	.1163	17	.1249
31	.1743	33	.1896
60	.2636	97	.3697
98	.3645	138	.4593
146	.4612	170	.5186
181	.5241	213	.5910
224	.5967	237	.6262
279	.6703	334	.6979
420	.7000	364	.7000

With Field data

t	W	t	W
5	.0506	5	.0575
15	.1122	15	.121
32	.1833	30	.1852
60	.2763	61	.2907
92	.3651	90	.3683
127	.4500	124	.4548
176	.5499	151	.5062
226	.6342	200	.5982
255	.6713	334	.7000
440	.7000		

APPENDIX D

EQUIPMENT DESCRIPTIONS

APPENDIX D

EQUIPMENT DESCRIPTIONS

(1) 'SPELLMAN' High Voltage D.C. Supply

Range: 0-20 KV
(see Figure D.1)

(2) 'CAHN' Gram Electrobalance

(Adapted for remoted weighing)
Precision = 0.1 microgram
Accuracy = 0.05% of range
Maximum Load on Loop B (used in this work) = 1 g
Sensitivity = .001 mg
6 V Calibration battery replaced by filtered and stabilized D.C. power supply.
(see Figure D.2)

(3) Blue M 'Magni Whirl' Constant Temperature Water Bath

(4) 'Simpson' Ultra High Sensitivity Volt Ohm Micro-Ammeter

(see Figure D.1)

(5) Model D-612T ELECTRO Filtered D.C. Power Supply

(see Figure D.1)

(6) 'RAYTHEON' Voltage Stabilizer

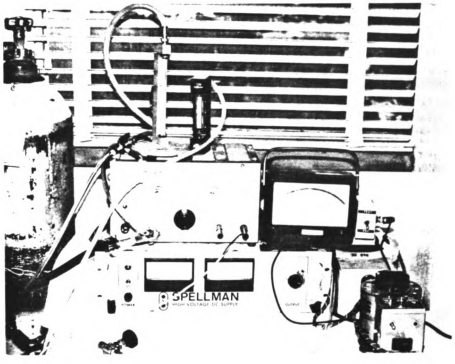

Figure D.1. 1) H.V. Supply; 2) Multimeter; 3) D.C. Power Supply; 4) Variacs.

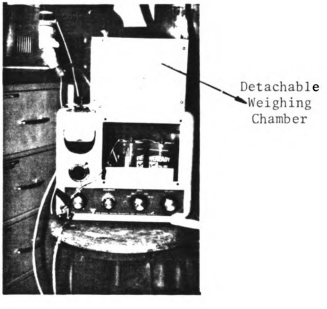

Figure D.2. CAHN Gram Electrobalance

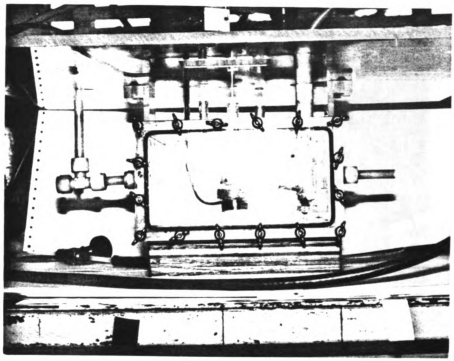

Figure D.3. Adsorption Chamber with Electrode Assembly.

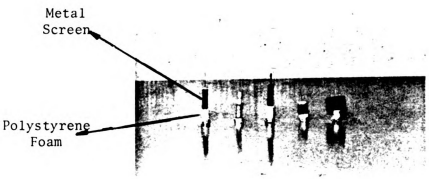

Figure D.4. Adsorbent Pans used in this work.

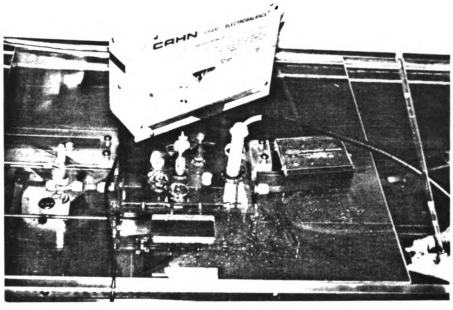

Figure D.5. Adsorption Chamber in Water Bath with Weighing Chamber.

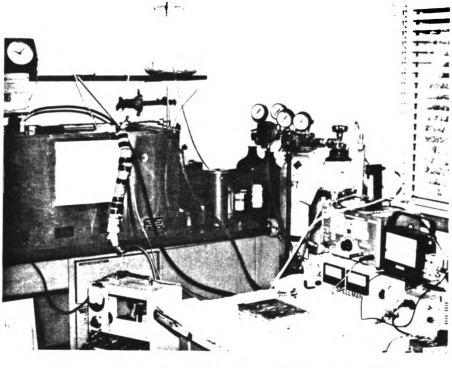

Figure D.6. Overall view of all equipment.

APPENDIX E

COMPUTER PROGRAM FOR SINGLE-PORE MODEL

APPENDIX E

COMPUTER PROGRAM FOR SINGLE-PORE MODEL

As mentioned in Chapter VI, the mathematical model for surface diffusion and adsorption in a single, open, cylindrical pore was solved on the computer by the 'Implicit Finite Difference' scheme. The following page represents the 'flow chart' for the various operations. Some of the terms used in the flow chart are described below:

C(I,N) = Surface adsorbate concentration (dimensionless)

G(I,N) = Gas phase concentration (dimensionless)

DZO = Surface diffusion coefficient (for monolayer)

D2(loc.) = Local, adsorbate dielectric constant

DP(loc.) = Local, particle dielectric constant

EP(loc.) = Local, particle field strength x r

ES(loc.) = Local, adsorbate phase field strength x r

EG(loc.) = Local, gas phase field strength x r

W = gms. adsorbed/gm. dry adsorbent

D2(avg) = Average adsorbate dielectric constant in bed

DP(avg) = Average particle dielectric constant in bed

D = Dielectric constant of overall bed

E = Average field strength in bed x r

EP(avg) = Average particle field strength in bed x r

ALPHA, BETA = (defined in program)

DC = Dielectric constant of surface hopping molecules

XA, XB, XC, XD = Matrix elements

FLOW CHART FOR COMPUTER PROGRAM

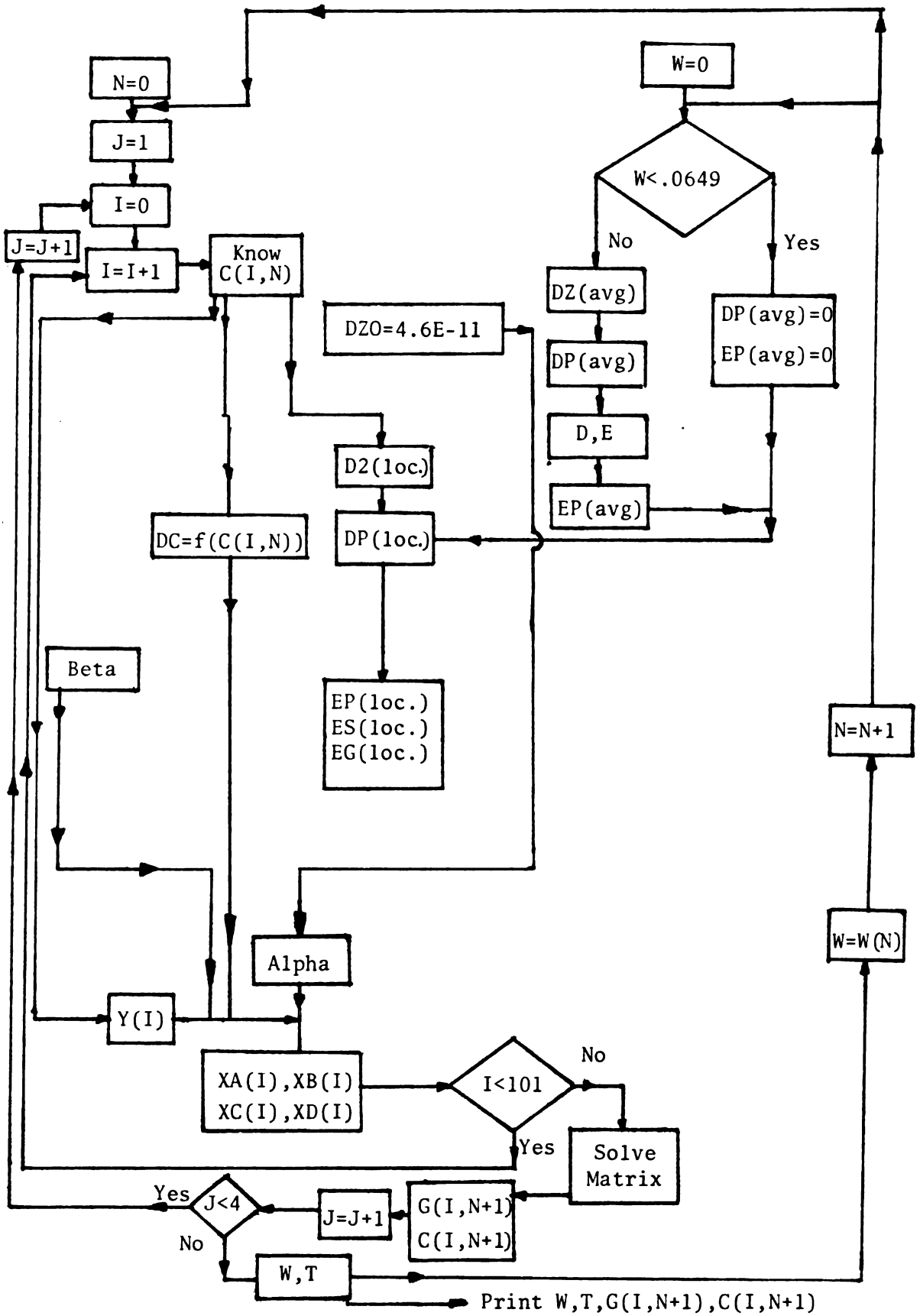

In Section E.1 is given a sample output for the variation of W with respect to time T when no external field is applied. Section E.2 represents the corresponding output when the field is imposed. Sections E.3 and E.4 give the dimensionless gas phase and adsorbate phase concentration profiles in a single, model pore for the 'no field' and 'with field' case, respectively.

Computer Program for 'Single Pore' Model

```
PROGRAM PONDER     74/175  OPT=1                    FTN 4.8+552        12/14/82  .17 00.43      PAGE     1

      1              PROGRAM PONDER (OUTPUT)
                     DIMENSION G(102,60),C(102,60),M(101),XA(101),XB(101),XC(101),XD(10
                    *1),S(101),V(102),U(101),F(101),EG(102),B(101),ES(102),Y(101),Z(101
                    *),Q(101),W0(37),T0(37),DM(37),EM(37),DC(101)
      5              REAL K1,LE,M
                C  SIGMA=THICKNESS OF LAYER FOR SURFACE DIFFUSION
                C DZO=SURFACE DIFFUSION COEFFICIENT TIMES SIGMA FOR MONOLAYER COVERAGE
                     DZO=4.6E-11
                C    ROS=DENSITY OF ADSORBATE GM/CC
     10         C    A= SPECIFIC AREA OF SILICA GEL S-2509,CM**2/GM
                C    RO=RADIUS OF EMPTY PORE, CM
                C    GO=CONCENTRATION OF SURROUNDING VAPOR, GM/CC
                C    CO=SURFACE ADSORBATE CONCENTRATION OF FILLED PORE, GM/CM**2
                C    DELZ=STEP SIZE IN Z
     15         C    LE=LENGHT OF PORE, CM
                     ROS=1.0 $A=4.561E+6 $ RO=30.7E-8 $ GO=2.3E-5 $ CO=1.535E-7 $ DELZ=
                    *.01  $ LE=.01693
                C  DO=DIELECTRIC CONSTANT OF DRY PARTICLE
                C   D1=DIELECTRIC CONSTANT OF SOLID SILICA
     20             DO=2.133 $ D1=6.173 $ DI=1.529
                C    BETA1=INTERPARTICLE VOID VOLUME FRACTION
                C    BETA2=1-BETA1
                       BETA1=.5285 $ BETA2=.4715 $ W=0.0
                C    XO=DIMENSIONLESS SURROUNDING GAS CONCENTRATION
     25         C    GM=GAS PHASE CONCENTRATION FOR MONOLAYER
                       XO=1.0
                       GM=.310
                C    INITIAL CONCENTRATIONS
                       DO 30 I=1,101
     30                G(I,1)=0.0001
                       C(I,1)=5E-5
                  30   CONTINUE
                       XT=60.0
                       DO 100 N=1,37
     35         C    ESTIMATION OF INTERNAL ELECTRIC FIELDS
                       IF (W.LT..0649) GO TO 25
                       IF(W.LE..1390) D2=((W-.0649)*43.26+.0649*1.05)/W
                       IF(W.GT..1390) D2=((W-.1390)*104+(.1390-.0649)*43.26+.0649*1.05)/W
                       DEL3=.6105*(1-W/0.7)
     40                A1=2.-6*(D2+2)/(3*(D2-1))
                       B1=5-9*DEL3-6*(DO-1)*(D1+2)/(3*(D1-1))+(6*DO-3)*(D2+2)/(3*(D2-1))
                       C1=2-3*(DO-1)*(D1+2)/(3*(D1-1))+3*DO*(D2+2)/(3*(D2-1))
                C    DP=PARTICLE DIELECTRIC CONSTANT
                       DP=(-B1-(B1**2.-4*A1*C1)**0.5)/(2.*A1)
     45                A2=2*(DP+2)/(DP-1)-2.
                       B2=-(DP+2)/(DP-1)-5+9*BETA2
                       C2=-(DP+2)/(DP-1)-2
                C    D=OVERALL DIELECTRIC CONSTANT OF BED
                       D=(-B2+(B2**2-4*A2*C2)**0.5)/(2*A2)
     50                DM(N)=D
                C    E=OVERALLL ELECTRIC FIELD*R(AVG)
                C    EP=PARTICLE ELECTRIC FIELD*R(AVG)
                       E=60000/((2.890*2.056*D)*.067)
                       EM(N)=E
     55                EP=((D+2)/3-3*D*BETA2/(2*D+1))*3*E/((DP+2)*BETA1)
                       EPA=EP $ DPA=DP
                       GO TO 26
                  25   EPA=0.0 $ DPA=0.0
                  26   J=1    $  W=0.0
     60                IF(N.LT.11) DELT=2*XT
                       IF(N.GE.11.AND.N.LT.19) DELT=5*XT
                       IF(N.GE.19.AND.N.LT.27) DELT=15*XT
                       IF(N.GE.27) DELT=20*XT
                  20   DO50 I=1,101
     65                IF(J.EQ.1) V(I)=G(I,N)
                       IF(J.EQ.1) U(I)=C(I,N)
                C    VALUES OF K1 AND K2 FOR LINEAR RELATION BETWEEN G AND C
                       IF(G(I,N).GE..0000.AND.G(I,N).LT..1477) GO TO 61
                       IF(G(I,N).GE..1477.AND.G(I,N).LT..3480) GO TO 62
     70                IF(G(I,N).GE..3480.AND.G(I,N).LT..5217) GO TO 63
                       IF(G(I,N).GE..5217.AND.G(I,N).LT..6435) GO TO 64
                       IF(G(I,N).GE..6435.AND.G(I,N).LT..7391) GO TO 65
                       IF(G(I,N).GE..7391.AND.G(I,N).LT..8000) GO TO 66
                       IF(G(I,N).GE..8000.AND.G(I,N).LT..8522) GO TO 67
     75                IF(G(I,N).GE..8522.AND.G(I,N).LT..8957) GO TO 68
                       IF(G(I,N).GE..8957.AND.G(I,N).LT..9652) GO TO 69
                       IF(G(I,N).GE..9652.AND.G(I,N).LE.1.000) GO TO 70
```

```
      61  K1=3.176E-3 $ C1=0.0
          GO TO 71
80    62  K1=1.5652E-3 $ C1=5.5E-9
          GO TO 71
      63  K1=2.00E-3 $ C1=2.0E-9
          GO TO 71
      64  K1=4.357E-3 $ C1=-2.628E-8
85        GO TO 71
      65  K1=9.045E-3 $ C1=-9.567E-8
          GO TO 71
      66  K1=1.807E-2 $ C1=-2.491E-7
          GO TO 71
90    67  K1=3.90E-2 $ C1=-6.342E-7
          GO TO 71
      68  K1=1.56E-2 $ C1=-1.7556E-7
          GO TO 71
      69  K1=4.125E-3 $ C1=6.0825E-8
95        GO TO 71
      70  K1=1.2493E-3 $ C1=1.2467E-7
      71  S(I)=K1 $ F(I)=C1
          IF(J.EQ.3) GO TO 50
          IF(J.EQ.1) GO TO 73
100       GO TO 72
      73  B(I)=K1 $ Z(I)=C1
C     DEL3=FRACTION OF GAS PHASE IN PORE
      72  DEL3=.6105*(1-C(I,N))
C     D2=AVERAGE DIELECTRIC CONSTANT OF ADSORBATE
105   80  IF(C(I,N).LE..0927) D2=1.05
          IF(C(I,N).GT..0927.AND.C(I,N).LE..1986) D2=(C(I,N)-.0927)*43.26/C(
         *I,N) +.0927*1.05/C(I,N)
          IF(C(I,N).GT..1986) D2=((C(I,N)-.1986)*104+(.1986-.0927)*43.26+.09
         *27*1.05)/C(I,N)
110       A1=2.-6*(D2+2)/(3*(D2-1))
          B1=5-9*DEL3-6*(DO-1)*(D1+2)/(3*(D1-1))+(6*DO-3)*(D2+2)/(3*(D2-1))
          C1=2-3*(DO-1)*(D1+2)/(3*(D1-1))+3*DO*(D2+2)/(3*(D2-1))
          DP=(-B1-(B1**2.-4*A1*C1)**0.5)/(2.*A1)
          EP=EPA*(DPA+2)/(DP+2)
115       DEL2=.6105-DEL3
C     ES(I)=FIELD IN ADSORBATE PHASE IN PORE
C     EG(I)=FIELD IN GAS PHASE IN PORE
          ES(I)=((DP-DO)*EP/(DEL2*(D2-1)))**2.
          EG(I)=(3*DP*EP/(2*DP+1))**2.
120   C   DC(I)=DIELECTRIC CONSTANT OF SURFACE HOPPING MOLECULES
          IF(C(I,N).LT..0927) DC(I)=1.05
          IF(C(I,N).GT..0927.AND.C(I,N).LE..1986) DC(I)=43.26
          IF(C(I,N).GT..1986) DC(I)=104
      50  CONTINUE
125       IF(J.EQ.3) GO TO 77
      82  DO 51 I=1,101
C     P=FRACTION OF PORE FILLED WITH ADSORBATE
          P=2.*C(I,N)*CO/(RO*ROS)
          R=RO*(1-P)**0.5
130   C   Y(I)=RADIUS OF CICULAR C.S. FOR DIFFUSION (DIMENSIONLESS)
          Y(I)=(R+3E-8)/RO
          Y(I)=Y(I)*(G(I,N)+V(I))/(2.*GM)
          IF(C(I,N).LT..0927) Y(I)=1.0
135   51  CONTINUE
          ALPHA=LE**2./DZO
          DO 101 I=2,100
          XA(I)=Y(I)/DELZ**2.-(Y(I+1)-Y(I-1))/(4.*DELZ**2.)
          XC(I)=Y(I)/DELZ**2. +(Y(I+1)-Y(I-1))/(4.*DELZ**2.)
          XB(I)=-2.*Y(I)/DELZ**2. -ALPHA*S(I)/DELT
140   C   BETA=M*EO/(2.*R*T*GO)
          BETA=3.218E-16/GO
          XD(I)=-ALPHA*(B(I)*V(I)+Z(I)/GO-F(I)/GO)/DELT+BETA*((DC(I)-1.)*Y(I
         *)*(EG(I+1)-2.*EG(I)+EG(I-1))/(DELZ**2.)+Y(I)*(EG(I+1)-EG(I-1))*(DC
         *(I+1)-DC(I-1))/(4.*DELZ**2.)+(DC(I)-1)*(EG(I+1)-EG(I-1))*(Y(I+1)-Y
145      *(I-1))/(4.*DELZ**2.))
     101  CONTINUE
          XD(2)=XD(2)-XA(2)*XO
          XD(100)=XD(100)-XC(100)*XO
C     SOLVING THE TRI-DIAGONAL MATRIX FOR CONCNTRATIONS
150       CALL TRIDAG (XA,XB,XC,XD,M)
C     GAS PHASE CONCENTRATION IN PORE
          DO 85 I=2,100
          G(I,N+1)=M(I)
      85  CONTINUE
```

```
155           G(1,N+1)=X0 $ G(101,N+1)=X0
          C   SURFACE ADSORBATE CONCENTRATIONS IN PORE
            77 DO 90 I=1,101
               C(I,N+1)=U(I)+(S(I)*G(I,N+1)*GO+F(I)-B(I)*V(I)*GO-Z(I))/CO
            90 CONTINUE
160           C(1,N+1)=C(2,N+1)
              C(101,N+1)=C(100,N+1)
          C   ITERATION FOR BETTER AVERAGE GUESSES
              J=J+1
              IF(J.EQ.4) GO TO 87
165           DO 86 I=1,101
              G(I,N)=G(I,N+1)
              C(I,N)=(C(I,N+1)+U(I))/2.
            86 CONTINUE
              GO TO 20
170       C   W=GMS ADSORBED/GM ADSORBENT DRY
            87 DO 54 I=1,100
              W=W +(C(I,N+1)+C(I+1,N+1))*CO*.01*A/2.
            54 CONTINUE
              IF(N.LT.11) T=N*2
175           IF(N.GE.11.AND.N.LT.19) T=20.+(N-10)*5
              IF(N.GE.19.AND.N.LT.27) T=60+(N-18)*15
              IF(N.GE.27) T=180+(N-26)*20
              WO(N)=W $ TO(N)=T
           100 CONTINUE
180           PRINT 204
           204 FORMAT(20X,* PROFILE OF OVERALL W.D.E. VS T (MIN ) FOR SINGLE PORE
             **,/)
              PRINT 205
           205 FORMAT(20X,*W*,11X,*T*,10X,*D*,12X,*E*/)
185           DO 206 I=1,37
              PRINT 210,WO(I),TO(I),DM(I),EM(I)
           210 FORMAT(/,12X,E13.5,3X,F7.2,3X,F7.2,5X,F9.2,3X,/)
           206 CONTINUE
          C   GAS PHASE CONCENTRATION PROFILE IN PORE
190       C   SURFACE ADSORBATE CONCENTRATION PROFILE IN PORE
              PRINT 161
           161 FORMAT(1H1,20X,*GAS AND ADSORBED PHASE CONCEN. PROFILE IN PORE*/)
              PRINT 162
           162 FORMAT(/,9X,*G(2,N+1)*,3X,*G(3,N+1)*,3X,*G(25,N+1)*,2X,*G(26,N+1)*
             *,2X,*G(27,N+1)*,2X,*G(50,N+1)*,2X,*G(51,N+1)*,2X,*G(52,N+1)*/)
195           PRINT 169
           169 FORMAT(/,9X,*C(2,N+1)*,3X,*C(3,N+1)*,3X,*C(25,N+1)*,2X,*C(26,N+1)*
             *,2X,*C(27,N+1)*,2X,*C(50,N+1)*,2X,*C(51,N+1)*,2X,*C(52,N+1)*/)
              DO 163 I=1,11
200           IF(I.LT.3) N=5*I
              IF(I.GE.3.AND.I.LT.5) N=12+(I-3)*6
              IF(I.GE.5.AND.I.LT.9) N=20+(I-5)*2
              IF(I.GE.9) N=29+(I-9)*3
              PRINT 164,TO(N)
205           164 FORMAT(/,20X,*T= *,F4.0,3X,/)
              PRINT 160,G(2,N+1),G(3,N+1),G(25,N+1),G(26,N+1),G(27,N+1),G(50,N+1
             *),G(51,N+1),G(52,N+1)
           160 FORMAT(/,9X,F7.5,4X,F7.5,4X,F7.5,4X,F7.5,4X,F7.5,4X,F7.5,4X,F7.5,4
             *X,F7.5,3X,/)
210           PRINT 170,C(2,N+1),C(3,N+1),C(25,N+1),C(26,N+1),C(27,N+1),C(50,N+1
             *),C(51,N+1),C(52,N+1)
           170 FORMAT(/,9X,F7.5,4X,F7.5,4X,F7.5,4X,F7.5,4X,F7.5,4X,F7.5,4X,F7.5,4
             *X,F7.5,3X,/)
           163 CONTINUE
215           END
```



```
  1           SUBROUTINE TRIDAG (XA,XB,XC,XD,M)
              DIMENSION XA(101),XB(101),XC(101),XD(101),BETA(101),GAMMA(101),M(1
             *01)
              REAL M
  5           BETA(2)=XB(2)
              GAMMA(2)=XD(2)/BETA(2)
              DO 40 I=3,100
              BETA(I)=XB(I)-XA(I)*XC(I-1)/BETA(I-1)
              GAMMA(I)=(XD(I)-XA(I)*GAMMA(I-1))/BETA(I)
 10            40 CONTINUE
              M(100)=GAMMA(100)
              DO 50 I=2,99
              K=101-I
              M(K)=GAMMA(K)-XC(K)*M(K+1)/BETA(K)
 15            50 CONTINUE
              RETURN
              END
```

E.1. Variation of W with time T (no field) in single model pore.

PROFILE OF OVERALL W.D.E. VS T (MIN) FOR SINGLE PORE

W	T	D	E				
.65671E-01	2.00	-I	-I				
.99539E-01	4.00	1.55	14719.20	.46292E+00	90.00	12.15	3214.15
.12709E+00	6.00	2.08	12500.17	.48936E+00	105.00	13.28	2966.33
.14993E+00	8.00	2.40	11445.07	.51286E+00	120.00	14.27	2778.89
.16973E+00	10.00	2.82	10303.79	.53380E+00	135.00	15.15	2630.42
.18711E+00	12.00	3.34	9183.32	.55271E+00	150.00	15.94	2510.44
.20279E+00	14.00	3.81	8349.28	.56990E+00	165.00	16.66	2410.82
.21738E+00	16.00	4.26	7689.23	.58567E+00	180.00	17.31	2326.67
.23091E+00	18.00	4.69	7142.03	.60460E+00	200.00	17.92	2254.33
.24345E+00	20.00	5.11	6686.48	.62156E+00	220.00	18.64	2173.03
.27085E+00	25.00	5.50	6303.78	.63673E+00	240.00	19.29	2104.95
.29452E+00	30.00	6.40	5581.68	.65016E+00	260.00	19.87	2047.43
.31573E+00	35.00	7.20	5063.18	.66181E+00	280.00	20.38	1999.01
.33478E+00	40.00	7.93	4665.79	.67170E+00	300.00	20.83	1958.79
.35213E+00	45.00	8.60	4353.57	.67973E+00	320.00	21.21	1925.86
.36818E+00	50.00	9.22	4100.47	.68596E+00	340.00	21.52	1899.92
.38304E+00	55.00	9.79	3889.35	.69053E+00	360.00	21.76	1880.28
.39686E+00	60.00	10.33	3710.99	.69384E+00	380.00	21.94	1866.10
.43247E+00	75.00	10.84	3558.20	.69617E+00	400.00	22.06	1855.97

E.2. Variation of W, D, E (V/cm) with time T (when ΔV = 6 KV) in single model pore.

PROFILE OF OVERALL W,D,E, VS T (MIN) FOR SINGLE PORE

W	T	D	E				
.65671E-01	2.00	-I	-I				
.10204E+00	4.00	1.55	14719.20	.49181E+00	90.00	13.25	2971.12
.12171E+00	6.00	2.11	12394.54	.51700E+00	105.00	14.36	2762.67
.14540E+00	8.00	2.34	11636.56	.53919E+00	120.00	15.31	2605.85
.16773E+00	10.00	2.71	10595.10	.55892E+00	135.00	16.15	2481.25
.18899E+00	12.00	3.28	9287.27	.57662E+00	150.00	16.90	2379.75
.20653E+00	14.00	3.86	8266.02	.59263E+00	165.00	17.57	2295.28
.22830E+00	16.00	4.37	7542.96	.60718E+00	180.00	18.18	2223.77
.24541E+00	18.00	5.03	6770.88	.62445E+00	200.00	18.74	2162.40
.26104E+00	20.00	5.57	6247.14	.63971E+00	220.00	19.40	2093.74
.29378E+00	25.00	6.07	5823.59	.65302E+00	240.00	19.98	2036.49
.32102E+00	30.00	7.17	5078.17	.66442E+00	260.00	20.49	1989.00
.34399E+00	35.00	8.11	4575.17	.67398E+00	280.00	20.93	1949.99
.36427E+00	40.00	8.93	4215.84	.68165E+00	300.00	21.30	1918.44
.38230E+00	45.00	9.65	3938.91	.68739E+00	320.00	21.59	1893.84
.39866E+00	50.00	10.30	3719.53	.69158E+00	340.00	21.81	1875.80
.41359E+00	55.00	10.90	3539.25	.69459E+00	360.00	21.98	1862.86
.42732E+00	60.00	11.45	3388.41	.69668E+00	380.00	22.09	1853.67
.46228E+00	75.00	11.96	3260.00	.69793E+00	400.00	22.17	1847.34

E.3. Concentration profiles in single pore at different times (no field).

GAS AND ADSORBED PHASE CONCEN. PROFILE IN PORE

G(2,N+1)	G(3,N+1)	G(25,N+1)	G(26,N+1)	G(27,N+1)	G(50,N+1)	G(51,N+1)	G(52,N+1)
C(2,N+1)	C(3,N+1)	C(25,N+1)	C(26,N+1)	C(27,N+1)	C(50,N+1)	C(51,N+1)	C(52,N+1)
	T= 10.						
.94361	.89442	.52876	.51604	.50330	.29100	.29055	.29100
.97790	.93792	.16549	.15991	.15556	.09113	.09102	.09113
	T= 20.						
.95861	.92255	.67605	.67012	.66444	.59300	.59286	.59300
.98750	.96401	.26993	.26356	.25742	.19819	.19810	.19819
	T= 30.						
.96461	.93444	.72175	.71692	.71227	.65815	.65806	.65815
.99178	.97245	.34163	.33473	.32811	.25612	.25603	.25612
	T= 60.						
.97809	.95839	.79466	.79168	.78882	.75623	.75618	.75623
.99498	.98686	.50464	.49609	.48793	.40056	.40045	.40056
	T= 90.						
.98302	.96689	.81810	.81548	.81304	.78769	.78765	.78769
.99599	.99237	.61861	.60332	.58895	.49036	.49023	.49036
	T= 120.						
.98613	.97289	.83530	.83257	.83002	.80462	.80459	.80462
.99665	.99404	.72604	.71029	.69558	.55509	.55494	.55509

T= 150.

.98832	.97716	.84979	.84684	.84410	.81641	.81637	.81641
.99710	.99492	.81360	.79674	.78103	.62184	.62160	.62184

T= 180.

.99016	.98072	.86591	.86289	.85993	.83001	.82997	.83001
.99744	.99559	.86980	.86261	.85350	.69619	.69593	.69619

T= 240.

.99278	.98583	.89227	.88957	.88701	.85617	.85610	.85617
.99794	.99657	.93107	.92466	.91856	.83297	.83275	.83297

T= 300.

.99543	.99101	.92709	.92511	.92318	.89614	.89609	.89614
.99844	.99753	.96553	.96419	.96288	.93531	.93519	.93531

T= 360.

.99805	.99614	.96402	.96301	.96204	.95113	.95111	.95113
.99895	.99853	.98898	.98830	.98766	.98025	.98024	.98025

E.4. Concentration profiles in single pore at different times (ΔV = 6 KV).

GAS AND ADSORBED PHASE CONCEN. PROFILE IN PORE

G(2,N+1)	G(3,N+1)	G(25,N+1)	G(26,N+1)	G(27,N+1)	G(50,N+1)	G(51,N+1)	G(52,N+1)
C(2,N+1)	C(3,N+1)	C(25,N+1)	C(26,N+1)	C(27,N+1)	C(50,N+1)	C(51,N+1)	C(52,N+1)
	T= 10.						
.93099	.87525	.57974	.57198	.55853	35856	.35811	.35856
.97005	.89238	.18966	.18389	.17698	.10140	.10126	.10140
	T= 20.						
.95385	.91332	.70698	.70299	.69902	.66877	.66868	.66877
.98402	.95697	.31383	.30815	.30242	.26247	.26240	.26247
	T= 30.						
.96321	.93172	.74973	.74664	.74375	.71276	.71271	.71276
.99033	.96964	.38773	.38125	.37517	.32872	.32864	.32872
	T= 60.						
.97847	.95915	.80811	.80587	.80378	.78108	.78105	.78109
.99503	.98720	.55737	.54750	.53822	.46805	.46794	.46805
	T= 90.						
.98374	.96820	.82704	.82480	.82274	.80329	.80326	.80329
.99612	.99284	.67405	.66127	.64943	.54631	.54617	.54631
	T= 120.						
.98684	.97430	.84278	.84028	.83796	.81550	.81546	.81550
.99678	.99431	.77109	.75682	.74359	.61630	.61612	.61630

T= 150.

.98905	.97859	.85761	.85473	.85207	.82711	.82707	.82711
.99723	.99518	.84865	.83750	.82703	.68499	.68478	.68490

T= 180.

.99094	.98227	.87462	.87183	.86916	.84016	.84012	.84016
.99759	.99587	.88982	.88316	.87651	.75623	.75600	.75623

T= 240.

.99378	.98780	.90552	.90285	.90033	.87402	.87398	.87402
.99812	.99692	.95082	.94695	.94330	.88355	.88344	.88355

T= 300.

.99671	.99352	.94543	.94405	.94273	.92695	.92692	.92695
.99867	.99798	.97629	.97531	.97436	.96211	.96209	.96211

T= 360.

.99874	.99751	.97600	.97521	.97440	.96446	.96444	.96446
.99909	.99881	.99401	.99384	.99356	.98921	.98919	.98921

BIBLIOGRAPHY

BIBLIOGRAPHY

A1 Agaev, A. A., and Abdullaev, P. Kh., Izv. VUZ, Neft'i Gaz, 3, p. 53 (1969).

A2 Agzamkhodzhaev, A. A.; Zhurav'lev, L. T.; Kiselev, A. V.; and Shengeliya, K. Ya., Izv. Akad. Nauk SSSR, Seriya Khimicheskaya, No. 10 (1969).

B1 Bickelhaupt, R. E. "Surface Resistivity and the Chemical Composition of Fly Ash." J. Air Pollut. Control Assn., 25, 148-52 (1975).

B2 Bickelhaupt, R. E. Environ. Sci. Technol., 9 (4), 336 (1975).

B3 Brunauer, S.; Emmett, P. H.; and Teller, E. J. Am. Chem. Soc., 60, 309 (1938).

B4 Brunauer, S.; Copeland, L. E.; and Kantro, D. L. "The Langmuir and B.E.T. Theories." Chapter 3, The Solid-Gas Interface. Vol. 1, Marcel Dekker, Inc., N.Y. (1967).

B5 Barrer, R. M. "Surface and Volume Flow in Porous Media." Chapter 19, The Solid-Gas Interface. Vol. 2, Marcel Dekker, Inc., N.Y. (1967).

B6 Bottcher, C. J. F. Rec. Trav. Chim., 64, 47 (1945).

B7 Bennett, A. J. "The Effect of Applied Electric Fields on Chemisorption." Surf. Sci., 50, No. 1, 77-94 (1975).

B8 Banczyk, L. "Effect of the Electric Field on Mass Transfer in Liquid-Liquid Systems." Inz. Chem., 3, p. 469 (1975).

B9 Bailes, P. J., and Larkai, S. K. L. "An Experimental Investigation into the Use of High-Voltage D.C. Fields for Liquid Phase Separation." Trans. IChemE, 59, 229-37 (1981).

C1 Cohan, L. H. J. Amer. Chem. Soc., 60, 433 (1938).

C2 Clausing, P. Ann. d. Physik, 7, 521 (1930).

C3 Carnahan, B.; Luther, H. A.; and Wilkes, J. O. Applied Numerical Methods. Wiley (1969).

D1 Ditl, P., and Coughlin, R. W. "Sorption and Diffusion Interactions with Fly Ash of SO_2 in Air, SO_3 in Air, SO_2 + H_2O in Air, SO_3 + H_2O in Air." Environ. Sci. and Tech., 11, No. 7, 701-6 (1977).

D2 Ditl, P., and Coughlin, R. W. "Improving Efficiency of Electrostatic Precipitation by Physicochemical Modification of the Electrical Resistivity of Fly Ash." AIChE J., 22, No. 4, 730-36 (1976).

D3 de Groot, S. R., and Mazur, P. Non-Equilibrium Thermodynamics. North Holland, Amsterdam (1962).

D4 Dushchenko, V. P.; Panchenko, M. S.; Romanovskii, I. A.; and Slinkyakova, I. B. "Interaction of Moisture with Model Capillary-Porous Hydrophilic Materials." Inzh.-Fiz. zh., 15, No. 4 (1968).

D5 de Boer, J. H. The Dynamical Character of Adsorption. Oxford (1953).

D6 Domke, M.; Block, J. H.; and Drechsler, M. "The Influence of Electric Fields on Adsorbed Gases: FEM of O_2 on Tungsten Single Crystal Faces." Surf. Sci. (Netherlands), 51, No. 2, 451-68 (1968).

D7 Devyatov, V. G.; Mikheeva, E. P.; and Keier, N. P. "Influence of External Electric Field on Oxygen and Carbon Monoxide Adsorption." React. Kinet. Lett., 9, 199-204 (1978).

D8 Defay, R., and Mazur, P. Bull. Soc. Chim. Belges, 63, 562 (1954).

F1 Flood, E. A. "Thermodynamic Descriptions of Adsorption." Chapter 2, The Solid-Gas Interface. Vol. 1, Marcel Dekker, Inc., N.Y. (1967).

G1 Gregg, S. J., and Sing, K. S. W. Adsorption, Surface Area and Porosity. Academic Press (1967).

G2 Gordeev, Yu. N.; Bologa, M. K.; and Smirnov, G. F. (Kishinev, USSR), Elektron. Obrab. Mater., (4), 38-40 (Russ.), (1980).

G3 Gilliland, E. R.; Baddour, R. F.; George, G. P.; and Sladek, K. I. Ind. Eng. Chem., Fundam., 13, 95 (1974).

H1 Higuti, I. Bull. Inst. Phys. Chem. Research, Tokyo, 20, 489 (1941).

H2 Hirshfelder, J. O.; Curtis, C. F.; and Bird, R. B. Molecular Theory of Gases and Liquids. John Wiley & Sons, Inc., 847 (1954).

H3 Hoenig, S. A., and Lane, J. R. "Chemisorption of Oxygen on Zinc-Oxide, Effect of a D.C. Electric Field." Surf. Sci., 2, 163-74 (1968).

H4 Harker, J. D., and Ahmadzadeh, J. "The Effect of Electric-Fields on Mass Transfer from Falling Drops." Int. J. Heat Mass Transfer, 17, 1219-1225 (1974).

H5 Higashi, K.; Ito, H.; and Oishi, J. J. Japan Atom. Energy Soc., 5, 846 (1963).

K1 Kurosaki, S. J. Phys. Chem., 58, 320 (1954).

K2 Kirkwood, J. G., and Ruoss, R. M. J. Am. Chem. Soc., 63, 385 (1941).

K3 Kaptsov, N. S. The Corona Discharge (in Russ.). Gostckhizdat, Moscow-Leningrad (1975).

K4 Kuliev, A. M.; Teimurova, F. A.; Dzhafarova, F. Sh.; and Gasanov, N. G. "Mechanism of Adsorption in an Electric Field." Zh. Fiz. Khim., 52 (3), 712-13 (Russ.), (1978).

K5 Kuliev, A. M.; Rasulov, A. M.; Teimurova, F. A.; and Dzhamalova, S. T. "Adsorption of Hydrocarbons of Different Structure in an Electric Field." Zh. Prikl. Khim. (Leningrad), 47 (11), 2570-1 (Russ.), (1974).

K6 Kowalski, W., and Ziolkowski, Z. "Increase in Rate of Mass Transfer in Extraction Columns by Means of an Electric Field." Int. Chem. Engg., 21, No. 2 (1981).

K7 Kokin, A. S., and Popov B. G. "Effect of an Electrostatic Field on the Evaporation Processes in Disperse Media." Teor. Osn. Khim. Tekhnol., (4), 626-9 (Russ.), (1977).

K8 Kuliev, A.M.; Teimurova, F. A.; Kwieva, N. N.; and Gasonov, N. G. "Study of the Adsorption of Hydrogen Sulfide from Natural Gas by an Acqueous Solution of Monoethanolamine in an Electric Field." Izv. Vyssh. Uchebn. Zaved, Neft Gaz, 23 (10), 53-5 (Russ.), (1980).

K9 Kirkwood, J. G. J. Chem. Phys., 7, 911 (1939).

L1 Lincoln, W. W., and Olinger, J. L. "Enhancement of Gaseous Adsorption on Metal Surfaces Through the Use of an Applied A.C. Voltage." Adsorption and Ion Exchange. AIChE Symp. Ser. (1975).

M1 Maclean, K. J. "Influence of Electric Field on the Resistivity of a Particulate Layer." Proc. IEE, Vol. 121, No. 1, 76-80 (1974).

M2 McIntosh, R.; Rideal, E. K.; and Snelgrove, J. A. Proc. Roy. Soc. (London), A208, 292 (1951).

M3 McIntosh, R. L. Dielectric Behaviour of Physically Adsorbed Gases. Marcel Dekker, Inc., N.Y. (1966).

M4 McIntosh, R. L., and Channen, E. W. Can. J. Chem., 33, 172 (1955).

M5 Mosievich, A. S. "Effect of an Electric Field on Internal Mass Transfer During Sorption of Moisture by Natural Polymers Under Different Temperature Conditions." Teploprovodnost Konvektivinyi Teploobmen, 7th, 90-4 (Russ.), (1976).

M6 Mazur, P., and Prigogine, I. Mem. Acad. Roy. Belg., 23, 1 (1953).

M7 Mandel, M. Thesis, Universite Libre de Bruxelles (1955).

P1 Panchenko, M. S.; Dushchenko, V. P.; Panasyuk, A. L.; Mosievich, A. S.; and Karpovich, I. N. "Enhancement of the Internal Mass Transfer Under Isothermal Conditions." Inzh.-Fiz. zh., 25, No. 2 (1973).

P2 Panasyuk, A. L.; Panchenko, M. S.; Starov, V. M.; and Churaev, N. V. "Influence of Inhomogeneous Electric and Magnetic Fields on Internal Mass Transfer in Capillary Porous Bodies." Inzh.-Fiz. zh., 5, No. 7 (1978).

P3 Panchenko, M. S.; Dushchenko, V. P.; Panasyuk, A. L.; and Mosievich, A. S. "Effect of an Electric Field on the Kinetics of Water Sorption by a Capillary-Porous Material." Inzh.-Fiz. zh., 22, No. 5 (1972).

P4 Panchenko, M. S.; Panasyuk, A. L.; and Mosievich, A. S. "On the Thermodynamics of Moisture Retained in Pores of Capillary-Porous Models." Inzh.-Fiz. zh., 20, No. 5 (1971).

P5 Panchenko, M. S.; Dushchenko, V. P.; Panasyuk, A. L.; Mosievich, A. S.; and Zhenevskii, N. V. "Effect of Electrical and Magnetic Fields on Internal Mass Transfer Coefficients During Moisture Sorption by Typical Capillary-Porous Materials Under Different Temperature Conditions." Teplo-Massoperenos, Dokl. Vses. Sovesch, 4th, 6, 118-23 (Russ.), (1972).

P6 Panchenko, M. S.; Dushchenko, V. P.; Panasyuk, A. L.; Mosievich, A. S.; and Semko, O. Ya. "Effect of Electrical and Magnetic Fields and Structure of Capillary-Porous Bodies on the Kinetics of Sorption of Water Molecules." Elektron. Obrab. Mater., (3), 56-61 (Russ.), (1972).

P7 Panchenko, M. S.; Dushchenko, V. P.; Mosievich, A. S.; and Panasyuk, A. L. "Effect of an Electrical Field on Internal Mass Transfer in Dispersed Systems of Different Physicochemical Nature." Zh. Fiz. Khim., 52 (5), 1278-9 (Russ.), (1978).

P8 Panchenko, M.S.; Mosievich, A. S.; and Dushchenko, V. P. "Effect of an Electric Field on Internal Mass Transfer in Dispersed Bodies in their Drying Process." Elektron. Obrab. Mater., (2), 50-2 (Russ.), (1981).

P9 Panchenko, M. S.; Mosievich, A. S.; Dushchenko, V. P.; and Plotnitskii, B. F. "Characteristics of Hydration of the KU-2 Cation Exchanger in Different Ionic Forms in the Presence of a Heterogeneous Electric Field." Zh. Fiz. Khim., 52 (4), 1008-11 (Russ.), (1978).

P10 Panchenko, M. S.; Mosievich, A. S.; Panasyuk, A. L.; and Karpovich, I. N. "Effect of Electrical and Magnetic Fields on the Geometry of the Interstice and on the Sorption Capacity of Dispersed Bodies." Elektron. Obrab. Mater., (6), 40-4 (Russ.), (1976).

P11 Panchenko, M. S.; Panasyuk, A. L.; Karpovich, I. N.; and Kisel' chuk, N. Ya. "Drying Kinetics of a Capillary-Porous Body in an Electric Field." Inzh. Fiz. zh., 33, No. 2, 356-57 (1977).

P12 Panchenko, M. S.; Karpovic, I. N.; and Churaev, N. V. "Effect of a Corona Discharge Field on Evaporation of Liquids from Capillaries." Inzh. Fiz. zh., 41, No. 6, 1049-56 (1981).

P13 Prigogine, I. J. Chim. Phys., 49, 79 (1952).

P14 Prigogine, I.; Mazur, P.; and Defay, R. J. Chem. Phys., 50, 146 (1953).

P15 Prigogine, I., and Mazur, P. Physica, 19, 241 (1953).

P16 Prigogine, I. Introduction to Thermodynamics of Irreversible Processes. Springfield (Illinois), (1955).

P17 Prigogine, I., and Defay, R. Thermodynamique Chimique. Desoer, Liege (1952).

P18 Ponzi, M.; Papa, J.; Rivalora, J. B. P.; and Zgrablich, G. AIChE J., 23 347 (1977).

R1 Robinson, M. "Electrostatic Precipitation." Chapter 9, Electrostatics and its Applications. John Wiley & Sons (1973).

R2 Rasulov, A. M.; Teimurova, F. A.; and Dzhamalova, S. T. "Change in Adsorbent Surface Properties in an Electric Field." Podgot. Pererab. Gaza Gazov. Kondens., (10), 24-7 (Russ.), (1978).

R3 Rozova, T. T.; Ivanov, V. G.; and Fursei, G. N. "Effect of a Strong Electric Field on Oxygen Adsorption on Germanium." Fiz. Tverdogo Tela, 17, No. 1, 64-66 (1975).

R4 Rubashov, Ya. B., and Bortnikov Ya. S. Electrogazdinamika (Electrogas Dynamics). Atomizdat (1971).

R5 Reitz, J. R.; Milford, F. J.; and Christy, R. W. Foundations of Electromagnetic Theory. Addison Wesley (1979).

S1 Steele, W. A. The Interaction of Gases with Solid Surfaces. Pergamon Press (1974).

S2 Shukla, P. N. Ph.D. Dissertation, Michigan State University (1980).

S3 Somarjai, G. A. Principles of Surface Chemistry. Prentice-Hall, Inc. (1972).

S4 Sawistowski, H.; Austin, L. J.; and Banczyk, L. "Effect of Electric Field on Mass Transfer Across a Plane Interface." Chem. Engg. Sci., 26, 2120 (1969).

S5 Sawistowski, H., and Iyer, P. V. R. "Effect of Electric Field on Mass Transfer Across a Plane Interface." Proc. Int. Solvent Extr. Conf., 2, 1029-46 (1974).

S6 Sanfeld, A. Introduction to the Thermodynamics of Charged and Polarised Layers (Vol. 10, Monographs in Statistical Physics). John Wiley & Sons, Ltd. (1968).

S7 Smith, R. K., and Metzner, A. G. J. Phys. Chem., 68, 2741 (1964).

S8 Stewart, W. E.; Bird, R. B.; and Lightfoot, E. N. Transport Phenomena. John Wiley & Sons, Inc. (1960).

T1 Tishin, E. A. "Effect of an External Electric Field on Various Concentrations of Adatoms." Ukr. Fiz. Zh. (Russ. Ed.), 16, No. 9, 1552-4 (Russ.), (1971).

T2 Thornton, J. D. "The Applications of Electrical Energy to Chemical and Physical Rate Processes." Rev. Pure and Appl. Chem., 18, 197 (1968).

T3 Tamon, H.; Kyotani, S.; Wada, H.; Okazaki, M.; and Toei, R. "Surface Flow Phenomenon of Adsorbed Gases on Activated Alumina." J. Chem. Engg. Japan, 14, No. 2, 136 (1981).

W1 White, H. J. "SO_3 Injection to Aid Stack Cleanup?" Electrical World, 22 (1970).

W2 White, H. J. "Resistivity Problems in Electrostatic Precipitation." J. Air Pollut. Contr. Assn., 24 (1974).

W3 Weaver, J. A., and Metzner, A. B. AIChE J., 12, 655 (1964).

W4 White, H. J. "Chemical and Physical Conductivity Factors in Electrical Precipitation." Chem. Engg. Prog., 52, 244 (1956).

Z1 Zettlemoyer, A. C.; McCafferty, E.; and Pravdic, V. "Dielectric Behaviour of Adsorbed Water Films on the α-Fe_2O_3 Surface." Trans. Faraday Soc., 66, 1720 (1970).